2012

Identification and Quantification of Protein Carbonylation by Mass Spectrometry

Qingyuan Liu
Virginia Commonwealth University

COPYRIGHT PAGE

IDENTIFICATION AND QUANTIFICATION OF PROTEIN CARBONYLATION BY MASS SPECTROMETRY

A dissertation submitted in partial fulfillment of the requirements for the degree of Doctor of Philosophy at Virginia Commonwealth University.

by

Qingyuan Liu

Director: Prof. Scott Gronert

Department of Chemistry

Virginia Commonwealth University

Richmond, Virginia

January 2012

Abstract

IDENTIFICATION AND QUANTIFICATION OF PROTEIN CARBONYLATION BY MASS SPECTROMETRY

By Qingyuan Liu, Ph.D.

A dissertation submitted in partial fulfillment of the requirements for the degree of Doctor of Philosophy at Virginia Commonwealth University.

Virginia Commonwealth University, 2012

Director: Professor Scott Gronert, Department of Chemistry

Accumulated evidence indicates oxidative stress plays important roles in disease and aging. Under oxidative stress, lipid peroxidation (LPO) leads to reactive carbonyl species (RCS) that can modify a wide range of biomolecules including protein, DNA and carbohydrate. In this dissertation, we investigate the modification of two model proteins, human serum albumin (HSA) and aconitase (ACO), by the LPO-relevant α, β-unsaturated aldehydes, acrolein (ACR) and 4-hydroxy-2-nonenal (HNE). The investigation is focused on the characterization and quantification ACR and HNE addition to the model proteins. A correlation between HNE modification and ACO activity is also determined. These results provide insights into the impact of oxidative stress at the molecular level and are relevant to aging and disease states. We finally

investigate protein carbonylation in ischemic mouse heart mitochondia, and develop a quantitative method for detecting carbonylated protein in this system. The research is based on liquid chromatography/mass spectrometry (LC/MS), Western Blots, and enzymatic assay.

Acknowledgements

First and foremost, I would like to express my sincerest gratitude to my research advisor, Dr. Scott Gronert for his wonderful guidance. I experience an incredible research life from the first day I started my career in his lab. He is always here to support me with his remarkable knowledge, direct me with his intensive experience, and inspire me with his intelligent suggestion. Without his help, the dissertation could not have been completed.

I also would like to extend my heartfelt gratitude to Dr. Edward J. Lesnefsky's, Dr. Suzanne Ruder, Dr. Mike Grotewiel, Dr. Julio C. Alvarez, and Dr. Matthew C.T. Hartman for their vital advice during my research and thesis writing.

I own my deepest gratitude to Dr. Kristina T. Nelson, Dr. Chen Qun, and Dr. David C. Simpson for their technical support to my research. I gain thoughtful suggestions and creative ideas from the discussion with them every time. I am also grateful to all faculty and staff in the Department of Chemistry of Virginia Commonwealth University for their countless assistance.

I am also obliged to my colleagues and friends during my graduate student life, Melanie Paillard, Keyanna Conner, Dr. Jun Yin, Dr. Hongwei Xie, Bo Zhao, Suresh Narayanasamy, and Mark Davis, for their invaluable and unselfish help on both an academic and a personal level.

My most especially goes to my parents, husband, and the other family members. Their unconditional and endless love encourages me forward to achieve my goals.

Finally, I would like to acknowledge the academic and financial support of the National Institute of Health and Philip Morris USA Inc. for this research.

Table of Contents

List of Tables

List of Figures

List of Schemes

List of Abbreviations

ROS	reactive oxygen species
RNS	reactive nitrogen species
RCS	reactive carbonyl species
GSH	glutathione
CAT	catalase
SOD	superoxide dismutase
GPX	glutathione peroxidase
LPO	lipid peroxidation
LOOH	lipid hydroperoxide
MeSOX	methionine sulfoxide
PUFA	polyunsaturated fatty acid
MDA	malondialdehyde
ONE	4-oxo-2-nonenal
HNE	4-hydroxy-2-nonenal
MCO	metal catalyzed oxidation
ACR	acrolein
ELISA	enzyme-linked immunosorbent assay
PTMs	post-translational modifications
HPLC	high performance liquid chromatography
CE	capillary electrophoresis
FDP-lysine	N^{ε}-(3-formyl-3,4-dehydropiperidino)lysine
MP-lysine	N^{ε}-(3-methylpyridinium)lysine
dG	deoxyguanosine
HMPA	*S*-(3-hydroxy-propyl)-*N*-acetylcysteine
HSA	human serum albumin
NEM	N-ethylmaleimide
DTT	1,4-dithio-DL-threitol
PBS	phosphate buffered saline
TFA	trifluoroacetic acid
ETD	electron-transfer dissociation
CID	collision-induced dissociation
IAM	iodoacetamide
SASA	solvent accessible surface area
HPODE	hydroperoxy-octadecadienoic acid
LOX	lipoxygenase
HPL	hydroperoxide lyase
HNA	4-hydroxynon-2-enoic acid
HPNE	4-hydroperoxy-2*E*-nonenal

DHN	1,4-dihydroxy-2-nonene
GST	glutathione-S-transferase
HAA	4-hydroxynonanal
BCA	bicinchoninic acid assay
iTRAQ	isobaric tag for relative and absolute quantitation
PQD	pulsed-Q dissociation
MS/MS	tandem mass spectrometry
HCD	higher-energy C-trap dissociation
PIC	phenylisocyanate
IRP	iron-regulatory protein
IRE	iron-responsive elements
ACO	aconitase
m-aconitase	mitochondrial aconitase
c-aconitase	cytoplasmic aconitase
SDS-PAGE	sodium dodecyl sulfate-polyacrylamide gel electrophoresis
PVDF	polyvinylidene difluoride
HRP	horseradish peroxidase
TBST	tris-buffered saline with tween 20
BSA	bovine serum albumin
ECL	enhanced chemiluminescence
HEPES	4-(2-hydroxyethyl)-1-piperazineethanesulfonic acid
NADPH	nicotinamide adenine dinucleotide phosphate
OBP	bathophenanthroline disulfonic acid disodium salt
ETC	electron-transport chain
mtDNA	mitochondrial DNA
ATP	adenosine-5'-triphosphate
NADH	nicotinamide adenine dinucleotide
ADP	adenosine diphosphate
SSM	sub-sarcolemmal mitochondria
IFM	inter-fibrillar mitochondria
MES	2-(N-morpholino) ethanesulfonic acid
DNPH	2,4-dinitrophenylhydrazine

Chapter 1: Introduction

Introduction

Oxidative stress and disease

Evidence of oxidative stress playing important roles in disease and aging has accumulated over many years. Oxidative stress is caused by an imbalance between the production of pro-oxidants and the anti-oxidant defense capacity of an organism.[1] This imbalance is induced by one of three factors: 1) increased pro-oxidant generation, 2) decreased anti-oxidant protection, or 3) failure to repair oxidative damage.[2]

Chemically, a substance that can accept electrons is an oxidant and one that can donate electrons is a reductant. In biological environments, they are identified as pro-oxidant and anti-oxidant.[3] Generally the pro-oxidants are referred to as reactive oxygen species (ROS) and reactive nitrogen species (RNS). The ROS and RNS are generally oxidizing molecules and can be classified into two types of compounds, free radicals and nonradicals. The free radicals include compounds such as hydroxyl radical, superoxide ion radical, oxygen, peroxyl radical and nitric oxide radical.[4] These compounds contain at least one unpaired electron. The unpaired electron makes these compounds highly reactive with a strong affinity to donate or obtain another electron to attain stability.[5] The nonradicals include compounds such as hydrogen peroxide, organic peroxide, peroxynitrite, ozone, singlet oxygen, hypochlorous acid and aldehydes.[4] Most of the ROS have a short life span, and often the half-life depends on the environment of the medium. In some cases, a relatively long life span for the ROS might imply a stronger toxicity because it provides adequate time to reach a biological target and cause damage far from the site

of production.[6]

Generation of ROS and RNS can occur in response to diverse stimuli, which can come from both exogenous and endogenous sources.[7] Exogenous sources mainly include exposure to ionizing and nonionizing irradiation such as ultrasound, UV and γ irradiation,[8, 9] exposure to xenobiotics and chemicals such as toxins, pesticides and alcohol,[10, 11] or exposure to pollutants such as cigarette smoke, car exhaust and industrial contaminants.[12] Drugs, food, bacteria and viruses are also major exogenous sources of ROS and RNS.[13-16] Endogenous sources mainly include mitochondrial respiration,[17] direct and indirect ROS producing enzymes such as NO synthase and xanthin oxidase,[18] metabolism,[19] and diseases such as metal disorders and ischemic processes.[20] Generation of ROS and RNS from endogenous sources causes chronic problems because it is a constant process during the life of the cell.[21, 22]

Anti-oxidants are substances that prevent or repair oxidative damage. In general, anti-oxidants include exogenous small molecule anti-oxidants such as ascorbic acid (vitamin C) and tocopherol (vitamin E),[23] endogenous small molecule anti-oxidants such as glutathione (GSH),[24] small protein anti-oxidants such as thioredoxins and glutaredoxins,[25] and enzymes such as catalase (CAT), superoxide dismutase (SOD) and glutathione peroxidase (GPX).[26] These different anti-oxidants all act to reduce oxidative damage *in vivo*, but their mechanisms of action are highly diverse. Based on their mode of biochemical action, anti-oxidants are divided into preventive and chain-breaking anti-oxidants.[27-29] The preventive anti-oxidants prevent the generation of radical chain reactions by scavenging ROS directly or binding transition metals

needed to produce ROS. The chain-breaking anti-oxidants interrupt the reproduction of radical chain reactions by forming a stable product.[30, 31] The pro-oxidant/anti-oxidant balance maintains physiological homeostasis and determines the degree of oxidant stress. Any disruption of the balance will lead to cell death or to the acceleration of ageing and age related diseases (Figure 1-1).[32]

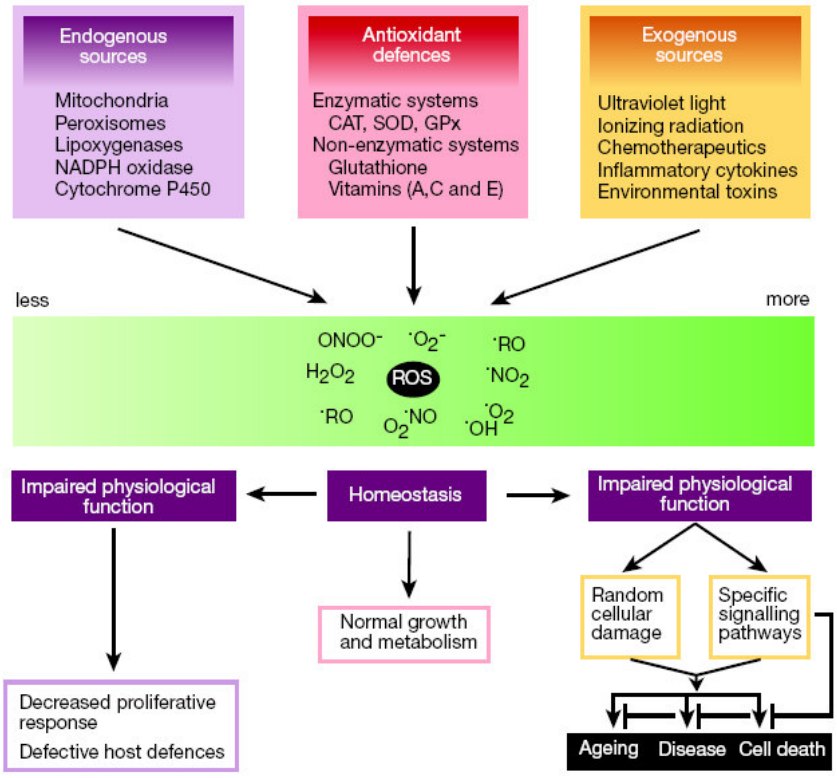

Figure 1-1. Oxidative stress and ROS caused interference to the balance in biological system.[32]

ROS and RNS react with various cellular components including proteins, DNA, lipids and carbohydrates. The reactions cause reversible or irreversible damage to these biological targets,

and thereby can lead to many cellular functional changes.[3, 33] The effects of oxidative stress depend on the levels of these damages. Severe oxidative stress can even cause cell apoptosis and necrosis. Oxidative stress induced modifications have been involved in many diseases, such as Alzheimer's disease, Parkinson's disease, heart failure, lung disease, atherosclerosis, chronic fatigue syndrom, and aging.[34, 35]

Direct determination of ROS/RNS concentration is difficult because they in general are too reactive and have too short lifetimes to be measured *in vivo*. However, the reactions of ROS/RNS with biomolecules typically generate specific products which are more stable than the reactive oxidants, i.e., aldehydes derived from oxidized lipids and carbonylated amino acids are more stable than the reactive species that cause these modifications. Thus the ROS/RNS measurement can be approximated by the determination of levels of their oxidation products.[36, 37] On this basis, some biological molecules (biomarkers) will become available for determining general oxidative stress and oxidant levels.

Protein oxidation

Proteins are major targets for oxidative stress. Oxidative damage to proteins is caused either directly by ROS or indirectly by the reaction of "secondary" products from oxidative stress, such as aldehydes from lipid peroxidation.[38-41] Oxidative damage to proteins can occur at protein side chains and the protein backbone. It leads to oxidation of the chains, protein cross-linking, and oxidation of the backbone resulting in protein fragmentation.[33, 42-44] Protein fragmentation caused

by backbone cleavage is rarely used as a marker of protein oxidation *in vivo* because of the function of proteases in protein hydrolysis. In contrast, the oxidation of amino acid side chains produces stable products that can be used as potential markers of oxidative damage, and disease progression.[37, 41, 44-46]

Protein oxidation caused by oxidative stress also can be divided into reversible and irreversible modifications (Figure 1-2).[47, 48] Reversible modifications usually occur at sulfide-containing amino acid residues, such as cysteine and methionine. Cysteine can be oxidized to a disulfide and methionine can be oxidized to methionine sulfoxide (MeSOX). Oxidized cysteine and methionine can be converted back to unmodified formation by disulfide and MeSOX reductase containing in biological systems.[33, 41, 42, 49, 50] Irreversible modifications can occur at the protein backbone or on various amino acid residues, leading to protein-protein cross-linking, protein fragmentation or the addition of oxidation sites on side chains, such as carbonyls. Irreversible modifications cannot be repaired and can lead to protein proteolytic degradation or aggregation, thus causing permanent loss of protein function.[42, 44, 51] Reversible modifications such as methionine oxidation can be used as a "built-in" ROS resistance system to prevent more damaging irreversible modifications that cannot be repaired.[52]

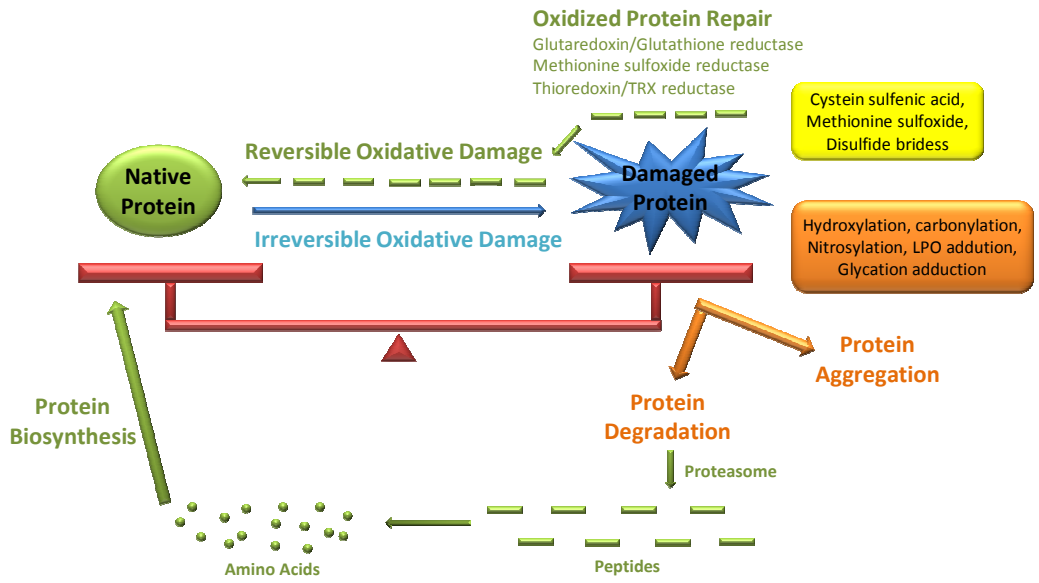

Figure 1-2. Intramolecular pathway of reversible and irreversible oxidized protein.[47]

Lipid peroxidation (LPO) and LPO-derived aldehydes

The peroxidation of lipids is commonly described as a ROS activated deterioration of unsaturated fatty acids, phospholipids, glycolipids, and cholesterol. The process can be an enzymatic or non-enzymatic reaction and involves the polyunsaturated fatty acids (PUFA).[53] Lipid peroxidation (LPO) generally goes through a free radical chain mechanism.[54] This chain reaction for lipids involves three steps: initiation, propagation and termination, as shown in Scheme 1-1.[53-55] In the initiation step, the lipid carbon-centered radical (L·) is formed by abstraction of a hydrogen atom from a bis allylic carbon in the PUFA, which is activated for attack by ROS. Next, the bis allylic carbon radical reacts with oxygen rapidly to form a lipid peroxyl radical (LOO·), which abstracts a bis allylic hydrogen atom from a neighboring PUFA to give a lipid hydroperoxide (LOOH) when an anti-oxidant does not mediate the process. At the

same time, a new carbon-centered radical is formed, and the propagation steps repeat. The propagation cycle can be terminated by reactions of the free radicals to form non-radical, stable products. Various free radical scavengers are able to cause chain termination.[55] Monounsaturated and saturated fatty acids are much less likely to participate in LPO because peroxyl radicals have difficulty abstracting a singly allylic hydrogen.

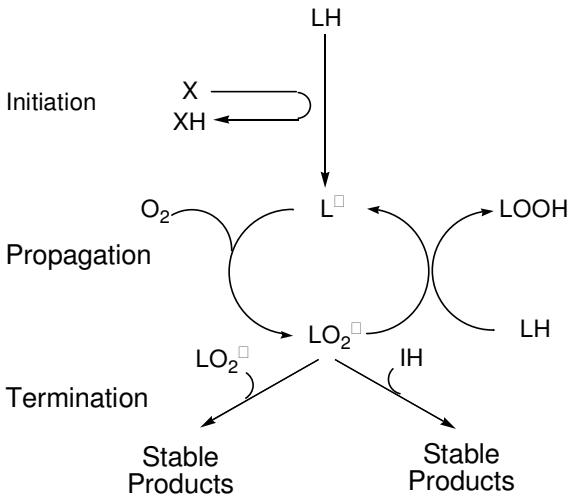

Scheme 1-1. General LPO process proceeding by a free radical chain mechanism.[55]

In the presence of transition metal ions, LOOH from the radical chain reaction can undergo decomposition and finally induces the generation of various secondary peroxidation products,[38, 56-58] such as malondialdehyde (MDA),[38, 56, 57] 4-oxo-2-nonenal (ONE),[38, 59] 4-hydroxy-2-nonenal (HNE),[38, 56, 57] 2-octenal,[60-62] 2-hydroxyalkanal[63] and so on (Scheme 1-2).[56] These bifunctional aldehydes are reactive, relatively stable, and diffusible. They can act locally or diffuse from the site of origin and cause oxidative damage remotely.

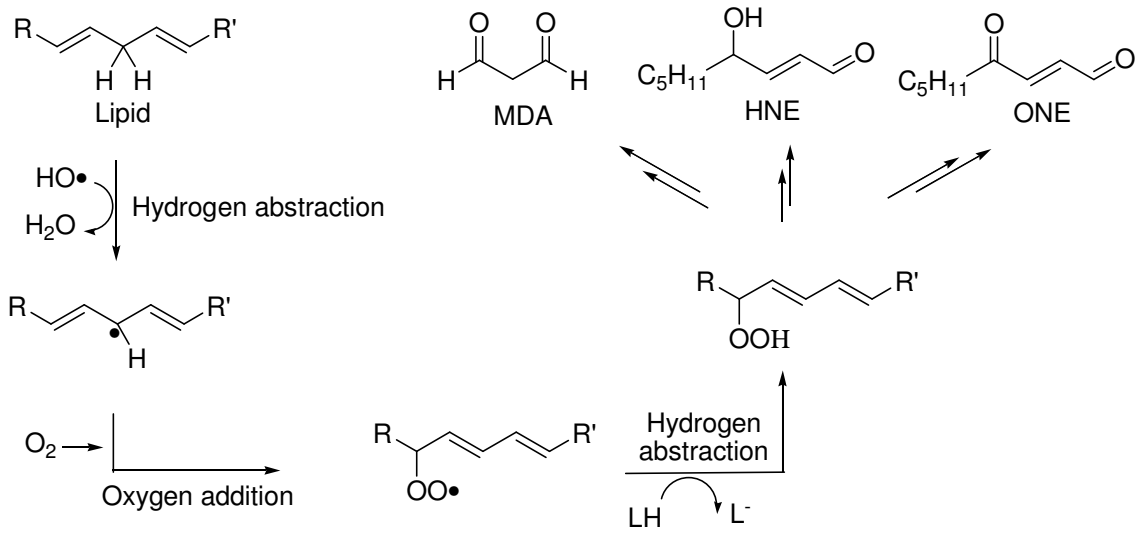

Scheme 1-2. Common aldehydes generated from LPO under oxidative stress.[56]

LPO has been considered as a major process in the production of oxidative damage from ROS.[40] Some hypotheses have been proposed to explain the connection between membrane LPO and cellular dysfunction that characterizes the process of aging and disease.[64] One of these hypotheses is that LPO changes the fluidity of membranes, which interrupts essential functions, such as signal transduction or the selectivity of membrane permeability (Figure 1-3).[40, 65-67] The other hypotheses involve the modifications of DNA and protein by LPO products. [43, 68-70]

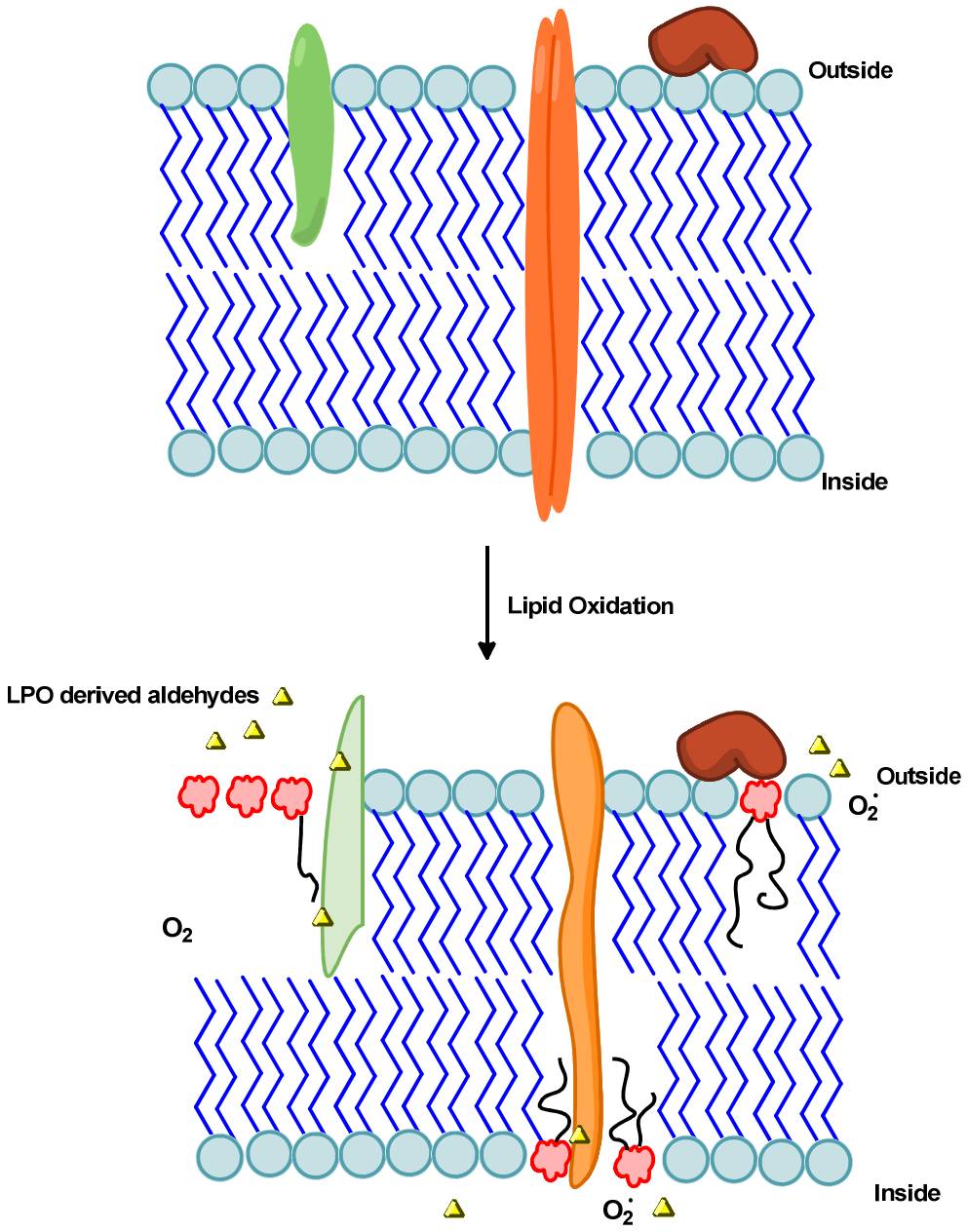

Figure 1-3. LPO induced modification to integral proteins in cell membrane under oxidative stress.[71]

Protein carbonylation and LPO-derived protein modification

Proteins can become modified by a large variety of reactive oxygen species under oxidative

stress, which can alter protein structure and function and finally cause cellular deterioration. Table 1-1 lists the common oxidations of amino acid residues of protein.[42] Among these modifications, protein carbonylation has attracted much attention due to its irreversible and unrepairable nature.[72] Many studies have shown that protein carbonylation plays a significant role in the development of various diseases and the aging of cells and tissues. Diseases involving increased protein carbonyl levels include neurodegenerative diseases, such as Parkinson's disease and Alzheimer's disease, cardiovascular diseases, such as atherosclerosis, chronic kidney, lung disease, cancer, cataractogenesis, diabetes, and aging process.[46, 72-74]

Amino acid residues	Oxidation products
Cysteine	disulfides, cysteic acid
Methionine	methionine sulfoxide, methionine sulfone
Tryptophan	*2-, 4-, 5-, 6-,* and *7*-hydroxytryptophan, nitrotryptophan, kynurenine, *3*-hydroxykynurinine, formylkynurinine
Phenylalanine	*2,3*-dihydroxyphenylalanine, *2-, 3-,* and *4*-hydroxyphenylalanine
Tyrosine	*3,4*-dihydroxyphenylalanine, tyrosine-tyrosine cross-linkages, cross-linked nitrotyrosine
Histidine	*2*-oxohistidine, asparagine, aspartic acid
Arginine	Glutamic semialdehyde
Lysine	α-aminoadipic semialdehyde
Proline	*2*-pyrrolidone, *4*- and *5*-hydroxyproline pyroglutamic acid, glutamic semialdehyde
Threonine	*2*-amino-*3*-ketobutyric acid
Glutamyl	oxalic acid, pyruvic acid

Table 1-1. Common oxidations of amino acid residues of protein.[42]

Protein carbonyl derivatives can be generated by four oxidative pathways:[42, 58, 72, 75] The first pathway is direct oxidation of arginine, lysine, proline and threonine side chains by metal catalyzed oxidation (MCO) involving hydroxyl radicals. This leads to glutamic semialdehyde from arginine and proline, 2-aminoadipic semialdehyde from lysine, and 2-amino-3-ketobutyric acid from threonine.[6, 42, 76] The second pathway is direct oxidation of the protein backbone, which can generate reactive protein carbonyl derivatives from cleavage of the protein backbone by either an α-amidation pathway leading to an α-ketoacyl derivatives, or a diamide pathway leading to an isocyanate (Scheme 1-3).[42] The third pathway is involves glycation and glycoxidation reactions of the primary amino group of lysine residues with reactive carbonyl derivatives (ketoamines, ketoaldehydes, deoxyosones) generated from carbohydrates or their secondary oxidation products (advanced glycation end products).[65] Finally, protein carbonylation also can be induced by adduction of reactive carbonyl derivatives generated during the peroxidation of PUFA. These LPO derived aldehydes include di-aldehydes such as MDA, which can react with lysine residues and form a Schiff-base product, α,β-unsaturated aldehydes such as acrolein (ACR) and HNE, which can react with amino acids that have nucleophilic side chains (i.e., cysteine, histidine and lysine), and keto-aldehydes such as ONE, which also react with nucleophilic amino acid side chains by Michael addition.[61, 77] The third and fourth pathways generate protein carbonyl derivatives from reactive carbonyl species (RCO). RCO are considered to be a major source of chemical modifications of proteins from oxidative stress. LPO-derived protein carbonyls play a key role in the development of Alzheimer's disease and diabetes.[78]

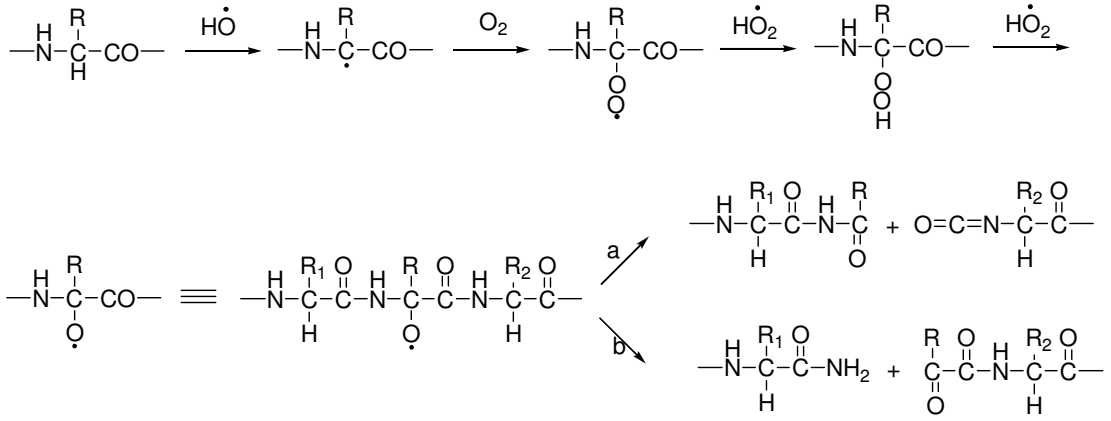

Scheme 1-3. General pathways of protein backbone cleavage under oxidative stress.[42]

Compared to ROS, LPO-derived RCO are more stable and diffusible. They can diffuse in or out of cells and attack targets far from the site of generation. LPO-derived protein carbonyls are more stable than ROS and more difficult to degrade by enzymes. Quantification of protein carbonyls can be used as a measure of the extent of oxidative damage. Various sensitive biochemical and immunological methods including Western blot, enzyme-linked immunosorbent assay (ELISA) and mass spectrometry have been developed for the identification and quantification of carbonylated proteins in cells, tissues and body fluids.[73, 79, 80] LPO-derived protein carbonylation is becoming one of the best characteristic biomarkers of several diseases and aging under oxidative stress and damage.

Protein carbonylation during disease development and aging is not random. Some proteins are more susceptive to be modified. However, the carbonylated proteins differ in different species.[75] The molecular cause for the evident selectivity of some proteins for carbonylation is not clear,

but some studies have suggested proteins binding with transition metals are more susceptible to undergo carbonylation by MCO,[43, 81] probably because protein-bound transition metals are sources of MCO which could modify nearby amino acid residues in proteins.[82] In addition, some proteins are more sensitive to be carbonylated, mainly because they are located close to the sites of producing ROS.

Protein carbonylation is irreversible and unrepairable. It has been argued that protein carbonylation can cause protein misfolding, resulting in cell dysfunction and hence disease.[75] Misfolded proteins not only lose their normal function, but also form toxic species, including oligomers or aggregates. Generally mild carbonylation reduces or eliminates protein function and increases the rate of protein proteolytic degradation by proteasome.[83] Heavily carbonylated and cross-linked proteins tend to aggregate in cells and eventually induce apoptosis.[84, 85]

Mass spectrometry based proteomics

In general, proteomics can directly determine the protein level of the large scale of gene and cellular function.[86-91] Various approaches have been developed in this area, including biochemical methods, immunological methods, mass spectrometric methods and any combination of these methods.[92-94] Compared to other available methods, mass spectrometry has been one of the most successful methods to analyze protein primary sequence, post-translational modifications (PTMs) and protein-protein interactions, especially for the analysis of low abundance and complex protein samples. Mass spectrometry provides more details about the

kinetics and mechanism of PTMs, as well as the stoichiometry and sites of modification.[95-100] In addition, mass spectrometry can be combined with various separation technologies, such as high performance liquid chromatography (HPLC) and capillary electrophoresis (CE), to provide necessary purification and improved sensitivity.[101-103]

Most recently, mass spectrometry based analysis approaches have been successfully applied to identify and quantify protein modification in both *in vitro* and *in vivo* experiments.[104, 105] Finally, data analysis software and bioinformatics tools have been developed to rapidly process the large number of peptide MS/MS spectra for characterization of the peptide fragmentations which are used to identify specific sites of modifications.[106-109]

The long-term goal of the project

Although protein carbonylation has been identified as an important factor in disease and aging processes, there is limited information available about the specific sites of carbonylation in the effected proteins. This knowledge gap hampers our ability to understand the mechanisms underlying the molecular changes that occur with oxidative stress. The key question is whether site selectivity can offer information about the nature of the disease state or the origin of the oxidative stress that caused the protein modification. This question only can be answered by gathering more data and establishing whether or not correlations exist between carbonylation patterns and disease states or environmental conditions.

Our central hypothesis is that protein carbonylation does not occur randomly on reactive residues in a protein, but is localized at sites with vulnerable structural motifs and more inportantly, dependent on the nature of the oxidant. The research aims are to identify the sites of protein carbonylation both *in vitro* and *in vivo* by mass spectrometry. The data will test our hypothesis and provide critical information about the structural impacts of protein carbonylation and give insights into the functional ramifications of carbonylation. In the future, the modifications identified in this study could serve as biomarkers for disease states and aging processes. Finally, new analysis approaches aimed at improving the sensitivity and efficiency of identifying carbonylation sites will be developed.

Chapter 2: Identification of Acrolein Modified Human Serum Albumin

Background

Acrolein (2-propenal, ACR) was first isolated from the distillation of glycerin in the presence of a dehydration agent by Redtenbacher in 1893.[110, 111] Acrolein is a highly toxic, irritating and reactive molecule having two reactive centers consisting of a carbon-carbon double bond and an aldehyde group (Figure 2-1). In industry, acrolein has been an important intermediate in producing acrylic acid and plastic.[111] Human exposure to acrolein can be grouped into exogenous and endogenous. Acrolein is mainly introduced to the environment from incomplete combustion of materials (such as petroleum, wood, coal and plastic material), automobile exhaust, tobacco smoke and cooking emission (from fried vegetable oil and animal fat).[77, 111 112]The main endogenous sources of acrolein are LPO of PUFAs, cleavage of dehydrated carbohydrates, enzyme-mediated degradation of amino acids (such as methionine and threonine) and polyamines (such as spermine and spermidine), metabolism of some allyl compounds, and the widely used anticancer drug cyclophosphamide.[77, 111, 113]

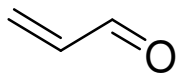

Figure 2-1. The structure of acrolein

Acrolein is one of the most electrophilic simple α, β-unsaturated aldehyde.[114] It is capable of modifying nucleophilic side chains of cysteines, histidines, lysines and arginines in proteins by Michael addition (Scheme 2-1).[111] A protein-ACR adduct can also be formed through a Schiff

base between the ε-amino group of the lysine residue and the aldehdye group of acrolein.[115] The bi-functionality of acrolein gives the possibilities of intra- and intermolecular crosslinks through both Michael addition and Schiff base formation.[116] Furthermore, a bis-adduct, N^{ε}-(3-formyl-3,4-dehydropiperidino)lysine (FDP-lysine) can be formed on reaction with lysine residues by two, sequential Michael additions, followed by an aldol condensation and dehydration.[115] Recently, a novel adduct, N^{ε}-(3-methylpyridinium)lysine (MP-Lys) has been detected immunochemically using the oxidized B chain of insulin as a model peptide.[58, 117] Similar to adduction of the guanidine group of arginine, acrolein can react with deoxyguanosine (dG) in DNA.[118, 119] It has been established that the relative reactivity of amino acid residues towards electrophilic aldehydes is Cys>>His>Lys. Histidine and lysine are considered as relatively weak nucleophiles and unlikely to be an immediate target for the soft acrolein electrophile.[120]

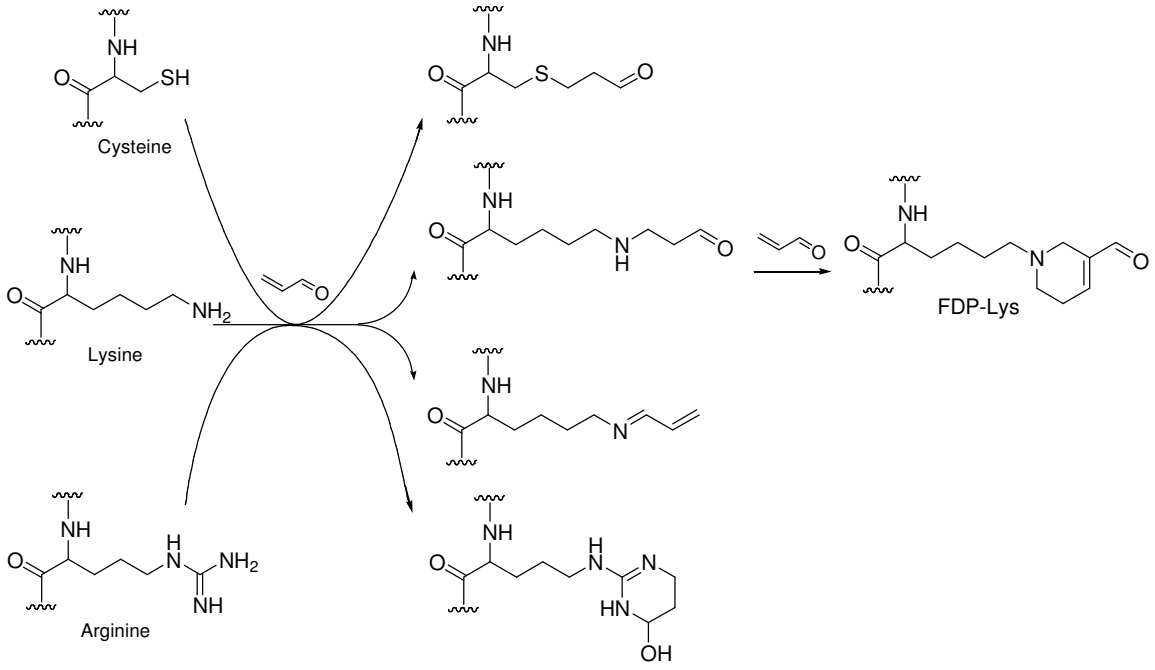

Scheme 2-1. Adduction of acrolein to amino acid residues in proteins.[111]

Exposure to acrolein is highly toxic. The respiratory system is the most common target organ. Exposure can cause pulmonary edema, respiratory irritation and distress.[112] Most of the cytotoxic effects of acrolein are involved in its high reactivity towards proteins. Irreversible acrolein adduction disrupts protein function and induces inhibition of protease activity and cell growth, disruption of metabolism and cell signaling, and modulation of cell apoptosis and necrosis.[121-123] Considering the relative reactivity of residues towards this electrophile, the toxic effects of histidine and lysine modifications are more likely under high dose intoxication or during the late stage of the chronic diseases when modifications on cysteine become saturated.[120]

Acrolein can pass through membranes by passive diffusion. The major pathway for metabolism of acrolein is conjugation with glutathione (GSH) in the liver, followed by cleavage of the

glycine and γ-glutamic acid residues in the presence of enzymes.[111] After enzyme induced N-acetylation and reduction, *S*-(3-hydroxy-propyl)-*N*-acetylcysteine (HPMA) is generated as the main metabolite of acrolein, and is found in urine.[124, 125]

Human serum albumin (HSA) was chosen as a model protein in this project. HSA is a 66 kDa carrier protein that is important in physiological transport of many compounds, including free fatty acids, steroids, metals and metabolites.[126-128] HSA is an attractive choice for biomarker studies because it is present in high concentration in serum, is known to form complexes and adducts with a variety of species, including acrolein and 4-hydroxy-2-nonenal (HNE), is a known target of oxidative stress, and is readily available.[77, 129, 130]

Experimental Procedures

Chemicals

Essentially fatty acid and globulin free HSA (Product A3782), (+) Biotin-hydrazide, iodoacetamide (IAM), N-ethylmaleimide (NEM), 1,4-dithio-DL-threitol (DTT), trifluoroacetic acid (TFA), sodium cyanoborohydride ($NaBH_3CN$) and 10×phosphate buffered saline (PBS) concentrate were purchased from Sigma-Aldrich (St. Louis, MO). Ammonium bicarbonate was obtained from J.T. Baker (Phillipsburg, NJ) and acrolein was obtained from Cayman Chemical (Ann Arbor, MI). Sequencing grade modified trypsin was from Promega (Madison, WI).

Experiments

HSA modification

HSA at 15 μM in 1× PBS buffer (pH 7.4) was incubated with acrolein at various final ACR:HSA molar ratios (1:4, 1:2, 1:1, 2:1, 5:1, 10:1). All reactions were carried out at 25°C with gentle shaking. The reaction time was 100 min for all experiments.

1. Method A: acrolein adducts were labeled by incubation with Biotin-hydrazide at room temperature for 2 h. Labeled modifications were stabilized by adding $NaBH_3CN$ to 15 mM and incubating for 60 min at 0°C. Reaction mixture was repeated washes employing centrifugal filter devices (VWR, West Chestrt, PA) to remove reagents and to exchange to 50 mM ammonium bicarbonate buffer (pH 8.0) for enzymatic digestion; the molecular weight cut-off for the centrifugal filter devices used was 30 kDa.

2. Method B/C: acrolein adducts were directly stabilized by adding $NaBH_4$ to 5 mM and incubating for 60 min at room temperature. Same centrifugal filter devices were employed to remove reagents and to exchange to 50 mM ammonium bicarbonate buffer (pH 8.0) for enzymatic digestion.

Enzymatic digestion

1. Method A: Modified HSA samples in 50 mM ammonium bicarbonate buffer were first reduced by incubating with 30 mM DTT for 20 min at 50°C and then alkylated by incubating with 55 mM IAM for 30 min at room temperature in the dark. Excess DTT and IAM were removed using the centrifugal filter devices (three washes were performed using 50 mM ammonium bicarbonate buffer). Sequencing grade trypsin (substrate to enzyme weight ratio 40:1) was added and the mixture incubated for 16 h at 37°C. Digestion was terminated by adding 1% formic acid (final pH = 2~3).

2. Method B: Same procedure was performed, but no reagent was added to alkylate.

3. Method C: Same procedure was performed, but NEM was used to alkylate instead of IAM.

μLC-MS/MS analysis

Adduct identification was performed using a Thermo (San Jose, CA) LTQ XL linear ion trap mass spectrometer, equipped with electron-transfer dissociation (ETD). The LTQ XL was interfaced with a Thermo Surveyor capillary HPLC system. Peptides were separated on a

reversed-phase, C18 column (150 μm × 10 cm, 5 μm particles, 300 Å pores; Column Technology, Fremont, CA) at a flow rate of about 1 μl min−1 using 0.1% formic acid in water as mobile phase A and 0.1% formic acid in methanol as mobile phase B. Approximately 2 μg peptides were injected and a Michrom (Auburn, CA) CapTrap trapping column was used for rapid sample injection. The gradient started from 2% B, then increased to 15% B over 5 min, then increased to 80% B over 70 min, and finally increased to 95% B over 15 min. The eluted peptides were introduced into the LTQ XL with a nanospray source operating at a spray voltage of 2.1 kV, a capillary voltage of 21 V, and a capillary temperature of 200°C. A full scan in the m/z range 300-2000 was performed to obtain precursor ions, followed by four data-dependent tandem mass spectrometry (MS/MS) scans (collision-induced dissociation, CID) for the three most abundant precursor ions in the full scan. Dynamic exclusion was used, that is, if the same precursor ion was picked for fragmentation twice within a 30 s window, it was excluded from further analysis for 180 s.

Database searching and data processing

Peptide sequences and modifications were identified using the BioWorks version 3.3.1, SP1 implementation of Sequest (Thermo). No scan grouping was performed in preparing peak lists for database searching. The protein sequence database used consisted of the NCBI RefSeq version of the complete human proteome and the UniProt sequence for porcine trypsin (Accession Number P00761); reversed versions of all sequences were also included to permit false discovery rate estimation. Sequences were downloaded on November 20, 2010, and the

final database contained 68040 entries. Only fully-tryptic peptides were considered and up to three missed cleavage sites were allowed. Precursor ion tolerances were ±2 Da for linear ion trap measurements. According to method A, Fixed mass shifts were applied for IAM alkylated cysteines (+57 Da) while differential amino acid mass shifts were incorporated for $NaBH_3CN$-reduced Biotin labeled Michael adducts at histidine and lysine (+298 Da) and at cysteine (+241 Da when the fixed mass shift at cysteine is considered), reduced Schiff base adducts at lysine (+40 Da), and oxidized methionines (+16 Da). According to method B, differential amino acid mass shifts were incorporated for $NaBH_4$-reduced Michael adducts at cysteine, histidine and lysine (+58 Da), reduced Schiff base adducts at lysine (+40 Da), and oxidized methionines (+16 Da). According to method C, Fixed mass shifts were applied for NEM alkylated cysteines (+125 Da) while differential amino acid mass shifts were incorporated for $NaBH_4$-reduced Michael adducts at histidine and lysine (+58 Da) and at cysteine (-67 Da when the fixed mass shift at cysteine is considered), reduced Schiff base adducts at lysine (+40 Da), and oxidized methionines (+16 Da). In addition, MS/MS spectra for modified peptides were manually examined and any found to be inconsistent with the proposed identification were rejected.

Results

The major mode of action of acrolein with proteins is Michael addition to the nucleophilic amino acid side chains of cysteine, histidine, lysine, and arginine to give stable adducts.[111] Acrolein can also form a Schiff base with lysine and propano adducts with the guanidine group of arginine.[131] Furthermore, a bis-adduct, FDP-lysine, can be formed on reaction with lysine residues by two Michael additions, followed by an aldol condensation and dehydration.[115] All of the Michael additions lead to products bearing an aldehyde functional group whereas the Schiff base contains an imine instead. Modifications on arginine and FDP-lysine have been reported by immunochemistry.[115] HSA is a 66 kDa protein with 35 cysteines, 16 histidines, and 59 lysines in its secreted form. There are 17 disulfide bridges, which leaves a single free cysteine in the protein.[126] If the nucleophilic residue does not have reasonable surface accessibility or is located in an environment that is too sterically crowded to accept the added acrolein, some modifications would be highly unlikely.

Sample preparations

In this project, the mass shift of stabilized acrolein adducts by Michael addition is 58 and the mass shift of cysteine carboxyamidomethylation by IAM is 57. This 1 unit mass difference in the two shifts is not easily discriminated by the LTQ and can lead to incorrect modification assignments by the Sequest search. Therefore, three different sample preparation methods were applied. In method A, (+) biotin-hydrazide was used to label adducts of Michael addition

(Scheme 2-2).[132] After stabilization by $NaBH_3CN$, the mass shift became 298. In method B, no labeling reagent was used after the initial modification, and no carboxyamidomethylation step was applied before the trypsin digestion. In method C, no labeling reagent was used after initial incubation. NEM was applied as the alkylating agent instead of IAM after treatment by DTT. The mass shift of NEM alkylation at cysteines is 125.

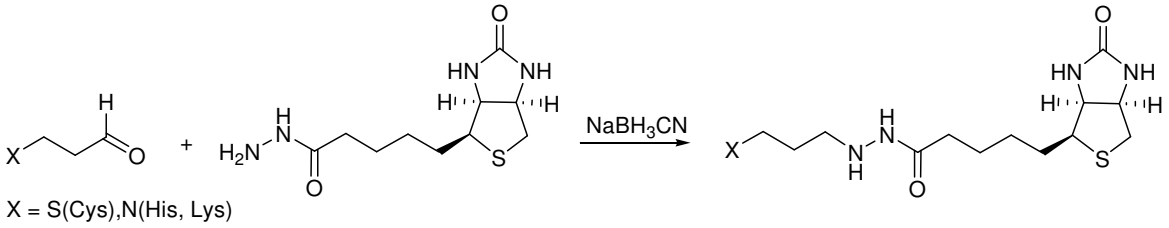

Scheme 2-2. Acrolein adducts labeled by (+) biotin-hydrazide.

Modification Sites

Our goal was to identify the key modification sites when HSA is treated with acrolein. Starting with an HSA concentration of 15 μM, ACR:HSA ratios from 1:4 to 10:1 were surveyed and data are reported for the 1:1 and 10:1 ratios (Table 2-1). All site identifications are supported by CID data.

Naturally, as the amount of acrolein was increased, it was possible to identify more modification sites. At a 1:1 ratio, a total of seven modification sites were identified in the three different sample preparations, but there were variations in the modification sites in the different preparations. In method A, five lysine residues (K^{51}, K^{162}, K^{262}, K^{351} and K^{545}) were identified as

Michael additions (the residue numbers are for the secreted protein; to convert to nascent protein numbering, add 24). In method B, one modified cysteine and histidine residue were found (C^{34} and H^{338}) as well as three lysine residues (K^{233}, K^{525} and K^{545}). In method C, one cysteine residue was found (C^{34}) as well as three lysine and histidine residues (K^{233}, K^{378}, K^{545}, H^{146}, H^{288} and H^{388}). At a 10:1 ratio, thirteen lysines and six histidines were modified in method A; one cysteine, fifteen lysines and three histidines were found modified in method B; one cysteine, eight lysines and three histidines were found in method C. The majority of the variability is due to the fact that we are operating at near detection thresholds. The different labeling procedures (A, B and C) introduce differences in the ionizability of the peptides and the quality of their CID spectra. Each of these can shift the detection threshold and affect the probability for detection. This effect is confirmed by the fact that modifications detected in a single preparation method at the 1:1 ratio are detected in multiple preparations at the 10:1 ratio in all but one case.

Table 2-1. Modification site identifications from different sample preparations. Manual MS/MS spectrum validation was required in all cases.

Modification Site[a]	Type[b]	1:1[c]	10:1[c]
Cys^{34}	**MA**	**B/C[d]**	**B/C**
His^{67}	**MA**	**not detected**	**A**
His^{146}	**MA**	**C**	**A/B/C**
His^{242}	**MA**	**not detected**	**A**
His^{247}	**MA**	**not detected**	**A**
His^{288}	**MA**	**C**	**A/B/C**
His^{338}	**MA**	**B/C**	**A/B/C**
Lys^{12}	**MA**	**not detected**	**B**
Lys^{51}	**MA**	**A**	**A**
Lys^{73}	**MA**	**not detected**	**B**

Lys^{137}	**MA**	**not detected**	**B/C**
Lys^{159}	**MA**	**not detected**	**B**
Lys^{162}	**MA**	**A**	**A/B**
Lys^{174}	**MA**	**not detected**	**A/B**
Lys^{205}	**MA**	**not detected**	**C**
Lys^{225}	**MA**	**not detected**	**B**
Lys^{233}	**MA**	**B/C**	**A/B/C**
Lys^{262}	**MA**	**A**	**A/B/C**
Lys^{351}	**MA**	**A**	**A/B**
Lys^{378}	**MA**	**C**	**A/B/C**
Lys^{414}	**MA**	**not detected**	**A/B/C**
Lys^{519}	**MA**	**not detected**	**A**
Lys^{525}	**MA**	**B**	**A/B/C**
Lys^{525}	**SB**	**not detected**	**B**
Lys^{545}	**MA**	**A/B/C**	**A/B/C**
Lys^{545}	**SB**	**not detected**	**B/C**
Lys^{545}	**FDP-Lys**	**not detected**	**B/C**
Lys^{574}	**MA**	**not detected**	**A/B**

[a] Secreted protein numbering; add 24 for nascent protein.

[b] MA indicates Michael adduct formation; SB indicates Schiff base formation; FDP-Lys indicates FDP-Lys product generation.

[c] Applied ACR:HSA ratio.

[d] Sample preparation method: A represented biotin labeling method; B represented method with no carboxyamidomethylation; C represented NEM alkylating method.

Finally, the sequence coverage from the tryptic digestion is around 80%. Five histidines and sixteen lysines are not in the covered sequence. It is possible that modifications at these residues occurred, but were not detected with our LC-MS conditions. Very short or long peptides are the most challenging to detect with the LTQ.

Discussion

Sample preparation methods

In this project, three different sample preparation methods were applied, but the identified modification sites from them were not entirely same. At a 1:1 molar ratio of ACR:HSA, no cysteine and histidine modifications were detected with method A, and only one modified lysine (K^{545}) was detected in all the methods. At a 1:1 ratio, methods B and C shared the most modification sites (C^{34}, H^{338}, K^{233} and K^{545}). At a 10:1 ratio, six modified histidines along with twelve modified lysines were identified with method A, but the cysteine modification still was not observed. There again is more consistency between methods B and C at the 10:1 molar ratio. Thirteen modifications are in common between these methods. Overall more sites are detected by multiple methods at the higher molar ratio, which probably is because the modification levels were more generally above the detection threshold. The identifications from repeats of the same sample preparation method are relatively reproducible, which implies that different sample preparations do impact the ability of a modification to be identified. The total number of modifications identified with method A was 18, with method B was 22, and with method C was 14. The greatest sensitivity was with the method with no cysteine blocking, method B.

Modification Sites

It has been accepted that Cys^{34} is the most reactive site in HSA because Cys^{34} is the only free cysteine and sulfur is known to be highly nucleophilic in Michael additions.[77, 129, 133] In this

project, there is evidence for acrolein addition at Cys^{34} in HSA at both concentrations. For sample preparation method A, no adduct of Cys^{34} was identified even when the concentration of acrolein was increased. It may due to limited detectability caused by the poor ionizability of the corresponding peptide after biotin labeling or due to the poor quality of its CID spectrum.

Only six modified histidines were identified and three of them were detected in all the sample preparation methods at a 10:1 molar ratio. Generally, the detection of modifications on histidines from the repeats on the same sample preparation were very reproducible even at a low acrolein concentration, which may imply that histidine modification occurs readily and gives peptides with robust detection characteristics. Using detection at the 1:1 molar ratio as a criterion, His^{146}, His^{288}, and His^{338} are viewed as the most reactive histidines towards acrolein.

Comparing the lysine and histidine modifications, more modification sites at lysines were identified. However, some lysine modifications had low reproducibility, especially at a lower concentration of acrolein. This suggests that lysine modifications are less favorable and are present at lower concentrations. Of all the identified lysine modifications, Lys^{545} was the only one found at a low concentration of acrolein in all three sample preparations. Schiff base formation adducts and FDP-lysine products at Lys^{545} were also detected when the concentration was increased. Therefore, Lys^{545} is likely one of the most reactive lysines towards acrolein. Other lysines active at the 1:1 molar ratio are Lys^{162}, Lys^{233}, Lys^{262}, Lys^{351}, Lys^{378}, and Lys^{525}.

It has been reported that acrolein also could form a propano adduct with the guanidine group of arginine.[115] However, no arginine adducts with acrolein were found in this project.

Correlation between Local Environment and Modification

The effect of local protein environments on acrolein modifications can be evaluated by examining the crystal structure of HSA.[134] At a low concentration of acrolein, it was observed that some modification sites were on the surface of HSA, such as Lys^{51}, Lys^{162}, Lys^{233}, Lys^{262}, Lys^{351} and Lys^{378} (Figure 2-2); some were near the surface or seams on the surface, but the side chains were recessed in grooves of the protein, such as Cys^{34}, His^{146}, His^{288}, His^{338}, Lys^{525} and Lys^{545}, (Figure 2-3). Meanwhile, some residues are on the very surface of HSA, such as His^{128}, gave no evidence of modification even at higher concentrations. This phenomenon also can be quantified using a simple calculation of the solvent accessible surface area (SASA) associated with the residues.[135, 136] It provides some insight into the local environments of the modified residues. The plots of side chain and backbone SASAs for the histidines and lysines in HSA were generated using the GETAREA program (Figure 2-4).[137] Although this small data set is not sufficient for confirming an absolute pattern, general tendencies can be suggested. Checking the SASA plots of histidines and lysines, the general properties of the more reactive sites, such as His^{338} and Lys^{545} seem to be moderate accessibility on the side chain and relatively low accessibility on the backbone. This phenomenon is more obvious in the histidine modifications. Moreover, some highly exposed sites were not generally reactive. His^{128} is a good negative control for this measurement. It has a relatively high SASA value for its side chain (95.2 $Å^2$) and

backbone (25.6 $Å^2$), but no modification of this site was detected even at higher concentrations of acrolein. Overall, the data suggest that factors aside from surface accessibility are important in determining the modification site, but that these preferences lead to limited selectivity.

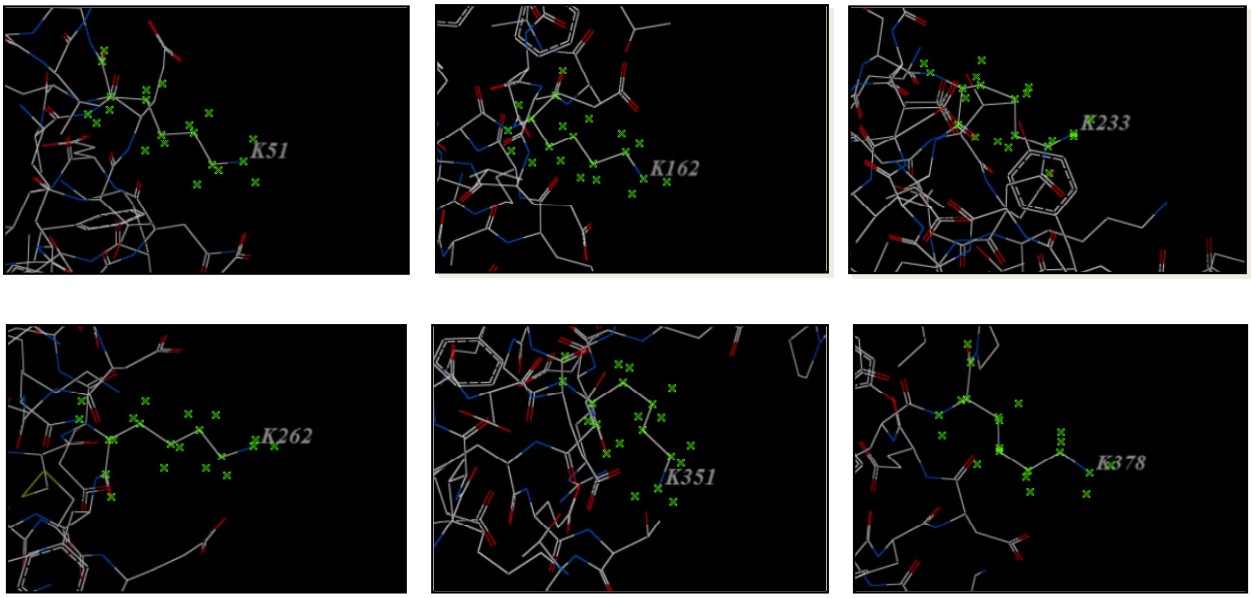

Figure 2-2. Crystal structures showing modified sites (K^{51}, K^{162}, K^{233}, K^{262}, K^{351} and K^{378}) on the very surface of protein.

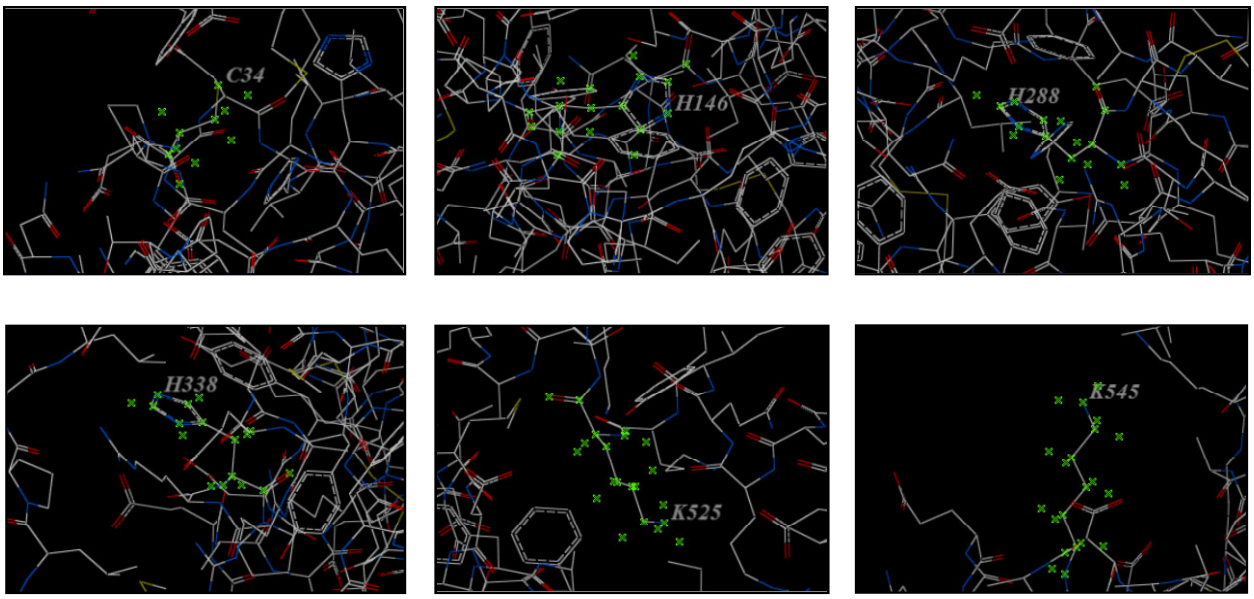

Figure 2-3. Crystal structures showing modified sites (C^{34}, H^{146}, H^{288}, H^{338}, K^{525} and K^{545}) recessed in the pocket of protein.

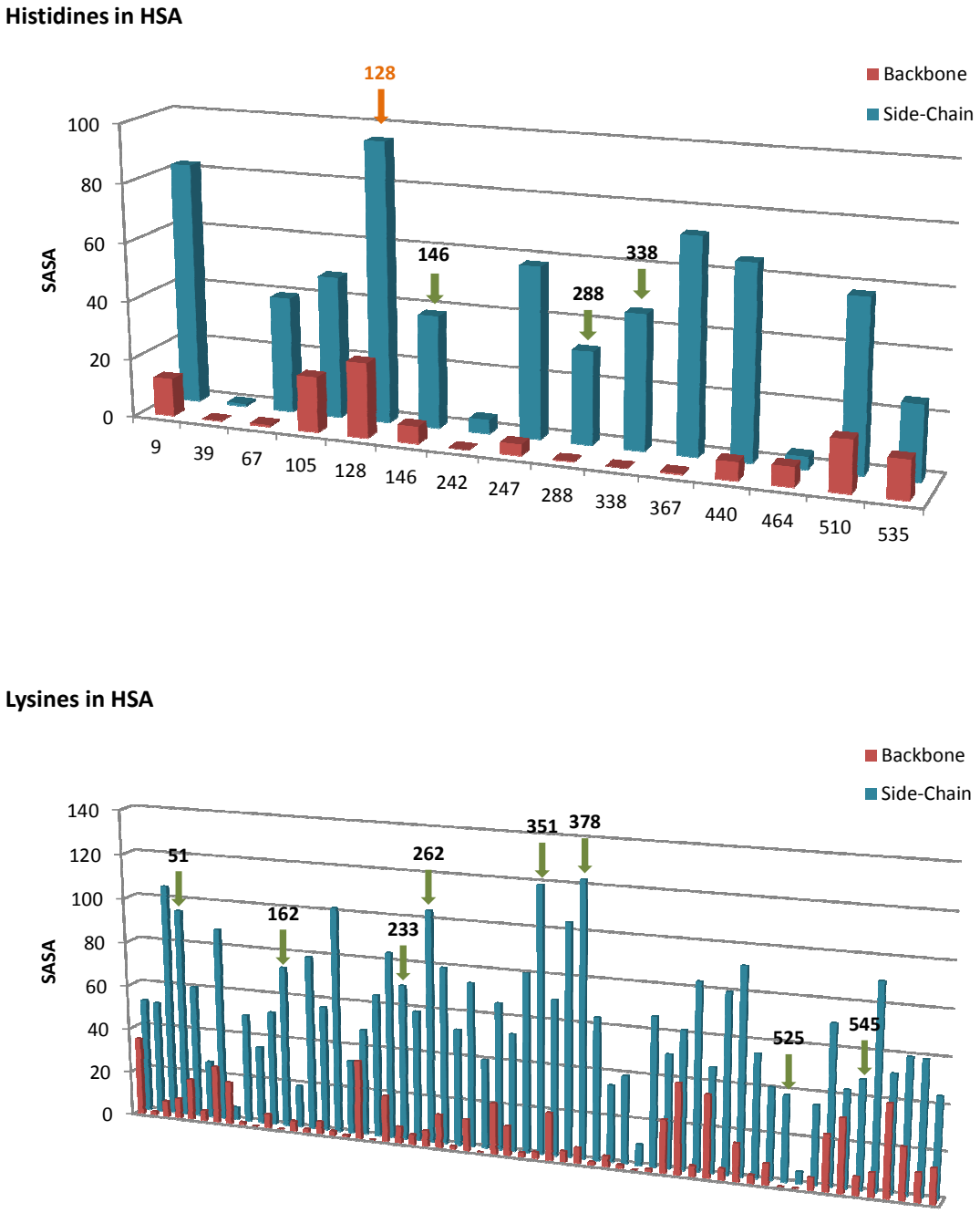

Figure 2-4. SASA in $Å^2$ for histidines and lysines of HSA. Red bars are the backbones and blue bars are the side chains. Green arrows indicate sites that were identified as modified at a 1:1 molar ratio of ACR:HSA. Orange arrow indicates a negative control.

Future Direction

This project has identified histidines and lysines in HSA that are most reactive towards acrolein. The data suggest that surface accessibility is an important component in determining reactivity, but other factors are also affecting the reactivity. To explore this system is greater detail, a more quantitative approach, such as that used in the next chapter is needed. Nonetheless, the present results provide a baseline for comparison to the system explored in the next chapter, HNE reacting with HAS.

Conclusions

The addition of a prototypical α, β-unsaturated aldehyde, acrolein, to HSA exhibits modest selectivity in this study. Modification sites were identified at the ACR:HSA molar ratios of 1:1 and 10:1 using a linear ion trap mass spectrometer.

Identified modifications were not entirely the same from three sample preparation methods, which suggests that different sample preparations impact the detectability of modified peptides by mass spectrometry. By examining the modification sites in the crystal structure of HSA, it appears that surface accessibility is important, particularly with lysine modifications. However this is not the only factor and many lysines with high surface accessibility were not modified. There is more limited data with histidine, but it appears that surface accessibility is less important. Finally, developing a quantification approach is necessary for analyzing reaction kinetics and accurately identifying the relative reactivity of the residues.

Chapter 3: The Reactivity of Human Serum Albumin Towards *trans*-4-Hydroxy-2-nonenal

Background

Since HNE (Figure 3-1) was recognized as a major product formed during CCl_4-induced lipid peroxidation in the rat liver microsome,[138] it has been identified as the most cytotoxic aldehyde. This initiated a large number of investigations about generation, quantitation and biological activity.

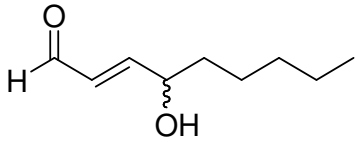

Figure 3-1. The lipid peroxidation product (E)-HNE.

HNE is the end-product of peroxidation of ω-6 polyunsaturated fatty acids, particularly arachidonic acid and linoleic acid, the most common ones in biomembranes.[139, 140] These peroxidation mechanisms have not been fully understood, although numerous pathways have been proposed, which include enzymatic and non-enzymatic pathways.[140, 141] Two distinct non-enzymatic pathways were proposed by Schneider, C. et al. in 2001, based on an oxidation study of 9*S* and 13*S*-hydroperoxy-octadecadienoic acid (HPODE). However, the pathway though 13S-HPODE has recently been disproved by the same group. The 9S-HPODE mediated pathway starts from a free radical intermediate formed at the bis-allyl position of linoleic acid, which is captured by molecular oxygen to generate 9-HPODE. The cleavage of 9-HPODE through a Hock rearrangement provides 3*Z*-nonenal - further oxidation and reduction gives HNE (Scheme 3-1). An example of an enzymatic pathway has been given for the fatty acid peroxidation in plants.[141,

[142] Linoleic acid is first oxidized by plant lipoxygenase (LOX), then cleaved by hydroperoxide lyase (HPL) to give 3Z-nonenal, which can be easily converted to 4-HNE through an non-enzymatic pathway (Scheme 3-2).[141] Recently, a peroxyl radical initiated dimerization or polymerization pathway has attracted attention. In essence, the peroxide bridges in the dimer or oligomer are prone to breakage to release aldhedyes, including the 4-HNE precursor, 4-hydroperoxy-2*E*-nonenal (4-HPNE).[141] Other hypotheses have also been reported, but further validations are required.

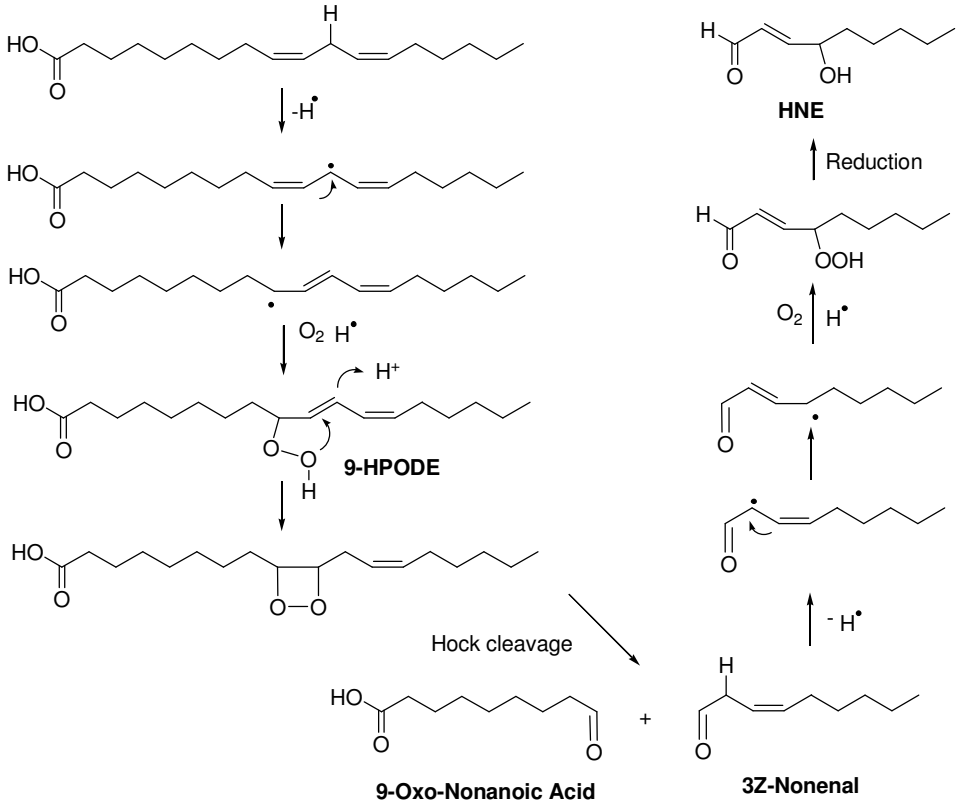

Scheme 3-1. Proposed 9S-HPODE mediated mechanism of HNE formation from ω-6 polyunsaturated fatty acids.[140]

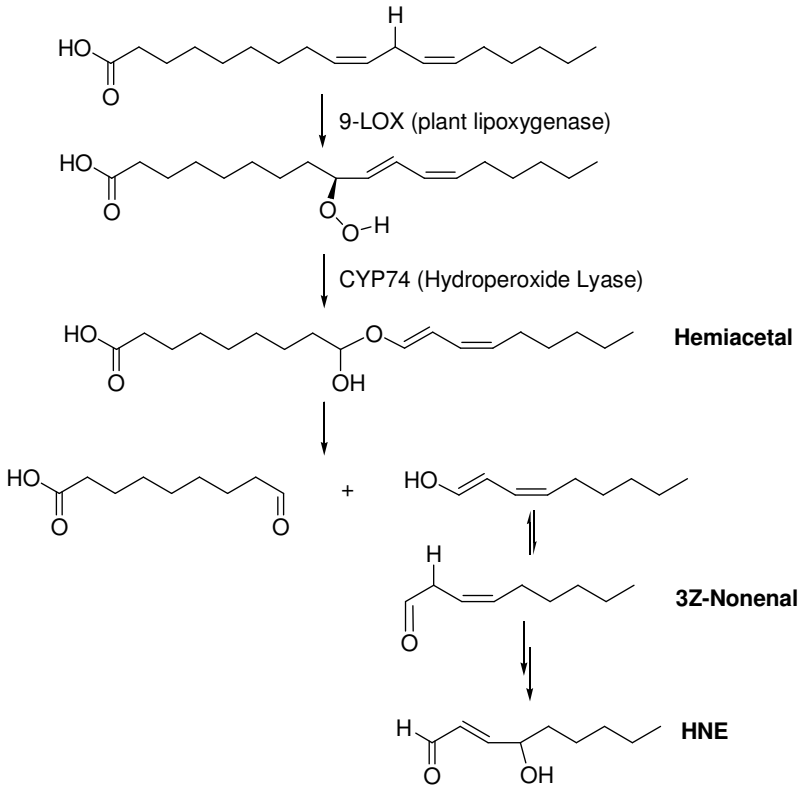

Scheme 3-2. Proposed enzymatic pathway of HNE formation from Linoleic acid.[141]

Studies have shown that basal levels of HNE (< 1 μM) are present in cells.[143, 144]. HNE could behave as a signaling molecule at these basal levels. However, HNE concentration could become higher (< 15 μM) under oxidative stress, causing unwanted modification of biological molecules and inducing a disease process. Some HNE concentrations may even reach the range of 100 μM in regions near or in oxidizing membranes because they are strongly lipophilic, which could yield acute and unspecific cytotoxic effects and finally lead to cell death (Figure 3-2).[77, 145, 146]

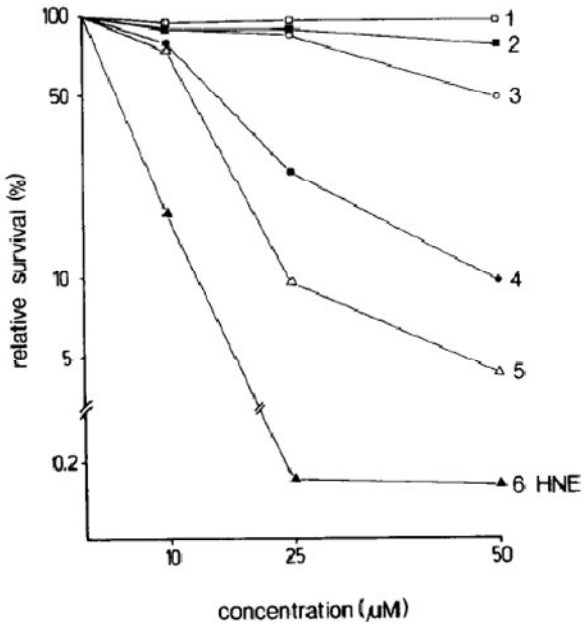

Figure 3-2. Toxicity of various aldehydes on growth arrested human fibroblasts.[77] 1: pentanal/hexanal; 2: 2-octenal; 3: 2-nonenal; 4: 2,4-nonadienal; 5: 2,4-decadienal; 6: 4-hydroxynonenal

Physiologically relevant concentrations of HNE could be detoxified by various enzymes in different cells and organs. These pathways include oxidation of HNE to 4-hydroxynon-2-enoic acid (HNA) by aldehyde dehydrogenase,[147] reduction of HNE to 1,4-dihydroxy-2-nonene (DHN) by aldehyde reductase,[148, 149] glutathione-S-transferase (GST) mediated addition of HNE with GSH to give a GS-HNE conjugate,[150] or reduction of HNE to 4-hydroxynonanal (HAA) by alkenal oxidoreductase.[146, 151]

Biological effects of HNE involve the capacity of HNE to act as an α,β-unsaturated aldehyde and react with a wide range of cellular nucleophiles, including DNA bases and proteins.[54, 77, 146] The protein-HNE adducts are mainly formed by Michael addition of the sulfhydryl of cysteine, the imidazole moiety of histidine, or the ε-amino group of lysine residues. The Michael adducts can

undergo cyclization to form a hemiacetal structure (Scheme 3-3A).[152] A protein-HNE adduct can also be formed through a Schiff base between the ε-amino group of a lysine residue and the aldehdye group of HNE, which can be followed by dehydration and cyclization to give a 2-pentylpyrrole moiety. Furthermore, the bi-functionality of HNE gives the possibility of intra and intermolecular crosslinks through both Michael addition and Schiff base formation (Scheme 3-3B).[152] Modifications by HNE are known to have wide-ranging biological effects including the attenuation of enzyme activity, apoptosis, and neurotoxicity.[143, 153] The presence of HNE modifications correlates with many disease states including Alzheimer's disease, diabetes, and atherosclerosis.[154, 155] In addition, an increase in HNE protein modifications has been observed with aging.[156] Finally, HNE has been implicated in signaling pathways, but details of its impact in this role are just emerging.[157] Overall, HNE has been viewed as a prime, potential biomarker for diseases or processes that induce oxidative stress, and several mass spectrometric studies of HNE protein modifications have been investigated.[152, 158-163]

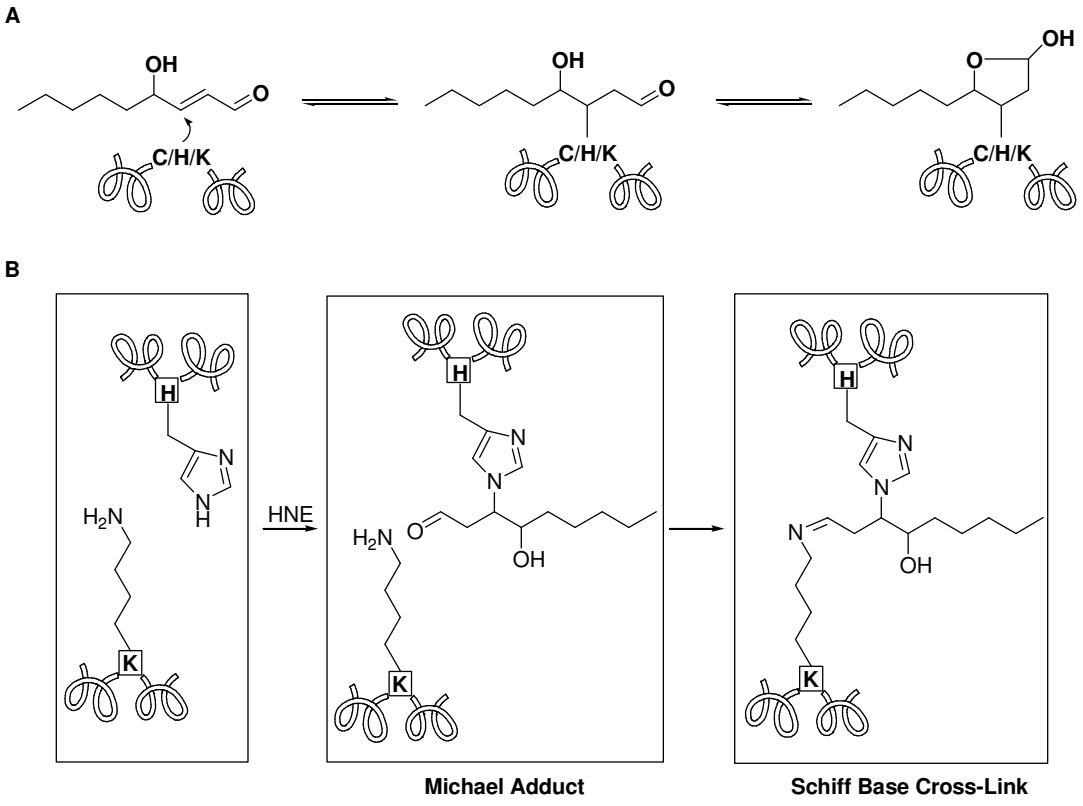

Scheme 3-3. (A) Reaction of HNE with the nucleophilic amino acid residues via Michael addition. (B) Proposed mechanism of protein crosslink by HNE addition.[152]

For these modifications to become useful biomarkers, an important step is a careful characterization of the chemical processes involved, which includes an understanding of the selectivity and kinetics of the protein modification reactions. In 2006, Aldini and Liebler presented separate studies aimed at characterizing the reaction of HNE with HSA.[164, 165] HSA is a natural choice for model studies because it is present in high concentration in serum, is known to form complexes and adducts with a variety of species, including HNE, is a known target of oxidative stress, and is readily available.[126, 128, 129] In the studies by Aldini and Liebler, the site selectivity and kinetics of the HNE additions were evaluated using mass spectrometric methods.

Different approaches were taken by the two groups, but generally the data were in accord; however, there were some noteworthy exceptions. Specifically, Aldini identified additional highly active modification sites not seen in the Liebler study. Furthermore, both groups assumed that the reactions were kinetically controlled and based their analyses on that assumption. However, it is possible that some processes reach equilibrium under the reaction conditions and this would have a significant impact on the interpretation of kinetic data.

Since most studies suggest that HNE signaling is the result of addition reactions rather than the result of allosteric interactions,[166] a better understanding of HNE adduction chemistry is clearly desirable. In the present work, we revisit the reaction of HNE with HSA and track the process as a function of time using an iTRAQ-labeling strategy.[167-169] We find that the kinetics are more complicated than may have been appreciated in previous work and have evidence that some processes may be controlled by thermodynamics rather than kinetics under conditions typically used for *in vitro* studies.

The iTRAQ™ (Isobaric Tag for Relative and Absolute Quantitation) system (Figure 3-3) is a multiplexed set of reagents for quantitative protein analysis. iTRAQ reagent has an NHS ester derivative to modify primary amino groups of proteolytic peptides in a digest mixture and link a mass balance group and a reporter group via an amide bond simultaneously.[167] When iTRAQ-tagged peptides are subjected to tandem mass spectrometry, the mass balance group is released as a neutral fragment, and reporter ions are used to quantify individual peptides in the digest mixture.[167, 169] In the iTRAQ labeling approach, peptides derived from proteins subjected

to different conditions are tagged with a set of isobaric labeling reagents, one for each condition studied. The labeling reagents are identical, except for the distribution of isotopes in the tag. This difference leads to fragment ions (immonium) with unique masses that correlate with the conditions. The beauty of the approach is that peptides from each of the conditions will have the same mass and should co-elute together, but once selected and fragmented will give characteristic peaks that are suitable for relative quantitation. One drawback of the approach is that the characteristic ions appear at low mass (114-117 in our case).

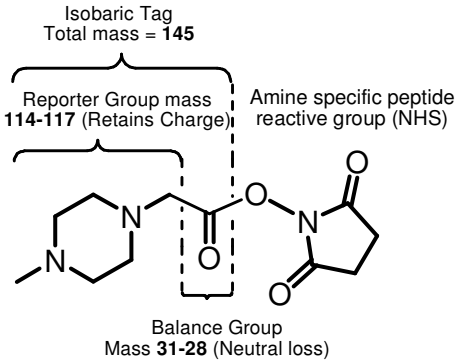

Figure 3-3. Structure of iTRAQ^{TM} reagents.[167]

Experimental Procedures

Chemicals

Essentially fatty acid and globulin free HSA (Product A3782), IAM, DTT and 10× PBS concentrate were purchased from Sigma-Aldrich (St. Louis, MO). Ammonium bicarbonate was obtained from J.T. Baker (Phillipsburg, NJ) and HNE was obtained from Cayman Chemical (Ann Arbor, MI). Sequencing grade modified trypsin was from Promega (Madison, WI). bicinchoninic acid assay (BCA) Protein Assay kits were purchased from Pierce (Rockford, IL) and iTRAQ reagent kits were obtained from Applied Biosystems (Foster City, CA).

Experiments

HSA modification

HSA at 15 μM in 1× PBS buffer (pH 7.4) was incubated with HNE at various final HNE:HSA molar ratios (1:4, 1:2, 1:1, 2:1, 5:1, 10:1, 50:1, 100:1). All reactions were carried out at 37°C with gentle shaking. The reaction time was 3 h for all experiments except those in which the reaction time was intentionally varied. Modified proteins were stabilized by adding $NaBH_4$ to 5 mM and incubating for 60 min at room temperature. Repeated washes employing centrifugal filter devices (VWR, West Chester, PA) were used to remove reagents and to exchange to 50 mM ammonium bicarbonate buffer (pH 8.0) for enzymatic digestion; the molecular weight cut-off for the centrifugal filter devices used was 30 kDa.

Enzymatic digestion

Modified HSA samples in 50 mM ammonium bicarbonate buffer were first reduced by incubating with 30 mM DTT for 20 min at 50°C and then alkylated by incubating with 55 mM IAM for 30 min at room temperature in the dark. Excess DTT and IAM were removed using the centrifugal filter devices (three washes were performed using 50 mM ammonium bicarbonate buffer). Sequencing grade trypsin (substrate to enzyme weight ratio 40:1) was added and the mixture incubated for 24 h at 37°C. Digestion was terminated by adding 1% formic acid (final pH = 2~3).

iTRAQ reagent labeling

1. Effect of varying HNE:HSA molar ratio

After digestion with trypsin, the concentrations of the HNE-modified peptide mixtures were measured using the BCA protein assay (error has been reported to be less than 5%). Peptide mixtures prepared under four conditions (50 µg each) were placed in four different microcentrifuge tubes (two control samples, *i.e.*, no HNE in prep, plus samples from 50:1 and 100:1, HNE:HSA experiments). Peptide mixtures were then dried using a centrifugal evaporator and reconstituted in 25 µl iTRAQ dissolution buffer. The iTRAQ reagents (114-117) were dissolved in 70 µl ethanol separately. Each iTRAQ reagent aliquot was added to one of the peptide mixtures in the following sequence: 114 to a control sample; 115 to 50:1 ratio sample; 116 to 100:1 ratio sample; and 117 to a control sample. After incubation for 3 h at room temperature, all four peptide mixtures were combined and then purified using a Waters (Milford,

MA) Oasis MCX solid phase extraction cartridge. The final sample was dried using a centrifugal evaporator and then resuspended in HPLC equilibration mobile phase for μLC-MS/MS analysis.

2. Effect of varying reaction time

HSA was incubated with HNE at a HNE:HSA molar ratio of 100:1. The reactions were quenched by adding $NaBH_4$ at 1, 3, and 24 h. After digestion, peptide mixtures from different time frames (containing 50 μg total peptides) were labeled separately using the four iTRAQ reagents: 114 for the 0 h sample (control); 115 for the 1 h sample; 116 for the 3 h sample; and 117 for the 24 h sample. Labeling and subsequent processing were performed as described for the varying molar ratio experiment.

μLC-MS/MS analysis

1. HNE adduct identification

Adduct identification was performed using a Thermo (San Jose, CA) LTQ XL linear ion trap mass spectrometer, equipped with ETD, and a Thermo LTQ Orbitrap Velos mass spectrometer. The LTQ XL was interfaced with a Thermo Surveyor capillary HPLC system. Peptides were separated on a reversed-phase, C_{18} column (150 μm × 10 cm, 5 μm particles, 300 Å pores; Column Technology, Fremont, CA) at a flow rate of ~1 μl min^{-1} using 0.1% formic acid in water as mobile phase A and 0.1% formic acid in methanol as mobile phase B. Approximately 2 μg peptides were injected and a Michrom (Auburn, CA) CapTrap trapping column was used for rapid sample injection. The gradient started from 2% B, then increased to 15% B over 5 min,

then increased to 80% B over 70 min, and finally increased to 95% B over 15 min. The eluted peptides were introduced into the LTQ XL with a nanospray source operating at a spray voltage of 2.1 kV, a capillary voltage of 21 V, and a capillary temperature of 200°C. A full scan in the *m/z* range 300-2000 was performed to obtain precursor ions, followed by six data-dependent MS/MS scans (consisting of CID and ETD scans) for the three most abundant precursor ions in the full scan. Dynamic exclusion was used, that is, if the same precursor ion was picked for fragmentation twice within a 30 s window, it was excluded from further analysis for 180 s. For the Thermo LTQ Orbitrap Velos system, separations were performed on a Waters nanoACQUITY reversed-phase, C_{18} column (100 µm × 10 cm; 1.7 µm particles). Elution was achieved using a gradient of 0.1% formic acid in acetonitrile (B) versus 0.1% formic acid in water (A) at a flow rate of 0.4 µL min^{-1}. Approximately 2 µg peptides were injected, with the loading and equilibration mobile phase being 1% B. The linear gradient ran to 35% B over the first 30 min and then to 85% B over the next 5 min. The nanospray ion source was operated at 3.5 kV.

2. iTRAQ reagent-labeled peptide quantification

For iTRAQ reagent-labeled samples, the linear ion trap-based system was operated largely as described above for HNE adduct identification except that pulsed-Q dissociation (PQD) replaced CID and ETD. The top four most abundant ions in each precursor ion scan were subjected to PQD fragmentation. Settings for PQD were normalized collision energy at 36%, activation Q at 0.7, and activation time at 0.1 ms. A targeted mass list was used and, therefore, dynamic

exclusion was not enabled. Similarly, for the Orbitrap-based system, most operating parameters remained the same as those used for HNE adduct identification except that higher-energy C-trap dissociation (HCD)[170] replaced CID. For HCD, the normalized collision energy was 40 and the activation time was 0.1 ms; the top eight most abundant ions in each precursor ion scan were subjected to HCD fragmentation. Dynamic exclusion was not enabled and the same targeted mass list was used. The chromatographic gradient was also lengthened; after loading at 1% B there was an initial increase to 15% B over 25 min, followed by an increase to 25% B over 35 min, followed by an increase to 35% B over 40 min, followed by an increase to 85% B over 20 min.

Database searching and data processing

Peptide sequences and modifications were identified using the BioWorks version 3.3.1, SP1 implementation of Sequest (Thermo). No scan grouping was performed in preparing peak lists for database searching. The protein sequence database used consisted of the NCBI RefSeq version of the complete human proteome and the UniProt sequence for porcine trypsin (Accession Number P00761); reversed versions of all sequences were also included to permit false discovery rate estimation. Sequences were downloaded on November 20, 2010, and the final database contained 68040 entries. Only fully-tryptic peptides were considered and up to two missed cleavage sites were allowed. Precursor ion tolerances were ±2 Da for linear ion trap measurments and ±15 ppm for Orbitrap measurements. Fixed mass shifts were applied for alkylated cysteines (+57 Da) while differential amino acid mass shifts were incorporated for

$NaBH_4$-reduced Michael adducts at histidine and lysine (+158 Da) and at cysteine (+101 Da when the fixed mass shift at cysteine is considered), $NaBH_4$-reduced Schiff base adducts at lysine (+140 Da), and oxidized methionines (+16 Da). In searches with the iTRAQ labels present, fixed mass shifts of +144 Da were used for the peptide N-terminus and non-carbonylated lysine residues, which resulted in the differential mass shifts associated with HNE modification at lysine being changed to +14 Da (Michael adducts) and −4 Da (Schiff base adducts). Addition of the iTRAQ tag at tyrosine (+144 Da differential modification) was also considered, but was found not to be common. Mass shifts were added to Sequest parameters files at high-precision (see Appendix Table A1 for non-iTRAQ and Table A2 for iTRAQ experiments) for compatibility with highly accurate Orbitrap precursor ion measurements and a maximum of three variable modifications were permitted for each peptide. Sequest output was refined using the Trans-Proteomic Pipeline (version 4.4; Institute for Systems Biology, Seattle, WA) software package. Specifically, PeptideProphet was used,[171] in semi-supervised mode,[172] to improve identification confidence. A PeptideProphet score threshold of 0.9 was applied. In addition, MS/MS spectra for modified peptides were manually examined and any found to be inconsistent with the proposed identification were rejected. Intensity measurements for iTRAQ reporter ions (114-117) were processed using Microsoft Access. MS/MS spectra for which all four reporter ion intensities were zero were first rejected and then reporter ion counts for all MS/MS spectra supporting each peptide were combined by averaging. Depletion plots were scaled to 100% for the control to allow comparison on the same axes while accumulation plots were not altered. Reporter ion counts should only be used to obtain relative abundance information for the same

peptide under different conditions and should not be compared between peptides, even between modified and corresponding unmodified peptides.

Results

As noted in the background, the major mode of action of HNE with proteins is Michael addition to the nucleophilic amino acid side chains of cysteine, histidine, and lysine to give stable adducts. HNE can also form a Schiff base with lysine. All of the Michael additions lead to products bearing an aldehyde functional group whereas the Schiff base contains an imine instead. The relevant reaction products, along with the final $NaBH_4$-reduced products that were analyzed, are given in Scheme 3-4. HSA is a 66 kDa protein with 35 cysteines, 16 histidines, and 59 lysines in its secreted form. There are 17 disulfide bridges, which leaves a single free cysteine in the protein.[126] The net result is the possibility of 135 different single addition modifications by HNE; however, some would be highly unlikely if the nucleophilic residue does not have reasonable surface accessibility or is located in an environment that is too sterically crowded to accept the added HNE group.

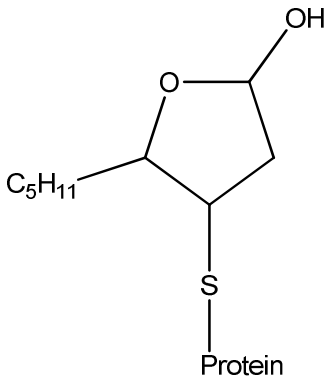

Michael addition at cysteine

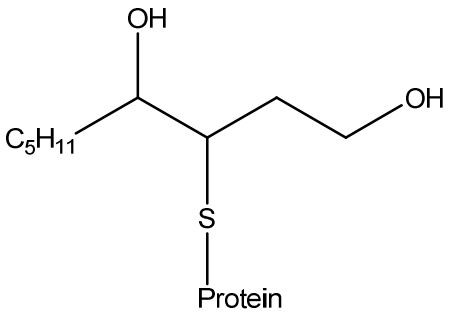

Reduced Michael addition at cysteine

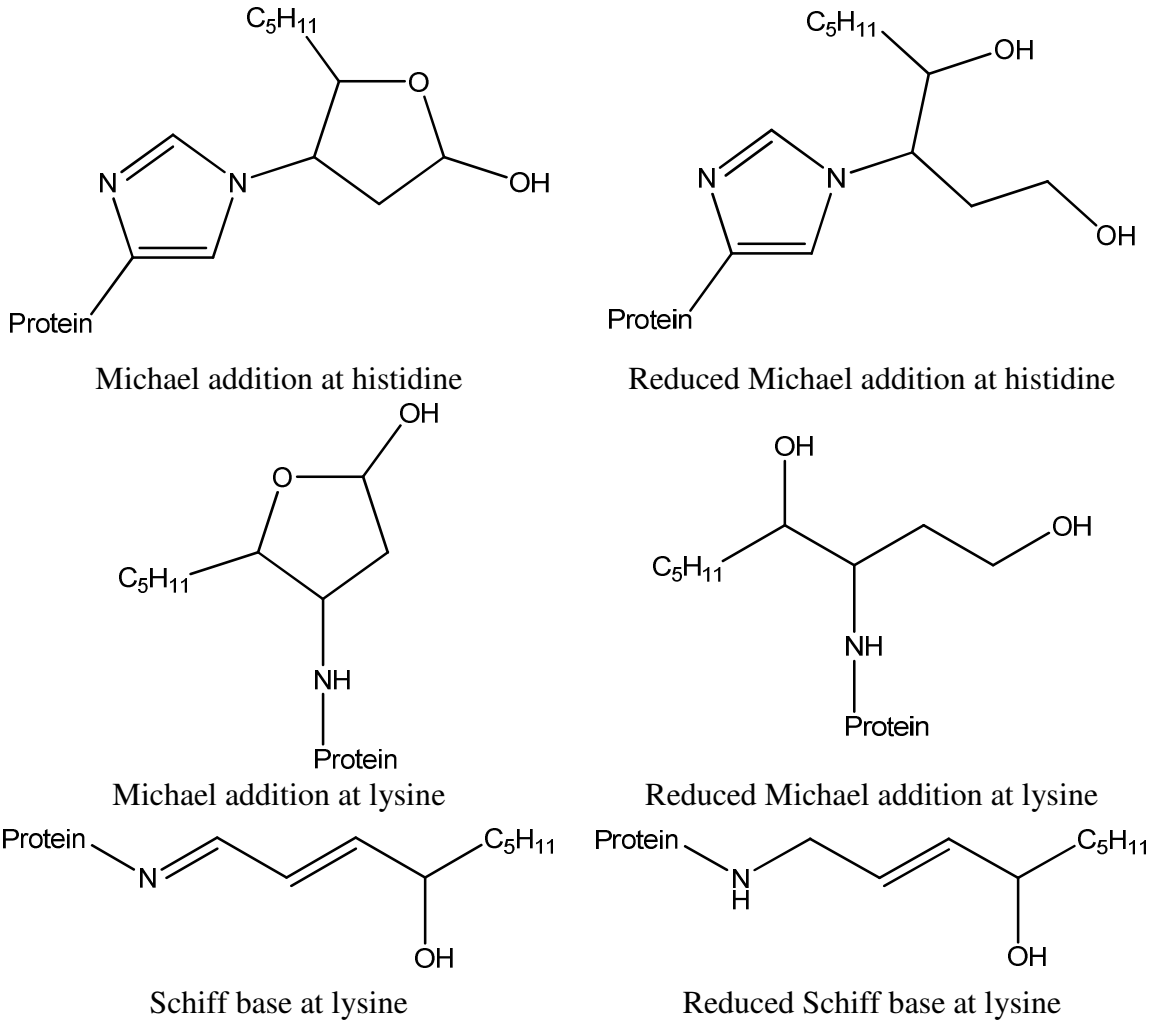

Scheme 3-4. Reaction products for the Michael addition of HNE to cysteine, histidine and lysine residues, and for Schiff base formation with lysine. Initial products are shown in the left column while the results of $NaBH_4$ reduction are shown in the right column. Hemiacetal structures are given for the non-reduced Michael adducts.

Modification Sites

Our first goal was to identify the key modification sites when HSA is treated with HNE. Starting with an HSA concentration of 15 μM, HNE:HSA ratios from 1:4 to 100:1 were surveyed and data are reported for the 1:1 and 10:1 ratios (Table 3-1). The exposure of HSA to HNE

experiment was repeated five times at the 1:1 and 10:1 ratios. These ratios result in HNE concentrations far in excess of those found in plasma, but they could be representative of HNE levels found transiently in membranes under oxidative stress conditions. Four repeats were analyzed using the linear ion trap system while one was investigated using the Orbitrap system. In all cases, three replicate LC-MS/MS runs were recorded for each preparation. Modifications found using the linear ion trap instrument and validated by manual inspection of the MS/MS spectra were regarded as medium confidence; those confirmed with complementary data from the Orbitrap system were regarded as high confidence. These data are also presented in terms of modified peptide (rather than modification site as found in Table 3-1) as Appendix Table A3, for counts of LC-MS/MS runs in which the modified peptides was detected. Most site identifications were supported by CID data, but numerous acceptable ETD detections were also obtained.

For peptides modified with non-reduced HNE Michael adducts, CID, but not ECD, fragmentation patterns are dominated by the neutral loss of HNE.[159] Neutral loss peaks provide good evidence that the modification of interest is present, but suppression of other fragment ions can prevent peptide identification. Alternatively, reduction of HNE Michael adducts with $NaBH_4$ results in MS/MS data that are not dominated by neutral loss peaks.[173] Further advantages of reduction include (a) avoiding the close mass coincidence between non-reduced Michael adducts (156.1150) and arginine residues (156.1011) and (b) removing the possibility of the aldehyde reacting during later sample processing steps. Without the neutral loss, HNE-modified peptides did not seem to exhibit a characteristic fragmentation pattern.

Using the Sequest/Trans-Proteomic Pipeline approach, the initial survey data were also searched for non-reduced Michael adducts and Schiff bases. For Michael adducts, the monoisotopic mass shift was +156 while for Schiff bases it was +138. Orbitrap and linear ion trap data were analyzed. No convincing identifications of either type were obtained, indicating that the reduction and stabilization reaction had gone to completion or that the unstable, non-reduced adducts were in some way lost during sample processing. While the strong neutral losses expected for the non-reduced Michael adducts make modified peptide identification more difficult, it seems reasonable to assume that if numerous non-reduced adducts were present, at least some would generate MS/MS data of sufficient quality to pass the scoring threshold.

Naturally, as the amount of HNE was increased, it was possible to identify more modification sites. At a 1:1 ratio, only three sites were identified at high confidence: His^{67}, Lys^{199}, and Lys^{525} (the residue numbers are for the secreted protein; to convert to nascent protein numbering add 24). His^{67} and Lys^{199} were Michael adducts while Lys^{525} was a Schiff base. At 10:1, there are 15 high confidence modifications at 13 different residues (Table 3-1). In general, the identifications were very reproducible, but it is clear that in some cases the peptides were at a concentration that was close to the threshold for our identification criteria. In Liebler's work, ten modifications were identified with an HNE:HSA ratio of over 600:1.[165] Our full set (medium and high confidence) includes all of their set with the exception of Lys^{51} and His^{105}. Michael addition at Lys^{51} was only detected in one out of ten experiments in Liebler's study while the presence of an alternative Michael addition site at Lys^{106} makes confident detection of addition at His^{105}

challenging; however, modification at His^{105} can be confidently detected in experiments where iTRAQ labels are present and quantitative data were obtained for this site (see below). Aldini detected eleven modifications at their highest ratio (5:1).[164] In our studies, at a ratio of 10:1, we detected the majority of them at high confidence with the exceptions being Michael additions at His^{242} and His^{510}, which we detected at medium confidence, and Schiff base formations at Lys^{195} and Lys^{199}, which we did not detect. Identification of His^{242} is challenging because the underlying tryptic peptide contains a second addition site at His^{247}, requiring very high quality MS/MS spectra for certainty in modification localization. Aldini's identification of Schiff base formation at Lys^{195} required a careful manual search for new peaks in the HNE-treated sample's chromatogram (searches were conducted in chromatograms covering a series of mass ranges). With our global approach for identifying modifications, the observation of this modification site, which appeared to be a minor one, was much less likely.

It is not surprising that our approach apparently detected more modifications than the one used by Aldini, 15/34 (high/medium confidence) vs. 11, because we used a somewhat higher concentration (10:1 vs. 5:1) and a longer reaction time (3 h vs. 2 h). In addition, they relied to some extent on manual matching in the chromatograms so there was a possibility that some modification combinations were not considered, the full sensitivity of their instrument was not realized, or peaks were obscured in some way. On the other hand, their approach has advantages in some situations and led to identifications that we did not detect. It is more surprising that we identified significantly more sites than Liebler despite using methodologies that were fairly

similar. It is unclear why so few modifications were identified in their study given the high concentrations employed, but nonetheless, there is reasonable consistency across the three studies of HNE/HSA reactivity in terms of the preferred sites of modification.

It is interesting to note that at a 1:1 ratio, the HNE addition appears to be relatively selective. Only two of the 59 lysines and one of the sixteen histidines are identified at high confidence as modified (considering both high and medium confidence identifications, there are four histidine and eight lysine modification sites at this concentration). It might be tempting to conclude that the reactions with histidine are less selective because a higher percentage of them are modified, but the larger number of modification sites is also driven by the fact that the reaction is more favorable (see below) and, therefore, at a given ratio, more of the HNE is naturally adducted to histidines.

Finally, there is evidence for HNE addition at the single free cysteine in HSA (Cys^{34}) at both concentrations. Although it has been accepted that Cys^{34} is the most reactive Michael addition site,[129, 133] the MS/MS data for this site are not as consistent as those for other modifications. This does not appear to be the result of a low level of modification, but instead is probably due to cysteinylation at Cys^{34}, a common post-translational modification that is often found in HSA preparations.[174] However, for all sites, poor detectability could be due to the ionizability of the corresponding peptide as well as the quality of its CID fragmentation pattern. Therefore, some care needs to be exercised in analyzing data from these types of experiments because effects other than concentration can have a major impact on the ability to identify modifications. As a

result, more direct concentration measures, such as those from an iTRAQ-labeling scheme are needed for ranking reactivities.[169]

Table 3-1. High (bolded) and medium (italicized) confidence modification site identifications. Medium confidence hits based on low mass accuracy precursor ion measurements (linear ion trap) while high confidence hits included high mass accuracy precursor ion measurements (Orbitrap). Manual MS/MS spectrum validation was required in all cases.

Modification Site[a]	Type[b]	1:1[c]	10:1[c]
Cys^{34}	**MA**	**9/1/0**	**9/3/3**
His^{67}	**MA**	**12/0/3**	**12/5/3**
His^{128}	*MA*	*0/2/0*	*2/3/0*
His^{146}	**MA**	**12/11/0**	**12/12/3**
His^{242}	*MA*	*8/7/0*	*11/11/0*
His^{247}	*MA*	*not detected*	*11/10/0*
His^{288}	**MA**	**10/0/0**	**12/1/3**
His^{338}	**MA**	**4/6/0**	**12/11/3**
His^{367}	*MA*	*not detected*	*9/0/0*
His^{510}	*MA*	*1/8/0*	*12/11/0*
Lys^{73}	*MA*	*not detected*	*3/0/0*
Lys^{106}	*SB*	*not detected*	*0/1/0*
Lys^{137}	*MA*	*not detected*	*1/0/0*
Lys^{159}	**MA**	**not detected**	**0/2/1**
Lys^{162}	**MA**	**not detected**	**12/2/2**
Lys^{162}	*SB*	*not detected*	*10/1/0*
Lys^{199}	**MA**	**6/0/2**	**11/0/3**
Lys^{212}	**MA**	**not detected**	**12/0/1**
Lys^{233}	*MA*	*not detected*	*9/4/0*
Lys^{240}	*MA*	*8/0/0*	*3/0/0*
Lys^{262}	*MA*	*not detected*	*5/3/0*
Lys^{351}	*MA*	*10/0/0*	*9/0/0*
Lys^{351}	*SB*	*not detected*	*3/1/0*
Lys^{359}	*MA*	*not detected*	*1/3/0*
Lys^{378}	*MA*	*not detected*	*5/1/0*
Lys^{402}	**MA**	**not detected**	**4/0/2**
Lys^{414}	**MA**	**not detected**	**11/1/3**
Lys^{414}	**SB**	**8/0/0**	**12/1/3**
Lys^{475}	*MA*	*not detected*	*1/0/0*

Lys^{519}	*MA*	*not detected*	*1/0/0*
Lys^{525}	**MA**	**not detected**	**0/1/3**
Lys^{525}	**SB**	**3/0/3**	**8/3/3**
Lys^{545}	**MA**	**4/7/0**	**11/11/3**
Lys^{545}	*SB*	*not detected*	*4/7/0*

[a] Secreted protein numbering; add 24 for nascent protein

[b] MA indicates Michael adduct formation; SB indicates Schiff base formation

[c] Applied HNE:HSA ratio. Values are counts of LC-MS/MS runs in which the modified site was identified using linear ion trap CID scans (maximum = 12)/linear ion trap ETD scans (maximum = 12)/linear ion trap CID scans associated with high mass accuracy Orbitrap precursor ion mass measurements (maximum = 3)

Relative Modification Levels Based on iTRAQ Labeling

In a quadrupole ion trap, such as that found in the LTQ XL instrument used in this work, it is very difficult to simultaneously trap low-mass iTRAQ reporter ions and the b- and y-ions needed for peptide identification because the mass window is fundamentally limited. However, in the LTQ XL, PQD can be used in place of CID to significantly widen the window and to simultaneously trap high- and low-mass ions (the approach shifts the q_z value during the activation and fragmentation timeframes).[175] Although PQD allows implementation of the iTRAQ approach with ion trap instrumentation, the intensities of the label ions are rather low and extensive signal averaging is needed to obtain reproducible results (based on our results, single PQD scans for both peptide identification and reporter ion intensity measurements were more effective than collecting, for each precursor ion, a CID scan for identification and a PQD scan for reporter ion measurements). Consequently, the most efficient approach in these systems is to use a targeted mass list of anticipated peptides (modified and unmodified) rather than dynamically determining masses for fragmentation. By targeting masses and not employing a dynamic

exclusion protocol, many more MS/MS spectra containing iTRAQ reporter ions can be recorded and averaged during a chromatographic run. The mass list approach was also used with the LTQ Orbitrap Velos instrument, both to allow comparisons to be made and to improve accuracy by collecting as many measurements as possible. A list of the 21 modified peptides targeted in these studies is given in Table 3-2; 20 modifications at 18 residues were considered (two variants are present for one modification to take account of the possibility of methionine oxidation). In addition, unmodified versions of the listed modified peptides and peptides resulting from cleavage with trypsin of unmodified versions of the listed modified peptides were also targeted (a full list of all targeted peptides with *m/z* values used is given as Appendix Table A4). Since it was not practical to monitor all possible modification sites in HSA in this way (there are hundreds of potential peptide masses), sites that had been identified previously by other workers as well as sites identified in the present study whose spectra suggested significant modification levels were included.

Table 3-2. List of modified peptides included in the targeted mass list.

Modified Peptide[a]	Modification Site[b]	Type[c]
ALVLIAFAQYLQQC#PFEDHVK	Cys^{34}	MA
SLH@TLFGDK	His^{67}	MA
NECFLQH@K	His^{105}	MA
VH@TECCHGDLLECADDR	His^{242}	MA
VHTECCH@GDLLECADDR	His^{247}	MA
SH@CIAEVENDEM*PADLPSLAADFVESK	His^{288}	MA
SH@CIAEVENDEMPADLPSLAADFVESK	His^{288}	MA
CCAAADPH@ECYAK	His^{367}	MA
EFNAETFTFH@ADICTLSEK	His^{510}	MA
LVNEVTEFAK^TCVAD	Lys^{51}	MA

YK^AAFTECCQAADK	Lys^{162}	MA
LK^CASLQK	Lys^{199}	MA
AFK^AWAVAR	Lys^{212}	MA
AEFAEVSK^LVTDLTK	Lys^{233}	MA
ADLAK^YICENQDSISSK	Lys^{262}	MA
LAK^TYETTLEK	Lys^{351}	MA
VFDEFK^PLVEEPQNLIK	Lys^{378}	MA
K^VPQVSTPTLVEVSR	Lys^{414}	MA
K~VPQVSTPTLVEVSR	Lys^{414}	SB
K^QTALVELVK	Lys^{525}	MA
K~QTALVELVK	Lys^{525}	SB

[a] Unmodified versions of the listed modified peptides and peptides resulting from cleavage with trypsin of unmodified versions of the listed modified peptides were also targeted; C# indicates HNE Michael addition at Cys followed by reduction; H@ indicates HNE Michael addition at His followed by reduction; K^ indicates HNE Michael addition at Lys followed by reduction; K~ indicates Schiff base formation with HNE at Lys followed by reduction; M* indicates oxidation at Met

[b] Secreted protein numbering; add 24 for nascent protein

[c] MA indicates Michael addition; SB indicates Schiff base formation

Effect of HNE Concentration on the Level and Distribution of Modifications

Using 3 h incubations at 37°C, we report pilot data here on two HNE:HSA ratios: 50:1 and 100:1. Linear ion trap data alone were collected for this comparison (more extensive data, including Orbitrap measurements, are provided in the next section). These ratios provide sufficient conversion at 3 h to limit the inherent uncertainty in using PQD to assess iTRAQ labels. The data are the result of three separate LC-MS/MS replicate runs on a single sample preparation. Using duplicate (no HNE present) controls allows the consistency between iTRAQ counts to be evaluated: the $\log_{10}$-transformed average 114:117 ratio (masses of the duplicate, control iTRAQ labels) was 0.0068, but the $\log_{10}$-transformed standard deviation was 0.33 (single standard deviation 114:117 ratio range is from 0.47 to 2.18). As noted above, a highly targeted

peptide list (Table 3-2) was used in the analysis to maximize the iTRAQ detection count obtained for each peptide. Although 20 modifications were targeted, useful data were obtained for only 15 of them. Furthermore, of the 15 identified modifications, detections counts for Cys^{34}, Lys^{199}, and Lys^{262} were very low (see Appendix Table A5). Results for the histidines and lysines are presented in Figure 3-4. In panels (a) and (c), depletion plots are shown for the unmodified histidines and lysines, respectively, scaled to 100% for the control samples. In panels (b) and (d) are the corresponding accumulation plots (average reporter ion intensities for each modified peptide are displayed; no scaling has been performed). The measurements supporting Figure 3-4 are listed in tabular form in Appendix Table A5.

(a) Depletion of unmodified peptides containing the indicated histidine modification site

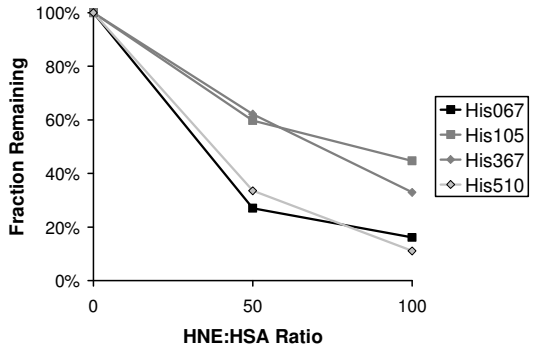

(b) Accumulation of modified peptides containing the indicated modified histidine residue

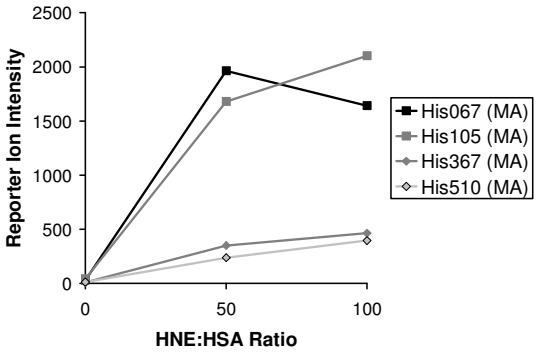

(c) Depletion of unmodified peptides containing the indicated lysine modification site

(d) Accumulation of modified peptides containing the indicated modified lysine residue

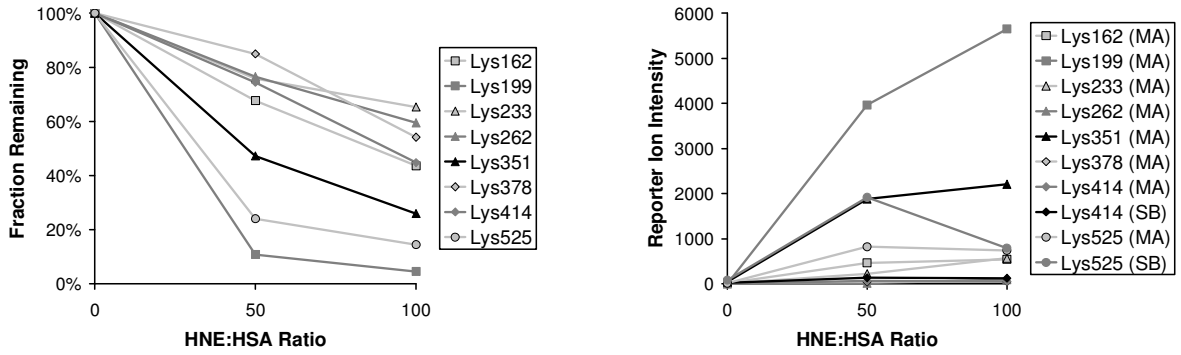

Figure 3-4. Effect of varying HNE:HSA ratio on reaction progress measured using iTRAQ reporter ion intensity (linear ion trap/PQD) for targeted histidine and lysine sites. The targeted mass list was used. Depletion plots are average reporter ion intensities scaled to 100% for the control while average reporter ion intensities are given unaltered in the accumulation plots. Relative abundance measurements were not obtained for His^{242}, His^{247}, His^{288}, Lys^{51}, and Lys^{212}. MA indicates Michael addition while SB indicates Schiff base formation. When more than one unmodified peptide for a particular modification site was available, the most frequently-detected unmodified peptide was used.

In Figures 3-4a and 3-4c, one sees a reasonable dose/response relationship for the unmodified histidines and lysines—as the HNE concentration increases, there is a consistent drop in the intensity of the parent peptides. Looking at Figures 3-4a and 3-4c, the data indicate that His^{67} and His^{510} are the most reactive of the histidines and that Lys^{199} and Lys^{525} are the most reactive lysines under these conditions. In Figures 3-4b and 3-4d, the accumulation plots present a somewhat different picture in terms of relative reactivity. First, it is clear that the peptides have very different ionization/detection properties, which leads to much greater variations in the response in the accumulation plots than is seen in the depletion plots (those are normalized relative to the control response). The variation in response suggests that much care must be taken

in evaluating relative reactivity on the basis of the detectability of products (*i.e.*, methods that use titrations to identify relative detection thresholds and then equate them with relative reactivity). Since intensities alone provide no guide, we are left with curve shape—the most reactive sites would be expected to show a greater increase in reporter ion intensity between the 0 and 50:1 points than between the 50:1 and 100:1 points because they would approach saturation (*i.e.*, 100% conversion to product). For the histidines, His^{67} remains a candidate for the most reactive site (reporter ion intensity at 50:1 is about the same as that at 100:1), in agreement with the depletion plots, but His^{510} now appears to be least reactive (the increase in intensity between 0 and 50:1 is similar to that between 50:1 and 100:1), though the differences are modest. In the accumulation plots for the lysine series, Lys^{199} stands out, but the jump between the 0 and 50:1 points is only a little larger than that between the 50:1 and 100:1 points; furthermore, the peptide supporting this modification was only detected once (see Appendix Table A5). Lys^{525} appears to still be relatively reactive, but the signal is split between the formation of a Michael adduct and a Schiff base, complicating interpretation. Looking for the least reactive targeted lysines, the accumulation plots suggest Lys^{262} and Lys^{233} (most relative intensity is found for the 100:1 HNE:HSA ratio data points), which is broadly in agreement with the depletion plots. In general, the availability of only curve shape for the accumulation plots makes then particularly hard to interpret; we have only relative abundances and no knowledge of how close the reaction is to completion. Furthermore, the accumulation plots contain high degrees of uncertainty because signals are often low for the modified peptides (especially for Lys^{378}), particularly at low conversions (intensities appear to be systematically low for the HNE-modified peptides,

probably because they offer alternative fragmentation pathways). In contrast, the depletion plots are much easier to compare since the degree of modification (i.e., depletion) must be zero if no HNE has been added. Therefore, the depletion plots would seem to be the best measure of relative reactivity. A critical point with respect to the data in Figure 4 is the impact of whether or not the systems are reaching equilibrium in this time frame. This issue is addressed with a more comprehensive analysis in the following section.

Effect of Incubation Time on the Level and Distribution of HNE Modifications

Incubation times of 1, 3, and 24 h were used with an HNE:HSA ratio of 100:1. The linear ion trap- and Orbitrap-based instruments were used with the same list of targeted peptides (Table 3-2) to maximize the number of MS/MS spectra collected for each peptide, thus enhancing the signal-to-noise ratio in the iTRAQ data. The data presented are the result of three complete repeat preparations, for each of which three replicate LC-MS/MS runs performed on each instrumental platform. We anticipated that the longest timeframe would lead to extensive modification and potentially an equilibrium mixture.

Data for targeted histidines are shown in Figure 3-5. All targeted histidines were detected except His^{247}, which is difficult to confidently identify because it is located on the same tryptic peptide as His^{242}. Modified and unmodified peptides for the His^{288} site were detected both with and without an oxidized methionine; the non-oxidized form was detected more frequently and was used in constructing these plots. Figures 3-5a and 3-5b illustrate the depletion of parent peptides

and the accumulation of modified peptides, respectively, for the linear ion trap while Figures 3-5c and 3-5d provide the same information for the Orbitrap. The same unmodified peptides were used in constructing depletion plots for both instrumental platforms (see Appendix Table A6). Looking first at the depletion plots, there is good agreement between the methods on the least reactive targeted histidines (His^{105} and His^{367}). This result is in good agreement with the HNE:HSA ratio versus unmodified peptide depletion comparison given in Figure 1a. His^{67} and His^{510}, which were most reactive in the concentration study, are again among the most reactive sites. However, the two additional detections, $His^{242/7}$ and His^{288}, appear most reactive, although $His^{242/7}$, by both methods, shows a greater degree of depletion at 1 h than 3 h. Moving to the modified peptide accumulation plots, His^{105} and His^{367} are again confirmed as being among the least reactive targeted histidines (not approaching saturation). Again, in agreement with the depletion plots, His^{67}, His^{288}, and His^{510} are confirmed as being the most reactive targeted histidines (saturated by 24 hours). His^{242} displays a more confusing picture, but this is probably caused by the low number of identifications obtained. This is due, as mentioned above, to two modification sites (His^{242} and His^{247}) being present on the same tryptic peptide (very high quality MS/MS spectra are required to unambiguously identify one particular site when another site on the same peptide must also be considered). Taking all Figure 3-5 plots together, it appears that the modification reaction is moving towards completion, but a reaction time of greater than 24 h is required.

(a) Linear ion trap measurement of the depletion of unmodified peptides containing the indicated histidine modification site

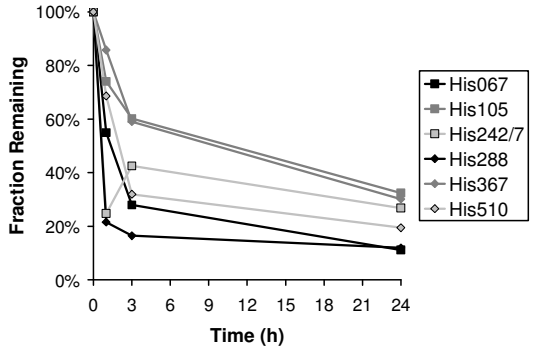

(b) Linear ion trap measurement of the accumulation of modified peptides containing the indicated modified histidine residue

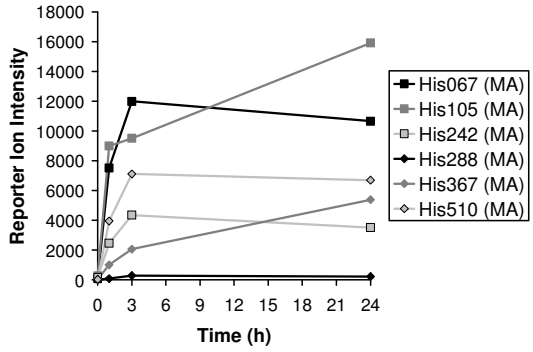

(c) Orbitrap measurement of the depletion of unmodified peptides containing the indicated histidine modification site

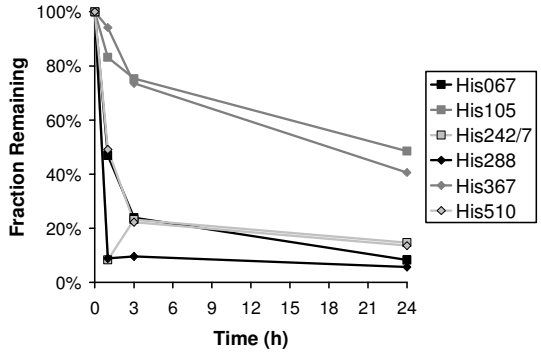

(d) Orbitrap measurement of the accumulation of modified peptides containing the indicated modified histidine residue

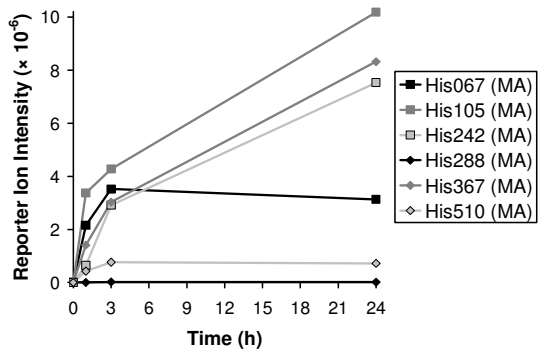

Figure 3-5. Effect of varying reaction duration, at a fixed HNE:HSA ratio of 100:1, on reaction progress measured using iTRAQ reporter ion intensity for targeted histidine sites. Linear ion trap/PQD and Orbitrap/HCD data are presented. The targeted mass list was used. Depletion plots are average reporter ion intensities scaled to 100% for the control while average reporter ion intensities are given unaltered in the accumulation plots. Relative abundance measurements were not obtained for targeted site His^{247}, although this site shares the same unmodified peptide with His^{242}. MA indicates Michael addition while SB indicates Schiff base formation. When more than one unmodified peptide for a particular modification site was available, the most frequently-detected unmodified peptide was used.

The data for the lysines are presented in Figure 3-6. Eleven of twelve targeted modifications were identified using the Orbitrap, with the exception being Lys^{51}; with the linear ion trap, Lys^{51} and Lys^{212} were missed. Figures 3-6a and 3-6b show the depletion of parent peptides and the accumulation of modified peptides, respectively, for the linear ion trap while Figures 3-6c and 3-6d provide the same information for the Orbitrap. The same unmodified peptides were used in constructing depletion plots for both instrumental platforms (see Appendix Table A7); furthermore, the same unmodified peptides were used in constructing Figures 3-4, 3-5, and 3-6. The lysines present a different picture to the histidines. Not only are the extents of depletion lower, but the plots indicate that lysine modifications become saturated and level off at what appear to be equilibrium levels. The curve shapes for the lysine depletion plots are clearly different to those observed for the histidine depletion plots. A group of three sites, Lys^{233}, Lys^{262}, and Lys^{378}, show very little depletion by both instrumental methods and appear to represent the set of least reactive targeted lysines (Lys^{212}, although only detected on the Orbitrap platform, could also be added to this group). The most reactive targeted lysine is clearly Lys^{199} while the second most reactive is Lys^{525}. The accumulation plots again provide a roughly complementary picture, but they tend to suggest that there is a slow accumulation in some modification sites in the 3-24 h time frame that is not reflected in the depletion plots. This is most evident for Lys^{233} and it is unclear why there is a substantial increase in modified peptide signal here despite the small drop in parent peptide intensity for this site; however, it is important to note that what looks like a large change at the level of reporter ion intensity may only represent a small change in concentration. In any case, the drift up in the 3-24 h range for the all of the other peptides

suggests a rate that is well below that indicated for the first three hours and suggests the process is slowing, presumably to an equilibrium level. Interestingly, the Schiff base products show reduced relative abundance at longer reaction times, possibly indicating that the Michael adduct is the thermodynamically favored product.

These experiments were not designed to provide quantitative kinetic data—the iTRAQ system employed provides too few data points and the uncertainties are significant. However, it is possible to extract crude rate constants from the data in Figures 3-5 and 3-6. In this analysis, a pseudo first-order approach was used, focusing on the first three hours of reaction. PQD and HCD measurements were averaged at equal weight when calculating rate constants. For the slowest targeted histidines, His^{105} and His^{367}, rate constants of 0.027 ± 0.004 and 0.025 ± 0.001 M^{-1} s^{-1}, respectively, were obtained. For the pair of histidines that showed intermediate reactivity, His^{67} and His^{510}, the respective rate constants calculated were 0.088 ± 0.009 and 0.083 ± 0.004 M^{-1} s^{-1} (the listed uncertainties only consider the precision of the kinetic plots—including other experimental factors, uncertainties in the 10-20% range are expected). For the most reactive histidines, $His^{242/7}$ and His^{288}, the errors were much larger in the kinetic plots and the rate constants for both sites are probably best expressed as 0.2 ± 0.1 M^{-1} s^{-1}. Errors were perhaps more significant because very low intensity reporter ions were being masked by noise in the mass spectrum. This approach is not possible with the lysines because they are approaching equilibrium and we do not have enough data points at early times. Nonetheless, the plots suggest that the most reactive lysine, Lys^{199}, has a rate constant comparable to $His^{242/7}$ and His^{288}.

(a) Linear ion trap measurement of the depletion of unmodified peptides containing the indicated lysine modification site

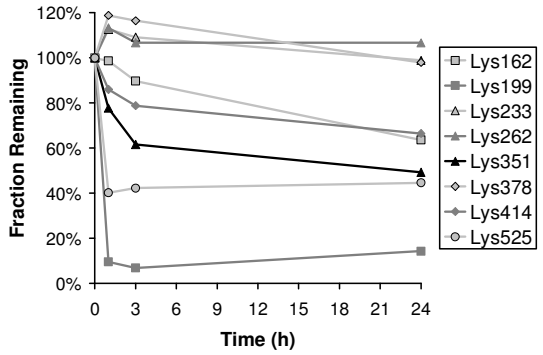

(b) Linear ion trap measurement of the accumulation of modified peptides containing the indicated modified lysine residue

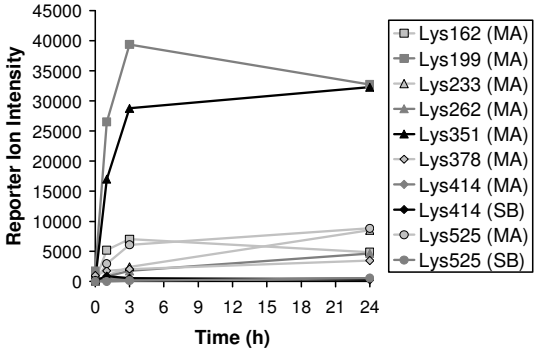

(c) Orbitrap measurement of the depletion of unmodified peptides containing the indicated lysine modification site

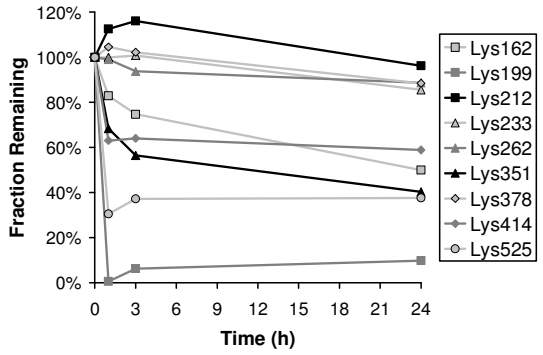

(d) Orbitrap measurement of the accumulation of modified peptides containing the indicated modified lysine residue

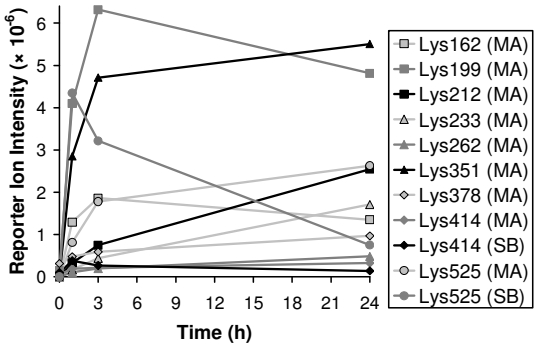

Figure 3-6. Effect of varying reaction duration, at a fixed HNE:HSA ratio of 100:1, on reaction progress measured using iTRAQ reporter ion intensity for targeted lysine sites. Linear ion trap/PQD and Orbitrap/HCD data are presented. The targeted mass list was used. Depletion plots are average reporter ion intensities scaled to 100% for the control while average reporter ion intensities are given unaltered in the accumulation plots. Relative abundance measurements were not obtained for Lys^{51} by either instrumental approach and were obtained for Lys^{212} only using the Orbitrap approach. MA indicates Michael addition while SB indicates Schiff base formation. When more than one unmodified peptide for a particular modification site was available, the most frequently-detected unmodified peptide was used.

Discussion

Comparison to Previous Work

Our strategy for the initial identification of HNE-modified sites was similar to Liebler's, with some differences being found in the computational details (for modified peptide identification Liebler used Sequest and P-Mod while we used Sequest and Trans-Proteomic Pipeline software). However, we were able to add high mass accuracy precursor ion measurements, obtained using an Orbitrap mass spectrometer, significantly improving identification confidence. Moreover, Liebler used a very high HNE:HSA ratio, 640:1, while we report the use of two much lower ratios, 1:1 and 10:1.

Aldini's approach resulted in a similar list of identified modified peptides, but it was distinct and comprehensive. Briefly, a tryptic digest of untreated HSA was analyzed using an LC-MS/MS with Sequest searching approach to build a list of detectable unmodified peptides. Reductions in selected ion chromatogram peak areas for HNE-exposed HSA versus control HSA, for each peptide, were then used to locate putative modification sites. These sites were then confirmed by collecting MS/MS data for the expected modified peptides. Chymotrypsin and chymotrypsin/trypsin hybrid digests were added in some cases to aid in distinguishing between two sites located on the same tryptic peptide. Furthermore, a search was made for additional peaks found in the HNE-exposed but not in the control total ion chromatogram that could indicate modified peptides for which the associated unmodified peptides had not been detected. However, this resulted in the identification of only one additional site, Lys^{195}. Figure 3-7 shows

the divided and shared modification sites obtains from Aldini's, Liebler's, and our experiments at respectively highest HNE concentrations.

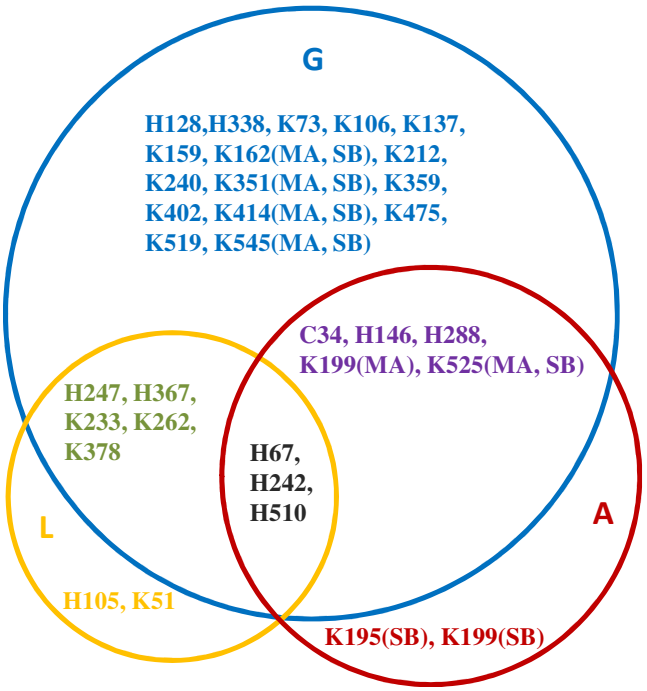

Figure 3-7. Divided and shared modification sites from Aldini's, Liebler's, and our experiments. A (red): Aldini's approach; L (yellow): Liebler's approach; G (blue): our approach.

Aldini also used depletion of unmodified peptides, again measured by precursor ion selected ion chromatogram peak area, to rank site reactivity. MS/MS data was not employed. At an HNE:HSA ratio of 1:4, only the tryptic peptide containing site Cys^{34} showed significant depletion, making Cys^{34} the most reactive site. At an HNE:HSA ratio of 1:2, His^{146} and Lys^{199} were added, with comparisons of the degree of depletion used to identify Lys^{199} as second most reactive site. MS/MS data was required to determine whether the depletion at site Lys^{199} was due to the Michael adduct or to Schiff base formation. No attempt to monitor reaction progression

over time or to rank the remaining sites was reported. Using selected ion chromatograms of precursor ions can be problematic when interfering species are encountered. Moving to the monitoring of characteristic MS/MS transitions would significantly improve confidence. Furthermore, excellent reproducibility is essential when comparing separate LC-MS/MS runs; methods, such as iTRAQ, where the peak areas to be compared are taken from the same spectrum are more robust.

In contrast, Liebler's strategy for ranking site reactivities is more similar to our iTRAQ approach than Aldini's. Liebler employed a self-developed system where phenylisocyanate (PIC) was used as a peptide N-terminus tag. Time point samples are labeled with $^{12}C_6$-PIC and are compared with a duplicate of the final time point labeled with $^{13}C_6$-PIC. Time point and standard samples are mixed and then subjected to LC-MS/MS analysis. Using ^{13}C-labeling ensures that light and heavy versions of each labeled peptide will co-elute and will therefore experience the same ionization environment. Liebler's approach uses a targeted mass list to ensure that both the light and heavy tagged peptides are selected for fragmentation, and then uses selected ion chromatogram peak areas for three characteristic fragment ions for each peptide as a measure of relative abundance. However, Liebler only monitored modified peptides; the depletion of unmodified peptides was not considered. Assigning the 24 h time point as a standard made it easy to regard this time point as representing the reaction going to completion, whereas our study indicates that this is not always the case. Finally, Liebler's method required targeting two masses for MS/MS spectra to provide relative quantification fro each peptide, so all other things being

equal, twice as many sites can be monitored with and iTRAQ approach where a single MS/MS spectrum provides the needed relative quantification.

As noted above, the present data share many of the same features as those obtained by Aldini in terms of modification sites. Comparisons focused on the relative reactivity of the sites are more difficult to make because the most reactive sites reported in the study by Aldini were difficult sites to quantify with our methods as well as with Aldini's methods. Aldini reports the following order of reactivity: $Cys^{34} > Lys^{199} > His^{146}$. In the case of Cys^{34} and His^{146}, they were not able to identify the modification products in tryptic digests, but had to rely on trypsin/chymotrypsin combination digests to identify them. Their conclusion was based on a combination of depletion data, comparisons of selected-ion chromatograms, and titrations identifying initial adducts at low HNE:HSA ratios. More recently, Aldini determined a rate constant of 30 M^{-1} s^{-1} for the reaction of Cys^{34} with HNE,[133] a value about two orders of magnitude greater than our approximate value for the most reactive histidines, suggesting that the free cysteine is exceptionally reactive. While we were able to identify adducts at Cys^{34}, His^{146}, and Lys^{199} at high confidence in our initial survey, there were problems with each of these sites. His^{146} was not included in the targeted mass list because this modification was observed in control runs where no HNE had been added and was not detected in initial Orbitrap test runs performed without a mass list; however, the chief peptide supporting His^{146}, RH@PYFYAPELLFFAK, is supported by convincing MS/MS spectra, with peak intensities conforming to the 'proline effect'.[176] Cys^{34} and Lys^{199} were added to the mass list, but for both residues relatively small numbers of acceptable MS/MS spectra

were obtained. Lys^{199} has been included in the accumulation and depletion plots, but Cys^{34} was not due to the probable presence of extensive cysteinylation at this site in HSA as mentioned above. Although Aldini did not rank the reactivity of their other modification sites, the limited quantitative data that they provide is consistent with the more extensive results shown here in Figures 3-(4-6).

Comparisons with Liebler's data are more difficult because the detected sites are somewhat different than those presented here. First, at an HNE:HSA ratio of 10:1, we find 15/34 (high/medium confidence) modifications whereas Liebler reports only ten at an HNE:HSA ratio of 640:1. The differences in the kinetic data are also significant. Liebler obtained the following order of reactivity for the histidines: $His^{242} > His^{67} \sim His^{510} > His^{367} > His^{247}$. Their rate constants vary by a factor of 600, from 0.0005 for His^{247} to 0.3 $M^{-1}s^{-1}$ for His^{242} (Sigma HSA numbers); in contrast, using the depletion of unmodified peptides, we see a much smaller variation in rate (from 0.02 for His^{105} to circa 0.2 $M^{-1}s^{-1}$ for $His^{242/7}$ and His^{288}). Due to the requirement for very high quality MS/MS spectra to confidently identify isobaric modifications on the same peptide and the consequent low numbers of detections for His^{242} and His^{247}, we can only realistically use the depletion of the unmodified peptide to provide a combined rate for His^{242} and His^{247}. Our results indicate the following ranking that is broadly in agreement with Liebler: $His^{242/7} \sim His^{288} > His^{67} \sim His^{510} > His^{105} \sim His^{367}$. Liebler identified but did not provide kinetic data for His^{105} and did not detect His^{288}. Overall, the major difference in the kinetic data centers on the rate constant of the less reactive histidines, which were found to be much slower in the Liebler study.

The origin of this difference is probably rooted in the methodologies that were used. In the Liebler study, the intensity of the HNE addition product was tracked as a function of time with the assumption that at 24 h there would be 100% modification at each site. The danger in this approach is that if the modification does not go to completion for some reason, such as equilibrium formation, or if the kinetics is more complex than expected, the approach can be skewed by the use of an errant reference point (*i.e.*, assumption of 100% conversion at longest reaction time). In addition, if the modification site undergoes any secondary reactions, it is not included as a productive reaction and would lead to underestimation of the reaction rate. In our approach, we have based our kinetics on the disappearance of the unmodified peptide. In this case, the reference point (*i.e.*, 0% conversion in the control) is well defined. However, it is possible to overestimate the rate of a particular reaction if there are hidden pathways depleting the signal for the unmodified peptide. As a result, the present data should be viewed as upper-limits on the rates. In any case, neither our accumulation of modified peptide nor depletion of unmodified peptide data are consistent with His^{242} having exceptional reactivity among the histidines. Liebler gives kinetic data for only one lysine, Lys^{233}, which like in our results, they identify as being a relatively less reactive site. Overall, the present data are broadly consistent with those from Liebler, but suggest that other histidines compete much more effectively with His^{242} than the previous data indicated.

Reactivity of Amino Acids

As noted above, it has been established that Cys^{34} is the most reactive site in HSA. This is not surprising in that it is the only free cysteine and sulfur is known to be highly nucleophilic in Michael additions.[77] Comparison of the lysines and histidines is more complicated because the lysines do not react to completion and are under a mix of kinetic and thermodynamic control with our reaction conditions. Nonetheless, some general conclusions can be drawn from the data at 1 h because the reactions, for the most part, have not reached equilibrium or completion at this point. If we look at the three most reactive lysines that were characterized, averaging the linear ion trap and Orbitrap data at equal weight, we see approximately 95% (Lys^{199}), 65% (Lys^{525}), and 27% (Lys^{351}) depletion at 1 h. For the four most reactive histidines, again combining linear ion trap and Orbitrap data, we see approximately 85% ($His^{242/7}$), 85% (His^{288}), 49% (His^{67}), and 46% (His^{510}) depletion at 1 h. These data indicate that histidines and lysines exhibit roughly the same kinetic reactivity with HNE and that local, specific interactions are mainly responsible for the variation in their rates of addition. However with lysine, some sites are thermodynamically unfavorable and therefore will not be competitive because their reactions do not proceed to completion despite having reasonable intrinsic addition rates (*i.e.*, they must also have fairly high off-rates). The next question is what local environmental factors control the reactivity of the histidines and lysines.

<u>Relative Histidine Reactivity</u>

The targeted histidines divide clearly into a fast set (His^{67}, $His^{242/7}$, His^{288}, and His^{510}) and a slower set (His^{105} and His^{367}). His^{464} is a site at which no evidence of modification was found, making it suitable as a negative control for environmental factors that affect HNE reactivity. In examining the crystal structure of HSA,[134] one finds that in general the most active sites have good, but not exceptional, surface accessibility. This can be quantified by a simple calculation of the SASA associated with the residue.[135, 136] Although not a perfect measure of the environment, it provides some insight. Using the GETAREA program,[137] a plot of side chain and backbone SASAs for the histidines in HSA can be generated (Figure 3-7a). Although there is not an absolute pattern in this small data set, the general tendency is for moderate accessibility on the side chain and low relative accessibility on the backbone. This corresponds with sites that are near the surface, but recessed in pockets or seams on the protein surface. The obvious exception is His^{242}. In fact, His^{242} matches the characteristics of the negative control, His^{464}. Liebler and co-workers noted the unusual location of His^{242} and suggested its reactivity was linked to it being buried in a hydrophobic pocket with its imidazole having very low basicity. We cannot clearly separate the reactivity of His^{242} and His^{247} in our data so definite conclusions cannot be made. Of all the modification sites we have identified (His and Lys), none has exhibited a side chain SASA as low as His^{242} (see below), so high reactivity here would be unique for the protein.

(a)

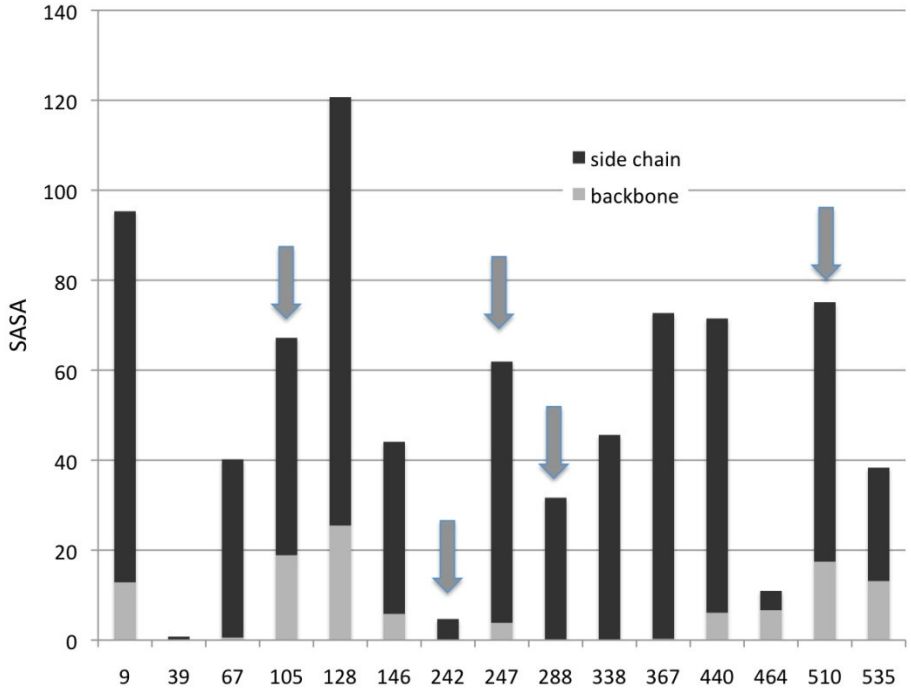
140
120
100
80
60
40
20
0
SASA
side chain
backbone
9
39
67
105
128
146
242
247
288
338
367
440
464
510
535

(b)

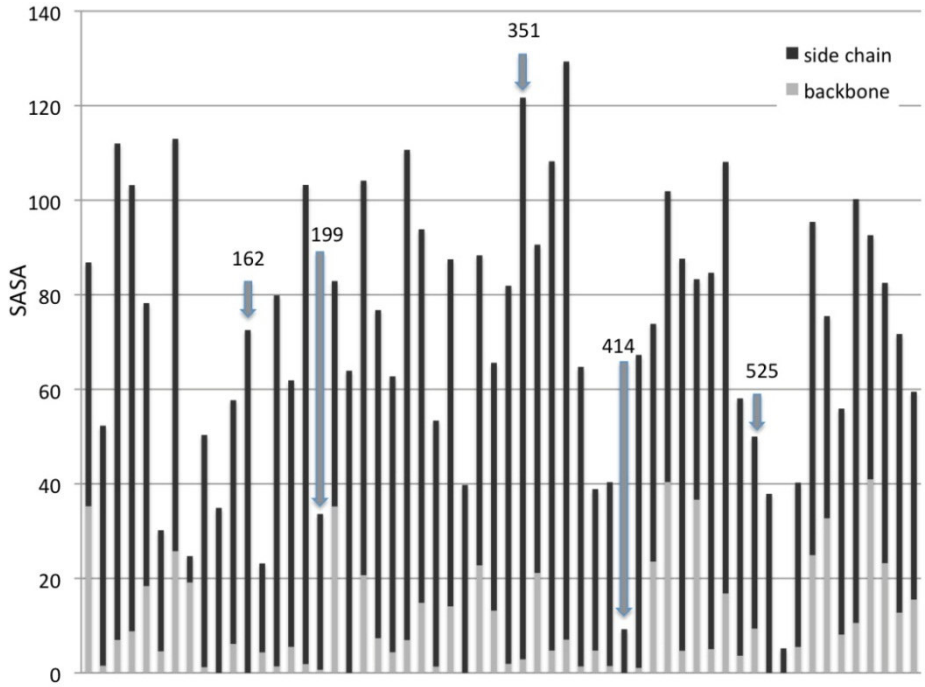
140
120
100
80
60
40
20
0
SASA
side chain
backbone
351
162
199
414
525

Figure 3-8. SASA in Å^2 for the (a) histidines and (b) lysines of HSA. Grey bars are the backbones and black bars are the side chains. Arrows indicate sites that were identified as being particularly reactive. In panel (b), the data is too extensive to include residue numbers, but highly reactive sites are labeled.

Relative Lysine Reactivity

The lysines are more interesting in that we have identified larger variations in rate/equilibrium constants and a larger data set is available. A similar pattern emerges in the plot of SASAs (Figure 3-7b). The most stable lysine adducts that we identified are Lys^{162}, Lys^{199}, Lys^{351}, Lys^{414}, and Lys^{525}. These residues follow the same general pattern as the histidines—one sees well to moderate accessibility on the side chains and very low accessibility on the backbone in the more reactive sites. Lys^{414} appears to be an exception, but it is in a groove and will have reasonable accessibility in some side-chain conformations. In fact, Lys^{414} is known to play a role in fatty acid binding (see below); in a crystal structure with myristic acid,[177] its SASA rises to 31.6 Å^2, a value consistent with other reactive lysines. It is interesting to note that of the 12 lysines that the GETAREA algorithm defines as exposed on the basis of their SASA values (side chain SASA > 82 Å^2 for lysine), only two were found to be modified in this study, Lys^{262} (a low reactivity site) and Lys^{351}, suggesting that high accessibility poorly correlates with the probability of HNE modification.

Overall Reactivity Patterns

Comparisons of relative site reactivity were made from experiments where HNE was used at

1.5 mM, a concentration almost certainly higher than any occurring naturally. It must be remembered that extensive protein modification could have occurred at long reaction times and caused changes in protein conformation that exposed normally unavailable residues to the solution. Furthermore, undetected modifications, which would enhance depletion of the corresponding unmodified peptide, could exist. Since rates were estimated from unmodified peptide depletion data, undiscovered pathways would result in an overestimation of the rate. However, for some of the lysines, alternative depletion pathways caused by modification of nearby residues might be detectable. Since modification at lysine prevents cleavage by trypsin, there is often more than one unmodified peptide that can be used to determine the rate (*i.e.*, either of the peptides flanking the missed cleavage point in the modified peptide). If the calculated rate was significantly different between these unmodified peptides, it would imply that another depletion pathway existed for the more rapidly depleted unmodified peptide. Comparative data is available for Lys^{233}, Lys^{262}, Lys^{351}, Lys^{414} and Lys^{525}. All except the unmodified peptides for Lys^{414} are similar, which given the supporting peptides, implies that there may be some reactivity at Lys^{413}.

We have a relatively small sample set, but it is possible to draw some general conclusion about the factors that control the relative reactivity of histidine and lysine residues of HSA with HNE. As noted above, some degree of surface accessibility is necessary, but highly exposed sites are generally unreactive. The presence of nearby hydrophobic grooves or patches is a common theme in the more reactive residues identified in this study. This is not completely surprising

given the fact that HNE does have a moderately hydrophobic tail and could benefit from hydrophobic interactions. Liebler noted this in his study and suggested a strong link between the hydrophobicity of the environment and reactivity.[165] It is well known that HSA has multiple binding sites for fatty acids and crystal structures are available for complexes.[177, 178] These binding sites provide a guide for locations that offer favorable hydrophobic interactions linked to a salt bridge interaction with a basic site. Interestingly, two of the strong lysine HNE binding sites, Lys^{414} and Lys^{525}, correspond directly with myristate binding sites (the carboxylate of a myristate binds to the ammoniums of these lysine residues).[177] In addition, two other strong HNE binding sites, Lys^{162} and His^{288}, are located adjacent to the hydrophobic pockets occupied by myristic acid. There certainly is not a one-to-one correspondence between the HNE and myristate binding sites (and one should not be expected given the differences in structure/binding), but the overlap that we have observed is at least suggestive and indicates that hydrophobicity might be playing a significant role in the HNE binding preferences. Liebler also suggested that the pK_a of a histidine played an important role in its relative reactivity.[165] This conclusion was driven by their identification of His^{242} as the most reactive histidine and an estimate of its imidazolium's pK_a that indicated that it was unusually acidic. As shown above, although we see evidence of high reactivity in the peptide containing His^{242} and His^{247}, the consensus of our data is not consistent with His^{242} being exceptionally reactive among the histidines (His^{288} is similar); therefore, the low, predicted pK_a does not appear to be a strong predictor of HNE reactivity.

Comparison to acrolein induced modifications

The overall modification sites in HSA induced by both aldehydes (acrolein and HNE) do not entirely overlap. Cys^{34} was detected as modified when both aldehydes were incubated with HSA. More modified histidines were identified from HNE treated HSA at a 1:1 molar ratio of aldehyde to HSA than with the acrolein treated HSA. All of the identified histidine modifications (His^{146}, His^{288} and His^{338}) found in the acrolein treatment was also found in the HNE treatment. However the His^{128} and His^{510} modifications found with HNE were not detected with acrolein treatment even at higher concentrations. The results are more diverse for lysine modifications. More modified lysines were identified with acrolein treated HSA than with HNE at the lower concentration of aldehydes. Only three lysine modifications (Lys^{351}, Lys^{525} and Lys^{545}) of the eight from the acrolein treatment were identified with HNE. The Lys^{51} modification was detected in acrolein treated HSA but not in HNE treatment; Lys^{199} and Lys^{240} were found to be modified by HNE but not by acrolein, even at a 10:1 molar ratio of aldehyde to HSA. A major, general difference is that acrolein tends to target lysines with greater surface accessibility than HNE. This is most likely a result of HNE being more hydrophobic and preferring sites near hydrophobic patches on the protein.

Conclusions

The addition of a prototypical α,β-unsaturated aldehyde, HNE, to HSA exhibits relatively high selectivity with only three of the potential 135 single addition modifications being identified at high confidence at an HNE:HSA ratio of 1:1. Even at high HNE:HSA ratios (100:1), our data suggests that only ten sites reach modification levels of 50% or more (assuming that most of the depletion of the unmodified peptide containing His^{242} and His^{247} is due to the generation of His^{242}). Our data indicate that aside from the highly reactive Cys^{34}, the next most kinetically reactive sites are Lys^{199}, $His^{242/7}$, and His^{288}. Although this reaction system has been studied in the past, it has not previously been recognized that the lysine modifications are under thermodynamic rather than kinetic control under typical *in vitro* experimental conditions and do not go to completion even with HNE:HSA ratios as high as 100:1. This result suggests that lysine modifications by HNE will only have biological relevance when local HNE concentrations are anomalously high or if secondary reactions make the additions irreversible. In contrast, the monitored histidine reactions in the study appeared to be going to completion under our conditions. Finally, the work demonstrates that care must be taken in the quantification of HNE modified residues by mass spectrometry because the modification can greatly alter the ionization/detection efficiency of the peptide. In this respect, the iTRAQ approach, with monitoring of both the modified and unmodified peptides, offers a powerful tool for quantifying the reaction progressions.

Chapter 4: *trans*-4-Hydroxy-2-nonenal Induced Aconitase Carbonylation and Its Impact to Enzyme Activity

Background

Aconitase (ACO) is a Krebs cycle (tricarboxylic acid cycle) dehydratase, which catalyzes the stereospecific conversion of citrate to isocitrate via the intermediate formation of cis-aconitate (Scheme 4-1).[179] It was first reported by Carl Martius in 1937.[180] Aconitase is present in both mitochondria and the cytosol of cells.[181, 182] Mitochondrial aconitase (m-aconitase) and cytoplasmic aconitase (c-aconitase) are associated, however obviously different enzymes. They have about 30% amino acids sequence similarity. M-aconitase is abundant in heart, but c-aconitase is abundant in liver. Both types of aconitase contain an ion-sulfur cluster. The cubic iron-sulfur cluster is essential for their catalytic activities in the active state. C-aconitase can be converted to an iron-regulatory protein (IRP) by disassembling its iron-sulfur cluster when the iron is insufficient. IRP binds to iron-responsive elements (IRE) on either the 5' or the 3' untranslated region of various mRNAs that encode proteins related to iron storage and transport.[179, 183-185] The two forms of the protein coexist *in vivo* depending on the iron level of cells. M-aconitase is similar to the c-aconitase form as an enzyme, containing an iron-sulfur cluster as well, but it does not act as an IRP.

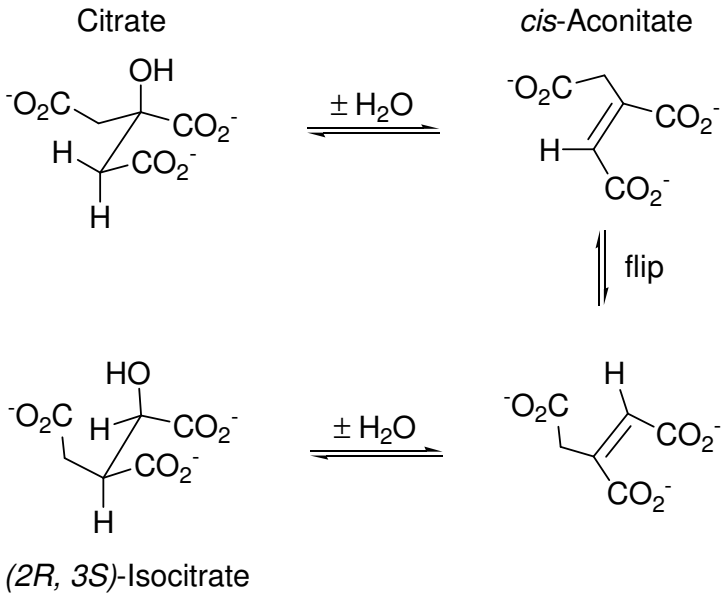

Scheme 4-1. Conversion of citrate to isocitrate via the intermediate formation of cis-aconitate by aconitase in a Krebs cycle.[179]

The porcine heart m-aconitase precursor consists of 781 amino acids (the first 27 residues is a mitochondrial targeting sequence) and an iron-sulfur cluster which plays the critical role in the enzymatic reaction.[186-188] In the active state of aconitase, the iron and inorganic sulfur are organized as a cubic $[4Fe\text{-}4S]^{2+}$ cluster.[189] An aconitase can be inactivated by oxygen damage resulting in the loss of the forth iron (Fe_α) from a specific site in the cluster and reform a new, stable $[3Fe\text{-}4S]^{+}$ cluster.[190-192] But inactivated aconitase can be rapidly reactivated by addition of Fe^{2+} and a reducing agent such as DTT, resulting in the formation of the $[4Fe\text{-}4S]^{2+}$ cluster.[193, 194] Each of three iron atoms in the iron-sulfur cluster forms a coordinate bond with one cysteine sulfur (C^{358}, C^{421} and C^{424}) of the protein backbone (Figure 4-1).[182, 186, 195] The Fe_α is ligated to inorganic sulfur and bound to hydroxyl from solvent.[187, 196]

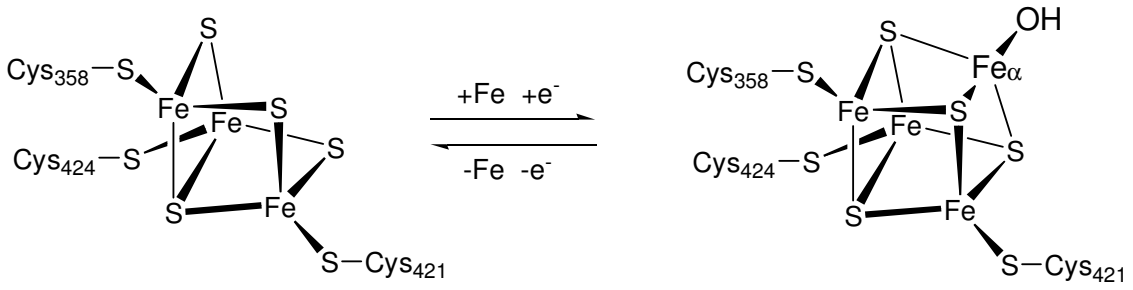

Figure 4-1. The formation of cysteine ligand with iron-sulfur cluster and transformation from $[3Fe\text{-}4S]^{+}$ to $[4Fe\text{-}4S]^{2+}$.[195]

During the tricarboxylic acid cycle, the Fe_{α} in the $[4Fe\text{-}4S]^{2+}$ cluster directly participates in the binding of the substrate to the enzyme by coordinating to hydroxide and the Cβ carboxyl of citrate (Figure 4-2).[195, 197] The coordination number of Fe_{α} increases to six from the substrate-free state. The intermediate product, cis-aconitate, binds with Fe_{α} in two ways, a citrate mode and an isocitrate mode. The two binding conformations transform by a 180° rotation around a perpendicular axis of the cis-aconitate double bond. The isocitrate coordinates with Fe_{α} by the hydroxyl and the Cα carboxyl.[192, 198-200]

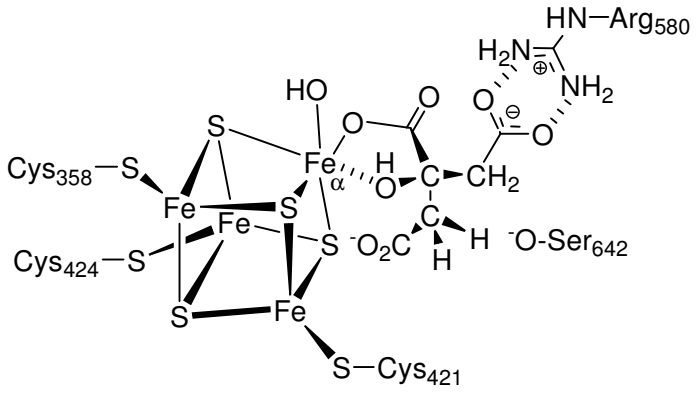

Figure 4-2. Binding of citrate with $[4Fe\text{-}4S]^{2+}$ and some residues in the active site region.

Although the fourth Fe could be considered as the critical active site of participating in substrate binding and catalysis, the cluster function is also controlled by the constraints imposed by the protein structure through the amino acid ligands and the amino acid residues surrounding the cluster.[200] The crystal structure has revealed that the active site region of aconitase involves the iron-sulfur cluster as well as 21 key amino acids side chains from all four domains of the protein (Figure 4-3).[182, 201] Active site residues are considered as such if they are in contact with the cluster or bound substrate, or are involved in hydrogen bonding with residues that directly bind with substrate.[182] The active site residues can be sorted into seven groups: cluster ligand cysteines (Cys^{358}, Cys^{421} and Cys^{424}); asparagines hydrogen bonding with inorganic or cysteine sulfur (Asn^{258} and Asn^{446}); histidines with aspartic acid or glutamic acid pairs (His^{101}/Asp^{100}, His^{147}/Asp^{165} and His^{167}/Glu^{262}); arginines in contact with substrate carboxyl groups (Arg^{447}, Arg^{452}, Arg^{580} and Arg^{644}); the catalytic base serine (Ser^{642}); serines and glutamine hydrogen bonding with substrate (Gln^{72}, Ser^{166} and Ser^{643}); isoleucine (Ile^{425}), which has a significant hydrophobic contact with the cluster; and an aspartic acid (Asp^{568}), which is hydrogen bonded to active site residues Arg^{452} and Arg^{644}.[182] Overall, the active site region is a mixed combination of residues which forms hydrogen-bonding network with the iron-sulfur cluster, substrate, water molecules and other residues etc..[182, 200] The involvement of 21 residues may provide a partial explanation of why aconitase is a large protein.[182] Mutational studies of some of the active site residues have proved that these residues are essential for the catalytic activity of aconitase.[202] The mutation of ligand cysteines to serines caused complete loss of activity. The mutations of Ser^{642} to alanine and Arg^{580} to lysine showed a 10^5 fold decrease in activity. The mutation of

His[101] to asparagine and Asp[100] to serine caused enzymatic activity to drop 3 orders of magnitude.[182, 202]

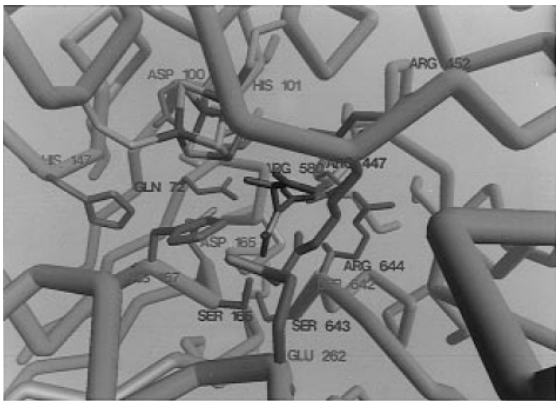

Figure 4-3. The active site region in mitochondrial aconitase. The side chains of 14 key active residues, iron-sulfur cluster and bound isocitrate are shown with labels.[201]

It was reported that m-aconitase is sensitive to reactive oxygen and nitrogen species.[203] Superoxide anion (O_2^-), hydrogen peroxide (H_2O_2) and peroxynitrite ($ONOO^-$) have been shown to inactivate mitochondrial aconitase through disturbing the $[4Fe\text{-}4S]^{2+}$ cluster.[196, 204-207] During this reaction, iron (II) is released from the cluster resulting in an inactive $[3Fe\text{-}4S]^{1+}$ form. The oxidation of m-aconitase plays an important role in mitochondrial oxidative damage, which is related to several diseases and aging.[208-210] However, there is not much details related to modulating aconitase activity through the oxidative modifications of amino acids.

As a reactive carbonyl species, HNE may modulate m-aconitase activity by modifying amino acids in the active site of the enzyme. In this project, we investigate the reaction of HNE with

m-aconitase *in vitro*. The reaction also was tracked as a function of time using an iTRAQ labeling strategy.

Experimental Procedures

Chemicals

Mitochondrial aconitase from porcine heart (Product A5384), IAM, DTT, urea, 10×PBS and 4-(2-hydroxyethyl)-1-piperazineethanesulfonic acid (HEPES) concentrate were purchased from Sigma-Aldrich (St. Louis, MO). HNE and enzymatic assay kits were obtained from Cayman Chemical (Ann Arbor, MI). Sequencing grade modified trypsin was from Promega (Madison, WI) and chymotrypsin was from Roche Diagnostics (Indianapolis, IN). Laemmli sample buffer was from Bio-Rad (Hercules, CA). Anti-HNE monoclonal antibody was purchased from Japan Institute for the Control of Aging (Haruoka, Japan). Enhanced chemiluminescence (ECL) kits were obtained from GE Healthcare (Pittsburgh, PA). BCA Protein Assay kits and Imperial protein stain were purchased from Thermo Fisher Scientific (Rockford, IL) and iTRAQ reagent kits were obtained from Applied Biosystems (Foster City, CA).

Experiments

Aconitase modification

Aconitase at 12 μM in 1× PBS buffer (pH 7.4) was incubated with HNE at various final HNE:ACO molar ratios (1:1, 2:1, 10:1, 50:1, 100:1). All reactions were carried out at 37°C with gentle shaking. The reaction time was 2 h for all experiments except those in which the reaction time was intentionally varied. Excess HNE were consumed by reacting with 10 times DTT at room temperature for 30 min. Modified proteins were denatured by adding 6 M urea and

stabilized by adding $NaBH_4$ to a final concentration of 5 mM and incubating for 60 min at room temperature. Repeated washes employing centrifugal filter devices (Millipore, Billerica, MA) were used to remove reagents and concentrate the sample for sodium dodecyl sulfate-polyacrylamide gel electrophoresis (SDS-PAGE) separation; the molecular weight cut-off for the centrifugal filter devices used was 50 kDa.

SDS-PAGE and in-gel enzymatic digestion

Modified protein was heated at 95°C for 5 min after mixing with the same volume of 2×Laemmli sample buffer. Aliquota of the mixture were loaded into each well and then separated by a homemade 4% stacking gel and 8% running gel. The final gel was stained using Imperial protein stain. The molecular weight of the different proteins in the sample was indicated by a protein ladder. The gel band containing aconitase was carefully cut out and washed. Prior to digestion, proteins in the sliced gel band were reduced with DTT and alkylated with IAM. The tryptic and chymotryptic digestion was carried out overnight at 37°C. Digestion products were extracted from the gel using 0.1% formic acid/5% acetonitrile and 0.1% formic acid/50% acetonitrile followed by centrifugal evaporation.

Western Blot

A similar amount of nonreducing, modified aconitase (40 µg) from various HNE to ACO molar ratios (0:1, 1:1, 5:1 and 10:1) was loaded on an 8% SDS-PAGE gel, and then transferred to a polyvinylidene difluoride (PVDF) membrane. The membrane was blocked for 1 h at room

temperature with 5% milk in tris-buffered saline with tween 20 (TBST) and incubated with anti-HNE in 5% bovine serum albumin (BSA) (1:1000) overnight at 4°C. The blocked membrane was then washed with TBST and incubated with horseradish peroxidase (HRP) conjugated anti-mouse in 5% BSA (1:5000) for 1 h at room temperature. Following washing with TBST, the signal was developed with ECL detection reagents.

iTRAQ reagent labeling

Aconitase was incubated with HNE at a HNE:ACO molar ratio of 10:1 at 37°C. The reactions were quenched by adding DTT, urea and $NaBH_4$ in turn at 0, 1, 2, and 6 h. After SDS-PAGE separation and in-gel tryptic digestion, the concentrations of the HNE-modified peptide mixtures were measured using the BCA protein assay. Peptide mixtures were desalted using C18 MicroSpin columns (The Nest Group, Southboro, MA) and dried using a centrifugal evaporator. Solid peptide mixtures (containing 25 ug total peptides) were then reconstituted in 25 ul iTRAQ dissolution buffer. Four iTRAQ reagents (114-117) were dissolved in 70 µl ethanol separately. Each iTRAQ reagent aliquot was added to one of the peptide mixtures in the following sequence: 114 for the 0 h sample (control); 115 for the 1 h sample; 116 for the 2 h sample; and 117 for the 6 h sample. After incubation for 2 h at room temperature with gentle shaking, all four peptide mixtures were combined and then purified using a Waters (Milford, MA) Oasis MCX solid phase extraction cartridge. The final sample was dried using a centrifugal evaporator and then re-suspended in HPLC equilibration mobile phase for µLC-MS/MS analysis.

Enzymatic assay

Aconitase at 12 μM in 1× HEPES buffer (pH 7.4) was incubated with HNE at various final HNE:ACO molar ratios (1:0, 1:1, 10:1, 50:1) for 2 h or at a HNE:ACO molar ratio of 10:1 with various reaction time frames (0 h, 1 h, 2 h, 6 h). All reactions were carried out at 37°C with gentle shaking. Modified proteins were precipitated and washed with 80% $(NH_4)_2SO_4$ on ice. The concentrations of the HNE-modified proteins from different molar ratios or time frames were determined using the BCA protein assay. Aconitase activity assay was performed following the manufacture's protocol. Modified aconitase from different preparations were activated by incubating with activation solution (50 mM cysteine hydrochloride and 1 mM ferrous ammonium sulfate in 1× Tris-Cl buffer) for 1 h on ice. Activated samples, nicotinamide adenine dinucleotide phosphate ($NADP^+$), isocitric dehydrogenase and citrate were added into wells of an assay plate in the order, followed by incubation at room temperature for 30 min. All the samples were assayed in triplicate in the presence and absence of inhibitor. The absorbance was monitored once every other minute at 340 nm for 30 min by a plate reader.

μLC-MS/MS analysis

1. HNE adduct identification

Adduct identification was performed using a Thermo (San Jose, CA) LTQ XL linear ion trap mass spectrometer, equipped with ETD, and by a Thermo LTQ Orbitrap Velos mass spectrometer. The LTQ XL was interfaced with a Thermo Surveyor capillary HPLC system. Peptides were separated on a reversed-phase, C18 column (150 μm × 10 cm, 5 μm particles, 300

Å pores; Column Technology, Fremont, CA) at a flow rate of ~1 µl min^{-1} using 0.1% formic acid in water as mobile phase A and 0.1% formic acid in methanol as mobile phase B. Approximately 2 µg of peptides were injected and a Michrom (Auburn, CA) CapTrap trapping column was used for rapid sample injection. The gradient started from 2% B, then increased to 15% B over 5 min, then increased to 80% B over 70 min, and finally increased to 95% B over 15 min. The eluted peptides were introduced into the LTQ XL with a nanospray source operating at a spray voltage of 2.1 kV, a capillary voltage of 21 V, and a capillary temperature of 200°C. A full scan in the m/z range 300-2000 was performed to obtain precursor ions, followed by four data-dependent CID MS/MS scans for the four most abundant precursor ions in the full scan. Dynamic exclusion was used, that is, if the same precursor ion was picked for fragmentation twice within a 30 s window, it was excluded from further analysis for 180 s. For the Thermo LTQ Orbitrap Velos system, separations were performed on a Waters nanoACQUITY reversed-phase, C18 column (100 µm × 10 cm; 1.7 µm particles). Elution was achieved using a gradient of 0.1% formic acid in acetonitrile (B) versus 0.1% formic acid in water (A) at a flow rate of 0.4 µL min−1. Approximately 2 µg peptides were injected, with the loading and equilibration mobile phase being 1% B. The linear gradient ran to 15% B after loading at 1% B over 25 min, followed by an increase to 25% B over 35 min, followed by an increase to 35% B over 40 min, and followed by an increase to 85% B over 20 min. The nanospray ion source was operated at 3.5 kV.

2. iTRAQ reagent-labeled peptide quantification

Analysis of iTRAQ reagent-labeled samples was performed only by a Thermo LTQ Orbitrap Velos mass spectrometer. For the Orbitrap-based system, most operating parameters remained the same as those used for HNE adduct identification except that HCD replaced CID.[170] For HCD, the normalized collision energy was 40 and the activation time was 0.1 ms; the top eight most abundant ions in each precursor ion scan were subjected to HCD fragmentation. A targeted mass list was used and, therefore, dynamic exclusion was not enabled.

Database searching and data processing

Peptide sequences and modifications were identified using the BioWorks version 3.3.1, SP1 implementation of Sequest (Thermo). No scan grouping was performed in preparing peak lists for database searching. The protein sequence database used consisted of the NCBI RefSeq version of the complete porcine proteome and reversed versions of all sequences. Reversed sequences permit false discovery rate estimation. Sequences were downloaded on October 1, 2009, and the final database contained 43958 entries. Only fully-tryptic peptides were considered and up to three missed cleavage sites were allowed. Precursor ion tolerances were ±2 Da for linear ion trap measurments and ±15 ppm for Orbitrap measurements. Fixed mass shifts were applied for alkylated cysteines (+57 Da) while differential amino acid mass shifts were incorporated for $NaBH_4$-reduced Michael adducts at histidine and lysine (+158 Da) and at cysteine (+101 Da when the fixed mass shift at cysteine is considered), $NaBH_4$-reduced Schiff base adducts at lysine (+140 Da), and oxidized methionines (+16 Da). Mass shifts were added to Sequest parameters files at high-precision (see Appendix Table A1 for non-iTRAQ and Table A2

for iTRAQ experiments) for compatibility with highly accurate Orbitrap precursor ion measurements and a maximum of four variable modifications were permitted for each peptide. In searches with the iTRAQ labels present, fixed mass shifts of +144.104 Da were used for the peptide N-terminus and non-carbonylated lysine residues, which resulted in the differential mass shifts associated with HNE modification at lysine being changed to +14.027 Da (Michael adducts) and −3.984 Da (Schiff base adducts). MS/MS spectra for modified peptides were manually examined and any found to be inconsistent with the proposed identification were rejected.

Intensity measurements for iTRAQ reporter ions (114-117) were processed using Microsoft Access. MS/MS spectra for which all four reporter ion intensities were zero were first rejected. Reporter ion counts for all MS/MS spectra supporting each identified peptide were combined by averaging and then normalized by dividing the combined intensity of relative reporter ion from the targeted internal standard peptide (WVVIGDENYGEGSSR). Depletion plots were scaled to 100% for the control to allow comparison on the same axes while accumulation plots were not altered. Accumulation plots were simply the normalized raw intensity or the logarithm of it.

Results

HNE is a reactive carbonyl species and a byproduct from lipid peroxidation. The major mode of reaction of HNE with proteins is Michael addition to the nucleophilic amino acid side chains of cysteine, histidine and lysine to give stable adducts. HNE can also form a Schiff base with lysine's side chain.[77, 146] All of the Michael additions lead to products bearing an aldehyde functional group whereas the Schiff base contains an imine instead. The m-aconitase is an 82 kDa protein with 12 cysteines, 25 histidines and 53 lysines. There are no disulfide bridges, but side chains of three cysteines are coordinated with the iron-sulfur cluster as ligands.[186, 187] Some mutation studies of active site residues in m-aconitase have confirmed that changes in the active site can reduce or eliminate the catalytic activity of the enzyme.[182, 202] HNE may modulate m-aconitase activity by modifications of amino acids in the active site of the enzyme.

Western Blotting

To confirm the modification of the protein, monoclonal anti-HNE was used to detect HNE modifications in samples of aconitase treated with HNE. The anti-HNE is particularly sensitive to modified histidines in proteins. Both reduced and unreduced samples were analyzed (i.e., treated or not treated with $NaBH_4$ after HNE modification). HNE-modified proteins were detected only from an unreduced sample. This is not surprising because the antibody is designed for the unreduced form of the HNE modification. An increased modification level was observed at the higher molar ratios of HNE to aconitase (Figure 4-4). The band position of aconitase only

could be determined roughly because the anti-aconitase antibody used to identify it was only weakly responsive in this study. The other present bands having steady blotting with the increased HNE concentrations are mostly caused by the unspecific binding of antibody.

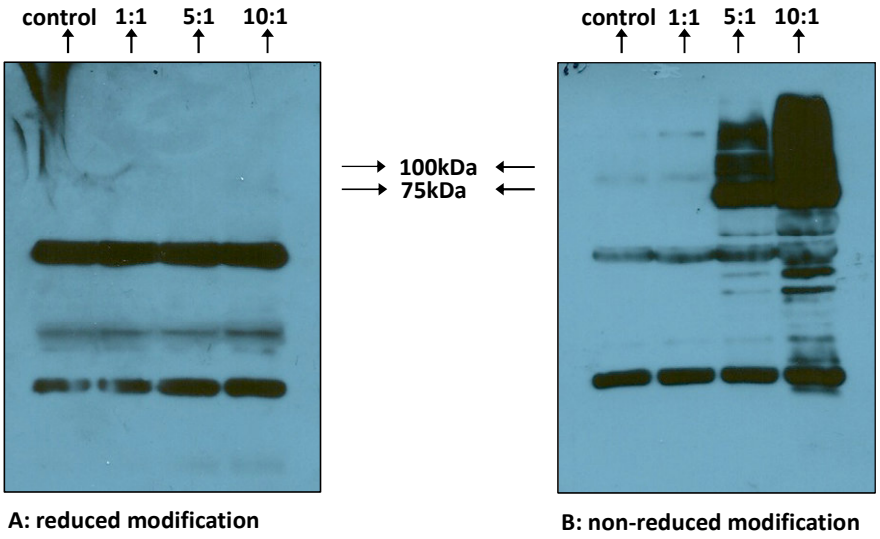

Figure 4-4. Western blot of HNE modifications. A: reduced modifications with increasing molar ratios of HNE to aconitase (control, 1:1, 5:1 and 10:1); B: non-reduced modifications with increasing molar ratios of HNE to aconitase (control, 1:1, 5:1 and 10:1).

Modification Sites

The first aim of the project was to identify the key modification sites when m-aconitase was treated with HNE. Starting with an aconitase concentration of 12 μM, HNE:ACO ratios from 1:1 to 50:1 were surveyed and data are report in Table 4-1. The experiment was repeated four times at each of the different ratios. Three repeats were analyzed using the linear ion trap system while one was investigated using the Orbitrap system. Results from trypsin and chymotrypsin digestions were combined together. Only one LC-MS/MS run was recorded for each sample

preparation due to the limited amount of sample from the in-gel digestion. Modifications detected using the liner ion trap instrument and validated by manual inspection of the MS/MS spectra were regarded as medium confidence; those confirmed with complementary data from the orbitrap system were regarded as high confidence. These data are also presented in terms of modified peptide (rather than modification site as found in Table 4-1) as Appendix Table A8. Site identifications were supported only by CID data. ETD was not used in this study.

It was possible to identify more modification sites when the amount of HNE was increased. At a 1:1 ratio of HNE to aconitase, five sites were identified: Cys^{358}, Cys^{421}, Cys^{565}, His^{13} and His^{98} (the residue numbers are for the secreted protein; to convert to nascent protein numbering add 27). Only Cys^{358} and Cys^{565} were identified at high confidence. As the molar ratio increased to 2:1, eight modifications were detected. Four of them are at high confidence. At a ratio of 10:1, there are 22 identified modifications and 14 of them are at high confidence. When the molar ratio was raised to 50:1, more modified histidine and lysine residues were detected, but the four cysteine modifications found at lower ratios became less apparent and gave less confident identifications. In general, the identifications were very reproducible, but the concentration dependence indicates that in some cases, the peptides were at a concentration that was close to the threshold for our identification criteria. The combined sequence coverage is around 78% for the LTQ analysis and 68% for the Orbitrap analysis. It is possible that some peptide fragments having modification sites were not detected. Schiff base formation of lysine adducts were found only on Lys^{384} and Lys^{564}. However, they were not investigated further.

Three of the five modifications that were identified at the lowest HNE concentrations were cysteines. Two of these, Cys^{358} and Cys^{421} are in the active site and involved in the iron-sulfur cluster. This result matches previous research that showed that cysteine is the most reactive Michael addition site in proteins, but it is noteworthy that the iron-sulfur cluster is available for modification by HNE. As the amount of HNE increases, first more histidines appear as modified, then more lysines. It might be tempting to conclude that the reactions with histidine are less selective because a higher percentage of them are modified, but the larger number of modification sites is also driven by the fact that the reaction is more favorable and more of the HNE is naturally adducted to histidines at a given ratio. However, effects other than concentration also can have a major impact on the ability to identify modifications. Some care needs to be employed in analyzing data from these types of experiments. Therefore, a more direct quantification method, such as iTRAQ reagent labeling is needed for ranking reactivities.

It is also interesting to note that the solubility of the incubated sample declined as the amount of HNE or incubation time increased. Furthermore, some of the identified modification sites at the low molar ratios were not detected at higher ratios. The quantity of corresponding MS/MS spectra also dropped. This is possibly explained by cross linking between HNE-modified residues and lysine side chains by Schiff base formation, leading to peptides that could not be identified by our SEQUEST approach. This cross-linking is also expected to reduce solubility and potentially inhibit digestion by trypsin and chymotrypsin.

Table 4-1. List of identified modification sites based on linear ion trap data (represented by number) and Orbitrap data (represented by *). Bolded with underscore sites represent active site residues. Manual MS/MS spectrum validation was required in all cases.

Modification Site[a]	Enzyme[b]	1:1[c]	2:1[c]	10:1[c]	50:1[c]
Cys^{99}	T	0	1*	1*	2
Cys^{305}	C	0	1	2	0
$\underline{Cys^{358}}$	**T**	**3***	**3***	**3***	**3***
$\underline{Cys^{421}}$	**T**	**2**	**1**	**3***	**1**
$\underline{Cys^{424}}$	**T**	**0**	**0**	**3***	**1***
Cys^{565}	T	3*	3*	3*	3*
His^{9}	T	0	0	0	1
His^{13}	T	1	1	3*	3*
His^{46}	T	0	0	3*	3*
His^{46}	C	0	0	3*	3*
His^{98}	T	1	1	2	3*
$\underline{His^{101}}$	**T**	**0**	**0**	**3***	**3***
$\underline{His^{147}}$	**C**	**0**	**0**	**0**	**1**
His^{321}	C	0	0	2*	3*
His^{379}	T	0	0	0*	0*
His^{460}	T	0	1*	3*	3*
His^{460}	C	0	0	3	3*
His^{519}	T	0	0	3	3*
His^{569}	T	0	0	2	2*
His^{668}	T	0	0	1*	2*
His^{717}	T	0	0	1	1
His^{729}	T	0	0	0	1*
Lys^{23}	T	0	0	1	2
Lys^{117}	T	0	0	3*	3*
Lys^{218}	T	0	0	1	2
Lys^{490}	T	0	0	0	3
Lys^{496}	T	0	0	2	3
Lys^{674}	T	0	0	0	1*

[a] Secreted protein numbering; add 24 for nascent protein

[b] T indicates Trypsin digestion; C indicates Chymotrypsin digestion

[c] Applied HNE:ACO molar ratio. Values are counts of LC-MS/MS runs in which the modified site was identified using linear ion trap CID scans (maximum=3) and linear ion trap CID scans associated with high mass accuracy Orbitrap precursor ion mass measurements (*)

Relative Modification Levels Based on iTRAQ labeling

In a quadrupole ion trap, such as that found in the LTQ XL instrument used to identify modification sites, it is very difficult to simultaneously trap low mass iTRAQ reporter ions and the b- and y-ions needed for peptide identification because the mass window is fundamentally limited. Although PQD technology[175] has partially alleviated this limitation, in this project, the signal of iTRAQ reporter ions from PQD analysis was still low. Thus, the LTQ Orbitrap Velos instrument was applied to improve accuracy. A targeted mass list of anticipated peptides (modified and unmodified) was used. A list of the 12 modified peptides targeted in these studies is given in Table 4-2; 17 modifications at 12 residues were considered. In addition, unmodified versions of these peptides were also targeted (a full list of all targeted peptides with *m/z* values used is given as Appendix Table A9). In some cases, more than one unmodified version was needed because the modified peptides contained a missed cleavage – a version with and without the missed cleavage was included in the list. A peptide with no HNE addition sites was put in the list as an internal standard (WVVIGDENYGEGSSR) for normalizing the intensity of reporter ions. Since the methods in this project may impact the stability of imines formed between HNE and lysine, Schiff base formation of lysine adducts was not included in the iTRAQ analysis (actually, the detected Schiff base formation was very limited). By targeting masses and not employing a dynamic exclusion protocol, many more MS/MS spectra containing iTRAQ reporter ions can be recorded and averaged during a chromatographic run. However, it was not practical to monitor all the potential HNE modifications in m-aconitase in this way (there are too many

potential peptides masses). Only the sites identified at significant modification levels were included. Most of the modification sites from Table 4-1 were included.

Table 4-2. List of modified peptides included in the targeted mass list.

Modified Peptide[a]	**Modification Site**[b]
VAVPSTIHC@DHLIEAQLGGEK	Cys^{99}
VAVPSTIH^C@DHLIEAQLGGEK	Cys^{99} /His^{98}
VAVPSTIHC@DH^LIEAQLGGEK	Cys^{99} / His^{101}
VAVPSTIH^C@DH^LIEAQLGGEK	Cys^{99} / His^{98} / His^{101}
VAVPSTIH^C*DHLIEAQLGGEK	His^{98}
VAVPSTIHC*DH^LIEAQLGGEK	His^{101}
VAVPSTIH^C*DH^LIEAQLGGEK	His^{98} / His^{101}
VGLIGSC@TNSSYEDMGR	Cys^{358}
VGLIGSC@TNSSYEDM#GR	Cys^{358}
DVGGIVLANAC@GPC*IGQWDR	Cys^{421}
DVGGIVLANAC*GPC@IGQWDR	Cys^{424}
DVGGIVLANAC@GPC@IGQWDR	Cys^{421} / Cys^{424}
C@TTDHISAAGPWLK	Cys^{565}
C@TTDH^ISAAGPWLK	Cys^{565} / His^{569}
C*TTDH^ISAAGPWLK	His^{569}
VAMSH^FEPHEYIR	His^{9}
VAM#SH^FEPHEYIR	His^{9}
VAMSHFEPH^EYIR	His^{13}
VAM#SHFEPH^EYIR	His^{13}
VAMSH^FEPH^EYIR	His^{9} / His^{13}
VAM#SH^FEPH^EYIR	His^{9} / His^{13}
IVYGH^LDDPANQEIER	His^{46}
NDANPETH^AFVTSPEIVTALAIAGTLK	His^{460}
AEFDPGQDTYQH^PPK	His^{519}
AK~DINQEVYNFLATAGAK	Lys^{117}
FNPETDFLTGK~DGK	Lys^{490}
FK~LEAPDADELPR	Lys^{496}
K~QGLLPLTFADPADYNK	Lys^{674}
[a] Unmodified versions of the listed modified peptides were included in the list. If the modified peptide contains a missed cleavage, an additional peptide (without the missed cleavage) was also included. A peptide	

(WVVIGDENYGEGSSR) without HNE modification sites was also included as an internal standard; C* indicates carboxyamidomethylation at Cys; C@ indicates HNE Michael addition at Cys followed by reduction; H^ indicates HNE Michael addition at His followed by reduction; K~ indicates HNE Michael addition at Lys followed by reduction; M# indicates oxidation at Met
[b] Secreted protein numbering; add 27 for nascent protein

Effect of Incubation Time on the Level and Distribution of HNE Modifications

Incubation times of 1, 2, and 6 h were used with an HNE:ACO ratio of 10:1. The Orbitrap-based instruments was employed with the list of targeted peptides (Table 4-2) to maximize the number of MS/MS collected for each peptide, thus enhancing the signal-to-noise ratio in the iTRAQ data. The data presented are the result of three replicated LC-MS/MS runs from a single preparation. In this study, higher HNE concentrations and longer incubation times cannot be applied due to the poor solubility of aconitase under these experimental conditions. One unmodified peptide was chosen as an internal standard (WVVIGDENYGEGSSR) to correct for declining overall signal intensity caused by possible protein precipitation during long incubations. The measurements are listed in tabular form in Appendix Table A10.

Data for targeted cysteines are shown in Figure 4-5. All the targeted cysteines were detected except Cys^{424}, which is difficult to confidently identify because it is located on the same tryptic peptide as Cys^{421}. Very high quality MS/MS are required to unambiguously identify one particular site when another site on the same peptide must also be considered. In this case, strong evidence was only found for Cys^{421}. Tryptic peptides having both Cys^{421} and Cys^{424} modified were not found. In the listed sites, Cys^{99}/$His^{(98/101)}$ and Cys^{565}/His^{569} also share the same tryptic

peptides. In these cases, all the possible modifications share the same unmodified parent peptide and cannot be distinguished in plots of parent peptide depletion rates. Modified and unmodified peptides for the Cys^{358} site were both detected, with and without an oxidized methionine; the oxidized and non-oxidized forms had a similar contribution in constructing these plots. Figures 4-5a and 4-5b illustrate the depletion of parent peptides and the accumulation of modified peptides from Orbitrap measurements. Generally, the depletion plots are easier to compare because the starting and end points are well defined - 100% intensity at time zero and 0% intensity at reaction completion. In contrast, we have no information about the expected absolute intensity at 100% conversion (standards are not available). As a result, it is not possible to relate the intensity of the modified peptides to relative concentrations. In addition, the modified peptides often give low signal intensities due to low concentrations in some cases and potentially poor ionization properties in others. Unfortunately, three of the four identified cysteine modifications are on peptides with more than one potential site. The simple case is Cys^{358}, which exhibits about 20% depletion at 6 hours in its parent peptide. Much of the reaction appears to be complete in the 1^{st} hour and this is confirmed in the accumulation plot. The modifications at Cys^{421} and Cys^{424} share the same peptide. Because both are part of the iron-sulfur cluster, distinguishing between them is not as critical. They exhibit over 60% depletion at 6 hours. The cysteines that share peptides with histidine modifications are more difficult to analyze. However, some insight can be gained by examining the kinetic profiles. For the peptides containing Cys^{99} and Cys^{565}, most of the observed depletion occurs in the first 2 hours. This is mirrored in the accumulation plots for the two modifications. In contrast, the accumulation plots for the

corresponding histidine modifications are more linear and substantial accumulation occurs between 2 hours and 6 hours (Figure 4-6b). The match of kinetic profiles (accumulation *vs*. depletion) for the cysteines strongly suggests that the majority of the depletion in the parent peptide is due to cysteine modification. It is likely that the histidines represent only a small fraction of the depletion at early times and play a greater role late in the kinetic studies. As a result, it is reasonable to assume that the depletion of the parent peptides of Cys^{99} and Cys^{565} is mainly caused by cysteine modifications at the 6 h time point.

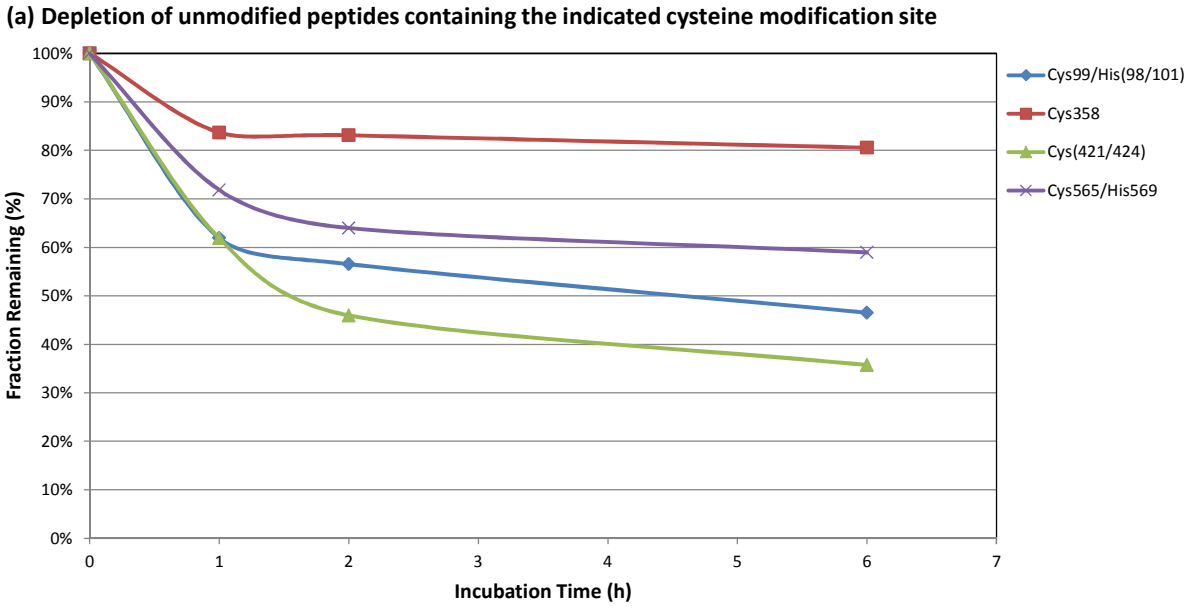

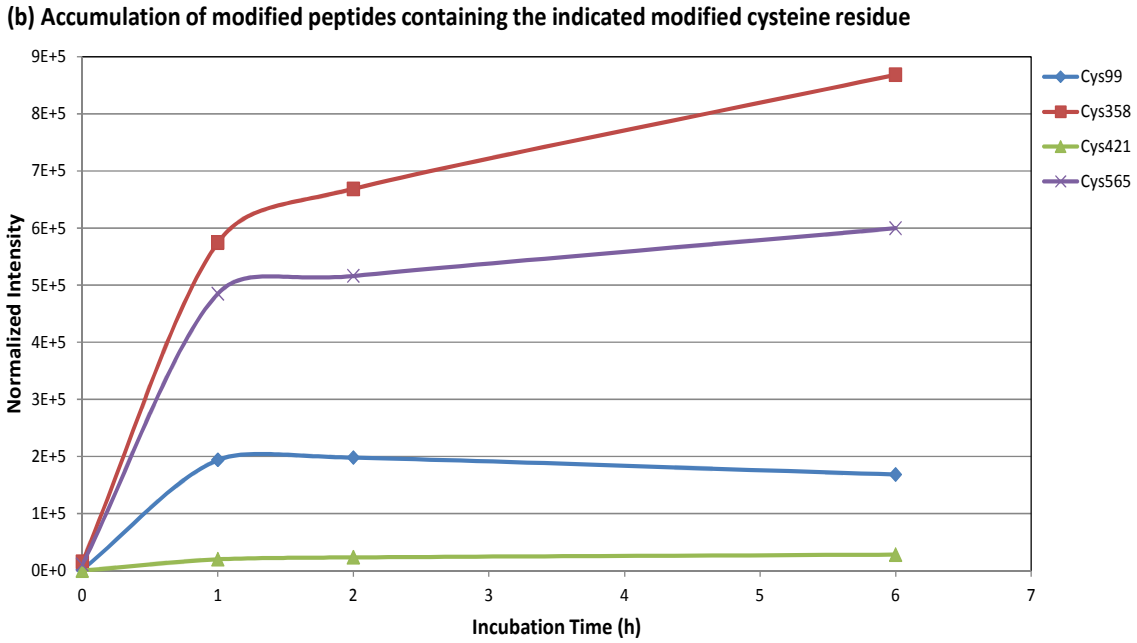

Figure 4-5. Effect of varying reaction duration, at a fixed HNE:ACO ratio of 10:1, on reaction progress measured using iTRAQ reporter ion intensity for targeted cysteine sites. The targeted mass list was used with Orbitrap/HCD measurement. Depletion plots are scaled to 100% for the control while normalized absolute intensities are given in the accumulation plots. Relative abundance measurements were not obtained for targeted site Cys^{424}, although this site shares the same unmodified peptide with Cys^{421}.

Data for the histidines are presented in Figure 4-6. Seven of eight targeted modification sites were identified using the Orbitrap, with the exception being His^{101}, which is located on the same tryptic peptide as His^{98}. Two tryptic peptides containing two sites $His^{(9/13)}$ and $His^{(98/101)}$ were also detected. Modified and unmodified peptides for sites $His^{(9/13)}$ were both detected, with and without an oxidized methionine - the oxidized and non-oxidized forms had the similar contributions in constructing these plots. Figure 4-6a and 4-6b illustrate the depletion of parent peptides and the accumulation of modified peptides from Orbitrap measurements. As discussed above, it is likely that much of the depletion seen in peptides sharing a cysteine and histidine is

due to the cysteine. As a result, His^{460} stands out as an exceptionally reactive histidine. Only modest depletion is seen for the other histidines and the accumulation plots indicate that many of the histidines are far from reaching complete reaction at 6 hours; they still retain nearly peak reaction velocities.

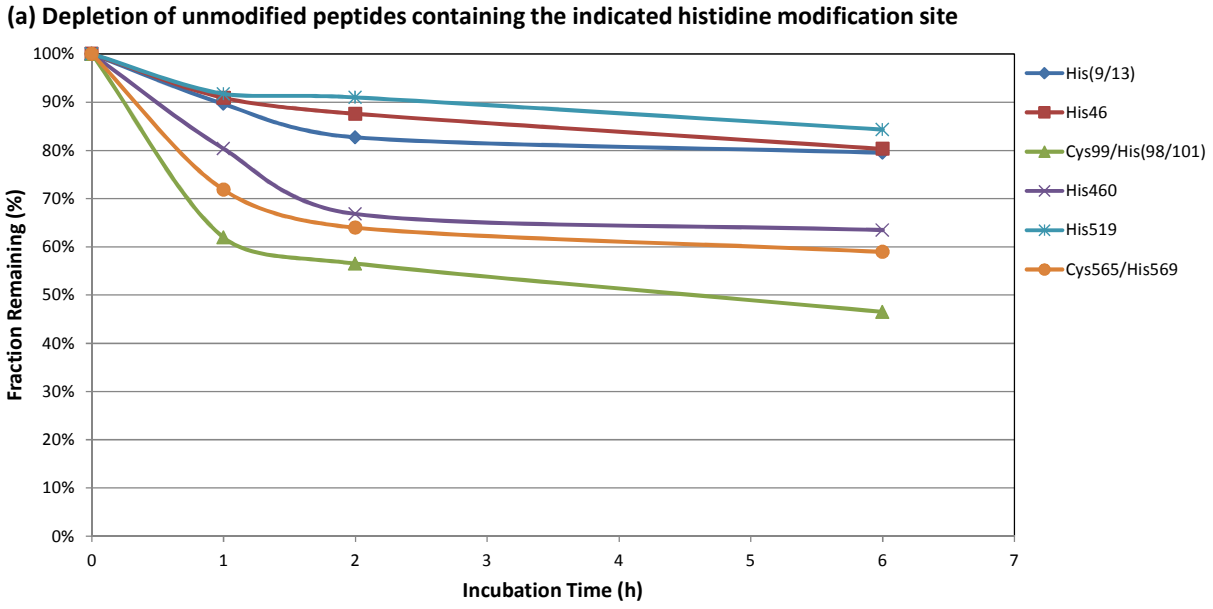

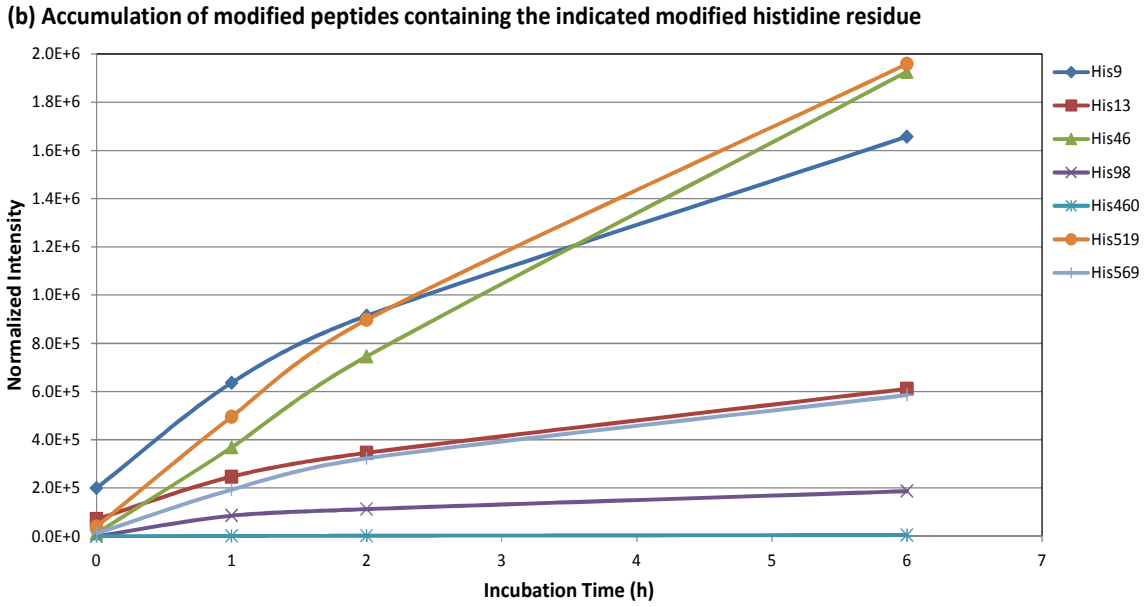

Figure 4-6. Effect of varying reaction duration, at a fixed HNE:ACO ratio of 10:1, on reaction progress measured using iTRAQ reporter ion intensity for targeted histidine sites. The targeted mass list was used with Orbitrap/HCD measurement. Depletion plots are scaled to 100% for the control while normalized absolute intensities are given in the accumulation plots. Relative abundance measurements were not obtained for targeted site His^{101}.

Data for the listed lysines are presented in Figure 4-7. Three of the four targeted lysines were detected - the exception is Lys^{490}. Figures 4-7a and 4-7b illustrate the depletion of the parent peptides and the accumulation of the modified peptides from Orbitrap measurements. In the depletion plots for the listed lysine series, the depletion for all parent peptides is very limited. The changes seen in the plot are at the uncertainty of the measurement and not meaningful. It indicates that the lysine reaction towards HNE is inefficient. In the accumulation plots, significant background modification is seen at time zero. This may represent a small concentration of the modification present in the starting aconitase or be background noise in the iTRAQ ion region of the spectrum. In either case, the plots in Figure 4-7 indicate that lysine

modifications are not significant under these conditions and only reach concentrations suitable for detection, but not quantification.

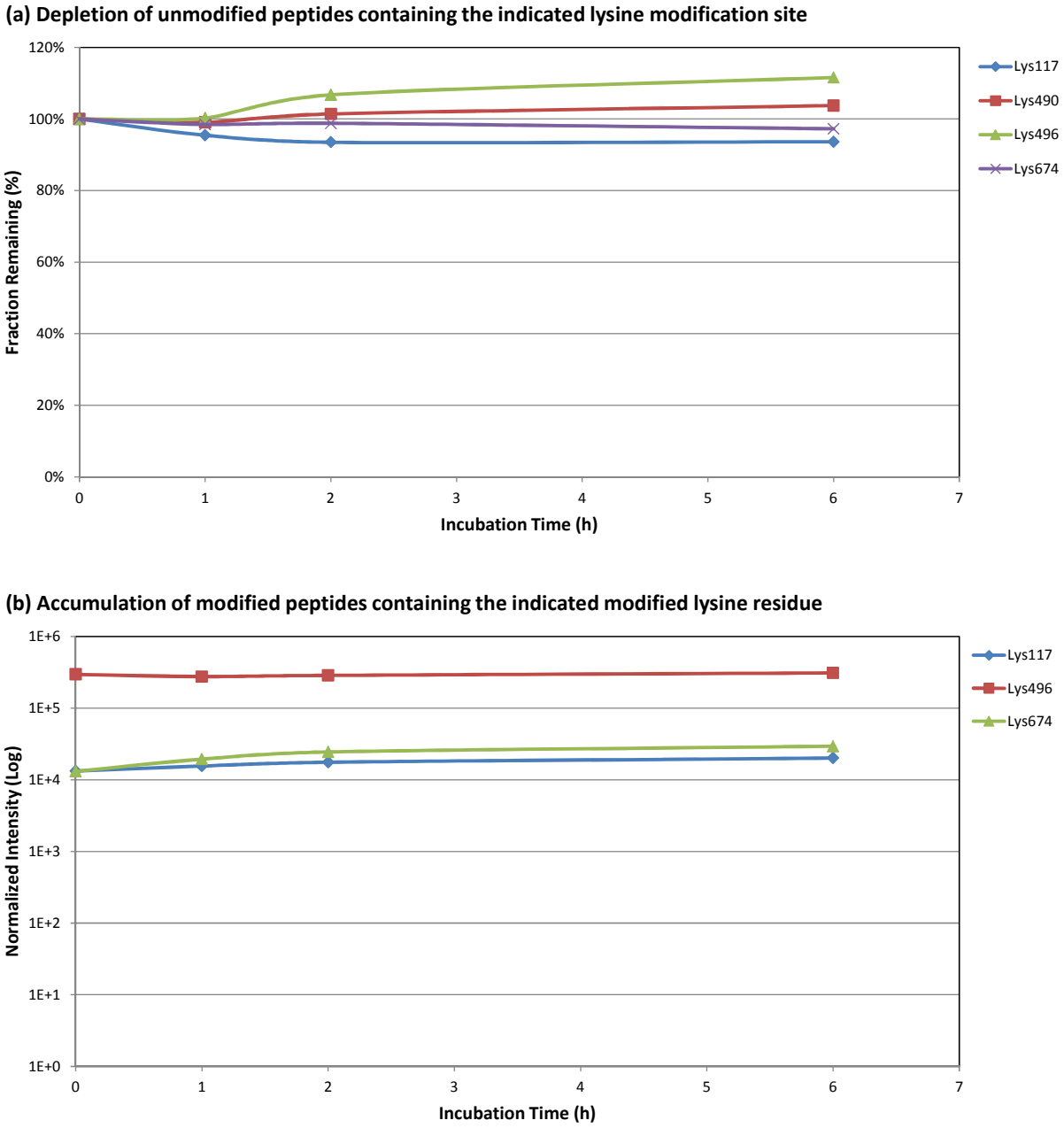

Figure 4-7. Effect of varying reaction duration, at a fixed HNE:ACO ratio of 10:1, on reaction progress measured using iTRAQ reporter ion intensity for targeted lysine sites. The targeted

mass list was used with Orbitrap/HCD measurement. Depletion plots are scaled to 100% for the control while normalized absolute intensities are given in the accumulation plots. Relative abundance measurements were not obtained for targeted site His[490].

Enzymatic Assay

Aconitase activity was determined using an established assay. This method is based on measuring the rate of NADPH generation at a wavelength of 340 nm (Scheme 4-2).[211, 212]

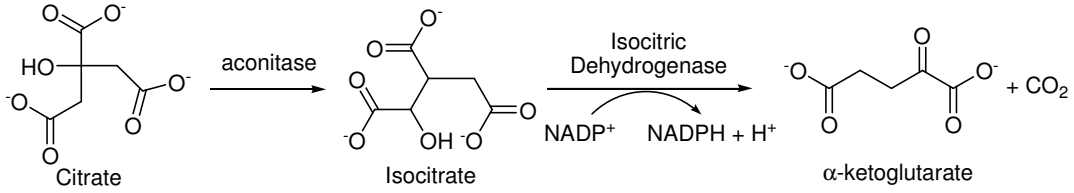

Scheme 4-2. Generation of NADPH in aconitase enzymatic assay.[211]

The activity of two preparations of modified aconitase was measured: One set was prepared from various molar ratios of HNE to aconitase (0:1, 1:1, 10:1 and 50:1) with a 2 h incubation (Figure 4-8); another set was prepared from various incubation time frames (0h, 1h, 2h and 6h) at a molar ratio of 10:1 (Figure 4-9). Sample preparations were done in triplicate and the activity of each sample was measured three times. The average absorbance value from each sample was plotted as a function of time and the linear portion of the assay's calibration curve was used in the analysis. Relative activity was obtained after correcting for blank activity and normalizing against the rate of the aconitase positive control (activity of positive control was considered as 100%).

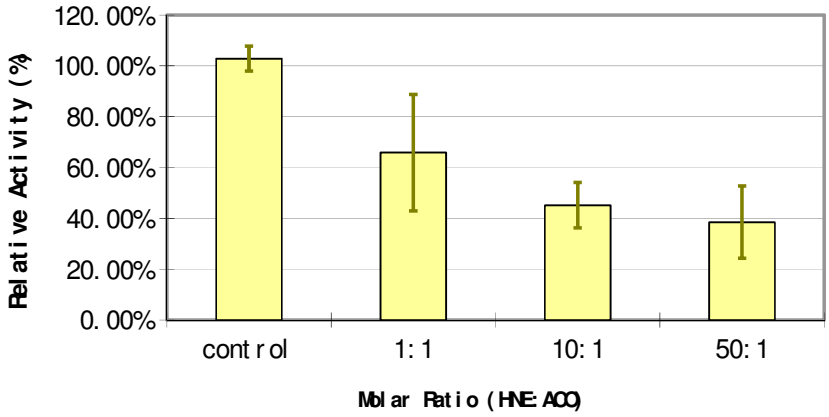

Figure 4-8. Enzymatic assay of HNE modified m-aconitase. Samples were prepared at different molar ratios (0:1, 1:1, 10:1 and 50:1) with 2 h incubation.

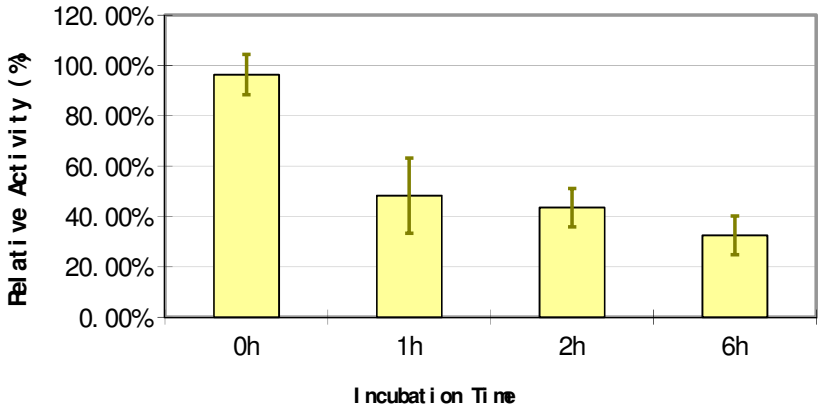

Figure 4-9. Enzymatic assay of HNE modified m-aconitase. Samples were prepared from different incubation time frames (0 h, 1 h, 2 h and 6 h) at a molar ratio of 10:1.

The relative activity of the 0 to 1 molar ratio or the 0 h incubation time was around 100% as expected. It shows that the process of sample preparation does not cause enzyme activity to be lost. In both assay experiments, with the elevation of HNE amount or incubation time, aconitase activity dropped. In the molar ratios experiments, catalytic activity was at 70%, 45% and 40% of

original sample when the molar ratios were 1:1, 10:1 and 50:1 with a 2 h incubation. In the incubation time experiments, enzyme activity remained around 50%, 45% and 35% when the time frames were 1 h, 2 h, and 6 h at a 10:1 molar ratio. The two experiments overlapped at the 10:1 molar ratio with a 2 h incubation, and results from the overlap measurements were quite consistent. The activity decline of modified aconitase in both sets did not drop off at a consistent rate and it appears that the modification stalled at long reaction times or high concentrations. At a 50:1 molar ratio or 6 h incubation, 35% - 40% of activity still remained. Higher molar ratios or longer incubation times cannot be examined due to the poor solubility caused by presumably cross-linking.

Discussion

Method Development

Porcine heart aconitase purchased from Sigma-Aldrich was used in this project. At the beginning, the project suffered from low coverage and poor signal in the tandem mass spectrometry, which limited our ability to detect modifications. Some experiments were attempted to improve the results. Various enzymes (Trypsin, GluC, Chymotrypsin and AspN) were combined. HNE was substituted by a more active carbonyl reagent, acrolein. A chelating reagent, bathophenanthroline disulfonic acid disodium salt (OBP), was added before enzymatic digestion to try to break ligation between the cysteines and the cluster. The coverage and number of detected modification could not be dramatically improved with these approaches.

Analysis of the commercial sample using SDS-PAGE separation and mass spectrometry revealed the purity of aconitase is much lower than reported (Figure 4-10). The purchased sample is a mixture of various proteins. Porcine serum albumin in a large portion was added to stabilize aconitase. The low purity of aconitase made the identification of modification sites difficult by the method described in the previous HSA project. In this project, SDS-PAGE separation and in-gel digestion were applied after modification instead of gel-free digestion.

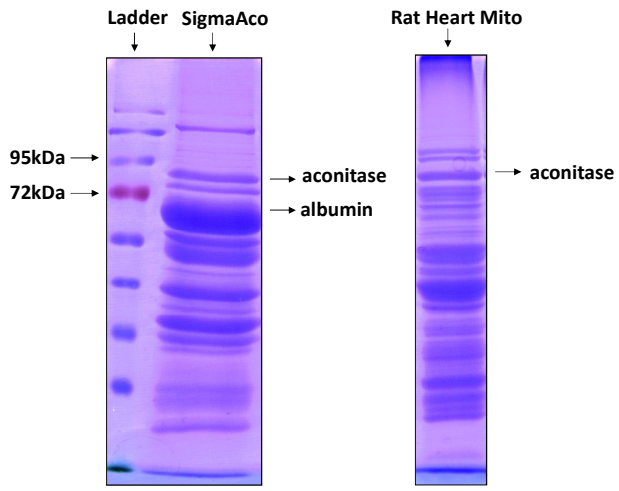

Figure 4-10. 10% SDS-PAGE running of Sigma-Aldrich aconitase and rat heart mitochondria.

During the incubation of HNE with aconitase, the solution was observed to become cloudy with increased incubation time. This phenomenon was more obvious at higher molar ratios of HNE and finally caused smeared gel bands and poor tandem mass spectra. It was assumed to be due to intra and intermolecular cross-links involving Michael additions and Schiff base formations. To limit this problem, excess DTT was added after incubation of HNE with aconitase to consume the remaining HNE. Urea was then used to denature the modified proteins before adding reductant. This method was applied to possibly break down any imines involved in cross-linking. Analysis of samples with this approach showed a clearer gel band from the SDS-PAGE and improved tandem mass spectrum quantity at a 50:1 molar ratio (Figure 4-11). The drawback of this method is that the added DTT may compete for adducted HNE or impact the ligated cysteines. Additionally, it probably would be difficult to detect Schiff base formation under the conditions. However, product analyses from the two methods at a 10:1 molar ratio showed

similar modifications. This implies that the added DTT did not impact the modifications significantly at room temperature and pH 7.4.

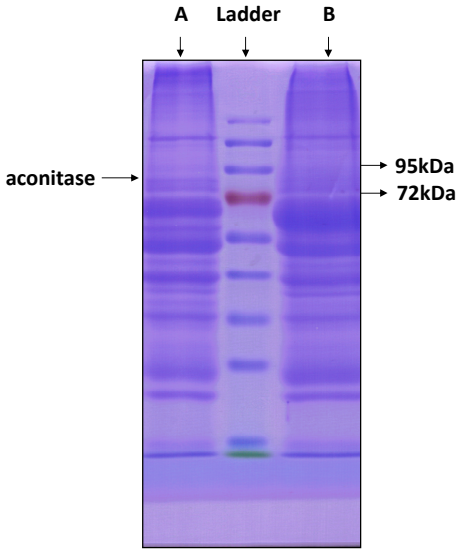

Figure 4-11. 10% SDS-PAGE running of modified aconitase (HNE:ACO=50:1) with or without adding DTT and urea before reduction. A: treated with DTT and urea; B: without DTT and urea added.

Correlation between HNE Modifications and Enzyme Activity

Superoxide anion (O_2^-), hydrogen peroxide (H_2O_2) and peroxynitrite ($ONOO^-$) have been shown to inactivate mitochondrial aconitase through disturbing the $[4Fe\text{-}4S]^{2+}$ cluster.[196, 204-207] Aconitase activity may also be modulated by modifications of amino acids. Peroxynitrite ($ONOO^-$) has been reported to modulate m-aconitase activity through modifications of cysteines and tyrosines.[204, 205] In this project, some of the identified HNE modifications are in the active site region of aconitase. Cys^{358}, Cys^{421} and Cys^{424} contribute ligands to the iron-sulfur cluster. The replacement of any of these cysteines with serine causes enzymatic activity to be lost. It has

been shown that Cys^{565} is the most reactive cysteine in aconitase towards electrophiles and can bind to various alkylation reagents, causing a decrease in aconitase activity.[181, 213] Although this cysteine is not in the active site, modification of this residue could inhibit substrate entry to the cluster. His^{101} and His^{147} are also active sites in aconitase because they directly or indirectly provide protons when paired with Asp^{100} and Asp^{165} in hydrogen bonds with the substrate.[182] The mutation of His^{101}/Asp^{100} and His^{147}/Asp^{165} pairs to Asn/Ser pairs shows varying-levels of decrease in aconitase activity.[202] Our enzymatic assay results show reduced catalytic activities when the amount of HNE or incubation time increases. Before performing the assay, an effort was made to rebuild the $[4Fe\text{-}4S]^{2+}$ cluster by providing the necessary components for the cluster. Assuming that the conditions used were favorable for cluster formation (near 100% activity was seen in the control samples subjected to the same procedures), it appears that protein modifications by the HNE must be the cause of the reduced aconitase activity. This could be a direct result of modification at active site residues or a result of poor folding due to cross-linking. The iTRAQ data provides evidence for the former.

In this project, iTRAQ reagent labeling quantification was employed to measure the relative reactivity of targeted sites. There is evidence that critical residues are modified. The high degree of modification at the cysteines in the iron-sulfur cluster suggests that HNE would have a large impact on aconitase activity. The depletion plots for the unmodified peptides containing these cysteines are quite similar in profile to the aconitase activity plots. Each drops rapidly in the first 2 hours to about 40-50% of the control value and then begins to level off in the 2-6 hour period.

This correlation strongly suggests that HNE modification of a cysteine in the iron-sulfur cluster leads to the elimination of aconitase activity.

The enzyme activity assay as well as the cysteine modification analysis (iTRAQ) suggests that the HNE alteration of the protein does not go to completion. In each case, about 30% - 40% of the protein appears to resist alteration despite higher HNE concentrations or longer incubation times. This indicates that some portion of the protein is protected from reaction in the incubation process. There is not enough information from these studies to pinpoint the cause. A possible explanation is that some HNE modifications do not reduce function, but do alter the structure or solubility of aconitase in a way that inhibits reaction of HNE with active site residues. In such a scenario, the aconitase could retain activity and avoid critical cysteine modifications despite extended reaction times or greater HNE concentrations.

Reactivity of Amino Acids

As noted above, there are twelve cysteines, but no disulfide bridges in aconitase. Three cysteines, Cys^{358}, Cys^{421} and Cys^{424}, coordinate with the iron-sulfur cluster as ligands.[189] In reactions with electrophiles, Cys^{565} has been reported as the most reactive site in the enzyme.[213] All detectable cysteines, except Cys^{358}, share the same tryptic peptides with other amino acids, which makes it hard to rank the reactivity of the cysteines using the iTRAQ quantification. If we assume that the cysteines are more reactive than the histidines in the peptides that contain both, the data in Figure 5a suggest the following order of reactivity: $Cys^{421/424} > Cys^{99} > Cys^{565} > Cys^{358}$. The high level

of modification in the peptide containing $Cys^{421/424}$ may be a result of it having two reactive cysteines. It is somewhat surprising that Cys^{99} reacts faster than Cys^{565}, which had been identified in previous studies as being the most reactive with electrophiles. It is true that the peptide with Cys^{99} has contributions in its modification from $His^{98/101}$, but as discussed earlier, these are expected to be small. In any case, the data suggest that all of these cysteines, Cys^{99}, $Cys^{421/424}$, and Cys^{565} have high reactivity. In the histidines, it is more difficult to identify an order of reactivity because $His^{98/101}$ and His^{569} have their reactivity masked by the more reactive cysteines in the peptides that contain them. Excluding these, we are left with $His^{460} > His^{46} \sim His^{9/13} > His^{519}$. Of these, His^{460} separates itself out as being significantly more reactive than the others. Based on their very limited reactivity, nothing can be stated about the relative lysine reactivity.

A simple calculation of the SASA associated with the residues can be done.[135, 136] It provides some insight into the environments of the reactive residues. Plots of side chain and backbone SASAs for the cysteines and histidines in aconitase can be generated using the GETAREA program[137] (Figure 4-12). Lysines are excluded because we have no useful reactivity data for them. From the SASAs plots of cysteines and histidines, there seems to be no relationship between the SASA and reactivity other than the need for marginal surface accessibility.

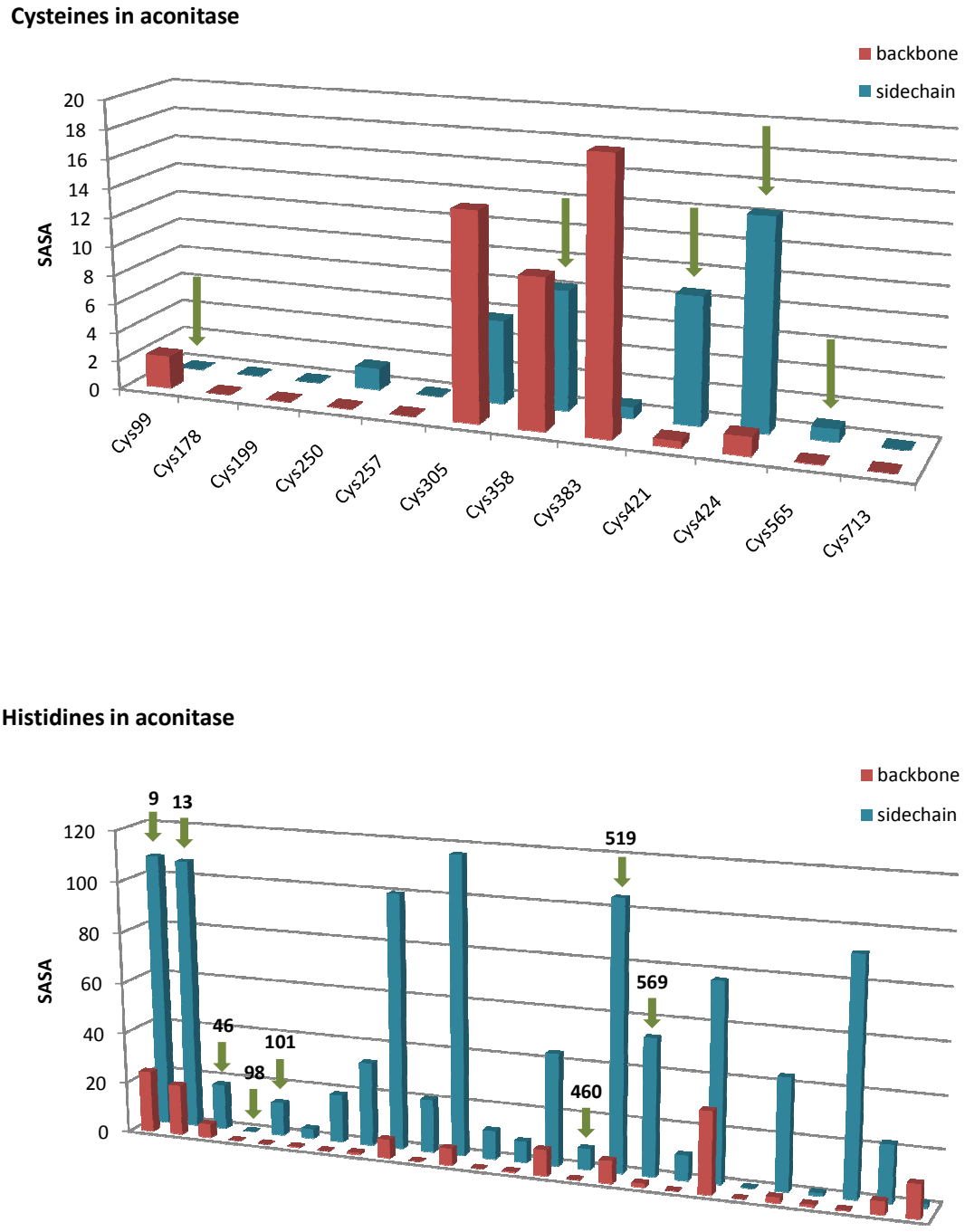

Figure 4-12. SASA in $Å^2$ for cysteines and histidines in aconitase. Red bars are the backbones and blue bars are the side chains. Green arrows indicate sites that were on the target list.

What the majority of the most reactive residues have in common is that they are physically close to the active site of the enzyme.[200] All the cysteines from the iron-sulfur cluster are reactive with HNE, as well as a number of histidines that are in close proximity to the active site. In addition to the cysteines of the iron-sulfur cluster, many other reactive sites are near the cluster. His^{101} and His^{147} are within 10 Å of the cluster and Cys^{99}, His^{98}, His^{460}, and His^{569} are all within about 20 Å of the cluster. This is an intriguing finding and suggests that features of the active site might direct HNE modification to residues in the vicinity. This would make aconitase very sensitive to HNE modification and potentially, active site residues might be catalyzing the HNE modification. This type of targeted modification was not seen in HSA and indicates that the local environment can play a strong role in directing HNE modification.

Conclusions

The addition of a reactive α, β-unsaturated aldehyde, HNE, to aconitase exhibits relatively high selectivity. The modification sites were determined at high confidence with various molar ratios of HNE to ACO (1:1, 2:1, 5:1 and 10:1) using mass spectrometry. In addition to the iron-sulfur cluster, other amino acids play a critical role in the enzymatic reaction and are considered as active site residues. Enzymatic assays of aconitase modified with HNE at various incubation times and molar ratios show decreased enzyme reactivity. iTRAQ quantification was applied to measure the relative reactivity of targeted amino acids towards HNE. The results suggest that cysteines have relatively high modification levels. The quantitation results for ligated cysteines (C^{358}, C^{421} and C^{424}) and an active site histidine (His^{101}) are consistent with the enzymatic assay results, which quantitatively indicated that the decreased aconitase activity correlates with the extent of modification of active sites. Finally, the crystal structure of aconitase and plots of SASAs indicate that surface accessibility does not correlate with reactivity in aconitase. Instead, reactivity seems to be targeted at residues near the active site.

Chapter 5: Determine The Level and Nature of Protein Carbonylation in Oxidatively Stressed Mouse Heart Mitochondria

Background

Mitochondria are a major source of ROS and target for oxidative damage. Mitochondria are involved in the production of ROS through one-electron carriers in the electron-transport chain (ETC), and mitochondria are also very susceptible to oxidative stress as evidenced by significant reports of LPO, protein oxidation and mitochondrial DNA (mtDNA) mutations. Mitochondria play a critical role in various apoptosis events since oxidative stress induced by ROS can cause apoptosis.[214] However, exact mechanisms of increased ROS formation in mitochondria and their induction of apoptotic signals are not deeply understood.[215]

The ETC is a powerful source of ROS during normal metabolism.[216, 217] These ROS primarily are superoxide radical ($O_2^{\cdot-}$) and hydrogen peroxide (H_2O_2). The latter is either as a product of SOD or spontaneous disproportionation of superoxide radical.[214, 218] It is calculated that 1-4% of the oxygen entering the ETC is incompletely reduced to ROS.[214, 219, 220] The ETC is composed of five multimeric complexes (Figure 5-1),[215, 221] which are NADH dehydrogenase, succinate dehydrogenase, ubiquinol cytochrome c reductase, cytochrome c oxidase, and adenosine-5'-triphosphate (ATP) synthase. Electron transport between complex I (nicotinamide adenine dinucleotide (NADH) dehydrogenase) to complex IV (cytochrome c oxidase) is coupled to extrusion of protons from complex I, III (ubiquinol cytochrome c reductase) and IV into the intermembrane space, generating an electrochemical potential across the mitochondrial inner membrane.[215] In this process, complex II (succinate dehydrogenase) only acts to transfer additional electrons into the quinone pool (Q) from succinate. Protons finally flow to complex V

(ATP synthase), which organizes the energy to synthesize ATP from adenosine diphosphate (ADP).[222] Complex I and complex III are two major ROS-producing regions in the ETC under normal conditions.[214] The rate of ROS generation from mitochondria is increased in various pathologic conditions including hypoxia, ischemia, aging, and chemical inhibition of ETC.[216, 223-228]

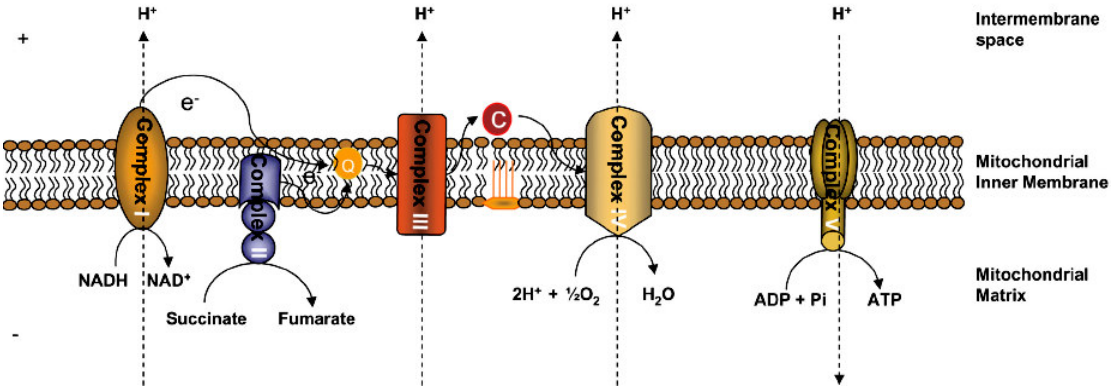

Figure 5-1. Component of ETC in mitochondria.[215]

Mitochondrial components are exposed to high concentrations of ROS because they are major producers of ROS, and may therefore be particularly susceptible to attack by ROS. Damage by oxidative stress to mitochondrial components includes LPO, protein oxidation and mtDNA mutations.[214, 229] LPO might be particularly harmful in mitochondria, especially because there are some highly unsaturated lipids in the inner mitochondrial membrane.[230] As a result of oxidative stress, protein oxidation may occur either directly or as a consequence of LPO. MtDNA is also highly susceptible to oxidative stress because it is located in the matrix and close to the major source of ROS. The damage to mtDNA is greater and lasts longer than that to nuclear DNA.[214]

Mitochondrial functional damage mostly impacts cells that have a high-energy demand, such as neurons and cardiac myocytes, because mitochondria play a critical role in cellular energy production by ETC dependent synthesis of ATP.[215, 231] It has been suggested that ROS contribute to myocardial injury during ischemia and reperfusion.[217, 232, 233] The rate of ROS generation from mitochondria is increased under ischemia and reperfusion conditions.[228, 232-235] Some research has been done to support that ischemic damage to ETC increases the generation of ROS from mitochondria, which was measured by H_2O_2 release from ischemic damaged sub-sarcolemmal mitochondria (SSM) and inter-fibrillar mitochondria (IFM). The results show that ischemic damage to the ETC increases the generation of H_2O_2 from both complex I and complex III, and could be a potential mechanism of cardiac injury.[228]

Although ischemic damage has been described to increase ROS by inhibiting ETC, there are not many details about how important proteins in mitochondria are impacted in this process. In this project, we are working with Dr. Edward J. Lesnefsky's group in the Department of Biochemistry at Virginia Commonwealth University. They provide the mouse heart mitochondrial samples. Our aim is to determine which mitochondrial proteins are oxidatively modified to give protein carbonyls during ischemic events in mouse hearts. Furthermore we will try to investigate the specific modification sites in these proteins.

Experimental Procedures

Materials

Isolated mouse heart mitochondria were provided by Dr. Lesnefsky's lab. They were prepared using standard techniques.[228, 236] (+) Biotin-hydrazide, SDS, 2-(N-morpholino) ethanesulfonic acid (MES), $NaBH_3CN$, IAM, DTT, and 10×PBS concentrate were purchased from Sigma-Aldrich (St. Louis, MO). Sequencing grade modified trypsin was from Promega (Madison, WI). HNE was obtained from Cayman Chemical (Ann Arbor, MI). Streptavidin magnetic beads were purchased from Invitrogen (Carlsbad, CA). Laemmli sample buffer was from Bio-Rad (Hercules, CA). The anti-HNE monoclonal antibody was purchased from Japan Institute for the Control of Aging (Haruoka, Japan). Enhanced chemiluminescence kits were obtained from GE Healthcare (Pittsburgh, PA) and oxyblot™ protein oxidation detection kits were obtained from Millipore (Billerica, MA). BCA Protein Assay kits, Imperial protein stain, streptavidin poly-HRP, and streptavidin resin were purchased from Thermo Scientific (Rockford, IL). iTRAQ reagent kits were obtained from Applied Biosystems (Foster City, CA).

Experiments

Biotinylation of protein carbonyls

The fresh isolated ischemic mouse mitochondria sample and control were incubated with 5 mM biotin-hydrazide for 60 min at room temperature separately. The mitochondrial membrane was broken by adding 2% SDS at room temperature. The insoluble materials were discarded with

centrifugation at 12800 g and the supernatant was collected. The collected supernatant was diluted using labeling buffer (50 mM MES buffer, pH 5.5) to a final concentration of 1 mg/ml. Biotin hydrazide stock solution (50 mM in DMSO) was then added to a final concentration of 5 mM. The mixture was incubated for 2 h at room temperature with gentle shaking. The hydrazone formed during labeling was stabilized by adding $NaBH_3CN$ to 15 mM and incubating for 60 min in an ice bath. Repeated washes employing centrifugal filter devices (Millipore, Billerica, MA) were used to remove reagents and to exchange to 200 ml 1×PBS buffer (pH 7.4) for enrichment; the molecular weight cut-off for the centrifugal filter devices used was 3 kDa. The protein concentration was determined using the BCA protein assay.

Purification of biotinylated proteins

After labeling, biotinylated proteins were enriched using streptavidin conjugated magnetic beads and streptavidin resins separately. The purification procedure was done according to the manufacturer's protocol with slight adjustment. Briefly, the same amount biotin labeled sample and control were measured and incubated with pre-washed streptavidin magnetic beads or streptavidin resins for 60 min at room temperature. The incubation was carried out on a rotary machine using gentle rotation. For streptavidin magnetic beads, protein-coated beads were collected with a magnet for 3 min, and the supernatant was then removed completely. Coated beads were washed three times using 1×PBS buffer with 0.01% Tween 20 and 0.1% SDS (pH 7.4) to avoid unspecific binding. For the streptavidin resin, the protein-attached slurry was separated with centrifugation at 4000 g for 2 min, and the supernatant was carefully removed by pipette.

The slurry was washed three times using 1×PBS buffer with 0.01% Tween 20 and 0.1% SDS (pH 7.4). Finally, the beads and slurry were collected for trypsin digestion.

Enzymatic digestion

1. Protein digestion after releasing from beads

The collected coated beads from the enrichment were resuspended in100 µl 1% SDS in 1×PBS buffer and incubated at 95 °C for 5 min. The beads were separated with a magnetic separator for 3 min and the supernatant containing enriched proteins was carefully collected. This step was repeated three times to completely collect the released proteins. The released proteins in the supernatant were reduced with DTT and alkylated with IAM. Repeated washes employing centrifugal filter devices (3 kDa molecular weight cut-off) were used to remove excess reagents and to exchange to a 50 mM ammonium bicarbonate buffer (pH 8.5) for digestion. The tryptic digestion was carried out overnight at 37°C. Digestion products were purified using a Waters (Milford, MA) Oasis MCX solid phase extraction cartridge. The final sample was dried using a centrifugal evaporator and then re-suspended in an HPLC equilibration mobile phase for µLC-MS/MS analysis.

2. Protein digestion on beads or resins

The collected protein bound beads and resins were resuspended and washed with 50 mM ammonium bicarbonate buffer (pH 8.5) twice. Samples were subsequently reduced with DTT and alkylated with IAM. The streptavidin beads and resins were separated by magnetic separator

or subjected to centrifugation again, and then were washed with 50 mM ammonium bicarbonate buffer (pH 8.5) twice. The supernatant was removed and discarded during this process. The samples were treated with 0.5 µg trypsin. The reaction was carried out at 37 °C for 2 h with gentle shaking. The tryptic digestion was repeated twice and the final incubation time was 16 h. After every trypsin treatment, beads and resins were isolated and supernatants containing tryptic peptides were collected for mass spectrometry analysis and iTRAQ labeling.

iTRAQ reagent labeling

Enriched peptide mixtures were desalted using C18 MicroSpin columns (The Nest Group, Southboro, MA) and dried using a centrifugal evaporator. Solid peptide mixtures of both sample and control were then reconstituted in 25 ul of iTRAQ dissolution buffer. Two iTRAQ reagents were dissolved in 70 µl of ethanol separately. Each iTRAQ reagent aliquot was added to one of the peptide mixtures in the following sequence: mass 114 for the enriched control using streptavidin magnetic beads; mass 116 for the enriched ischemic sample using streptavidin magnetic beads, mass 115 for the enriched control using streptavidin resin, and mass 117 for the enriched ischemic sample using streptavidin resin. After incubation for 2 h at room temperature with gentle shaking, the iTRAQ labeled sample and control were combined and then purified using a Waters (Milford, MA) Oasis MCX solid phase extraction cartridge. The final products from both enrichment methods were dried using a centrifugal evaporator and then re-suspended in the HPLC equilibration mobile phase for µLC-MS/MS analysis.

Western Blot

1. Detection of mitochondria carbonylation *in vitro*

Fresh isolated mitochondria at a concentration of 1 mg/ml were treated with HNE at various concentrations (25 µM, 50 µM, 100 µM and 200 µM). All reactions were incubated at 37 °C for 3 h. Modified mitochondria (100 µg) were mixed with a Laemmli sample buffer. After heating at 95 °C for 5 min, the protein mixtures were separated on a 12% SDS-PAGE gel, and then transferred onto a PVDF membrane by electroblot. The membrane was blocked for 1 h at room temperature with a 5% fatty acid-free milk in TBST and incubated with anti-HNE diluted to 1:500 in 5% BSA overnight at 4°C. Blocked membrane was then washed with TBST and incubated with HRP conjugated anti-mouse antibody in 5% BSA (1:5000 dilution) for 1 h at room temperature. Following washing with TBST, the membrane was developed with ECL detection reagents.

2. Immunobloting of mitochondria carbonylation using streptavidin-conjugated HRP

Equal amounts of biotinylated control and ischemic mitochondria samples (10 µg) were loaded on a 4-20% gradient polyacrylamide gel, and then transferred onto a PVDF membrane. The PVDF membrane was blocked overnight at 4 °C with 4% fatty acid-free BSA in PBST (pH 7.2). Blots were then incubated with streptavidin poly-HRP diluted to 0.02 µg/ml in 4% BSA at room temperature for 1 h. Following rinsing with PBST, the membrane was developed with ECL detection reagents.

3. Identification of mitochondria carbonylation using Oxyblot

The procedure for the Oxyblot detection was taken directly from the manufacturer's protocol. Briefly, fresh, isolated control and ischemic mitochondria samples (10 µg) were denatured by adding 12% SDS to a final concentration of 6% SDS, and then were derivatized by adding 10 µl of a 2,4-dinitrophenylhydrazine (DNPH) solution. The derivatization reaction was carried out at room temperature for 15 min. Samples were neutralized and reduced by adding 7.5 µl of neutralization solution and 1 µl of 2-mercaptoethanol. Mixtures were loated on 4-20% gradient polyacrylamide gel, and then transferred onto a PVDF membrane by electroblot. The membrane was blocked for 1 h at room temperature with 5% fatty acid-free BSA in PBST and incubated with anti-DNP diluted to 1:150 in 1% BSA/PBST at room temperature for 1 h. The blocked membrane was then washed with PBST and incubated with HRP conjugated anti-goat antibody in 1% BSA (1:2000 dilution) for 1 h at room temperature. Following washing with PBST, the membrane was developed with ECL detection reagents.

µLC-MS/MS analysis

1. Mitochondria carbonylation identification

Carbonylation identification was performed using a Thermo (San Jose, CA) LTQ XL linear ion trap mass spectrometer equipped with ETD. The LTQ XL was interfaced with a Thermo Surveyor capillary HPLC system. Peptides were separated on a reversed-phase, C18 column (150 µm × 10 cm, 5 µm particles, 300 Å pores; Column Technology, Fremont, CA) at a flow rate of ~1 µl min^{-1} using 0.1% formic acid in water as mobile phase A and 0.1% formic acid in methanol as mobile phase B. Approximately 2 µg peptides were injected and a Michrom

(Auburn, CA) CapTrap trapping column was used for rapid sample injection. The gradient started from 2% B, then increased to 15% B over 5 min, then increased to 80% B over 70 min, and finally increased to 95% B over 15 min. The eluted peptides were introduced into the LTQ XL with a nanospray source operating at a spray voltage of 2.1 kV, a capillary voltage of 21 V, and a capillary temperature of 200°C. A full scan in the m/z range 300-2000 was performed to obtain precursor ions, followed by four data-dependent CID MS/MS scans for the four most abundant precursor ions in the full scan. Dynamic exclusion was used-if the same precursor ion was picked for fragmentation twice within a 30 s window, it was excluded from further analysis for 180 s.

2. iTRAQ reagent-labeled on-beads digests

Analysis of iTRAQ reagent-labeled samples was performed only by a Thermo LTQ Orbitrap Velos mass spectrometer. Separations were performed on a Waters nanoACQUITY reversed-phase, C18 column (100 µm × 10 cm; 1.7 µm particles). Elution was achieved using a gradient of 0.1% formic acid in acetonitrile (B) versus 0.1% formic acid in water (A) at a flow rate of 0.4 µL min^{-1}. Approximately 2 µg peptides were injected, with the loading and equilibration mobile phase being 1% B. The linear gradient ran to 15% B after loading at 1% B over 25 min, followed by an increase to 25% B over 35 min, followed by an increase to 35% B over 40 min, and followed by an increase to 85% B over 20 min. The nanospray ion source was operated at 3.5 kV. A full scan in the m/z range 400-7500 was performed to obtain precursor ions, followed by eight data-dependent HCD MS/MS scans for the eight most abundant

precursor ions in the full scan. Dynamic exclusion was used. For HCD, the normalized collision energy was 40 and the activation time was 0.1 ms.

Database searching and data processing

Peptide sequences and modifications were identified using the BioWorks version 3.3.1, SP1 implementation of Sequest (Thermo). No scan grouping was performed in preparing peak lists for database searching. The protein sequence database used consisted of the NCBI RefSeq version of the complete mouse proteome and reversed versions of all sequences. Reversed sequences permit a false discovery rate estimation. Sequences were downloaded on June 27, 2011, and the final database contained 70499 entries. Only fully-tryptic peptides were considered and up to three missed cleavage sites were allowed. Precursor ion tolerances were ±2 Da for linear ion trap measurments and ±15 ppm for Orbitrap measurements. Fixed mass shifts were applied for alkylated cysteines (+57 Da) while differential amino acid mass shifts were incorporated for biotin hydrazide labeled carbonylation at lysines (+241 Da), at arginines (+199 Da), at proleins (+258 Da), at threonines (+240 Da), and oxidized methionines (+16 Da). A maximum of four variable modifications were permitted for each peptide. In searches with the iTRAQ labels present, fixed mass shifts of +144.102 Da were used for the peptide N-terminus and non-carbonylated lysine residues while differential amino acid mass shifts were incorporated for cysteines carboxyamidomethylation (+57.0513 Da) and methionines oxidation (+15.9994). Sequest output was refined using the Trans-Proteomic Pipeline (version 4.4; Institute for Systems Biology, Seattle, WA) software package. Specifically, PeptideProphet[171] was used, in

semi-supervised mode[172], to improve identification confidence. A PeptideProphet score threshold of 0.9 was applied. Intensity measurements for iTRAQ reporter ions (114-117) were processed using Microsoft Access.

Results

In this project, fresh mitochondria samples were prepared by Dr. Lesnefsky's laboratory. Briefly, a mouse heart ischemia model was set up by submerging isolated hearts in saline within an Eppendorff tube. The tube was then incubated in a water bath at 37 °C for 30 min with shaking. Simultaneously, control hearts were kept in the same buffer on ice for the same period of time. Finally, mitochondria were isolated from both ischemic and control hearts following a standard procedure.[228, 236]

DNPH derivatization was applied for protein carbonylation detection in this project. DNPH is often used to qualitatively identify carbonyl groups associated with aldehydes and ketones. DNPH can react with carbonyl groups of oxidized amino acid residues in proteins (Scheme 5-1). The formed hydrazone derivatives can be used to detect carbonyl functionality in the protein by a color change or by a western blot analysis with anti-DNP.[237, 238]

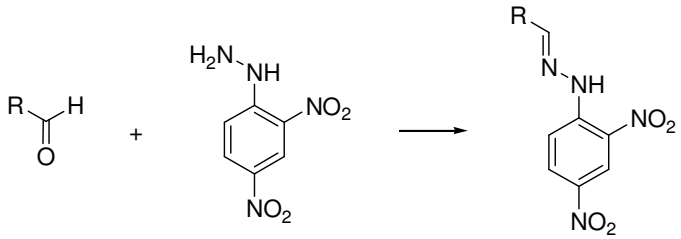

Scheme 5-1. Protein carbonylations labeling by DNPH.

In addition, (+) biotin-hydrazide was used to label the carbonylated proteins.[132] Biotinylated proteins were then purified using streptavidin-conjugated beads and resins. The interaction

between streptavidin and biotin is a non-covalent and highly specific biological binding. The binding between streptavidin and biotin is very tight, rapid and unaffected by pH or organic solvent.[239, 240] The streptavidin-biotin interaction can only be broken under harsh conditions, which can often denature the proteins involved in the interaction. However, it has been reported recently a mild incubation at elevated temperatures in water can break the interaction.[241] Streptavidin is also widely applied in western blots; an immunoblotting can detect protein biotinylation when conjugated with reporter molecules.[242, 243]

Western Blotting

In vitro modification with HNE

An *in vitro* experiment was designed to examine the possibility of mitochondrial protein modification by HNE. A monoclonal anti-HNE antibody was used to detect the HNE modifications. The anti-HNE is particularly sensitive to modified histidines in proteins. An increased modification level was observed at higher molar ratios of HNE to mitochondria (Figure 5-2). A band from the corresponding electrophoresis gel was cut out to perform in-gel trypsin digestion. One of the blotted proteins was identified as being aconitase by mass spectrometry analysis (see Figure 5-2). The western blot results indicate that HNE entered the mitochondria and modified a variety of proteins. Relatively high HNE concentrations were needed to observe wide spread modifications.

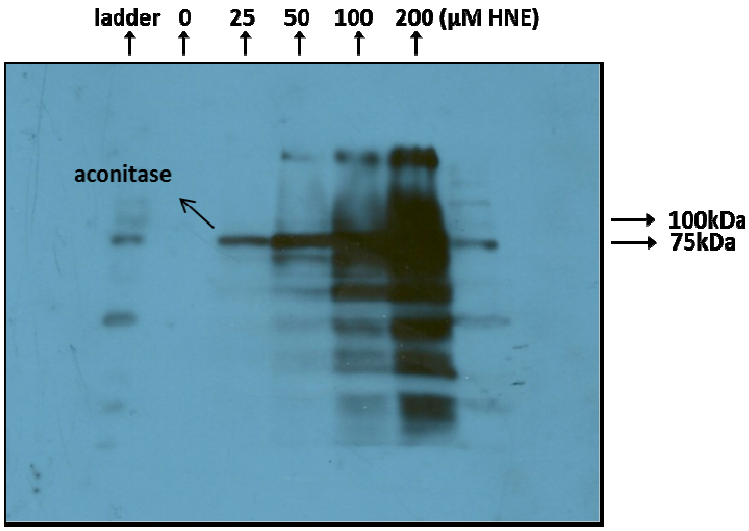

Figure 5-2. Western blot of mitochondria modifications by HNE *in vitro*. HNE was at increasing concentrations (0, 25, 50, 100 and 200 µM). One band was identified as aconitase by mass spectrometry analysis.

Carbonylated proteins from ischemia model

Streptavidin conjugated poly-HRP was employed to detect biotinylated carbonylations in ischemia model mitochondria samples. The detection is based on the specific interaction between streptavidin and biotin.[242, 243] Blotting detected multiple protein biotinylations from both biotin-hydrazide treated control (negative control 2, NC2)) and the ischemia sample (Figure 5-3). The modified proteins from both samples appeared at the same general positions on the gel. There is slightly higher intensity in the ischemia model sample. The high background in NC2 suggests either significant modification in the control or significant non-specific binding in the western blot. No blotting from the buffer treated control (negative control 1, NC1) was found.

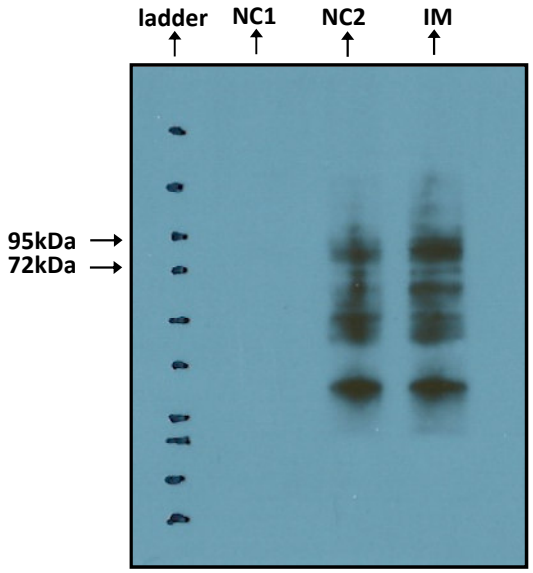

Figure 5-3. Streptavidin conjugated poly-HRP identification of biotin-hydrazide treated control (NC2), ischemic mitochondria (IM), and buffer treated control (NC1) in Western blot. Protein molecular weight was decided by protein marker roughly.

Oxyblot was also used to detect the carbonylated proteins in ischemic mitochondria. It is based on DNPH induced derivatization of carbonylated proteins.[237, 238] Anti-DNP antibodies were used to detect the derivatization. Western blot results show specific, positive blotting from the ischemia model mitochondria sample. Limited signals of derivatization were found in the DNPH treated control (negative control 2, NC2) and none in the blank solution control (negative control 1, NC1) were observed (Figure 5-4). A band from the corresponding gel electrophoresis analysis was cut out to perform in-gel trypsin digestion. Mass spectrometry analysis of this band at around 95 kDa showed the band contained aconitase.

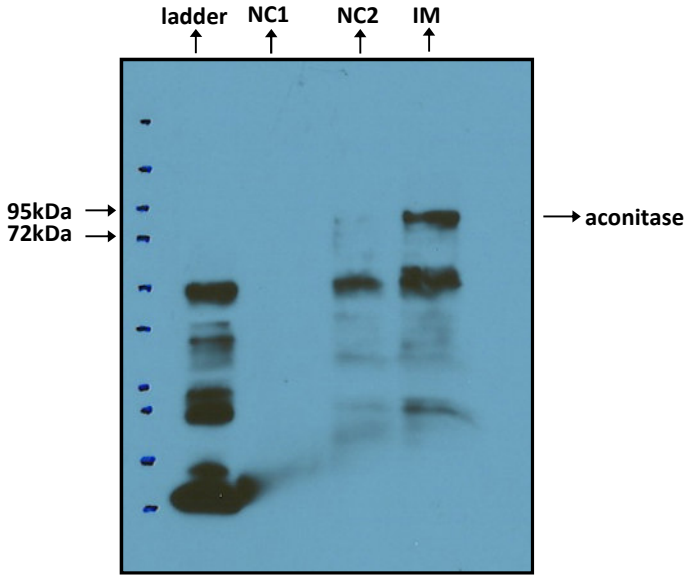

Figure 5-4. Oxyblot of DNPH treated control (NC2), ischemic mitochondria (IM), and buffer treated control (NC1). One blotting was identified as aconitase by mass spectrometry analysis.

The differences between Figure 5-3 and 5-4 suggest that the biotin-streptavidin strategy provides a greater amount of non-specific binding. The fact that patterns observed in this western blot are not reproduced in the Oxy blot is evidence of the non-specific binding. Careful comparison of the two methods shows that many of the bands with higher intensity in the Oxyblot of the ischemic model also give higher intensity in the biotin-streptavidin western blot, though somewhat obscured by the high degree of non-specific binding.

Carbonylation Identification

Our goal was to identify the carbonylated proteins from ischemia mitochondria. Fresh, isolated mouse mitochondria were treated with increasing amounts of HNE. Western blotting identified HNE modifications in the samples. The amount of apparent modification increased with

increasing amounts of HNE. Some blotted bands from the corresponding gel electrophoresis were subjected to in-gel trypsin digestion. The digests were analyzed by mass spectrometey and proteins were identified, such as aconitase and cytochrome c etc.. However, no peptides bearing HNE modifications were identified by mass spectrometry, even when the amount of HNE attained 200 μM. This concentration is higher than physiological HNE concentrations. Therefore, enrichment or other purification methods of the carbonylated proteins in the ischemia mitochondria sample was considered in this project. Streptavidin conjugated magnetic beads were primarily applied for the enrichment of potential protein carbonylation in this study. After releasing proteins from the beads and digestion, a very limited number of proteins were detected by mass spectrometry from both the control and the ischemia model mitochondria sample, and each protein was identified by only one peptide (Table 5-1). Also, no peptides bearing carbonylation sites were found. Comparing the search data from the control and the ischemia model mitochondria, the identified proteins were similar and it is hard to make any conclusions about which proteins were actually carbonylated. The limited detections probably were due to the very tight streptavidin-biotin binding, and as a result, carbonylated proteins were not efficiently released. Those that were identified were likely from non-specific binding on the beads. Next, the trypsin digestion was completed without releasing the proteins from the beads.[244] Around three hundred proteins were identified by mass spectrometry from both the control and the ischemia model mitochondria sample (Table 5-1). Obviously no carbonylation sites will be detected in this protocol because the biotin-bearing peptide remains on the bead. Comparing search data from the control and the ischemia model mitochondria, the number of

identified proteins from the ischemia model was a little higher than the amount from control. However, the number of MS/MS spectra for specific proteins were quite similar and it is hard to identify a pattern of modification. Non-specific binding to the streptavidin conjugated beads, especially for the hydrophobic proteins in mitochondria, might be a problem in this experiment. To gain more information, a quantitative approach was taken.

	Control Mitochondria	Ischemic Mitochondria
Digestion after Releasing	7*	7
On-Beads Digestion	288	254

Table 5-1. Protein identification from control and ischemic mitochondria samples with two digestion pathways. *: number of detected proteins.

Relative Carbonylation Levels Based on iTRAQ Labeling

In this project, the iTRAQ reagent labeling was used to measure the relative carbonylation levels of control and ischemia model mitochondria samples. The iTRAQ reagent-labeled samples were analyzed on a Thermo LTQ Orbitrap mass spectrometer. Peptide sequences were identified using tBioWorks, and the sequest output was refined using the Trans-Proteomic Pipeline software package. The ratios of iTRAQ reporter ions from the ischemia model and control mitochondria proteins were calculated and corrected by the ratio for trypsin peptides in the two samples. Because the same amount of trypsin was used in both digestions and no trypsin will be lost during the experiment, it can serve as an internal standard. Two batches of ischemia model mitchondria samples were quantified separately by applying the iTRAQ reagent after

streptavidin beads or resins. In the first preparation, all of the proteins enriched on the streptavidin magnetic beads showed significantly higher intensities for the iTRAQ ions in the ischemia model, as expected for a higher level of carbonylation. Table 5-2 lists the proteins that have the highest (>5) calculated ratios of ischemia model; control mitochondria proteins. In the Table 5-2, NADH dehydrogenase (ubiquinone) 1 alpha subcomplex, 13 shows the highest ratio (8.32). Next are ATP synthase subunit B1 and cytochrome c oxidase subunit IV isoform 1. For ischemia model proteins purified on streptavidin resins, even more proteins show significant increases in carbonylation compared to the control sample (Table 5-3). Among these proteins, NADH dehydrogenase (ubiquinone) 1 alpha subcomplex, 13 also shows the highest ratio (21.43) and it is higher than the one from the streptavidin magnetic beads. The sample from the resin enrichment let to more proteins with quantifiable intensities and generally double the ratios of the ischemia model to control. This variation in ratios may reflect a difference in the levels of non-specific and specific binding on the two avidin products. In any case, both approach highlighted a similar set of proteins as having exceptional carbonylation levels in the ischemia model. It is interesting to note that most of these proteins are in the ETC. However, in the second batch, none of the protein modification levels were found to be significantly increased in the ischemia model. This is a surprising result and suggests problems in the preparation of the ischemia model mitochondria. For ischemia model proteins purified on streptavidin magnetic beads, only one protein, NADH dehydrogenase (ubiquinone) flavoprotein 2, showed a slightly higher amount of carbonylation compared to the control sample. For the streptavidin resin enriched ischemic sample, several proteins, NADH dehydrogenase (ubiquinone) Fe-S protein 1,

NADH dehydrogenase (ubiquinone) Fe-S protein 7, isovaleryl-CoA dehydrogenase and enoyl-CoA delta isomerase, showed higher amounts of carbonylation compared to the control sample.

Proteins	**iTRAQ intensity Ratios (Ischemic/Control)**
NADH dehydrogenase (ubiquinone) 1 alpha subcomplex, 13	8.32
ATP synthase, H+ transporting, mitochondrial F0 complex, subunit B1	7.53
cytochrome c oxidase subunit IV isoform 1	7.04
ubiquinol-cytochrome c reductase, complex III subunit VII	6.32
NADH dehydrogenase (ubiquinone) 1 alpha subcomplex, 4	6.26
adenosine A3 receptor	6.00

Table 5-2. Streptavidin magnetic beads purified proteins showing the significantly increased amount of carbonylation from first preparation.

Proteins	**iTRAQ intensity Ratios (Ischemic/Control)**
NADH dehydrogenase (ubiquinone) 1 alpha subcomplex, 13	21.43
cytochrome c oxidase subunit IV isoform 1	20.67
ubiquinol-cytochrome c reductase, complex III subunit X	19.04
ATP synthase, H+ transporting, mitochondrial F0 complex, subunit B1	16.00
NADH dehydrogenase (ubiquinone) 1 beta subcomplex, 7	14.75
adenosine A3 receptor	14.45

ubiquinol-cytochrome c reductase binding protein	14.37
NADH dehydrogenase (ubiquinone) 1 alpha subcomplex, 8	13.98
NADH dehydrogenase (ubiquinone) 1 alpha subcomplex, 4	13.13
solute carrier family 4, sodium bicarbonate transporter-like, member 11	12.45
ATP synthase, H+ transporting mitochondrial F1 complex, beta subunit	12.19
ATP synthase, H+ transporting, mitochondrial F0 complex, subunit F2	11.48
cytochrome c oxidase, subunit VIb polypeptide 1	10.68
ATP synthase, H+ transporting, mitochondrial F1 complex, epsilon subunit	10.38
cytochrome c oxidase, subunit VIIa 2	10.01
cytochrome c oxidase subunit VIIb	8.54
succinate dehydrogenase complex, subunit C, integral membrane protein	8.27
acyl-CoA thioesterase 2	7.85
NADH dehydrogenase (ubiquinone) Fe-S protein 8	7.59
NADH dehydrogenase (ubiquinone) 1 alpha subcomplex, 6 (B14)	7.03
NADH dehydrogenase (ubiquinone) 1 beta subcomplex, 10	6.91
heat shock protein 1 (chaperonin)	6.62
hydroxyacyl-Coenzyme A dehydrogenase/3-ketoacyl-Coenzyme A thiolase/enoyl-Coenzyme A hydratase (trifunctional protein), beta subunit	6.59
NADH dehydrogenase (ubiquinone) 1 alpha subcomplex, 12	6.53
ATP synthase, H+ transporting, mitochondrial F0 complex, subunit d	6.45

NADH dehydrogenase (ubiquinone) Fe-S protein 3	6.22
aldehyde dehydrogenase 4 family, member A1	6.07

Table 5-3. Streptavidin resins purified proteins showing the significantly increased amount of carbonylation from first preparation.

Discussion

Method development

In the first part of this project, mitochondria were modified with HNE at various molar ratios. HNE modifications were detected in Western blot using a monoclonal anti-HNE antibody. The level of modification increased with increasing HNE concentration. However, no modification sites were identified by mass spectrometry from in-gel digestion of the corresponding gel band, even at the highest HNE concentration (200 μM). No enrichment was used in these experiments and the absence of identified modifications is probably due to the low modification level, which does not allow modified peptides to compete with background signal from unmodified peptides. An enrichment process is necessary for purifying modified peptides in order to reduce the background and improve the probability of detecting the modifications.

The frequently used strategies for isolating carbonylated proteins include Girard's reagent,[245] hydrazine-functionalized isotope-coded affinity tags,[246, 247] aldehyde reactive probes and solid-phase hydrazides.[248] In this project, we chose an aldehyde-reactive biotinylated derivative, biotin hydrazide, to tag the carbonylated proteins.[132] Streptavidin conjugated magnetic beads and resins were used to isolate biotinylated proteins. The general procedure for streptavidin beads and resins is to incubate the biotinylated proteins with the beads, and then release attached proteins after washing.[239, 240] The released proteins are then digested and the digested peptides are analyzed to identify modifications. During our experiment, we found that the bound proteins were very hard to release due to the strong interaction between the biotin tag and the

streptavidin. This is potentially more problematic in our system because the biotin-streptavidin conjugation point may be protected by the protein bearing the biotin tag. Therefore, we did the digestion on the beads. By choosing on-bead digestion, the proteins on the streptavidin are directly digested under relatively mild conditions. The digested peptides are easier to collect, and extra steps for sample purification before and after digestion are not necessary.[244] The shortcoming of the on-bead digestion is that it precludes the identification of specific modification sites.

We also applied iTRAQ reagents to quantify the streptavidin binding of control proteins and ischemia model mitochondria proteins. The quantitation by iTRAQ can eliminate the impact of non-specific binding caused by the very hydrophobic proteins in mitochondria. The total intensity ratio of the iTRAQ reporter ions from control and treated samples may give a measure of the enrichment provided by the streptavidin treatment and presumably the amount of carbonylation in each protein.

Western Blotting

In this project, Oxyblot was also used to detect the carbonylated proteins in ischemia model mitochondria. Oxy blotting results showed only one specific positive blotting from the ischemic mitochondria sample compared to negative controls. Although the blotted band appeared to contain aconitase, a more certain determination would require two-dimensional gel electrophoresis.[249, 250]

Streptavidin conjugated poly-HRP was employed to detect biotinylated carbonylations in western blotting too.[242, 243] The Oxy blotting technique suffers from severe limitations when applied to tissue extracts from mammalian sources. Compared to Oxy blotting, streptavidin conjugated HRP displays the specificity of streptavidin detection chemistries and is insensitive to immunoglobulin contamination of samples.[242] However, in this project, this method seems to have a relatively high background binding to the control sample. It is unclear if this was a result of non-specific binding or widespread oxidation in the control samples.

iTRAQ Reagent Quantitation for Relative Carbonylation Levels

For identifying the possible protein modifications, iTRAQ quantitation was used to measure the amount of biotin band binding in the control and treated samples. In one sample, large increases in carbonylation levels were seen in several proteins. Many of them are associated with the ETC. The two approaches of streptavidin enrichment gave similar general patterns, but the resin gave higher ratios. This may be related to the relative levels of non-specific binding. A second batch showed little difference in carbonylation levels between the ischemia model and control. This may be an issue in mitochondria preparation. Considering the two enrichment methods together, it seems the NADH dehydrogenase family proteins has the highest probability for modification, but more experiments are necessary. Overall, the quantification results from both sample purification methods are similar, but are dissimilar for different batches of ischemia michondria samples. More experiments for different ischemia sample preparations are demanded.

Nevertheless, the iTRAQ reagent based quantification method has been developed and can provide the comparison between treated and control samples.

Future Direction

The ultimate purpose of this project is to identify the specific modified sites from the ischemia model mouse heart mitochondria. Currently, we only could measure the relative protein carbonylation levels using iTRAQ reagent quantitation. In the future, we will try traditional two-dimensional gel electrophoresis to identify the carbonylated protein sites. We also will try different isolation methods, like Girard's P Reagent and SPH, for purifying the carbonylated proteins. Finally, we still could try the different experiment procedures, such as digestion before employing enrichment to capture the carbonylated peptides instead of proteins.

Conclusions

In this project, protein carbonylation in the ischemia model mouse heart mitochondria was investigated. Oxyblot was applied to identify the carbonylated proteins. Only one band suggested obvious modification and was identified as containing aconitase. Biotin hydrazide derivatives and streptavidin conjugated magnetic beads and resins were used to purify the protein carbonylations. No specific modified sites were detected with mass spectrometry after releasing proteins from the beads and digestion. iTRAQ reagent induced quantitation was employed to measure the levels of proteins in the control and ischemic samples binding to the beads and resins. Several proteins have elevated ratios in the ischemia model sample. However, more experiments are needed to validate this result.

References

1. Halliwell B, G. J., *Free Radicals in Biology and Medicine, 2nd ed.* **1999**.
2. Fiers, W.; Beyaert, R.; Declercq, W.; Vandenabeele, P., More than one way to die: apoptosis, necrosis and reactive oxygen damage. *Oncogene* **1999,** 18, (54), 7719-7730.
3. Nyska, A.; Kohen, R., Oxidation of biological systems: Oxidative stress phenomena, antioxidants, redox reactions, and methods for their quantification. *Toxicol. Pathol.* **2002,** 30, (6), 620-650.
4. Droge, W., Free radicals in the physiological control of cell function. *Physiol. Rev.* **2002,** 82, (1), 47-95.
5. Freeman, B. A.; Crapo, J. D., Free-Radicals and Tissue-Injury. *Lab. Invest.* **1982,** 47, (5), 412-426.
6. Requena, J. R.; Chao, C. C.; Levine, R. L.; Stadtman, E. R., Glutamic and aminoadipic semialdehydes are the main carbonyl products of metal-catalyzed oxidation of proteins. *Proc. Natl. Acad. Sci. U. S. A.* **2001,** 98, (1), 69-74.
7. Kohen, R.; Gati, I., Skin low molecular weight antioxidants and their role in aging and in oxidative stress. *Toxicology* **2000,** 148, (2-3), 149-157.
8. Shadyro, O. I.; Yurkova, I. L.; Kisel, M. A.; Brede, O.; Arnhold, J., Radiation-induced fragmentation of cardiolipin in a model membrane. *Int J Radiat Biol* **2004,** 80, (3), 239-245.
9. ScharffetterKochanek, K.; Wlaschek, M.; Brenneisen, P.; Schauen, M.; Blaudschun, R.; Wenk, J., UV-induced reactive oxygen species in photocarcinogenesis and photoaging. *Biol Chem* **1997,** 378, (11), 1247-1257.
10. Elsayed, N. M.; Omaye, S. T.; Klain, G. J.; Korte, D. W., Free Radical-Mediated Lung Response to the Monofunctional Sulfur Mustard Butyl 2-Chloroethyl Sulfide after Subcutaneous Injection. *Toxicology* **1992,** 72, (2), 153-165.
11. Jones, D. P.; Carlson, J. L.; Mody, V. C.; Cai, J. Y.; Lynn, M. J.; Sternberg, P., Redox state of glutathione in human plasma. *Free Radic. Biol. Med.* **2000,** 28, (4), 625-635.
12. Leikauf, G. D.; Kline, S.; Albert, R. E.; Baxter, C. S.; Bernstein, D. I.; Bernstein, J.; Buncher, C. R., Evaluation of a Possible Association of Urban Air Toxics and Asthma. *Environ Health Perspect* **1995,** 103, 253-271.
13. Furihata, C.; Matsushima, T., Mutagens and Carcinogens in Foods. *Annu Rev Nutr* **1986,** 6, 67-94.
14. Miller, E. C.; Miller, J. A., Carcinogens and Mutagens That May Occur in Foods. *Cancer* **1986,** 58, (8), 1795-1803.
15. Davis, W.; Ronai, Z.; Tew, K. D., Cellular thiols and reactive oxygen species in drug-induced apoptosis. *J. Pharmacol. Exp. Ther.* **2001,** 296, (1), 1-6.
16. Xu, C. J.; Li, C. Y. T.; Kong, A. N. T., Induction of phase I, II and III drug metabolism/transport by xenobiotics. *Arch. Pharm. Res.* **2005,** 28, (3), 249-268.
17. Richter, C.; Gogvadze, V.; Laffranchi, R.; Schlapbach, R.; Schweizer, M.; Suter, M.; Walter, P.; Yaffee, M., Oxidants in Mitochondria - from Physiology to Diseases. *Biochimica Et Biophysica Acta-Molecular Basis of Disease* **1995,** 1271, (1), 67-74.
18. Donko, A.; Peterfi, Z.; Sum, A.; Leto, T.; Geiszt, M., Dual oxidases. *Philosophical Transactions of the Royal Society B-Biological Sciences* **2005,** 360, (1464), 2301-2308.
19. Winston, G. W.; Harvey, W.; Berl, L.; Cederbaum, A. I., The Generation of Hydroxyl and Alkoxyl Radicals from the Interaction of Ferrous Bipyridyl with Peroxides - Differential Oxidation of Typical Hydroxyl-Radical Scavengers. *Biochem J* **1983,** 216, (2), 415-421.
20. Gutteridge, J. M. C., Free-Radicals in Disease Processes - a Compilation of Cause and Consequence. *Free*

Radic. Res. Commun. **1993,** 19, (3), 141-158.
21. Valko, M.; Rhodes, C. J.; Moncol, J.; Izakovic, M.; Mazur, M., Free radicals, metals and antioxidants in oxidative stress-induced cancer. *Chem-Biol Interact* **2006,** 160, (1), 1-40.
22. Dreher, D.; Junod, A. F., Role of oxygen free radicals in cancer development. *Eur. J. Cancer* **1996,** 32A, (1), 30-38.
23. Peponis, V.; Papathanasiou, M.; Kapranou, A.; Magkou, C.; Tyligada, A.; Melidonis, A.; Drosos, T.; Sitaras, N. M., Protective role of oral antioxidant supplementation in ocular surface of diabetic patients. *Br. J. Ophthalmol.* **2002,** 86, (12), 1369-1373.
24. Hayes, J. D.; McLellan, L. I., Glutathione and glutathione-dependent enzymes represent a Co-ordinately regulated defence against oxidative stress. *Free Radic. Res.* **1999,** 31, (4), 273-300.
25. Holmgren, A., Thioredoxin and Glutaredoxin Systems. *J. Biol. Chem.* **1989,** 264, (24), 13963-13966.
26. Wassmann, S.; Wassmann, K.; Nickenig, G., Modulation of oxidant and antioxidant enzyme expression and function in vascular cells. *Hypertension* **2004,** 44, (4), 381-386.
27. Reiter, R. J.; Tan, D. X.; Manchester, L. C.; Qi, W. B., Biochemical reactivity of melatonin with reactive oxygen and nitrogen species - A review of the evidence. *Cell Biochem. Biophys.* **2001,** 34, (2), 237-256.
28. Valachova, K.; Vargova, A.; Rapta, P.; Hrabarova, E.; Drafi, F.; Bauerova, K.; Juranek, I.; Soltes, L., Aurothiomalate as Preventive and Chain-Breaking Antioxidant in Radical Degradation of High-Molar-Mass Hyaluronan. *Chem. Biodivers.* **2011,** 8, (7), 1274-1283.
29. Radak, Z.; Chung, H. Y.; Goto, S., Systemic adaptation to oxidative challenge induced by regular exercise. *Free Radic. Biol. Med.* **2008,** 44, (2), 153-159.
30. Burton, G. W.; Ingold, K. U., Autoxidation of Biological Molecules .1. The Antioxidant Activity of Vitamin-E and Related Chain-Breaking Phenolic Antioxidants Invitro. *J Am Chem Soc* **1981,** 103, (21), 6472-6477.
31. Kumar, S.; Johansson, H.; Kanda, T.; Engman, L.; Muller, T.; Bergenudd, H.; Jonsson, M.; Pedulli, G. F.; Amorati, R.; Valgimigli, L., Catalytic Chain-Breaking Pyridinol Antioxidants. *J Org Chem* **2010,** 75, (3), 716-725.
32. Finkel, T.; Holbrook, N. J., Oxidants, oxidative stress and the biology of ageing. *Nature* **2000,** 408, (6809), 239-247.
33. Sies, H., Biochemistry of Oxidative Stress. *Angewandte Chemie-International Edition* **1986,** 25, (12), 1058-1071.
34. Marx, J. L., Oxygen Free-Radicals Linked to Many Diseases. *Science* **1987,** 235, (4788), 529-531.
35. Giustarini, D.; Dalle-Donne, I.; Tsikas, D.; Rossi, R., Oxidative stress and human diseases: Origin, link, measurement, mechanisms, and biomarkers. *Crit. Rev. Clin. Lab. Sci.* **2009,** 46, (5-6), 241-281.
36. Squadrito, G. L.; Cueto, R.; Dellinger, B.; Pryor, W. A., Quinoid redox cycling as a mechanism for sustained free radical generation by inhaled airborne particulate matter. *Free Radic. Biol. Med.* **2001,** 31, (9), 1132-1138.
37. Griffiths, H. R.; Olinski, R.; Coolen, S.; Collins, A.; Astley, S. B., Biomarkers. *Free Radic. Res.* **2002,** 36, 7-8.
38. Spiteller, P.; Kern, W.; Reiner, J.; Spiteller, G., Aldehydic lipid peroxidation products derived from linoleic acid. *Biochimica Et Biophysica Acta-Molecular and Cell Biology of Lipids* **2001,** 1531, (3), 188-208.
39. O'Brien, P. J.; Siraki, A. G.; Shangari, N., Aldehyde sources, metabolism, molecular toxicity mechanisms, and possible effects on human health. *Crit. Rev. Toxicol.* **2005,** 35, (7), 609-662.
40. Rikans, L. E.; Hornbrook, K. R., Lipid peroxidation, antioxidant protection and aging. *Biochimica Et Biophysica Acta-Molecular Basis of Disease* **1997,** 1362, (2-3), 116-127.
41. Dalle-Donne, I.; Scaloni, A.; Giustarini, D.; Cavarra, E.; Tell, G.; Lungarella, G.; Colombo, R.; Rossi, R.;

Milzani, A., Proteins as biomarkers of oxidative/nitrosative stress in diseases: The contribution of redox proteomics. *Mass Spectrom. Rev.* **2005,** 24, (1), 55-99.

42. Berlett, B. S.; Stadtman, E. R., Protein oxidation in aging, disease, and oxidative stress. *J. Biol. Chem.* **1997,** 272, (33), 20313-20316.

43. Stadtman, E. R., Protein Oxidation and Aging. *Science* **1992,** 257, (5074), 1220-1224.

44. Dean, R. T.; Fu, S. L.; Stocker, R.; Davies, M. J., Biochemistry and pathology of radical-mediated protein oxidation. *Biochem J* **1997,** 324, 1-18.

45. Davies, M. J.; Fu, S. L.; Wang, H. J.; Dean, R. T., Stable markers of oxidant damage to proteins and their application in the study of human disease. *Free Radic. Biol. Med.* **1999,** 27, (11-12), 1151-1163.

46. Dalle-Donne, I.; Rossi, R.; Giustarini, D.; Milzani, A.; Colombo, R., Protein carbonyl groups as biomarkers of oxidative stress. *Clin. Chim. Acta* **2003,** 329, (1-2), 23-38.

47. Friguet, B., Oxidized protein degradation and repair in ageing and oxidative stress. *FEBS Lett.* **2006,** 580, (12), 2910-2916.

48. Stadtman, E. R.; Berlett, B. S., Reactive oxygen-mediated protein oxidation in aging and disease. *Drug Metab. Rev.* **1998,** 30, (2), 225-243.

49. Carp, H.; Janoff, A.; Abrams, W.; Weinbaum, G.; Drew, R. T.; Weissbach, H.; Brot, N., Human Methionine Sulfoxide-Peptide Reductase, an Enzyme Capable of Reactivating Oxidized Alpha-1-Proteinase Inhibitor Invitro. *Am. Rev. Respir. Dis.* **1983,** 127, (3), 301-305.

50. Morrison, H. M.; Burnett, D.; Stockley, R. A., The Effect of Catalase and Methionine-S-Oxide Reductase on Oxidized Alpha-1-Proteinase Inhibitor. *Biol Chem Hoppe-Seyler* **1986,** 367, (5), 371-378.

51. Grune, T.; Merker, K.; Sandig, G.; Davies, K. J. A., Selective degradation of oxidatively modified protein substrates by the proteasome. *Biochem Biophys Res Commun* **2003,** 305, (3), 709-718.

52. Levine, R. L.; Mosoni, L.; Berlett, B. S.; Stadtman, E. R., Methionine residues as endogenous antioxidants in proteins. *Proc. Natl. Acad. Sci. U. S. A.* **1996,** 93, (26), 15036-15040.

53. Sevanian, A.; Hochstein, P., Mechanisms and Consequences of Lipid-Peroxidation in Biological-Systems. *Annu Rev Nutr* **1985,** 5, 365-390.

54. Porter, N. A., Chemistry of Lipid-Peroxidation. *Methods Enzymol* **1984,** 105, 273-282.

55. Niki, E., Antioxidants in Relation to Lipid-Peroxidation. *Chem. Phys. Lipids* **1987,** 44, (2-4), 227-253.

56. Spiteller, G., Lipid peroxidation in aging and age-dependent diseases. *Exp Gerontol* **2001,** 36, (9), 1425-1457.

57. Spiteller, G., Peroxidation of linoleic acid and its relation to aging and age dependent diseases. *Mech Ageing Dev* **2001,** 122, (7), 617-657.

58. Aldini, G.; Dalle-Donne, I.; Facino, R. M.; Milzani, A.; Carini, M., Intervention strategies to inhibit protein carbonylation by lipoxidation-derived reactive carbonyls. *Med. Res. Rev.* **2007,** 27, (6), 817-868.

59. Rindgen, D.; Nakajima, M.; Wehrli, S.; Xu, K. Y.; Blair, I. A., Covalent modifications to 2 '-deoxyguanosine by 4-oxo-2-nonenal, a novel product of lipid peroxidation. *Chem. Res. Toxicol.* **1999,** 12, (12), 1195-1204.

60. Luo, X. P.; Yazdanpanah, M.; Bhooi, N.; Lehotay, D. C., Determination of Aldehydes and Other Lipid-Peroxidation Products in Biological Samples by Gas-Chromatography Mass-Spectrometry. *Anal Biochem* **1995,** 228, (2), 294-298.

61. Grein, B.; Huffer, M.; Scheller, G.; Schreier, P., 4-Hydroxy-2-Alkenals and Other Products Formed by Water-Mediated Oxidative Decomposition of Alpha,Beta-Unsaturated Aldehydes. *J. Agric. Food. Chem.* **1993,** 41, (12), 2385-2390.

62. Alaiz, M.; Zamora, R.; Hidalgo, F. J., Antioxidative Activity of (E)-2-Octenal Amino-Acids Reaction-Products. *J. Agric. Food. Chem.* **1995,** 43, (3), 795-800.
63. Loidlstahlhofen, A.; Spiteller, G., Alpha-Hydroxyaldehydes, Products of Lipid-Peroxidation. *Biochimica Et Biophysica Acta-Lipids and Lipid Metabolism* **1994,** 1211, (2), 156-160.
64. Harman, D., Free-Radical Involvement in Aging - Pathophysiology and Therapeutic Implications. *Drugs Aging* **1993,** 3, (1), 60-80.
65. Yu, B. P.; Suescun, E. A.; Yang, S. Y., Effect of Age-Related Lipid-Peroxidation on Membrane Fluidity and Phospholipase-A2 - Modulation by Dietary Restriction. *Mech Ageing Dev* **1992,** 65, (1), 17-33.
66. Chen, J. J.; Yu, B. P., Alterations in Mitochondrial-Membrane Fluidity by Lipid-Peroxidation Products. *Free Radic. Biol. Med.* **1994,** 17, (5), 411-418.
67. Frankel, E. N., Chemistry of Free-Radical and Singlet Oxidation of Lipids. *Prog. Lipid Res.* **1984,** 23, (4), 197-221.
68. Oliver, C. N.; Ahn, B. W.; Moerman, E. J.; Goldstein, S.; Stadtman, E. R., Age-Related-Changes in Oxidized Proteins. *J. Biol. Chem.* **1987,** 262, (12), 5488-5491.
69. Mooradian, A. D.; Lung, C. C.; Shah, G.; Mahmoud, S.; Pinnas, J. L., Age-Related-Changes in Tissue Content of Malondialdehyde-Modified Proteins. *Life Sci* **1994,** 55, (20), 1561-1566.
70. Mahmoodi, H.; Hadley, M.; Chang, Y. X.; Draper, H. H., Increased Formation and Degradation of Malondialdehyde-Modified Proteins under Conditions of Peroxidative Stress. *Lipids* **1995,** 30, (10), 963-966.
71. Yuan, Q. Modification of biomolecules by lipoxidation derived aldehydes. Case Western Reserve University, Cleveland, OH, 2005.
72. Nystrom, T., Role of oxidative carbonylation in protein quality control and senescence. *EMBO J* **2005,** 24, (7), 1311-1317.
73. Dalle-Donne, I.; Giustarini, D.; Colombo, R.; Rossi, R.; Milzani, A., Protein carbonylation in human diseases. *Trends Mol. Med.* **2003,** 9, (4), 169-176.
74. Levine, R. L., Carbonyl modified proteins in cellular regulation, aging, and disease. *Free Radic. Biol. Med.* **2002,** 32, (9), 790-796.
75. Dalle-Donne, I.; Aldini, G.; Carini, M.; Colombo, R.; Rossi, R.; Milzani, A., Protein carbonylation, cellular dysfunction, and disease progression. *J. Cell. Mol. Med.* **2006,** 10, (2), 389-406.
76. Stadtman, E. R.; Levine, R. L., Free radical-mediated oxidation of free amino acids and amino acid residues in proteins. *Amino Acids* **2003,** 25, (3-4), 207-218.
77. Esterbauer, H.; Schaur, R. J.; Zollner, H., Chemistry and Biochemistry of 4-Hydroxynonenal, Malonaldehyde and Related Aldehydes. *Free Radic. Biol. Med.* **1991,** 11, (1), 81-128.
78. Januszewski, A. S.; Alderson, N. L.; Metz, T. O.; Thorpe, S. R.; Baynes, J. W., Role of lipids in chemical modification of proteins and development of complications in diabetes. *Biochem Soc Trans* **2003,** 31, 1413-1416.
79. Shacter, E., Quantification and significance of protein oxidation in biological samples. *Drug Metab. Rev.* **2000,** 32, (3-4), 307-326.
80. Conrad, C. C.; Choi, J. G.; Malakowsky, C. A.; Talent, J. M.; Dai, R.; Marshall, P.; Gracy, R. W., Identification of protein carbonyls after two-dimensional electrophoresis. *Proteomics* **2001,** 1, (7), 829-834.
81. Stadtman, E. R., Metal Ion-Catalyzed Oxidation of Proteins - Biochemical-Mechanism and Biological Consequences. *Free Radic. Biol. Med.* **1990,** 9, (4), 315-325.
82. Stadtman, E. R.; Berlett, B. S., Fenton Chemistry - Amino-Acid Oxidation. *J. Biol. Chem.* **1991,** 266, (26),

17201-17211.
83. Grune, T.; Merker, K.; Jung, T.; Sitte, N.; Davies, K. J. A., Protein oxidation and degradation during postmitotic senescence. *Free Radic. Biol. Med.* **2005,** 39, (9), 1208-1215.
84. Grune, T.; Jung, T.; Merker, K.; Davies, K. J. A., Decreased proteolysis caused by protein aggregates, inclusion bodies, plaques, lipofuscin, ceroid, and 'aggresomes' during oxidative stress, aging, and disease. *Int J Biochem Cell Biol* **2004,** 36, (12), 2519-2530.
85. Powell, S. R.; Wang, P.; Divald, A.; Teichberg, S.; Haridas, V.; McCloskey, T. W.; Davies, K. J. A.; Katzeff, H., Aggregates of oxidized proteins (lipofuscin) induce apoptosis through proteasome inhibition and dysregulation of proapoptotic proteins. *Free Radic. Biol. Med.* **2005,** 38, (8), 1093-1101.
86. Zhu, H.; Bilgin, M.; Snyder, M., Proteomics. *Annu Rev Biochem* **2003,** 72, 783-812.
87. Patterson, S. D.; Aebersold, R. H., Proteomics: the first decade and beyond. *Nat. Genet.* **2003,** 33, 311-323.
88. Anderson, N. L.; Anderson, N. G., Proteome and proteomics: New technologies, new concepts, and new words. *Electrophoresis* **1998,** 19, (11), 1853-1861.
89. Hanash, S., Disease proteomics. *Nature* **2003,** 422, (6928), 226-232.
90. Aebersold, R.; Mann, M., Mass spectrometry-based proteomics. *Nature* **2003,** 422, (6928), 198-207.
91. MacBeath, G., Protein microarrays and proteomics. *Nat. Genet.* **2002,** 32, 526-532.
92. Gevaert, K.; Vandekerckhove, J., Protein identification methods in proteomics. *Electrophoresis* **2000,** 21, (6), 1145-1154.
93. Patton, W. F., Detection technologies in proteome analysis. *Journal of Chromatography B-Analytical Technologies in the Biomedical and Life Sciences* **2002,** 771, (1-2), 3-31.
94. Cravatt, B. F.; Simon, G. M.; Yates, J. R., The biological impact of mass-spectrometry-based proteomics. *Nature* **2007,** 450, (7172), 991-1000.
95. Jensen, O. N., Modification-specific proteomics: characterization of post-translational modifications by mass spectrometry. *Curr. Opin. Chem. Biol.* **2004,** 8, (1), 33-41.
96. Aebersold, R.; Goodlett, D. R., Mass spectrometry in proteomics. *Chem. Rev.* **2001,** 101, (2), 269-295.
97. Mann, M.; Hendrickson, R. C.; Pandey, A., Analysis of proteins and proteomes by mass spectrometry. *Annu Rev Biochem* **2001,** 70, 437-473.
98. Domon, B.; Aebersold, R., Review - Mass spectrometry and protein analysis. *Science* **2006,** 312, (5771), 212-217.
99. Gygi, S. P.; Aebersold, R., Mass spectrometry and proteomics. *Curr. Opin. Chem. Biol.* **2000,** 4, (5), 489-494.
100. Witze, E. S.; Old, W. M.; Resing, K. A.; Ahn, N. G., Mapping protein post-translational modifications with mass spectrometry. *Nat. Methods* **2007,** 4, (10), 798-806.
101. Issaq, H. J., The role of separation science in proteomics research. *Electrophoresis* **2001,** 22, (17), 3629-3638.
102. Winnik, W. M.; Kitchin, K. T., Measurement of oxidative stress parameters using liquid chromatography-tandem mass spectroscopy (LC-MS/MS). *Toxicol. Appl. Pharmacol.* **2008,** 233, (1), 100-106.
103. Garza, S.; Moini, M., Analysis of complex protein mixtures with improved sequence coverage using (CE-MS/MS)(n). *Anal. Chem.* **2006,** 78, (20), 7309-7316.
104. Bantscheff, M.; Schirle, M.; Sweetman, G.; Rick, J.; Kuster, B., Quantitative mass spectrometry in proteomics: a critical review. *Anal. Bioanal. Chem.* **2007,** 389, (4), 1017-1031.
105. Ong, S. E.; Mann, M., Mass spectrometry-based proteomics turns quantitative. *Nat. Chem. Biol.* **2005,** 1, (5), 252-262.

106. Gasteiger, E.; Gattiker, A.; Hoogland, C.; Ivanyi, I.; Appel, R. D.; Bairoch, A., ExPASy: the proteomics server for in-depth protein knowledge and analysis. *Nucleic Acids Res* **2003,** 31, (13), 3784-3788.
107. Geer, L. Y.; Markey, S. P.; Kowalak, J. A.; Wagner, L.; Xu, M.; Maynard, D. M.; Yang, X. Y.; Shi, W. Y.; Bryant, S. H., Open mass spectrometry search algorithm. *Journal of Proteome Research* **2004,** 3, (5), 958-964.
108. Pedrioli, P. G. A.; Eng, J. K.; Hubley, R.; Vogelzang, M.; Deutsch, E. W.; Raught, B.; Pratt, B.; Nilsson, E.; Angeletti, R. H.; Apweiler, R.; Cheung, K.; Costello, C. E.; Hermjakob, H.; Huang, S.; Julian, R. K.; Kapp, E.; McComb, M. E.; Oliver, S. G.; Omenn, G.; Paton, N. W.; Simpson, R.; Smith, R.; Taylor, C. F.; Zhu, W. M.; Aebersold, R., A common open representation of mass spectrometry data and its application to proteomics research. *Nat. Biotechnol.* **2004,** 22, (11), 1459-1466.
109. Martens, L.; Hermjakob, H.; Jones, P.; Adamski, M.; Taylor, C.; States, D.; Gevaert, K.; Vandekerckhove, J.; Apweiler, R., PRIDE: The proteomics identifications database. *Proteomics* **2005,** 5, (13), 3537-3545.
110. Redtenbacher, J., Ueber die Zerlegungsprodukte des Glycer- inoxydes durch trockene Destillation. *Ann. Chem. Pharm.* **1843,** 47, 113-148.
111. Stevens, J. F.; Maier, C. S., Acrolein: Sources, metabolism, and biomolecular interactions relevant to human health and disease. *Mol. Nutr. Food Res.* **2008,** 52, (1), 7-25.
112. Beauchamp, R. O.; Andjelkovich, D. A.; Kligerman, A. D.; Morgan, K. T.; Heck, H. D., A Critical-Review of the Literature on Acrolein Toxicity. *CRC Crit. Rev. Toxicol.* **1985,** 14, (4), 309-380.
113. Al-Rawithi, S.; El-Yazigi, A.; Emst, P.; Al-Fiar, F.; Nicholls, P. J., Urinary excretion and pharmacokinetics of acrolein and its parent drug cyclophosphamide in bone marrow transplant patients. *Bone Marrow Transplant.* **1998,** 22, (5), 485-490.
114. LoPachin, R. M.; Barber, D. S.; Geohagen, B. C.; Gavin, T.; He, D.; Das, S., Structure-toxicity analysis of type-2 alkenes: In vitro neurotoxicity. *Toxicol. Sci.* **2007,** 95, (1), 136-146.
115. Uchida, K.; Kanematsu, M.; Morimitsu, Y.; Osawa, T.; Noguchi, N.; Niki, E., Acrolein is a product of lipid peroxidation reaction - Formation of free acrolein and its conjugate with lysine residues in oxidized low density lipoproteins. *J. Biol. Chem.* **1998,** 273, (26), 16058-16066.
116. Kuhla, B.; Haase, C.; Flach, K.; Luth, H. J.; Arendt, T.; Munch, G., Effect of pseudophosphorylation and cross-linking by lipid peroxidation and advanced glycation end product precursors on Tau aggregation and filament formation. *J. Biol. Chem.* **2007,** 282, (10), 6984-6991.
117. Furuhata, A.; Ishii, T.; Kumazawa, S.; Yamada, T.; Nakayama, T.; Uchida, K., N-epsilon-(3-methylpyridinium) lysine, a major antigenic adduct generated in acrolein-modified protein. *J. Biol. Chem.* **2003,** 278, (49), 48658-48665.
118. Chung, F. L.; Chen, H. J. C.; Nath, R. G., Lipid peroxidation as a potential endogenous source for the formation of exocyclic DNA adducts. *Carcinogenesis* **1996,** 17, (10), 2105-2111.
119. Chung, F. L.; Young, R.; Hecht, S. S., A Study of Chemical Carcinogenesis .61. Formation of Cyclic 1,N2-Propanodeoxyguanosine Adducts in DNA Upon Reaction with Acrolein or Crotonaldehyde. *Cancer Res.* **1984,** 44, (3), 990-995.
120. LoPachin, R. M.; Gavin, T.; Petersen, D. R.; Barber, D. S., Molecular Mechanisms of 4-Hydroxy-2-nonenal and Acrolein Toxicity: Nucleophilic Targets and Adduct Formation. *Chem. Res. Toxicol.* **2009,** 22, (9), 1499-1508.
121. Patel, J. M.; Block, E. R., Acrolein-Induced Injury to Cultured Pulmonary-Artery Endothelial-Cells. *Toxicol. Appl. Pharmacol.* **1993,** 122, (1), 46-53.
122. Nardini, M.; Finkelstein, E. I.; Reddy, S.; Valacchi, G.; Traber, M.; Cross, C. E.; van der Vliet, A.,

Acrolein-induced cytotoxicity in cultured human bronchial epithelial cells. Modulation by alpha-tocopherol and ascorbic acid. *Toxicology* **2002,** 170, (3), 173-185.
123. Tanel, A.; Averill-Bates, D. A., The aldehyde acrolein induces apoptosis via activation of the mitochondrial pathway. *Biochimica Et Biophysica Acta-Molecular Cell Research* **2005,** 1743, (3), 255-267.
124. Kaye, C. M., Biosynthesis of Mercapturic Acids from Allyl Alcohol, Allyl Esters and Acrolein. *Biochem J* **1973,** 134, (4), 1093-1101.
125. Hecht, S. S.; Carmella, S. G.; Chen, M. L.; Koch, J. F. D.; Miller, A. T.; Murphy, S. E.; Jensen, J. A.; Zimmerman, C. L.; Hatsukami, D. K., Quantitation of urinary metabolites of a tobacco-specific lung carcinogen after smoking cessation. *Cancer Res.* **1999,** 59, (3), 590-596.
126. He, X. M.; Carter, D. C., Atomic-Structure and Chemistry of Human Serum-Albumin. *Nature* **1992,** 358, (6383), 209-215.
127. Ishii, T.; Ito, S.; Kumazawa, S.; Sakurai, T.; Yamaguchi, S.; Mori, T.; Nakayama, T.; Uchida, K., Site-specific modification of positively-charged surfaces on human serum albumin by malondialdehyde. *Biochem Biophys Res Commun* **2008,** 371, (1), 28-32.
128. Giustarini, D.; Milzani, A.; Colombo, R.; Dalle-Donne, I.; Rossi, R., Nitric oxide and S-nitrosothiols in human blood. *Clin. Chim. Acta* **2003,** 330, (1-2), 85-98.
129. Aldini, G.; Vistoli, G.; Regazzoni, L.; Gamberoni, L.; Facino, R. M.; Yamaguchi, S.; Uchida, K.; Carini, M., Albumin is the main nucleophilic target of human plasma: A protective role against pro-atherogenic electrophilic reactive carbonyl species? *Chem. Res. Toxicol.* **2008,** 21, (4), 824-835.
130. Colombo, G.; Aldini, G.; Orioli, M.; Giustarini, D.; Gornati, R.; Rossi, R.; Colombo, R.; Carini, M.; Milzani, A.; Dalle-Donne, I., Water-Soluble alpha,beta-Unsaturated Aldehydes of Cigarette Smoke Induce Carbonylation of Human Serum Albumin. *Antioxidants & Redox Signaling* **2010,** 12, (3), 349-364.
131. Lambert, C.; Li, J.; Jonscher, K.; Yang, T. C.; Reigan, P.; Quintana, M.; Harvey, J.; Freed, B. M., Acrolein inhibits cytokine gene expression by alkylating cysteine and arginine residues in the NF-kappa B1 DNA binding domain. *J. Biol. Chem.* **2007,** 282, (27), 19666-19675.
132. Temple, A.; Yen, T. Y.; Gronert, S., Identification of specific protein carbonylation sites in model oxidations of human serum albumin. *J. Am. Soc. Mass Spectrom.* **2006,** 17, (8), 1172-1180.
133. Aldini, G.; Regazzoni, L.; Orioli, M.; Rimoldi, I.; Facino, R. M.; Carini, M., A tandem MS precursor-ion scan approach to identify variable covalent modification of albumin Cys34: a new tool for studying vascular carbonylation. *J. Mass Spectrom.* **2008,** 43, (11), 1470-1481.
134. Bhattacharya, A. A.; Curry, S.; Franks, N. P., Binding of the general anesthetics propofol and halothane to human serum albumin - High resolution crystal structures. *J. Biol. Chem.* **2000,** 275, (49), 38731-38738.
135. Richmond, T. J., Solvent Accessible Surface-Area and Excluded Volume in Proteins - Analytical Equations for Overlapping Spheres and Implications for the Hydrophobic Effect. *J. Mol. Biol.* **1984,** 178, (1), 63-89.
136. Fraczkiewicz, R.; Braun, W., Exact and efficient analytical calculation of the accessible surface areas and their gradients for macromolecules. *J. Comput. Chem.* **1998,** 19, (3), 319-333.
137. Fraczkiewicz, R. B., W. Calculation of Solvent Accessible Surface Areas, Atomic Solvation Energies and Their Gradients for Macromolecules. http://curie.utmb.edu/getarea.html
138. Benedetti, A.; Comporti, M.; Esterbauer, H., Identification of 4-Hydroxynoneal as a Cyto-Toxic Product Originating from the Peroxidation of Liver Microsomal Lipids. *Biochim Biophys Acta* **1980,** 620, (2), 281-296.
139. Pryor, W. A.; Porter, N. A., Suggested Mechanisms for the Production of 4-Hydroxy-2-Nonenal from the

Autoxidation of Polyunsaturated Fatty-Acids. *Free Radic. Biol. Med.* **1990,** 8, (6), 541-543.
140. Schneider, C.; Tallman, K. A.; Porter, N. A.; Brash, A. R., Two distinct pathways of formation of 4-hydroxynonenal - Mechanisms of nonenzymatic transformation of the 9-and 13-hydroperoxides of linoleic acid to 4-hydroxyalkenals. *J. Biol. Chem.* **2001,** 276, (24), 20831-20838.
141. Schneider, C.; Porter, N. A.; Brash, A. R., Routes to 4-hydroxynonenal: Fundamental issues in the mechanisms of lipid peroxidation. *J. Biol. Chem.* **2008,** 283, (23), 15539-15543.
142. Noordermeer, M. A.; Feussner, I.; Kolbe, A.; Veldink, G. A.; Vliegenthart, J. F. G., Oxygenation of (3Z)-alkenals to 4-hydroxy-(2E)-alkenals in plant extracts: A nonenzymatic process. *Biochem Biophys Res Commun* **2000,** 277, (1), 112-116.
143. Poli, G.; Schaur, R. J.; Siems, W. G.; Leonarduzzi, G., 4-hydroxynonenal: A membrane lipid oxidation product of medicinal interest. *Med. Res. Rev.* **2008,** 28, (4), 569-631.
144. Gil, L.; Siems, W.; Mazurek, B.; Gross, J.; Schroeder, P.; Voss, P.; Grune, T., Age-associated analysis of oxidative stress parameters in human plasma and erythrocytes. *Free Radic. Res.* **2006,** 40, (5), 495-505.
145. Kaneko, T.; Honda, S.; Nakano, S. I.; Matsuo, M., Lethal Effects of a Linoleic-Acid Hydroperoxide and Its Autoxidation Products, Unsaturated Aliphatic-Aldehydes, on Human-Diploid Fibroblasts. *Chem-Biol Interact* **1987,** 63, (2), 127-137.
146. Petersen, D. R.; Doorn, J. A., Reactions of 4-hydroxynonenal with proteins and cellular targets. *Free Radic. Biol. Med.* **2004,** 37, (7), 937-945.
147. Mitchell, D. Y.; Petersen, D. R., The Oxidation of Alpha-Beta-Unsaturated Aldehydic Products of Lipid-Peroxidation by Rat-Liver Aldehyde Dehydrogenases. *Toxicol. Appl. Pharmacol.* **1987,** 87, (3), 403-410.
148. Srivastava, S.; Watowich, S. J.; Petrash, J. M.; Srivastava, S. K.; Bhatnagar, A., Structural and kinetic determinants of aldehyde reduction by aldose reductase. *Biochemistry* **1999,** 38, (1), 42-54.
149. Jagt, D. L. V.; Kolb, N. S.; Jagt, T. J. V.; Chino, J.; Martinez, F. J.; Hunsaker, L. A.; Royer, R. E., Substrate-Specificity of Human Aldose Reductase - Identification of 4-Hydroxynonenal as an Endogenous Substrate. *Biochimica Et Biophysica Acta-Protein Structure and Molecular Enzymology* **1995,** 1249, (2), 117-126.
150. Alin, P.; Danielson, U. H.; Mannervik, B., 4-Hydroxyalk-2-Enals Are Substrates for Glutathione Transferase. *FEBS Lett.* **1985,** 179, (2), 267-270.
151. Dick, R. A.; Kwak, M. K.; Sutter, T. R.; Kensler, T. W., Antioxidative function and substrate specificity of NAD(P)H-dependent alkenal/one oxidoreductase - A new role for leukotriene B-4 12-hydroxydehydrogenase/15-oxoprostaglandin 13-reductase. *J. Biol. Chem.* **2001,** 276, (44), 40803-40810.
152. Carini, M.; Aldini, G.; Facino, R. M., Mass spectrometry for detection of 4-hydroxy-trans-2-nonenal (HNE) adducts with peptides and proteins. *Mass Spectrom. Rev.* **2004,** 23, (4), 281-305.
153. Kruman, I.; BruceKeller, A. J.; Bredesen, D.; Waeg, G.; Mattson, M. P., Evidence that 4-hydroxynonenal mediates oxidative stress-induced neuronal apoptosis. *J Neurosci* **1997,** 17, (13), 5089-5100.
154. Yoritaka, A.; Hattori, N.; Uchida, K.; Tanaka, M.; Stadtman, E. R.; Mizuno, Y., Immunohistochemical detection of 4-hydroxynonenal protein adducts in Parkinson disease. *Proc. Natl. Acad. Sci. U. S. A.* **1996,** 93, (7), 2696-2701.
155. Sayre, L. M.; Zelasko, D. A.; Harris, P. L. R.; Perry, G.; Salomon, R. G.; Smith, M. A., 4-hydroxynonenal-derived advanced lipid peroxidation end products are increased in Alzheimer's disease. *J Neurochem* **1997,** 68, (5), 2092-2097.
156. Lucas, D. T.; Szweda, L. I., Cardiac reperfusion injury: Aging, lipid peroxidation, and mitochondrial dysfunction. *Proc. Natl. Acad. Sci. U. S. A.* **1998,** 95, (2), 510-514.

157. Forman, H. J.; Fukuto, J. M.; Miller, T.; Zhang, H. Q.; Rinna, A.; Levy, S., The chemistry of cell signaling by reactive oxygen and nitrogen species and 4-hydroxynonenal. *Arch Biochem Biophys* **2008,** 477, (2), 183-195.
158. Tang, X. X.; Sayre, L. M.; Tochtrop, G. P., A mass spectrometric analysis of 4-hydroxy-2-(E)-nonenal modification of cytochrome c. *J. Mass Spectrom.* **2011,** 46, (3), 290-297.
159. Rauniyar, N.; Stevens, S. M.; Prokai-Tatrai, K.; Prokai, L., Characterization of 4-Hydroxy-2-nonenal-Modified Peptides by Liquid Chromatography-Tandem Mass Spectrometry Using Data-Dependent Acquisition: Neutral Loss-Driven MS(3) versus Neutral Loss-Driven Electron Capture Dissociation. *Anal. Chem.* **2009,** 81, (2), 782-789.
160. Rauniyar, N.; Prokai-Tatrai, K.; Prokai, L., Identification of carbonylation sites in apomyoglobin after exposure to 4-hydroxy-2-nonenal by solid-phase enrichment and liquid chromatography-electrospray ionization tandem mass spectrometry. *J. Mass Spectrom.* **2010,** 45, (4), 398-410.
161. Stevens, S. M.; Rauniyar, N.; Prokai, L., Rapid characterization of covalent modifications to rat brain mitochondrial proteins after ex vivo exposure to 4-hydroxy-2-nonenal by liquid chromatography-tandem mass spectrometry using data-dependent and neutral loss-driven MS3 acquisition. *J. Mass Spectrom.* **2007,** 42, (12), 1599-1605.
162. Bolgar, M. S.; Gaskell, S. J., Determination of the sites of 4-hydroxy-2-nonenal adduction to protein by electrospray tandem mass spectrometry. *Anal. Chem.* **1996,** 68, (14), 2325-2330.
163. Bruenner, B. A.; Jones, A. D.; German, J. B., Direct Characterization of Protein Adducts of the Lipid-Peroxidation Product 4-Hydroxy-2-Nonenal Using Electrospray Mass-Spectrometry. *Chem. Res. Toxicol.* **1995,** 8, (4), 552-559.
164. Aldini, G.; Gamberoni, L.; Orioli, M.; Beretta, G.; Regazzoni, L.; Facino, R. M.; Carini, M., Mass spectrometric characterization of covalent modification of human serum albumin by 4-hydroxy-trans-2-nonenal. *J. Mass Spectrom.* **2006,** 41, (9), 1149-1161.
165. Szapacs, M. E.; Riggins, J. N.; Zimmerman, L. J.; Liebler, D. C., Covalent adduction of human serum albumin by 4-hydroxy-2-nonenal: Kinetic analysis of competing alkylation reactions. *Biochemistry* **2006,** 45, (35), 10521-10528.
166. Riahi, Y.; Cohen, G.; Shamni, O.; Sasson, S., Signaling and cytotoxic functions of 4-hydroxyalkenals. *American Journal of Physiology-Endocrinology and Metabolism* **2010,** 299, (6), E879-E886.
167. Ross, P. L.; Huang, Y. L. N.; Marchese, J. N.; Williamson, B.; Parker, K.; Hattan, S.; Khainovski, N.; Pillai, S.; Dey, S.; Daniels, S.; Purkayastha, S.; Juhasz, P.; Martin, S.; Bartlet-Jones, M.; He, F.; Jacobson, A.; Pappin, D. J., Multiplexed protein quantitation in Saccharomyces cerevisiae using amine-reactive isobaric tagging reagents. *Molecular & Cellular Proteomics* **2004,** 3, (12), 1154-1169.
168. Wiese, S.; Reidegeld, K. A.; Meyer, H. E.; Warscheid, B., Protein labeling by iTRAQ: A new tool for quantitative mass spectrometry in proteome research. *Proteomics* **2007,** 7, (3), 340-350.
169. Griffin, T. J.; Xie, H. W.; Bandhakavi, S.; Popko, J.; Mohan, A.; Carlis, J. V.; Higgins, L., iTRAQ reagent-based quantitative proteomic analysis on a linear ion trap mass spectrometer. *Journal of Proteome Research* **2007,** 6, (11), 4200-4209.
170. Olsen, J. V.; Macek, B.; Lange, O.; Makarov, A.; Horning, S.; Mann, M., Higher-energy C-trap dissociation for peptide modification analysis. *Nat. Methods* **2007,** 4, (9), 709-712.
171. Keller, A.; Nesvizhskii, A. I.; Kolker, E.; Aebersold, R., Empirical statistical model to estimate the accuracy of peptide identifications made by MS/MS and database search. *Anal. Chem.* **2002,** 74, (20), 5383-5392.
172. Choi, H.; Nesvizhskii, A. I., Semisupervised model-based validation of peptide identifications in mass

spectrometry-based proteomics. *Journal of Proteome Research* **2008,** 7, (1), 254-265.
173. Crabb, J. W.; O'Neil, J.; Miyagi, M.; West, K.; Hoff, H. F., Hydroxynonenal inactivates cathepsin B by forming Michael adducts with active site residues. *Protein Sci.* **2002,** 11, (4), 831-840.
174. Kleinova, M.; Belgacem, O.; Pock, K.; Rizzi, A.; Buchacher, A.; Allmaier, G., Characterization of cysteinylation of pharmaceutical-grade human serum albumin by electrospray ionization mass spectrometry and low-energy collision-induced dissociation tandem mass spectrometry. *Rapid Commun. Mass Spectrom.* **2005,** 19, (20), 2965-2973.
175. Schwartz, J. C. S., J. P.; Quarmby, S. T., Improving the Fundamentals of Msn on 2D Ion Traps: New Ion Activation and Isolation Techniques;. In *53rd ASMS Conference on Mass Spectrometry,*, San Antonio, Texas, 2005.
176. Tabb, D. L.; Friedman, D. B.; Ham, A. J. L., Verification of automated peptide identifications from proteomic tandem mass spectra. *Nature Protocols* **2006,** 1, (5), 2213-2222.
177. Curry, S.; Mandelkow, H.; Brick, P.; Franks, N., Crystal structure of human serum albumin complexed with fatty acid reveals an asymmetric distribution of binding sites. *Nat. Struct. Biol.* **1998,** 5, (9), 827-835.
178. Petitpas, I.; Grune, T.; Bhattacharya, A. A.; Curry, S., Crystal structures of human serum albumin complexed with monounsaturated and polyunsaturated fatty acids. *J. Mol. Biol.* **2001,** 314, (5), 955-960.
179. Beinert, H.; Kennedy, M. C., Aconitase, a 2-Faced Protein - Enzyme and Iron Regulatory Factor. *FASEB J.* **1993,** 7, (15), 1442-1449.
180. Martius, C., Uber den Abbau der Citronensaure. *Z. Physiol. Chem.* **1937,** 247, 104-110.
181. Lauble, H.; Stout, C. D., Steric and Conformational Features of the Aconitase Mechanism. *Proteins-Structure Function and Genetics* **1995,** 22, (1), 1-11.
182. Beinert, H.; Kennedy, M. C.; Stout, C. D., Aconitase as iron-sulfur protein, enzyme, and iron-regulatory protein. *Chem. Rev.* **1996,** 96, (7), 2335-2373.
183. Chen, O. S.; Blemings, K. P.; Schalinske, K. L.; Eisenstein, R. S., Dietary iron intake rapidly influences iron regulatory proteins, ferritin subunits and mitochondrial aconitase in rat liver. *J Nutr* **1998,** 128, (3), 525-535.
184. Theil, E. C.; Eisenstein, R. S., Combinatorial mRNA regulation: Iron regulatory proteins and iso-iron-responsive elements (Iso-IREs). *J. Biol. Chem.* **2000,** 275, (52), 40659-40662.
185. Eisenstein, R. S., Iron regulatory proteins and the molecular control of mammalian iron metabolism. *Annu Rev Nutr* **2000,** 20, 627-662.
186. Robbins, A. H.; Stout, C. D., The Structure of Aconitase. *Proteins-Structure Function and Genetics* **1989,** 5, (4), 289-312.
187. Zheng, L. M.; Andrews, P. C.; Hermodson, M. A.; Dixon, J. E.; Zalkin, H., Cloning and Structural Characterization of Porcine Heart Aconitase. *J. Biol. Chem.* **1990,** 265, (5), 2814-2821.
188. Kennedy, C.; Gawron, O.; Rauner, R., Pig Heart Aconitase. *Biochem Biophys Res Commun* **1972,** 47, (4), 740-&.
189. Robbins, A. H.; Stout, C. D., Structure of Activated Aconitase - Formation of the [4fe-4s] Cluster in the Crystal. *Proc. Natl. Acad. Sci. U. S. A.* **1989,** 86, (10), 3639-3643.
190. Ruzicka, F. J.; Beinert, H., Mitochondrial Iron Protein with Properties of a High-Potential Iron-Sulfur Protein. *Biochem Biophys Res Commun* **1974,** 58, (3), 556-563.
191. Ruzicka, F. J.; Beinert, H., Soluble High Potential Type Iron-Sulfur Protein from Mitochondria Is Aconitase. *J. Biol. Chem.* **1978,** 253, (8), 2514-2517.
192. Emptage, M. H.; Kent, T. A.; Kennedy, M. C.; Beinert, H.; Munck, E., Mossbauer and

Electron-Paramagnetic-Res Studies of Activated Aconitase - Development of a Localized Valence State at a Subsite of the [4fe-4s] Cluster on Binding of Citrate. *Proceedings of the National Academy of Sciences of the United States of America-Biological Sciences* **1983,** 80, (15), 4674-4678.
193. Emptage, M. H.; Dreyer, J. L.; Kennedy, M. C.; Beinert, H., Optical and Electron-Paramagnetic-Res Characterization of Different Species of Active and Inactive Aconitase. *J. Biol. Chem.* **1983,** 258, (18), 1106-1111.
194. Kennedy, M. C.; Emptage, M. H.; Dreyer, J. L.; Beinert, H., The Role of Iron in the Activation-Inactivation of Aconitase. *J. Biol. Chem.* **1983,** 258, (18), 1098-1105.
195. Beinert, H.; Kennedy, M. C., Engineering of Protein-Bound Iron-Sulfur Clusters - a Tool for the Study of Protein and Cluster Chemistry and Mechanism of Iron-Sulfur Enzymes. *Eur J Biochem* **1989,** 186, (1-2), 5-15.
196. Bulteau, A. L.; Ikeda-Saito, M.; Szweda, L. I., Redox-dependent modulation of aconitase activity in intact mitochondria. *Biochemistry* **2003,** 42, (50), 14846-14855.
197. Werst, M. M.; Kennedy, M. C.; Houseman, A. L. P.; Beinert, H.; Hoffman, B. M., Characterization of the [4fe-4s]+ Cluster at the Active-Site of Aconitase by Fe-57, S-33, and N-14 Electron Nuclear Double-Resonance Spectroscopy. *Biochemistry* **1990,** 29, (46), 10533-10540.
198. Kent, T. A.; Emptage, M. H.; Merkle, H.; Kennedy, M. C.; Beinert, H.; Munck, E., Mossbauer Studies of Aconitase - Substrate and Inhibitor Binding, Reaction Intermediates, and Hyperfine Interactions of Reduced Fe-3 and Fe-4 Clusters. *J. Biol. Chem.* **1985,** 260, (11), 6871-6881.
199. Kennedy, M. C.; Werst, M.; Telser, J.; Emptage, M. H.; Beinert, H.; Hoffman, B. M., Mode of Substrate Carboxyl Binding to the [4fe-4s]+ Cluster of Reduced Aconitase as Studied by O-17 and C-13 Electron Nuclear Double-Resonance Spectroscopy. *Proc. Natl. Acad. Sci. U. S. A.* **1987,** 84, (24), 8854-8858.
200. Lauble, H.; Kennedy, M. C.; Beinert, H.; Stout, C. D., Crystal-Structures of Aconitase with Isocitrate and Nitroisocitrate Bound. *Biochemistry* **1992,** 31, (10), 2735-2748.
201. Goodsell, D. S.; Lauble, H.; Stout, C. D.; Olson, A. J., Automated Docking in Crystallography - Analysis of the Substrates of Aconitase. *Proteins-Structure Function and Genetics* **1993,** 17, (1), 1-10.
202. Zheng, L.; Kennedy, M. C.; Beinrt, H.; Zalkin, H., Mutational Analysis of Active-Site Residues in Pig-Heart Aconitase. *J. Biol. Chem.* **1992,** 267, (11), 7895-7903.
203. Imlay, J. A., Iron-sulphur clusters and the problem with oxygen. *Mol Microbiol* **2006,** 59, (4), 1073-1082.
204. Castro, L.; Rodriguez, M.; Radi, R., Aconitase Is Readily Inactivated by Peroxynitrite, but Not by Its Precursor, Nitric-Oxide. *J. Biol. Chem.* **1994,** 269, (47), 29409-29415.
205. Han, D.; Canali, R.; Garcia, J.; Aguilera, R.; Gallaher, T. K.; Cadenas, E., Sites and mechanisms of aconitase inactivation by peroxynitrite: Modulation by citrate and glutathione. *Biochemistry* **2005,** 44, (36), 11986-11996.
206. Andersson, U.; Leighton, B.; Young, M. E.; Blomstrand, E.; Newsholme, E. A., Inactivation of aconitase and oxoglutarate dehydrogenase in skeletal muscle in vitro by superoxide anions and/or nitric oxide. *Biochem Biophys Res Commun* **1998,** 249, (2), 512-516.
207. Verniquet, F.; Gaillard, J.; Neuburger, M.; Douce, R., Rapid Inactivation of Plant Aconitase by Hydrogen-Peroxide. *Biochem J* **1991,** 276, 643-648.
208. Yarian, C. S.; Rebrin, I.; Sohal, R. S., Aconitase and ATP synthase are targets of malondialdehyde modification and undergo an age-related decrease in activity in mouse heart mitochondria. *Biochem Biophys Res Commun* **2005,** 330, (1), 151-156.
209. Yan, L. J.; Levine, R. L.; Sohal, R. S., Oxidative damage during aging targets mitochondrial aconitase. *Proc. Natl. Acad. Sci. U. S. A.* **1997,** 94, (21), 11168-11172.

210. James, E. A.; Gygi, S. P.; Adams, M. L.; Pierce, R. H.; Fausto, N.; Aebersold, R. H.; Nelson, S. D.; Bruschi, S. A., Mitochondrial aconitase modification, functional inhibition, and evidence for a supramolecular complex of the TCA cycle by the renal toxicant S-(1,1,2,2-tetrafluoroethyl)-L-cysteine. *Biochemistry* **2002,** 41, (21), 6789-6797.
211. Rose, I. A.; Oconnell, E. L., Mechanism of Aconitase Action .I. Hydrogen Transfer Reaction. *J. Biol. Chem.* **1967,** 242, (8), 1870-&.
212. Kennedy, M. C.; Antholine, W. E.; Beinert, H., An EPR investigation of the products of the reaction of cytosolic and mitochondrial aconitases with nitric oxide. *J. Biol. Chem.* **1997,** 272, (33), 20340-20347.
213. Kennedy, M. C.; Spoto, G.; Emptage, M. H.; Beinert, H., The Active-Site Sulfhydryl of Aconitase Is Not Required for Catalytic Activity. *J. Biol. Chem.* **1988,** 263, (17), 8190-8193.
214. Lenaz, G., Role of mitochondria in oxidative stress and ageing. *Biochimica Et Biophysica Acta-Bioenergetics* **1998,** 1366, (1-2), 53-67.
215. Bayir, H.; Kagan, V. E., Bench-to-bedside review: Mitochondrial injury, oxidative stress and apoptosis - there is nothing more practical than a good theory. *Critical Care* **2008,** 12, (1).
216. Becker, L. B.; Vanden Hoek, T. L.; Shao, Z. H.; Li, C. Q.; Schumacker, P. T., Generation of superoxide in cardiomyocytes during ischemia before reperfusion. *American Journal of Physiology-Heart and Circulatory Physiology* **1999,** 277, (6), H2240-H2246.
217. Becker, L. B., New concepts in reactive oxygen species and cardiovascular reperfusion physiology. *Cardiovasc. Res.* **2004,** 61, (3), 461-470.
218. Fridovich, I., Superoxide Dismutases. *Adv. Enzymol. Relat. Areas Mol. Biol.* **1986,** 58, 61-97.
219. Chance, B.; Sies, H.; Boveris, A., Hydroperoxide Metabolism in Mammalian Organs. *Physiol. Rev.* **1979,** 59, (3), 527-605.
220. Richter, C., Do Mitochondrial-DNA Fragments Promote Cancer and Aging. *FEBS Lett.* **1988,** 241, (1-2), 1-5.
221. Enns, G. M., The contribution of mitochondria to common disorders. *Mol. Genet. Metab.* **2003,** 80, (1-2), 11-26.
222. Han YY, R. I., **Mitochondria in Acute Brain Injury**. *Brain Inj.* **2001**, 145-161.
223. Kevin, L. G.; Camara, A. K. S.; Riess, M. L.; Novalija, E.; Stowe, D. F., Ischemic preconditioning alters real-time measure of O-2 radicals in intact hearts with ischemia and reperfusion. *American Journal of Physiology-Heart and Circulatory Physiology* **2003,** 284, (2), H566-H574.
224. Herrero, A.; Barja, G., Sites and mechanisms responsible for the low rate of free radical production of heart mitochondria in the long-lived pigeon. *Mech Ageing Dev* **1997,** 98, (2), 95-111.
225. Chen, Q.; Vazquez, E. J.; Moghaddas, S.; Hoppel, C. L.; Lesnefsky, E. J., Production of reactive oxygen species by mitochondria - Central role of complex III. *J. Biol. Chem.* **2003,** 278, (38), 36027-36031.
226. Turrens, J. F.; Boveris, A., GENERATION OF SUPEROXIDE ANION BY THE NADH DEHYDROGENASE OF BOVINE HEART-MITOCHONDRIA. *Biochem J* **1980,** 191, (2), 421-427.
227. Sugioka, K.; Nakano, M.; Totsunenakano, H.; Minakami, H.; Terokubota, S.; Ikegami, Y., Mechanism of O-2-Generation in Reduction and Oxidation Cycle of Ubiquinones in a Model of Mitochondrial Electron-Transport Systems. *Biochim Biophys Acta* **1988,** 936, (3), 377-385.
228. Chen, Q.; Moghaddas, S.; Hoppel, C. L.; Lesnefsky, E. J., Ischemic defects in the electron transport chain increase the production of reactive oxygen species from isolated rat heart mitochondria. *American Journal of Physiology-Cell Physiology* **2008,** 294, (2), C460-C466.
229. Gusdon, A. M.; Chen, J.; Votyakova, T. V.; Mathews, C. E., Quantification, Localization, and Tissue

Specificities of Mouse Mitochondrial Reactive Oxygen Species Production. In *Methods in Enzymology, Vol 456: Mitochondrial Function, Part A: Mitochondrial Electron Transport Complexes and Reactive Oxygen Species*, 2009; Vol. 456, pp 439-457.
230. Capaldi, R. A., Arrangement of Proteins in the Mitochondrial Inner Membrane. *Biochim Biophys Acta* **1982,** 694, (3), 291-306.
231. Navarro, A.; Boveris, A., The mitochondrial energy transduction system and the aging process. *American Journal of Physiology-Cell Physiology* **2007,** 292, (2), C670-C686.
232. Barja, G., Mitochondrial free radical production and aging in mammals and birds. *Towards Prolongation of the Healthy Life Span - Practical Approaches to Intervention* **1998,** 854, 224-238.
233. Eefting, F.; Rensing, B.; Wigman, J.; Pannekoek, W. J.; Liu, W. M.; Cramer, M. J.; Lips, D. J.; Doevendans, P. A., Role of apoptosis in reperfusion injury. *Cardiovasc. Res.* **2004,** 61, (3), 414-426.
234. Chen, J. J.; Henderson, G. I.; Freeman, G. L., Role of 4-hydroxynonenal in modification of cytochrome c oxidase in ischemia/reperfused rat heart. *J. Mol. Cell. Cardiol.* **2001,** 33, (11), 1919-1927.
235. Di Lisa, F.; Bernardi, P., Mitochondria and ischemia-reperfusion injury of the heart: Fixing a hole. *Cardiovasc. Res.* **2006,** 70, (2), 191-199.
236. Kerbey, A. L.; Randle, P. J.; Cooper, R. H.; Whitehouse, S.; Pask, H. T.; Denton, R. M., Regulation of Pyruvate-Dehydrogenase in Rat-Heart - Mechanism of Regulation of Proportions of Dephosphorylated and Phosphorylated Enzyme by Oxidation of Fatty-Acids and Ketone-Bodies and of Effects of Diabetes - Role of Coenzyme-a, Acetyl-Coenzyme-a and Reduced and Oxidized Nicotinamide-Adenine Dinucleotideb. *Biochem J* **1976,** 154, (2), 327-348.
237. Yacoub, Y., Method procedures for sampling aldehyde and ketone using 2,4-dinitrophenylhydrazine - a review. *Proceedings of the Institution of Mechanical Engineers Part D-Journal of Automobile Engineering* **1999,** 213, (D5), 503-517.
238. Dalle-Donne, I.; Carini, M.; Orioli, M.; Vistoli, G.; Regazzoni, L.; Colombo, G.; Rossi, R.; Milzani, A.; Aldini, G., Protein carbonylation: 2,4-dinitrophenylhydrazine reacts with both aldehydes/ketones and sulfenic acids. *Free Radic. Biol. Med.* **2009,** 46, (10), 1411-1419.
239. Haukanes, B. I.; Kvam, C., Application of Magnetic Beads in Bioassays. *Bio-Technology* **1993,** 11, (1), 60-63.
240. Olsvik, O.; Popovic, T.; Skjerve, E.; Cudjoe, K. S.; Hornes, E.; Ugelstad, J.; Uhlen, M., Magnetic Separation Techniques in Diagnostic Microbiology. *Clin. Microbiol. Rev.* **1994,** 7, (1), 43-54.
241. Holmberg, A.; Blomstergren, A.; Nord, O.; Lukacs, M.; Lundeberg, J.; Uhlen, M., The biotin-streptavidin interaction can be reversibly broken using water at elevated temperatures. *Electrophoresis* **2005,** 26, (3), 501-510.
242. Hensley, K., Detection of Protein Carbonyls by Means of Biotin Hydrazide-Streptavidin Affinity Methods. **2009,** 536, 457-462.
243. Meany, D. L.; Xie, H. W.; Thompson, L. V.; Arriaga, E. A.; Griffin, T. J., Identification of carbonylated proteins from enriched rat skeletal muscle mitochondria using affinity chromatography-stable isotope labeling and tandem mass spectrometry. *Proteomics* **2007,** 7, (7), 1150-1163.
244. Soreghan, B. A.; Yang, F.; Thomas, S. N.; Hsu, J.; Yang, A. J., High-throughput proteomic-based identification of oxidatively induced protein carbonylation in mouse brain. *Pharm. Res.* **2003,** 20, (11), 1713-1720.
245. Mirzaei, H.; Regnier, F., Identification and quantification of protein carbonylation using light and heavy isotope labeled Girard's P reagent. *J Chromatogr A* **2006,** 1134, (1-2), 122-133.
246. Gygi, S. P.; Rist, B.; Gerber, S. A.; Turecek, F.; Gelb, M. H.; Aebersold, R., Quantitative analysis of complex

protein mixtures using isotope-coded affinity tags. *Nat. Biotechnol.* **1999,** 17, (10), 994-999.
247. Gygi, S. P.; Rist, B.; Griffin, T. J.; Eng, J.; Aebersold, R., Proteome analysis of low-abundance proteins using multidimensional chromatography and isotope-coded affinity tags. *Journal of Proteome Research* **2002,** 1, (1), 47-54.
248. Roe, M. R.; Xie, H. W.; Bandhakavi, S.; Griffin, T. J., Proteomic mapping of 4-hydroxynonenal protein modification sites by solid-phase hydrazide chemistry and mass spectrometry. *Anal. Chem.* **2007,** 79, (10), 3747-3756.
249. Gorg, A.; Weiss, W.; Dunn, M. J., Current two-dimensional electrophoresis technology for proteomics. *Proteomics* **2004,** 4, (12), 3665-3685.
250. Dunn, W. B.; Bailey, N. J. C.; Johnson, H. E., Measuring the metabolome: current analytical technologies. *Analyst* **2005,** 130, (5), 606-625.

Appendices-I: Calculation

Modification Description	Modification Composition	Monoisotopic Mass Shift	Type
Oxidation at Met	+O	+15.994915	Differential
Iodoacetamide Alkylation at Cys	$+C_2H_3NO$	+57.021464	Fixed or Differential
Michael Addition of HNE at Cys, Reduced	$+C_9H_{18}O_2$ –[acetamide cap]	+101.109216	Differential
Michael Addition of HNE at His, Reduced	$+C_9H_{18}O_2$	+158.130680	Differential
Michael Addition of HNE at Lys, Reduced	$+C_9H_{18}O_2$	+158.130680	Differential
Schiff Base Formation with HNE at Lys, Reduced	$+C_9H_{16}O$	+140.120115	Differential
Michael Addition of HNE at Cys, **Not** Reduced	$+C_9H_{16}O_2$ –[acetamide cap]	+99.093566	Differential
Michael Addition of HNE at His, **Not** Reduced	$+C_9H_{16}O_2$	+156.115030	Differential
Michael Addition of HNE at Lys, **Not** Reduced	$+C_9H_{16}O_2$	+156.115030	Differential
Schiff Base Formation with HNE at Lys, **Not** Reduced	$+C_9H_{14}O$	+138.104465	Differential

Table A1. Precise modification mass shifts considered in non-iTRAQ experiments; note that while oxidation at Met and iodoacetamide alkylation at Cys were always included, reduced and non-reduced HNE modifications were considered in separate Sequest searches.

Modification Description	Modification Composition	Monoisotopic Mass Shift	Type
Oxidation at Met	+O	+15.994915	Differential
Iodoacetamide Alkylation at Cys	$+C_2H_3NO$	+57.021464	Fixed or Differential
iTRAQ Label at Lys	$+{}^{12}C_5{}^{13}C_2{}^{1}H_{12}{}^{14}N_2{}^{18}O$/ $+{}^{12}C_4{}^{13}C_3{}^{1}H_{12}{}^{14}N^{15}N^{16}O$	+144.103991†	Fixed
iTRAQ Label at Peptide N-terminus	$+{}^{12}C_5{}^{13}C_2{}^{1}H_{12}{}^{14}N_2{}^{18}O$/ $+{}^{12}C_4{}^{13}C_3{}^{1}H_{12}{}^{14}N^{15}N^{16}O$	+144.103991†	Fixed

iTRAQ Label at Tyr‡	$+^{12}C_5{}^{13}C_2{}^{1}H_{12}{}^{14}N_2{}^{18}O$/ $+^{12}C_4{}^{13}C_3{}^{1}H_{12}{}^{14}N^{15}N^{16}O$	+144.103991†	Differential
Michael Addition of HNE at Cys, Reduced	$+C_9H_{18}O_2$ –[acetamide cap]	+101.109216	Differential
Michael Addition of HNE at His, Reduced	$+C_9H_{18}O_2$	+158.130680	Differential
Michael Addition of HNE at Lys, Reduced	$+C_9H_{18}O_2$ –[iTRAQ label]	+14.026689	Differential
Schiff Base Formation with HNE at Lys, Reduced	$+C_9H_{16}O$ –[iTRAQ label]	–3.983876	Differential

Table A2. Precise modification mass shifts considered in iTRAQ experiments; † iTRAQ label mass shift value was the average for the four tags (separation between heavy pair and light pair is circa 0.004 Da, too small to resolve with available instrumentation); ‡ iTRAQ label addition at tyrosine only tested with Orbitrap data and found to be uncommon.

Modified Peptide (with flanking residues)	**Modification Site or Sites (MA indicates Michael addition; SB indicates Schiff base formation)**	**Counts of LC–MS/MS runs in which the modified peptide was identified using LTQ XL CID scans (maximum = 12)/LTQ XL ETD scans (maximum = 12)/LTQ Orbitrap Velos CID scans associated with high mass accuracy Orbitrap precursor ion mass measurements (maximum = 3)**	
		1:1 HNE to HSA Ratio	**10:1 HNE to HSA Ratio**
K.DLGEENFKALVLIAFAQYLQQC#PFEDHVK.L	Cys-034 (MA)	not detected	0/0/1
K.ALVLIAFAQYLQQC#PFEDHVK.L	Cys-034 (MA)	9/1/0	9/3/3
K.SLH@TLFGDK.L	His-067 (MA)	12/0/3	12/5/3
K.SLHTLFGDK^LCTVATLR.E	Lys-073 (MA)	not detected	3/0/0
R.NECFLQHK~DDNPNLPR.L	Lys-106 (SB)	not detected	0/1/0
R.LVRPEVDVMCTAFH@DNEETFLK.K	His-128 (MA)	0/2/0	2/3/0

K.K^YLYEIAR.R	Lys-137 (MA)	not detected	1/0/0
R.RH@PYFYAPELLFFAK.R	His-146 (MA)	12/11/0	12/12/3
R.RH@PYFYAPELLFFAKR.Y	His-146 (MA)	not detected	1/0/0
R.RH@PYFYAPELLFFAK^R.Y	His-146 (MA) & Lys-159 (MA)	not detected	0/2/1
R.YK^AAFTECCQAADK.A	Lys-162 (MA)	not detected	12/2/2
R.YK~AAFTECCQAADK.A	Lys-162 (SB)	not detected	10/1/0
R.LK^CASLQK.F	Lys-199 (MA)	6/0/2	11/0/3
R.AFK^AWAVAR.L	Lys-212 (MA)	not detected	12/0/1
K.AEFAEVSK^LVTDLTK.V	Lys-233 (MA)	not detected	9/4/0
K.LVTDLTK^VH@TECCHGDLLECADDR.A	Lys-240 (MA) & His-242 (MA)	8/0/0	3/0/0
K.VH@TECCHGDLLECADDR.A	His-242 (MA)	0/7/0	0/7/0
K.VH@TECCH@GDLLECADDR.A	His-242 (MA) & His-247 (MA)	not detected	9/4/0
K.VH@TECCH@GDLLECADDRADLAK.Y	His-242 (MA) & His-247 (MA)	not detected	3/7/0
R.ADLAK^YICENQDSISSK.L	Lys-262 (MA)	not detected	5/3/0
K.SH@CIAEVENDEMPADLPSLAADFVESK.D	His-288 (MA)	10/0/0	12/1/3
K.SH@CIAEVENDEM*PADLPSLAADFVESK.D	His-288 (MA)	1/0/0	11/1/1
R.RH@PDYSVVLLLR.L	His-338 (MA)	4/0/0	12/3/3
R.H@PDYSVVLLLR.L	His-338 (MA)	not detected	2/0/0
R.H@PDYSVVLLLRLAKTYETTLEK.C	His-338 (MA)	0/6/0	1/9/0
R.LAK^TYETTLEK.C	Lys-351 (MA)	10/0/0	9/0/0
R.LAK~TYETTLEK.C	Lys-351 (SB)	not detected	3/1/0
K.TYETTLEK^CCAAADPHECYAK.V	Lys-359 (MA)	not detected	1/3/0
K.CCAAADPH@ECYAK.V	His-367 (MA)	not detected	9/0/0
K.VFDEFK^PLVEEPQNLIK.Q	Lys-378 (MA)	not detected	5/1/0
K.QNCELFEQLGEYK^FQNALLVR.Y	Lys-402 (MA)	not detected	4/0/2
K.K^VPQVSTPTLVEVSR.N	Lys-414 (MA)	not detected	11/1/3
K.K~VPQVSTPTLVEVSR.N	Lys-414 (SB)	8/0/0	12/1/3
R.VTK^CCTESLVNR.R	Lys-475 (MA)	not detected	1/0/0
K.EFNAETFTFH@ADICTLSEK.E	His-510 (MA)	1/8/0	12/11/0
K.EFNAETFTFHADICTLSEK^ER.Q	Lys-519 (MA)	not detected	1/0/0
K.K^QTALVELVK.H	Lys-525 (MA)	not detected	0/1/3
K.K~QTALVELVK.H	Lys-525 (SB)	3/0/3	8/3/3
K.EQLK^AVMDDFAAFVEK.C	Lys-545 (MA)	4/7/0	11/11/3
K.EQLK~AVMDDFAAFVEK.C	Lys-545 (SB)	not detected	4/7/0

Table A3. Counts of LC–MS/MS runs in which the indicated modified peptide was identified.

The PeptideProphet score threshold was 0.9. Five independent preparations were made for each HNE:HSA ratio. For each ratio, four preparations were analyzed using a Thermo LTQ XL linear ion trap mass spectrometer and one preparation was analyzed using a Thermo LTQ Orbitrap Velos instrument. In all cases, three replicate LC–MS/MS runs were recorded for each preparation. For the LTQ XL runs, one collision-induced dissocation (CID) and one electron-transfer dissociation (ETD) MS/MS were recorded for each precursor ion selected for fragmentation; resulting CID and ETD spectrum counts are presented separately. For the LTQ Orbitrap Velos runs, only CID MS/MS were recorded. C# indicates HNE Michael addition at Cys followed by reduction; H@ indicates HNE Michael addition at His followed by reduction; K^ indicates HNE Michael addition at Lys followed by reduction; K~ indicates Schiff base formation with HNE at Lys followed by reduction; M* indicates oxidation at Met.

Modification Site or Modification Site(s) Associated with Unmodified Peptide (MA indicates Michael addition; SB indicates Schiff base formation)	**Peptide**	**Mass List Constituents**		
		$[M+H]^+$	**$[M+2H]^{2+}$**	**$[M+3H]^{3+}$**
Cys-034 (MA)	ALVLIAFAQYLQQC#PFEDHVK	2879.60	1440.31	960.54
Cys-034-associated	ALVLIAFAQYLQQCPFEDHVK	2778.49	1389.75	926.84
His-067 (MA)	SLH@TLFGDK	1463.88	732.44	488.63
His-067-associated	SLHTLFGDK	1305.74	653.38	435.92
His-105 (MA)	NECFLQH@K	1521.84	761.42	507.95
His-105-associated	NECFLQHK	1363.71	682.36	455.24
Lys-162 (MA)	YK^AAFTECCQAADK	2109.06	1055.04	703.69
Lys-162-associated	YKAAFTECCQAADK	2095.04	1048.02	699.02
Lys-162-associated	AAFTECCQAADK	1659.78	830.39	553.93
Lys-199 (MA)	LK^CASLQK	1393.87	697.44	465.30
Lys-199-associated	LKCASLQK	1379.85	690.43	460.62
Lys-199-associated	CASLQK	994.56	497.79	332.19
Lys-212 (MA)	AFK^AWAVAR	1321.81	661.41	441.28
Lys-212-associated	AFKAWAVAR	1307.79	654.40	436.60
Lys-212-associated	AWAVAR	817.48	409.25	273.17
Lys-233 (MA)	AEFAEVSK^LVTDLTK	2097.23	1049.12	699.75
Lys-233-associated	AEFAEVSKLVTDLTK	2083.21	1042.11	695.07
Lys-233-associated	AEFAEVSK	1168.65	584.83	390.22
Lys-233-associated	LVTDLTK	1077.68	539.34	359.90

His-242 (MA)	VH@TECCHGDLLECADDR	2389.07	1195.04	797.03
His-247 (MA)	VHTECCH@GDLLECADDR	2389.07	1195.04	797.03
His-242-associated & His-247-associated	VHTECCHGDLLECADDR	2230.94	1115.97	744.32
Lys-262 (MA)	ADLAK^YICENQDSISSK	2388.26	1194.63	796.76
Lys-262-associated	ADLAKYICENQDSISSK	2374.23	1187.62	792.08
Lys-262-associated	ADLAK	805.51	403.26	269.17
Lys-262-associated	YICENQDSISSK	1731.85	866.43	577.96
His-288 (MA)	SH@CIAEVENDEM*PADLPSLAADFVESK	3436.68	1718.84	1146.23
His-288 (MA)	SH@CIAEVENDEMPADLPSLAADFVESK	3420.68	1710.85	1140.90
His-288-associated	SHCIAEVENDEM*PADLPSLAADFVESK	3278.55	1639.78	1093.52
His-288-associated	SHCIAEVENDEMPADLPSLAADFVESK	3262.55	1631.78	1088.19
Lys-351 (MA)	LAK^TYETTLEK	1743.04	872.03	581.69
Lys-351-associated	LAKTYETTLEK	1729.02	865.01	577.01
Lys-351-associated	TYETTLEK	1272.70	636.85	424.90
His-367 (MA)	CCAAADPH@ECYAK	1998.94	999.97	666.98
His-367-associated	CCAAADPHECYAK	1840.81	920.91	614.27
Lys-378 (MA)	VFDEFK^PLVEEPQNLIK	2491.43	1246.22	831.15
Lys-378-associated	VFDEFKPLVEEPQNLIK	2477.41	1239.21	826.47
Lys-378-associated	VFDEFK	1072.60	536.80	358.20
Lys-378-associated	PLVEEPQNLIK	1567.93	784.47	523.32
Lys-414 (MA)	K^VPQVSTPTLVEVSR	1942.17	971.59	648.06
Lys-414 (SB)	K~VPQVSTPTLVEVSR	1924.16	962.59	642.06
Lys-414-associated	KVPQVSTPTLVEVSR	1928.15	964.58	643.39
Lys-414-associated	VPQVSTPTLVEVSR	1655.95	828.48	552.65
His-510 (MA)	EFNAETFTFH@ADICTLSEK	2706.36	1353.68	902.79
His-510-associated	EFNAETFTFHADICTLSEK	2548.23	1274.62	850.08
Lys-525 (MA)	K^QTALVELVK	1575.04	788.02	525.68
Lys-525 (SB)	K~QTALVELVK	1557.03	779.02	519.68
Lys-525-associated	KQTALVELVK	1561.01	781.01	521.01
Lys-525-associated	QTALVELVK	1288.81	644.91	430.28

Table A4. List of targeted peptides and associated monoisotopic mass-to-charge ratios that were used as a targeted mass list for chosing parent ions for fragmentation. Mass-to-charge ratios in blue are outside the analyzed range (300-2000). Targeted peptides are grouped by modification site. C# indicates HNE Michael addition at Cys followed by reduction; H@ indicates HNE Michael addition at His followed by reduction; K^ indicates HNE Michael addition at Lys followed by reduction; K~ indicates Schiff base formation with HNE at Lys followed by

reduction; M* indicates oxidation at Met. Seventeen sites were targeted and both Schiff base formation and Michael addition were considered at two of these sites (Lys-414 and Lys-525).

Modification	Peptide	Detection Count	Averaged iTRAQ PQD Reporter Ion Intensity		
			No HNE Added	50:1 HNE: HSA	100:1 HNE: HSA
Cys-034-associated	*ALVLIAFAQYLQQCPFEDHVK*	*412*	*103*	*29*	*22*
Cys-034 (MA)	*ALVLIAFAQYLQQC#PFEDHVK*	*2*	*10*	*0*	*58*
His-067-associated	**SLHTLFGDK**	**795**	**15986**	**4323**	**2574**
His-105-associated	**NECFLQHK**	**345**	**8095**	**4837**	**3617**
His-242-associated & His-247-associated	*VHTECCHGDLLECADDR*	*239*	*184*	*73*	*54*
His-288-associated	*SHCIAEVENDEMPADLPSLAADFV ESK*	*433*	*198*	*40*	*19*
His-367-associated	**CCAAADPHECYAK**	**642**	**979**	**608**	**322**
His-510-associated	**EFNAETFTFHADICTLSEK**	**748**	**493**	**166**	**55**
His-067 (MA)	**SLH@TLFGDK**	**916**	**31**	**1963**	**1642**
His-105 (MA)	**NECFLQH@K**	**89**	**42**	**1681**	**2103**
His-367 (MA)	**CCAAADPH@ECYAK**	**326**	**9**	**351**	**465**
His-510 (MA)	**EFNAETFTFH@ADICTLSEK**	**126**	**13**	**239**	**397**
Lys-162-associated	**AAFTECCQAADK**	**527**	**1556**	**1053**	**679**
Lys-199-associated	**CASLQK**	**21**	**127**	**14**	**6**
Lys-233-associated	**AEFAEVSK**	**1018**	**2281**	**1729**	**1490**
Lys-233-associated	*LVTDLTK*	*313*	*6523*	*4854*	*4218*
Lys-262-associated	*ADLAK*	*6*	*542*	*337*	*353*
Lys-262-associated	**YICENQDSISSK**	**1195**	**886**	**678**	**527**
Lys-351-associated	**TYETTLEK**	**212**	**3714**	**1754**	**966**
Lys-378-associated	**VFDEFKPLVEEPQNLIK**	**895**	**718**	**610**	**389**
Lys-414-associated	**KVPQVSTPTLVEVSR**	**778**	**976**	**727**	**437**
Lys-414-associated	*VPQVSTPTLVEVSR*	*575*	*99*	*148*	*110*
Lys-525-associated	*KQTALVELVK*	*174*	*2206*	*480*	*151*
Lys-525-associated	**QTALVELVK**	**794**	**1789**	**430**	**259**
Lys-162 (MA)	**YK^AAFTECCQAADK**	**44**	**15**	**466**	**543**
Lys-199 (MA)	**LK^CASLQK**	**1**	**0**	**3965**	**5647**
Lys-233 (MA)	**AEFAEVSK^LVTDLTK**	**79**	**12**	**225**	**568**
Lys-262 (MA)	**ADLAK^YICENQDSISSK**	**2**	**0**	**16**	**96**

Lys-351 (MA)	**LAK^TYETTLEK**	**43**	**44**	**1880**	**2210**
Lys-378 (MA)	**VFDEFK^PLVEEPQNLIK**	**43**	**34**	**43**	**48**
Lys-414 (MA)	**K^VPQVSTPTLVEVSR**	**248**	**7**	**66**	**56**
Lys-414 (SB)	**K~VPQVSTPTLVEVSR**	**118**	**28**	**134**	**127**
Lys-525 (MA)	**K^QTALVELVK**	**135**	**15**	**823**	**740**
Lys-525 (SB)	**K~QTALVELVK**	**12**	**83**	**1917**	**793**

Table A5. Change in relative abundance for HNE-modified and corresponding unmodified HSA peptides in response to HNE-exposure at stated HNE:HSA molar ratios. Averaged iTRAQ reporter ion intensities are given here; since the control was duplicated, the average of the two reporter ion signal averages is given here. iTRAQ reporter ion intensities were obtained using pulsed-Q dissociation (PQD) in a linear ion trap mass spectrometer. This dataset is the result of a single repeat preparation subjected to three replicate LC–MS/MS runs. Incubation time with HNE was 3 h. The mass list described in Table A4 was used and only mass list peptides are included in this table. Bolded entries were used in constructing Figure 3-4 while italicized entries were not used. For a peptide identification to be accepted, a PeptideProphet score of 0.9 or greater was required. MS/MS where all four iTRAQ reporter ion intensities were zero were discarded. C# indicates HNE Michael addition at Cys followed by reduction; H@ indicates HNE Michael addition at His followed by reduction; K^ indicates HNE Michael addition at Lys followed by reduction; K~ indicates Schiff base formation with HNE at Lys followed by reduction.

Modification	**Peptide**	**Detection Count**	**Averaged iTRAQ PQD Reporter Ion Intensity**			
			100:1 HNE: HSA for 0 h	**100:1 HNE: HSA for 1 h**	**100:1 HNE: HSA for 3 h**	**100:1 HNE: HSA for 24 h**
Cys-034-associated	*ALVLIAFAQYLQQCPFEDHVK*	*342*	*212*	*121*	*122*	*100*
Cys-034 (MA)	*ALVLIAFAQYLQQC#PFEDHVK*	*70*	*2*	*24*	*17*	*38*
His-067-associated	**SLHTLFGDK**	**953**	**38165**	**20958**	**10653**	**4260**
His-105-associated	**NECFLQHK**	**437**	**5574**	**4126**	**3355**	**1806**
His-242-associated & His-247-associated	**VHTECCHGDLLECADDR**	**353**	**1289**	**319**	**548**	**346**

His-288-associated	*SHCIAEVENDEM*PADLPSL AADFVESK*	*857*	*88*	*311*	*58*	*47*
His-288-associated	**SHCIAEVENDEMPADLPSL AADFVESK**	**866**	**1135**	**244**	**186**	**135**
His-367-associated	**CCAAADPHECYAK**	**966**	**861**	**738**	**508**	**259**
His-510-associated	**EFNAETFTFHADICTLSEK**	**2204**	**1787**	**1226**	**571**	**348**
His-067 (MA)	**SLH@TLFGDK**	**3622**	**78**	**7515**	**11990**	**10650**
His-105 (MA)	**NECFLQH@K**	**260**	**269**	**8992**	**9506**	**15905**
His-242 (MA)	**VH@TECCHGDLLECADDR**	**8**	**168**	**2451**	**4349**	**3510**
His-288 (MA)	*SH@CIAEVENDEM*PADLPS LAADFVESK*	*834*	*7*	*89*	*302*	*242*
His-288 (MA)	**SH@CIAEVENDEMPADLPS LAADFVESK**	**2751**	**4**	**79**	**279**	**223**
His-367 (MA)	**CCAAADPH@ECYAK**	**1401**	**39**	**999**	**2063**	**5379**
His-510 (MA)	**EFNAETFTFH@ADICTLSEK**	**1722**	**29**	**3947**	**7110**	**6686**
Lys-162-associated	**AAFTECCQAADK**	**1052**	**3085**	**3044**	**2769**	**1962**
Lys-199-associated	**CASLQK**	**29**	**251**	**24**	**17**	**36**
Lys-233-associated	**AEFAEVSK**	**1404**	**4820**	**5431**	**5262**	**4765**
Lys-233-associated	*AEFAEVSKLVTDLTK*	*1*	*93*	*591*	*364*	*439*
Lys-233-associated	*LVTDLTK*	*499*	*17374*	*22540*	*24120*	*21831*
Lys-262-associated	*ADLAK*	*5*	*109*	*97*	*84*	*105*
Lys-262-associated	**YICENQDSISSK**	**1803**	**2797**	**3167**	**2985**	**2982**
Lys-351-associated	**TYETTLEK**	**344**	**5530**	**4297**	**3405**	**2725**
Lys-378-associated	**VFDEFKPLVEEPQNLIK**	**6292**	**5231**	**6216**	**6091**	**5124**
Lys-414-associated	**KVPQVSTPTLVEVSR**	**1293**	**8162**	**7017**	**6430**	**5426**
Lys-414-associated	*VPQVSTPTLVEVSR*	*1052*	*209*	*487*	*330*	*215*
Lys-525-associated	*KQTALVELVK*	*270*	*7350*	*2056*	*2005*	*1670*
Lys-525-associated	**QTALVELVK**	**1020**	**7644**	**3075**	**3230**	**3415**
Lys-162 (MA)	**YK^AAFTECCQAADK**	**210**	**155**	**5208**	**7024**	**4866**
Lys-199 (MA)	**LK^CASLQK**	**33**	**1720**	**26535**	**39406**	**32742**
Lys-212 (MA)	*AFK^AWAVAR*	*48*	*941*	*1771*	*2392*	*5858*
Lys-233 (MA)	**AEFAEVSK^LVTDLTK**	**355**	**73**	**961**	**2437**	**8534**
Lys-262 (MA)	**ADLAK^YICENQDSISSK**	**120**	**62**	**817**	**1777**	**4669**
Lys-351 (MA)	**LAK^TYETTLEK**	**222**	**295**	**17008**	**28787**	**32302**
Lys-378 (MA)	**VFDEFK^PLVEEPQNLIK**	**357**	**1000**	**1783**	**2071**	**3483**
Lys-414 (MA)	**K^VPQVSTPTLVEVSR**	**501**	**53**	**393**	**363**	**529**
Lys-414 (SB)	**K~VPQVSTPTLVEVSR**	**145**	**199**	**879**	**539**	**289**
Lys-525 (MA)	**K^QTALVELVK**	**345**	**128**	**2947**	**6102**	**8845**
Lys-525 (SB)	**K~QTALVELVK**	**1**	**0**	**0**	**141**	**556**

Table A6. Change in relative abundance for HNE-modified and corresponding unmodified HSA peptides in response to HNE-exposure time at a 100:1 HNE:HSA molar ratio. Averaged iTRAQ reporter ion intensities are given here. iTRAQ reporter ion intensities were obtained using pulsed-Q dissociation (PQD) in a linear ion trap mass spectrometer. This dataset is the result of a three repeat preparations subjected to three replicate LC–MS/MS runs each. The same set of three repeat preparations was analyzed using the LTQ Orbitrap Velos system (see Table A7). The mass list described in Table A4 was used and only mass list peptides are included in this table. Bolded entries were used in constructing Figures 3-5 and 3-6 while italicized entries were not used. For a peptide identification to be accepted, a PeptideProphet score of 0.9 or greater was required. MS/MS where all four iTRAQ reporter ion intensities were zero were discarded. C# indicates HNE Michael addition at Cys followed by reduction; H@ indicates HNE Michael addition at His followed by reduction; K^ indicates HNE Michael addition at Lys followed by reduction; K~ indicates Schiff base formation with HNE at Lys followed by reduction; M* indicates oxidation at Met.

Modification	**Peptide**	**Detection Count**	**Averaged iTRAQ HCD Reporter Ion Intensity**			
			100:1 HNE:HSA for 0h	**100:1 HNE:HSA for 1 h**	**100:1 HNE:HSA for 3 h**	**100:1 HNE:HSA for 24 h**
Cys-034-associated	*ALVLIAFAQYLQQCPFEDHVK*	*587*	*78,624*	*32,756*	*33,334*	*30,214*
Cys-034 (MA)	*ALVLIAFAQYLQQC#PFEDHVK*	*42*	*33*	*5,327*	*6,193*	*8,584*
His-067-associated	**SLHTLFGDK**	**415**	**13,952,918**	**6,539,486**	**3,337,288**	**1,158,342**
His-105-associated	**NECFLQHK**	**136**	**5,832,964**	**4,849,906**	**4,391,349**	**2,830,563**
His-242-associated & His-247-associated	**VHTECCHGDLLECADDR**	**165**	**3,822,606**	**320,141**	**888,666**	**562,688**
His-288-associated	*SHCIAEVENDEM*PADLPSLAADFVESK*	*427*	*21,440*	*3,763*	*2,908*	*2,669*
His-288-associated	**SHCIAEVENDEMPADLPSLAADFVESK**	**447**	**136,119**	**12,148**	**13,123**	**7,753**
His-367-associated	**CCAAADPHECYAK**	**242**	**1,956,960**	**1,843,165**	**1,439,056**	**795,689**

His-510-associated	**EFNAETFTFHADICTLSEK**	**3968**	**200,464**	**98,380**	**44,679**	**27,313**
His-067 (MA)	**SLH@TLFGDK**	**1726**	**13,109**	**2,156,987**	**3,519,615**	**3,131,642**
His-105 (MA)	**NECFLQH@K**	**144**	**4,630**	**3,374,603**	**4,273,392**	**10,184,120**
His-242 (MA)	**VH@TECCHGDLLECADDR**	**1**	**0**	**644,631**	**2,910,221**	**7,530,896**
His-288 (MA)	*SH@CIAEVENDEM*PADLPSLAADFVESK*	*432*	*94*	*989*	*6,542*	*5,691*
His-288 (MA)	**SH@CIAEVENDEMPADLPSLAADFVESK**	**517**	**89**	**1,456**	**22,830**	**15,411**
His-367 (MA)	**CCAAADPH@ECYAK**	**300**	**16,192**	**1,406,253**	**3,027,319**	**8,318,955**
His-510 (MA)	**EFNAETFTFH@ADICTLSEK**	**1709**	**489**	**429,024**	**762,804**	**720,107**
Lys-162-associated	**AAFTECCQAADK**	**326**	**27,423,946**	**22,733,690**	**20,503,814**	**13,714,238**
Lys-199-associated	**CASLQK**	**3**	**12,243,954**	**80,833**	**770,411**	**1,208,514**
Lys-212-associated	**AWAVAR**	**18**	**2,489,880**	**2,801,777**	**2,890,115**	**2,396,501**
Lys-233-associated	**AEFAEVSK**	**1405**	**8,509,280**	**8,504,345**	**8,576,027**	**7,285,145**
Lys-233-associated	*LVTDLTK*	*83*	*33,314,060*	*34,218,062*	*37,033,153*	*31,241,085*
Lys-262-associated	*ADLAK*	*33*	*169,516*	*187,289*	*204,700*	*204,112*
Lys-262-associated	**YICENQDSISSK**	**433**	**12,043,353**	**11,924,154**	**11,293,278**	**10,678,932**
Lys-351-associated	*LAKTYETTLEK*	*3*	*304,390*	*176,579*	*176,468*	*98,190*
Lys-351-associated	**TYETTLEK**	**318**	**31,796,143**	**21,735,695**	**17,967,937**	**12,827,925**
Lys-378-associated	**VFDEFKPLVEEPQNLIK**	**3490**	**1,155,907**	**1,208,714**	**1,181,820**	**1,022,525**
Lys-414-associated	**KVPQVSTPTLVEVSR**	**2689**	**927,400**	**585,347**	**594,473**	**546,458**
Lys-414-associated	*VPQVSTPTLVEVSR*	*335*	*1,889,170*	*2,012,382*	*2,697,308*	*3,472,855*
Lys-525-associated	*KQTALVELVK*	*105*	*11,562,546*	*2,307,665*	*2,613,592*	*1,917,802*
Lys-525-associated	**QTALVELVK**	**337**	**33,508,017**	**10,231,592**	**12,479,695**	**12,615,564**

Lys-162 (MA)	**YK^AAFTECCQAADK**	**109**	**5,108**	**1,294,683**	**1,862,666**	**1,353,267**
Lys-199 (MA)	**LK^CASLQK**	**82**	**148,821**	**4,099,255**	**6,318,518**	**4,813,055**
Lys-212 (MA)	**AFK^AWAVAR**	**183**	**15,885**	**328,737**	**750,455**	**2,543,724**
Lys-233 (MA)	**AEFAEVSK^LVTDLTK**	**259**	**213**	**166,208**	**442,734**	**1,710,775**
Lys-262 (MA)	**ADLAK^YICENQDSISSK**	**221**	**3,918**	**108,763**	**200,239**	**483,669**
Lys-351 (MA)	**LAK^TYETTLEK**	**358**	**9,234**	**2,853,576**	**4,711,145**	**5,505,777**
Lys-378 (MA)	**VFDEFK^PLVEEPQNLIK**	**222**	**315,488**	**476,860**	**591,517**	**970,454**
Lys-414 (MA)	**K^VPQVSTPTLVEVSR**	**168**	**53,292**	**194,219**	**214,435**	**329,460**
Lys-414 (SB)	**K~VPQVSTPTLVEVSR**	**139**	**102,784**	**383,309**	**269,070**	**142,050**
Lys-525 (MA)	**K^QTALVELVK**	**269**	**13,297**	**811,364**	**1,779,872**	**2,629,183**
Lys-525 (SB)	**K~QTALVELVK**	**150**	**1,202**	**4,346,272**	**3,215,159**	**753,301**

Table A7. Change in relative abundance for HNE-modified and corresponding unmodified HSA peptides in response to HNE-exposure time at a 100:1 HNE:HSA molar ratio. Averaged iTRAQ reporter ion intensities are given here. iTRAQ reporter ion intensities were obtained using higher-energy C-trap dissociation (HCD) in an Orbitrap mass spectrometer. This dataset is the result of a three repeat preparations subjected to three replicate LC–MS/MS runs each. The same set of three repeat preparations was analyzed using the LTQ XL system (see Table A6). The mass list described in Table A4 was used and only mass list peptides are included in this table. Bolded entries were used in constructing Figures 3-5 and 3-6 while italicized entries were not used. For a peptide identification to be accepted, a PeptideProphet score of 0.9 or greater was required. MS/MS where all four iTRAQ reporter ion intensities were zero were discarded. C# indicates HNE Michael addition at Cys followed by reduction; H@ indicates HNE Michael addition at His followed by reduction; K^ indicates HNE Michael addition at Lys followed by reduction; K~ indicates Schiff base formation with HNE at Lys followed by reduction; M* indicates oxidation at Met.

Modified Peptide (with flanking residues)	Modification Site or Sites (T indicates trypsin digestion; C indicates chymotrypsin digestion)	Counts of LC–MS/MS runs in which the modified peptide was identified using LTQ XL CID scans (maximum = 3) and LTQ Orbitrap Velos CID scans associated with high mass accuracy Orbitrap precursor ion mass measurements (*)			
		1:1 HNE to ACO Ratio	2:1 HNE to ACO Ratio	10:1 HNE to ACO Ratio	50:1 HNE to ACO Ratio
K.VAM(#)SH^FEPHEYIR.Y	His-009 (T)	not detected	not detected	not detected	1
K.VAM(#)SHFEPH^EYIR.Y	His-013 (T)	1	1	3*	3*
K.VAM(#)SH^FEPH^EYIR.Y	His-009 & His-013 (T)	not detected	not detected	not detected	1
R.YDLLEK~NIDIVR.K	Lys-023 (T)	not detected	not detected	1	2
K.IVYGH^LDDPANQEIER.G	His-046 (T)	not detected	not detected	3*	3*
Y.GH^LDDPANQEIERGKTY.L	His-046 (C)	not detected	not detected	3*	3*
K.VAVPSTIH^C*DHLIEAQLGGEK.D	His-098 (T)	1	1	2	1
K.VAVPSTIHC@DHLIEAQLGGEK.D	Cys-099 (T)	not detected	1*	1*	1
K.VAVPSTIHC*DH^LIEAQLGGEK.D	His-101 (T)	not detected	not detected	3	1*
K.VAVPSTIH^C@DHLIEAQLGGEK.D	His-098 & Cys-099 (T)	not detected	not detected	not detected	1
K.VAVPSTIH^C*DH^LIEAQLGGEK.D	His-098 & His-101 (T)	not detected	not detected	1	3*
K.VAVPSTIHC@DH^LIEAQLGGEK.D	Cys-099 & His-101 (T)	not detected	not detected	not detected*	1
K.VAVPSTIH^C@DH^LIEAQLGGEK.D	His-098 & Cys-099 & His-101 (T)	not detected	not detected	not detected	2
R.AK~DINQEVYNFLATAGAK.Y	Lys-117 (T)	not detected	not detected	3*	3*

W.RPGSGIIH^QIILENY.A	His-147 (C)	not detected	not detected	not detected	1
K.LTGSLSGWTSPK~DVILK.V	Lys-218 (T)	not detected	not detected	1	2
F.KDHLVPDPGC@HY.D	Cys-305 (C)	not detected	1	2	0
Y.DQVIEINLSELKPH^INGPF.T	His-321 (C)	not detected	0	2*	3*
R.VGLIGSC@TNSSYEDM(#)GR.S	Cys-358 (T)	3*	3*	3*	3*
K.QALAH^GLK.C	His-379 (T)	not detected	not detected	not detected*	not detected*
R.DVGGIVLANAC@GPC*IGQWDR.K	Cys-421 (T)	2	1	1	not detected
R.DVGGIVLANAC*GPC@IGQWDR.K	Cys-424 (T)	not detected	not detected	1	not detected*
R.DVGGIVLANAC@GPC@IGQWDR.K	Cys-421 & Cys-424 (T)	not detected	not detected	3*	1*
R.NDANPETH^AFVTSPEIVTALAIAGTLK.F	His-460 (T)	not detected	1*	3*	3*
F.TGRNDANPETH^AF.V	His-460 (C)	not detected	not detected	3	3*
K.FNPETDFLTGK~DGK.K	Lys-490 (T)	not detected	not detected	not detected	3
K.FK~LEAPDADELPR.A	Lys-496 (T)	not detected	not detected	2	3
R.AEFDPGQDTYQH^PPK.D	His-519 (T)	not detected	not detected	3	3*
K.C@TTDHISAAGPWLK.F	Cys-565 (T)	3*	3*	3*	3*
K.C*TTDH^ISAAGPWLK.F	His-569 (T)	not detected	not detected	2	2
K.C@TTDH^ISAAGPWLK.F	Cys-565 & His-569 (T)	not detected	not detected	2	2*
R.IH^ETNLK.K	His-668 (T)	not detected	not detected	1*	2*
K.K~QGLLPLTFADPADYNK.I	Lys-674 (T)	not detected	not detected	not detected	1*
K.H^PNGTQETILLNHTFNETQIEWFR.A	His-717 (T)	not detected	not detected	1	not detected
K.HPNGTQETILLNH^TFNETQIEWFR.A	His-729 (T)	not detected	not detected	not detected	not detected*

K.H^PNGTQETILLNH^TFNETQIEWFR.A	His-717 & His-729 (T)	not detected	not detected	not detected	1

Table A8. Counts of LC–MS/MS runs in which the indicated modified peptide was identified. Four independent preparations were made for each HNE:ACO ratio. For each ratio, three preparations were analyzed using a Thermo LTQ XL linear ion trap mass spectrometer and one preparation was analyzed using a Thermo LTQ Orbitrap Velos instrument. In all cases, only one LC–MS/MS run was recorded for each preparation. For the LTQ XL and the LTQ Orbitrap Velos runs, only collision-induced dissocation (CID) MS/MS were recorded for each precursor ion selected for fragmentation. C* indicates carboxyamidomethylation at Cys; C@ indicates HNE Michael addition at Cys followed by reduction; H^ indicates HNE Michael addition at His followed by reduction; K~ indicates HNE Michael addition at Lys followed by reduction; M# indicates oxidation at Met.

Modification Site or Modification Site(s) Associated with Unmodified Peptide	**Peptide**	**Mass List Constituents**		
		$[M+H]^{+}$	**$[M+2H]^{2+}$**	**$[M+3H]^{3+}$**
His-009	VAMSH^FEPHEYIR	1918.00	959.50	640.01
His-009	VAM#SH^FEPHEYIR	1934.00	967.50	645.34
His-013	VAMSHFEPH^EYIR	1918.00	959.50	640.01
His-013	VAM#SHFEPH^EYIR	1934.00	967.50	645.34
His-009 & His-013	VAMSH^FEPH^EYIR	2076.13	1038.57	692.72
His-009 & His-013	VAM#SH^FEPH^EYIR	2092.13	1046.57	698.05
His-009-associated & His-013-associated	VAMSHFEPHEYIR	1759.87	880.44	587.30
His-009-associated & His-013-associated	VAM#SHFEPHEYIR	1775.87	888.44	592.63
His-046	IVYGH^LDDPANQEIER	2171.15	1086.08	724.39
His-046-associated	IVYGHLDDPANQEIER	2013.02	1007.01	671.68
His-098	VAVPSTIH^C*DHLIEAQLGGEK	2720.49	1360.75	907.50
Cys-099	VAVPSTIHC@DHLIEAQLGGEK	2663.47	1332.24	888.49
His-101	VAVPSTIHC*DH^LIEAQLGGEK	2720.49	1360.75	907.50
His-098 & Cys-099	VAVPSTIH^C@DHLIEAQLGGEK	2821.60	1411.30	941.20
His-098 & His-101	VAVPSTIH^C*DH^LIEAQLGGEK	2878.62	1439.81	960.21
Cys-099 & His-101	VAVPSTIHC@DH^LIEAQLGGEK	2821.60	1411.30	941.20

His-098 & Cys-099 & His-101	VAVPSTIH^C@DH^LIEAQLGGEK	2979.73	1490.37	993.91
(His-098 & Cys-099 & His-101)-associated	VAVPSTIHC*DHLIEAQLGGEK	2562.36	1281.68	854.79
Lys-117	AK~DINQEVYNFLATAGAK	2399.34	1200.17	800.45
Lys-117-associated	AKDINQEVYNFLATAGAK	2385.31	1193.16	795.78
Lys-117-associated	DINQEVYNFLATAGAK	2042.08	1021.54	681.37
Cys-358	VGLIGSC@TNSSYEDMGR	2091.02	1046.01	697.68
Cys-358	VGLIGSC@TNSSYEDM#GR	2107.02	1054.01	703.01
Cys-358-associated	VGLIGSC*TNSSYEDMGR	1989.91	995.46	663.98
Cys-358-associated	VGLIGSC*TNSSYEDM#GR	2005.91	1003.46	669.31
Cys-421	DVGGIVLANAC@GPC*IGQWDR	2403.23	1202.12	801.75
Cys-424	DVGGIVLANAC*GPC@IGQWDR	2403.23	1202.12	801.75
Cys-421 & Cys-424	DVGGIVLANAC@GPC@IGQWDR	2504.34	1252.67	835.45
Cys-421-associated & Cys-424-associated	DVGGIVLANAC*GPC*IGQWDR	2302.12	1151.56	768.04
His-460	NDANPETH^AFVTSPEIVTALAIAGTLK	3226.78	1613.89	1076.27
His-460-associated	NDANPETHAFVTSPEIVTALAIAGTLK	3068.65	1534.83	1023.56
Lys-490	FNPETDFLTGK~DGK	2015.09	1008.05	672.37
Lys-490-associated	FNPETDFLTGKDGK	2001.07	1001.04	667.69
Lys-490-associated	FNPETDFLTGK	1556.82	778.91	519.61
Lys-496	FK~LEAPDADELPR	1803.00	902.00	601.67
Lys-496-associated	FKLEAPDADELPR	1788.97	894.99	597.00
Lys-496-associated	LEAPDADELPR	1369.71	685.36	457.24
His-519	AEFDPGQDTYQH^PPK	2176.12	1088.56	726.04
His-519-associated	AEFDPGQDTYQHPPK	2017.99	1009.50	673.33
Cys-565	C@TTDHISAAGPWLK	1946.07	973.54	649.36
His-569	C*TTDH^ISAAGPWLK	2003.09	1002.05	668.37
Cys-565 & His-569	C@TTDH^ISAAGPWLK	2104.20	1052.60	702.07
Cys-565-associated & His-569-associated	C*TTDHISAAGPWLK	1844.96	922.98	615.66
Lys-674	K~QGLLPLTFADPADYNK	2337.33	1169.17	779.78
Lys-674-associated	KQGLLPLTFADPADYNK	2323.30	1162.15	775.11
Lys-674-associated	QGLLPLTFADPADYNK	2051.10	1026.06	684.37
Internal Standard	WVVIGDENYGEGSSR	1811.87	906.44	604.63

Table A9. List of targeted peptides and associated monoisotopic mass-to-charge ratios that were used as a targeted mass list for chosing parent ions for fragmentation. Mass-to-charge ratios in blue are outside the analyzed range (300-2000). Targeted peptides are grouped by modification site. C* indicates carboxyamidomethylation at Cys; C@ indicates HNE Michael addition at Cys

followed by reduction; H^ indicates HNE Michael addition at His followed by reduction; K~ indicates HNE Michael addition at Lys followed by reduction; M# indicates oxidation at Met. Seventeen modifications at twelve residues were targeted.

Modification	**Peptide**	**Detection Count**	**Averaged iTRAQ HCD Reporter Ion Intensity**			
			10:1 HNE:ACO for 0h	**10:1 HNE:ACO for 1 h**	**10:1 HNE:ACO for 2 h**	**10:1 HNE:ACO for 6 h**
Internal Standard	WVVIGDENYGEGSSR	551	6,053,161	4,809,668	4,558,096	4,050,520
Cys-099	VAVPSTIHC@DHLIEAQLGGEK	121	2,551	229,961	222,621	168,247
Cys-358	VGLIGSC@TNSSYEDMGR	156	5,135	429,106	470,003	518,706
Cys-358	VGLIGSC@TNSSYEDM#GR	65	17,928	253,054	282,361	349,781
Cys-421	DVGGIVLANAC@GPC*IGQWDR	1	0	23,485	26,098	28,031
Cys-565	C@TTDHISAAGPWLK	92	15,842	575,998	580,750	599,727
Cys-565 & His-569	C@TTDH^ISAAGPWLK	145	2,757	123,904	252,470	517,238
(Cys-099 & His-098 & His-101)-associated	VAVPSTIHC*DHLIEAQLGGEK	87	1,237,639	609,098	527,023	385,229
Cys-358-associated	VGLIGSC*TNSSYEDMGR	80	2,909,994	1,878,845	1,712,891	1,444,203
Cys-358-associated	VGLIGSC*TNSSYEDM#GR	60	2,748,482	1,883,493	1,828,887	1,605,905
Cys-421-associated & Cys-424-associated	DVGGIVLANAC*GPC*IGQWDR	159	329,860	160,120	116,568	80,479
Cys-421-associated & Cys-424-associated	DVGGIVLANAC*GPC*IGQWDRK	2	6,804	5,449	0	0
Cys-565-associated & His-569-associated	C*TTDHISAAGPWLK	42	1,370,057	782,015	660,115	540,467
His-009	VAMSH^FEPHEYIR	1	0	324,755	519,955	828,189
His-009	VAM#SH^FEPHEYIR	2	298,354	430,856	508,790	828,993
His-013	VAMSHFEPH^EYIR	1	10,971	122,396	156,688	240,192
His-013	VAM#SHFEPH^EYIR	13	95,116	171,191	232,407	371,270
His-009 & His-013	VAMSH^FEPH^EYIR	11	21,608	43,299	73,096	191,010

His-009 & His-013	VAM#SH^FEPH^EYIR	13	15,945	27,321	46,278	126,248
His-046	IVYGH^LDDPANQEIER	107	17,499	437,198	838,855	1,926,070
His-098	VAVPSTIH^C*DHLIEAQLGGEK	1	0	101,458	126,504	186,825
His-098 & His-101	VAVPSTIH^C*DH^LIEAQLGGEK	1	3,942	12,086	28,348	114,005
His-460	NDANPETH^AFVTSPEIVTALAIAGTLK	111	236	1,029	2,372	5,178
His-519	AEFDPGQDTYQH^PPK	40	39,327	560,843	947,504	1,898,119
His-519	AEFDPGQDTYQH^PPKDSSGQR	1	20,404	27,054	62,686	60,425
His-569	C*TTDH^ISAAGPWLK	40	17,885	229,398	363,520	585,296
His-009-associated & His-013-associated	VAMSHFEPHEYIR	38	2,577,348	1,828,028	1,586,102	1,415,132
His-009-associated & His-013-associated	VAM#SHFEPHEYIR	99	1,279,880	919,430	816,214	636,920
His-046-associated	IVYGHLDDPANQEIER	1639	906,002	654,302	597,641	486,893
His-460-associated	NDANPETHAFVTSPEIVTALAIAGTLK	701	9,080	5,798	4,569	3,856
His-519-associated	AEFDPGQDTYQHPPK	212	2,213,658	1,613,471	1,523,537	1,252,205
His-519-associated	AEFDPGQDTYQHPPKDSSGQR	2	19,736	14,520	6,822	8,022
Lys-117	AK~DINQEVYNFLATAGAK	16	19,730	18,468	19,772	20,138
Lys-496	FK~LEAPDADELPR	27	442,284	327,440	322,685	310,301
Lys-674	K~QGLLPLTFADPADYNK	5	19,626	23,054	27,547	29,413
Lys-117-associated	AKDINQEVYNFLATAGAK	271	294,401	219,102	188,939	172,933
Lys-117-associated	DINQEVYNFLATAGAK	1077	288,322	222,843	221,252	192,174
Lys-490-associated	FNPETDFLTGKDGK	19	3,096,622	2,299,755	2,093,206	1,889,292
Lys-490-associated	FNPETDFLTGK	444	22,326,359	17,711,126	17,319,620	15,758,737
Lys-496-associated	FKLEAPDADELPR	678	994,196	754,689	690,847	642,682
Lys-496-associated	LEAPDADELPR	71	14,709,109	11,753,477	11,930,606	11,084,531
Lys-674-associated	KQGLLPLTFADPADYNK	112	393,637	326,304	300,272	257,119
Lys-674-associated	QGLLPLTFADPADYNK	692	570,630	428,138	417,142	370,419

Table A10. Change in relative abundance for HNE-modified and corresponding unmodified ACO peptides in response to HNE-exposure time at a 10:1 HNE:ACO molar ratio. Averaged iTRAQ reporter ion intensities are given here. iTRAQ reporter ion intensities were obtained using higher-energy C-trap dissociation (HCD) in an Orbitrap mass spectrometer. This dataset is the result of only one preparation subjected to three replicate LC–MS/MS runs. The mass list described in Table A9 was used and only mass list peptides are included in this table. All entries were used in constructing Figures 4-5, 4-6 and 4-7. For a peptide identification to be accepted, a PeptideProphet score of 0.9 or greater was required. MS/MS where all four iTRAQ reporter ion intensities were zero were discarded. C* indicates carboxyamidomethylation at Cys; C@ indicates HNE Michael addition at Cys followed by reduction; H^ indicates HNE Michael addition at His followed by reduction; K~ indicates HNE Michael addition at Lys followed by reduction; M# indicates oxidation at Met.

Appendices-II: Spectra

X-range: 200 - 1400
MassTol: 0.950 Y-zoom: 1.00
ImageSize: (•) Sm ( ) Lg
MassType: ( ) AVG (•) MONO
Axis: (•) 1 ( ) 2
Label: (•) I ( ) M ( ) -
Ions:

a	☐ +	☐ 2+	☐ 3+
b	☑ +	☑ 2+	☐ 3+
c	☐ +	☐ 2+	☐ 3+
x	☐ +	☐ 2+	☐ 3+
y	☑ +	☑ 2+	☑ 3+
z	☐ +	☐ 2+	☐ 3+

hide H_2O/NH_3 ☐
zoom 112-122 ☐
zoom 124-133 ☐
GO

ALVLIAFAQYLQQCPFEDHVK, MH+ 2591.5244, m/z 864.5130
1HNE-1HSA-37Trypsin3-LTQ2.7420.7420.3.dta

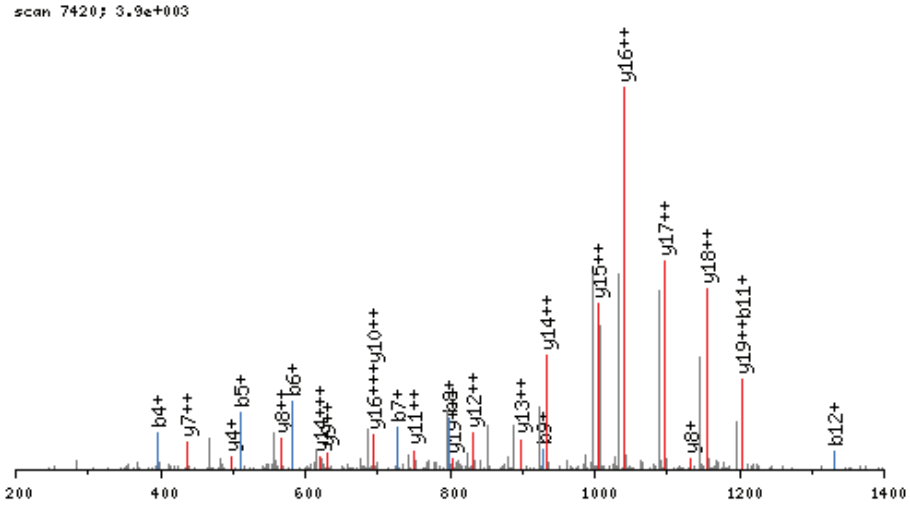

click image to zoom in; click top corners to zoom out [precursor±]

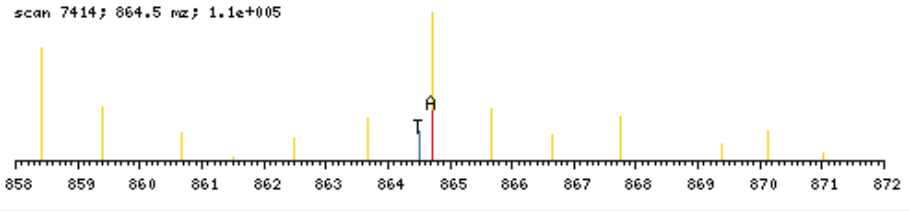

zoomed in precursor plot; T=theoretical m/z, A=acquired m/z

b^+	b^{2+}	#	AA	#	y^+	y^{2+}	y^{3+}
72.0449	36.5264	1	A	21			
185.1290	93.0684	2	L	20	2520.4873	1260.7476	840.8343
284.1974	142.6026	3	V	19	2407.4032	**1204.2055**	**803.1396**
397.2815	199.1447	4	L	18	2308.3348	**1154.6713**	770.1168
510.3655	255.6867	5	I	17	2195.2507	**1098.1293**	732.4221
581.4027	291.2052	6	A	16	2082.1667	**1041.5873**	**694.7274**
728.4711	364.7394	7	F	15	2011.1296	**1006.0687**	671.0484
799.5082	400.2580	8	A	14	1864.0611	**932.5345**	**622.0256**
927.5668	464.2873	9	Q	13	1793.0240	**897.0159**	598.3466
1090.6301	545.8190	10	Y	12	1664.9655	**832.9866**	555.6604
1203.7142	602.3610	11	L	11	1501.9021	**751.4550**	501.3059
1331.7727	666.3903	12	Q	10	1388.8181	**694.9129**	463.6112
1459.8313	730.4196	13	Q	9	1260.7595	**630.8837**	420.9250
1721.1008	861.0543	14	C	8	**1132.7009**	**566.8544**	378.2389
1818.1536	909.5807	15	P	7	871.4314	**436.2196**	291.1490
1965.2220	983.1149	16	F	6	774.3786	387.6932	258.7981
2094.2646	1047.6362	17	E	5	627.3102	314.1590	209.7753
2209.2915	1105.1497	18	D	4	**498.2676**	249.6377	166.7611
2346.3505	1173.6791	19	H	3	383.2407	192.1243	128.4188
2445.4189	1223.2133	20	V	2	246.1818	123.5948	82.7325
		21	K	1	147.1134	74.0606	49.7097

C(14):+261.27

X-range: 200 - 1800
MassTol: 0.950 Y-zoom: 1.00
ImageSize: Sm Lg
MassType: AVG MONO
Axis: 1 2
Label: I M -
Ions:

a	+	2+	3+
b	+	2+	3+
c	+	2+	3+
x	+	2+	3+
y	+	2+	3+
z	+	2+	3+

hide H_2O/NH_3
zoom 112-122
zoom 124-133
GO

ALVLIAFAQYLQQCPFEDHVK, MH+ 2591.5244, m/z 648.6366
10HNE-1HSA-37Trypsin2-LTQ1.7228.7228.4.dta

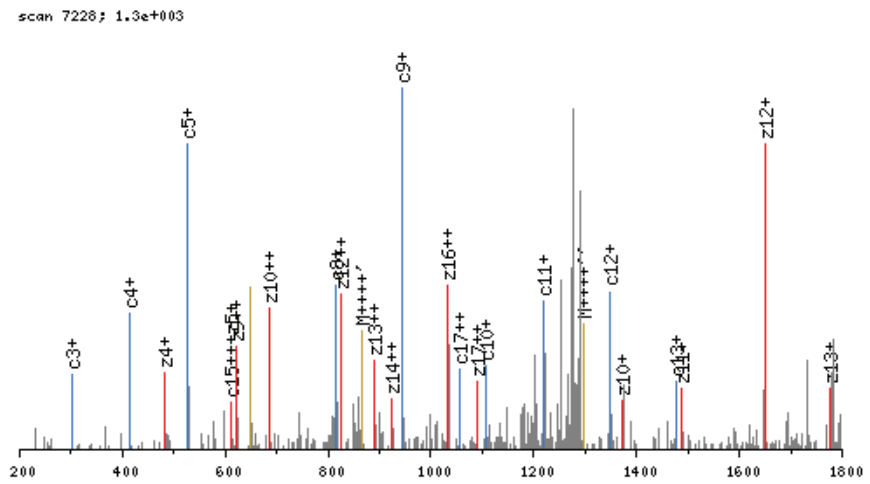

click image to zoom in; click top corners to zoom out [precursor±]

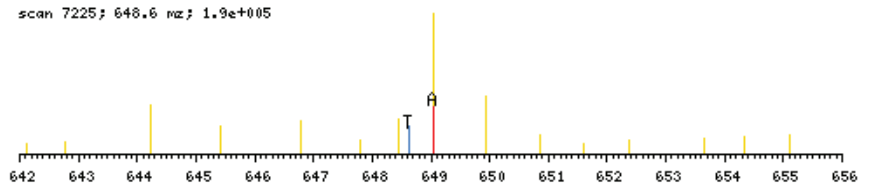

zoomed in precursor plot; T=theoretical m/z, A=acquired m/z

c^+	c^{2+}	c^{3+}	#	AA	#	z^+	z^{2+}	z^{3+}
89.0715	45.0397	30.3624	1	A	21			
202.1556	101.5817	68.0571	2	L	20	2504.4686	1252.7382	835.4947
301.2240	151.1159	101.0799	3	V	19	2391.3845	1196.1962	797.8000
414.3080	207.6579	138.7746	4	L	18	2292.3161	1146.6620	764.7772
527.3921	264.2000	176.4692	5	I	17	2179.2320	1090.1199	727.0826
598.4292	299.7185	200.1483	6	A	16	2066.1480	1033.5779	689.3879
745.4976	373.2527	249.1711	7	F	15	1995.1108	998.0593	665.7088
816.5347	408.7713	272.8501	8	A	14	1848.0424	924.5251	616.6860
944.5933	472.8006	315.5363	9	Q	13	1777.0053	889.0066	593.0070
1107.6566	554.3322	369.8908	10	Y	12	1648.9467	824.9773	550.3208
1220.7407	610.8743	407.5855	11	L	11	1485.8834	743.4456	495.9664
1348.7993	674.9036	450.2716	12	Q	10	1372.7993	686.9036	458.2717
1476.8579	738.9328	492.9578	13	Q	9	1244.7408	622.8743	415.5855
1738.1274	869.5676	580.0477	14	C	8	1116.6822	558.8450	372.8993
1835.1801	918.0940	612.3986	15	P	7	855.4127	428.2102	285.8094
1982.2486	991.6282	661.4214	16	F	6	758.3599	379.6839	253.4585
2111.2911	1056.1495	704.4356	17	E	5	611.2915	306.1497	204.4357
2226.3181	1113.6630	742.7779	18	D	4	482.2489	241.6284	161.4215
2363.3770	1182.1924	788.4642	19	H	3	367.2220	184.1149	123.0792
2462.4454	1231.7266	821.4870	20	V	2	230.1630	115.5854	77.3929
			21	K	1	131.0946	66.0512	44.3701

C(14):+261.27

X-range:
0 - 0
MassTol: Y-zoom:
0.950 1.00
ImageSize:
(•) Sm ( ) Lg
MassType:
( ) AVG (•) MONO
Axis:
(•) 1 ( ) 2
Label:
(•) I ( ) M ( ) -
Ions:

a	☐ +	☐ 2+	☐ 3+
b	☑ +	☑ 2+	☐ 3+
c	☐ +	☐ 2+	☐ 3+
x	☐ +	☐ 2+	☐ 3+
y	☑ +	☑ 2+	☑ 3+
z	☐ +	☐ 2+	☐ 3+

hide H_2O/NH_3 ☐
zoom 112-122 ☐
zoom 124-133 ☐
GO

SLHTLFGDK, MH+ 1175.7498, m/z 392.5881
10HNE-1HSA-37Trypsin3-LTQ1.4987.4987.3.dta

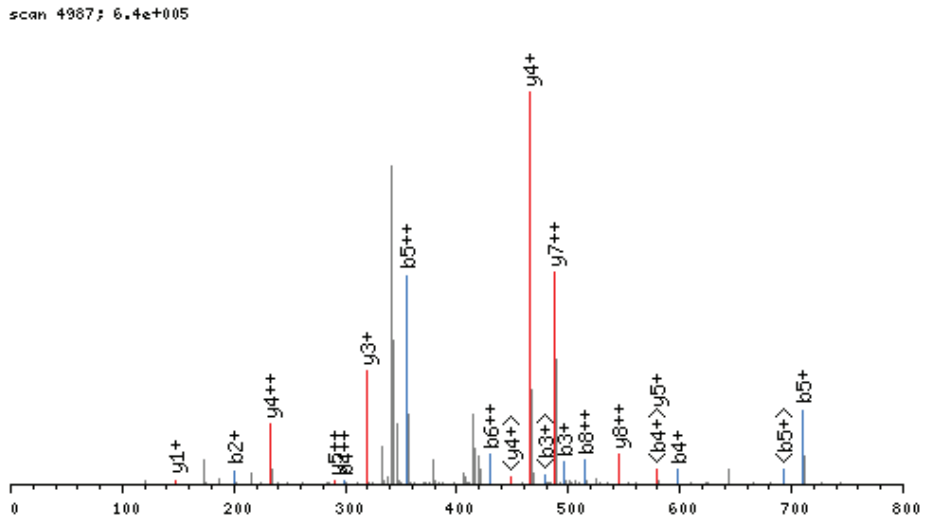

click image to zoom in; click top corners to zoom out [precursor±]

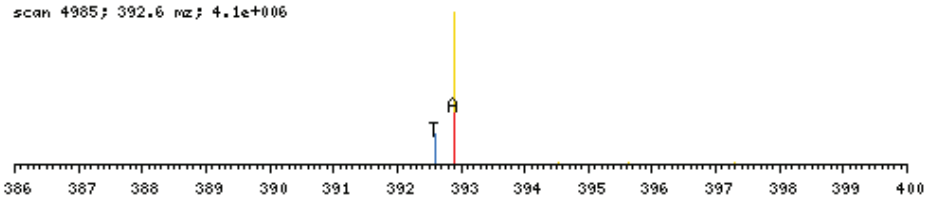

zoomed in precursor plot; T=theoretical m/z, A=acquired m/z

b^+	b^{2+}	#	AA	#	y^+	y^{2+}	y^{3+}
88.0399	44.5238	1	S	9			
201.1239	101.0659	2	L	8	1088.7178	**544.8628**	363.5778
496.3957	248.7018	3	H	7	975.6337	**488.3208**	325.8831
597.4434	**299.2256**	4	T	6	680.3619	340.6849	227.4592
710.5274	**355.7676**	5	L	5	**579.3142**	**290.1610**	193.7766
857.5959	**429.3018**	6	F	4	**466.2302**	**233.6190**	156.0819
914.6173	457.8126	7	G	3	**319.1618**	160.0848	107.0591
1029.6443	**515.3260**	8	D	2	262.1403	131.5741	88.0520
		9	K	1	**147.1134**	74.0606	49.7097

H(3):+295.27

X-range: 200 - 1200
MassTol: 0.950 Y-zoom: 1.00
ImageSize: (•) Sm ( ) Lg
MassType: ( ) AVG (•) MONO
Axis: (•) 1 ( ) 2
Label: (•) I ( ) M ( ) -
Ions:

a	☐ +	☐ 2+	☐ 3+
b	☐ +	☐ 2+	☐ 3+
c	☑ +	☑ 2+	☐ 3+
x	☐ +	☐ 2+	☐ 3+
y	☐ +	☐ 2+	☐ 3+
z	☑ +	☑ 2+	☑ 3+

hide H_2O/NH_3 ☐
zoom 112-122 ☐
zoom 124-133 ☐
GO

SLHTLFGDK, MH+ 1175.7498, m/z 392.5881
10HNE-1HSA-37Trypsin3-LTQ3.4874.4874.3.dta

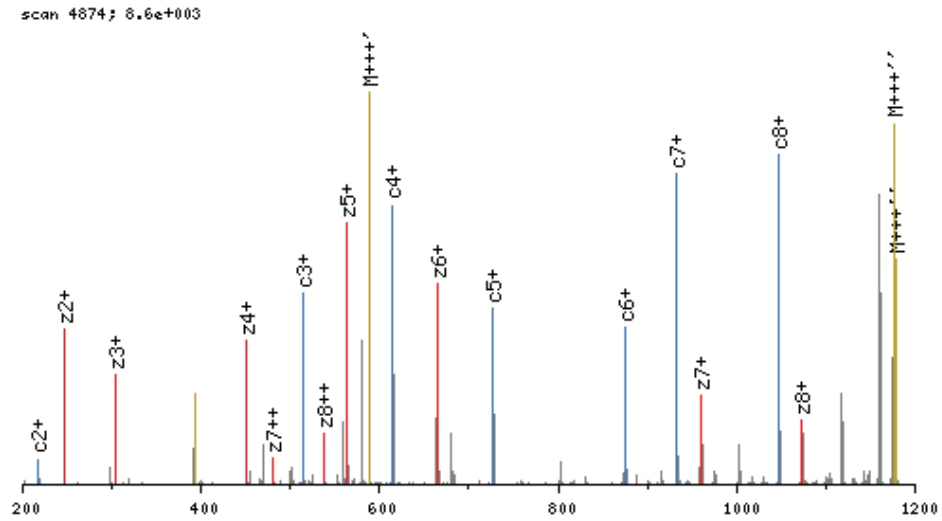

click image to zoom in; click top corners to zoom out [precursor±]

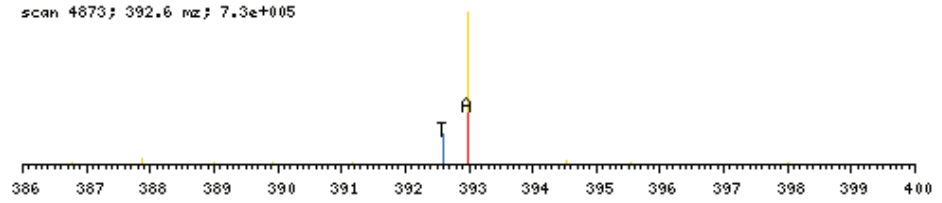

zoomed in precursor plot; T=theoretical m/z, A=acquired m/z

c^+	c^{2+}	#	AA	#	z^+	z^{2+}	z^{3+}
105.0664	53.0371	1	S	9			
218.1505	109.5791	2	L	8	1072.6990	536.8534	358.2382
513.4222	257.2150	3	H	7	959.6150	480.3114	320.5435
614.4699	307.7389	4	T	6	664.3432	332.6755	222.1196
727.5540	364.2809	5	L	5	563.2955	282.1517	188.4371
874.6224	437.8151	6	F	4	450.2114	225.6096	150.7424
931.6439	466.3258	7	G	3	303.1430	152.0754	101.7196
1046.6708	523.8393	8	D	2	246.1216	123.5647	82.7124
		9	K	1	131.0946	66.0512	44.3701

H(3):+295.27

X-range: 200 - 1200
MassTol: 0.950 Y-zoom: 1.00
ImageSize: (•) Sm ( ) Lg
MassType: ( ) AVG (•) MONO
Axis: (•) 1 ( ) 2
Label: (•) I ( ) M ( ) -
Ions:
a [ ] + [ ] 2+ [ ] 3+
b [x] + [x] 2+ [ ] 3+
c [ ] + [ ] 2+ [ ] 3+
x [ ] + [ ] 2+ [ ] 3+
y [x] + [x] 2+ [x] 3+
z [ ] + [ ] 2+ [ ] 3+
hide H_2O/NH_3 [ ]
zoom 112-122 [ ]
zoom 124-133 [ ]
GO

SLHTLFGDKLCTVATLR, MH+ 2090.3772, m/z 697.4639
10HNE-1HSA-37Trypsin5-LTQ3.5493.5493.3.dta

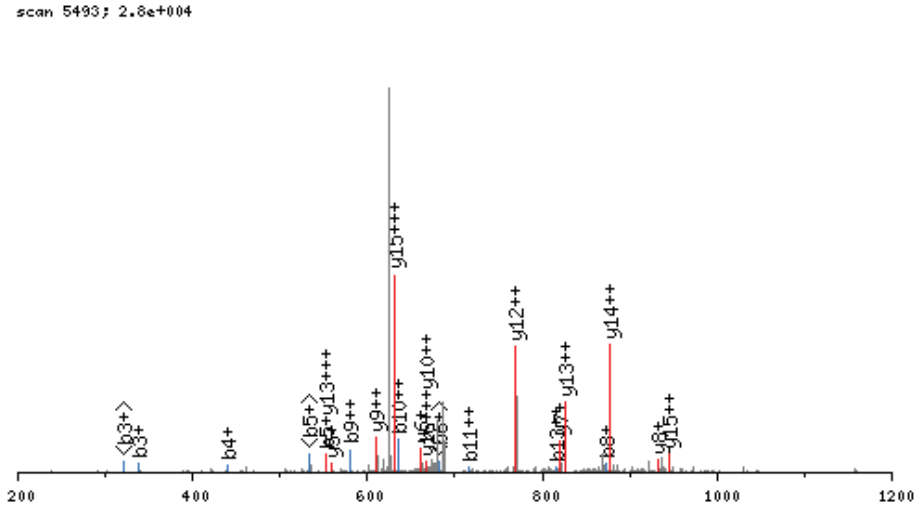

click image to zoom in; click top corners to zoom out [precursor±]

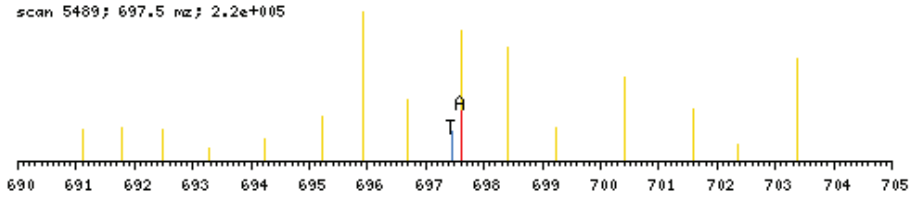

zoomed in precursor plot; T=theoretical m/z, A=acquired m/z

b^+	b^{2+}	#	AA	#	y^+	y^{2+}	y^{3+}
88.0399	44.5238	1	S	17			
201.1239	101.0659	2	L	16	2003.3451	1002.1765	**668.4536**
338.1828	169.5953	3	H	15	1890.2611	**945.6344**	**630.7589**
439.2305	220.1192	4	T	14	1753.2022	**877.1050**	585.0726
552.3146	276.6612	5	L	13	1652.1545	**826.5812**	**551.3900**
699.3830	350.1954	6	F	12	1539.0704	**770.0391**	513.6954
756.4044	378.7061	7	G	11	1392.0020	696.5049	464.6726
871.4314	436.2196	8	D	10	1334.9805	**667.9942**	445.6654
1157.7362	**579.3720**	9	K	9	1219.9536	**610.4807**	407.3231
1270.8202	**635.9140**	10	L	8	**933.6488**	467.3283	311.8882
1430.9805	**715.9942**	11	C	7	**820.5647**	410.7863	274.1935
1532.0282	766.5180	12	T	6	**660.4044**	330.7061	220.8067
1631.0966	**816.0522**	13	V	5	**559.3568**	280.1823	187.1241
1702.1337	851.5708	14	A	4	460.2884	230.6481	154.1013
1803.1814	902.0946	15	T	3	389.2512	195.1295	130.4223
1916.2655	958.6367	16	L	2	288.2036	144.6057	96.7397
		17	R	1	175.1195	88.0637	59.0451

K(9):+286.30 C(11):+160.16

X-range: 200 - 1800
MassTol: 0.950 Y-zoom: 1.00
ImageSize: Sm Lg
MassType: AVG MONO
Axis: 1 2
Label: I M -
Ions:

a	+	2+	3+
b	+	2+	3+
c	✓ +	✓ 2+	✓ 3+
x	+	2+	3+
y	+	2+	3+
z	✓ +	✓ 2+	✓ 3+

hide H_2O/NH_3
zoom 112-122
zoom 124-133
GO

NECFLQHKDDNPNLPR, MH+ 2137.2588, m/z 535.0702
10HNE-1HSA-37Trypsin2-LTQ2.4638.4638.4.dta

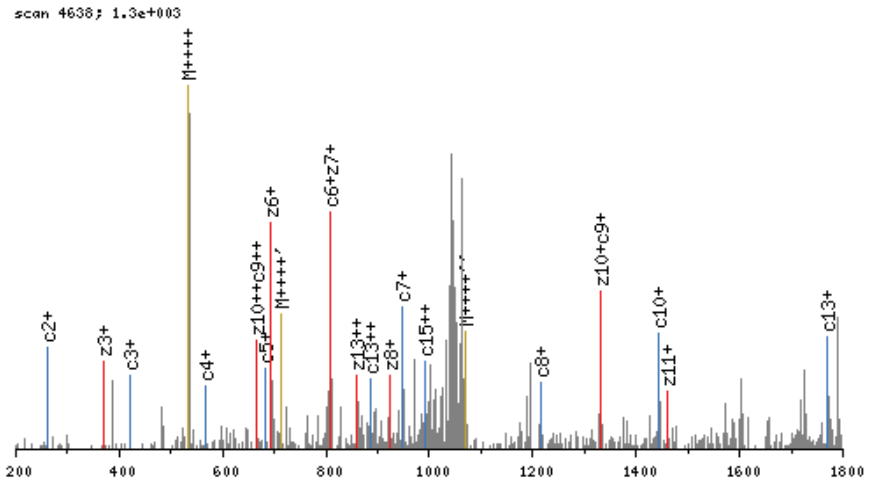

click image to zoom in; click top corners to zoom out [precursor±]

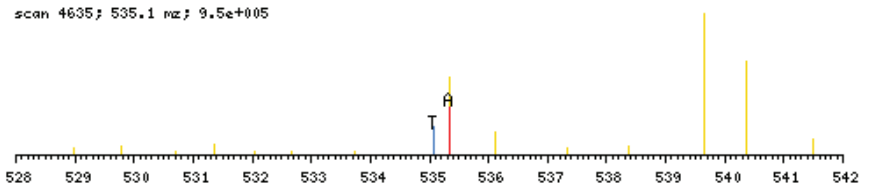

zoomed in precursor plot; T=theoretical m/z, A=acquired m/z

c^+	c^{2+}	c^{3+}	#	AA	#	z^+	z^{2+}	z^{3+}
132.0773	66.5426	44.6977	1	N	16			
261.1199	131.0639	87.7118	2	E	15	2007.1972	1004.1025	669.7376
421.2802	211.1440	141.0986	3	C	14	1878.1546	939.5812	626.7234
568.3486	284.6782	190.1214	4	F	13	1717.9943	**859.5011**	573.3366
681.4327	341.2202	227.8161	5	L	12	1570.9259	785.9669	524.3138
809.4913	405.2495	270.5023	6	Q	11	**1457.8418**	729.4248	486.6192
946.5502	473.7790	316.1886	7	H	10	**1329.7832**	**665.3955**	443.9330
1214.8444	607.9261	405.6200	8	K	9	1192.7243	596.8661	398.2467
1329.8713	**665.4396**	443.9623	9	D	8	**924.4301**	462.7190	308.8153
1444.8983	722.9530	482.3046	10	D	7	**809.4032**	405.2055	270.4729
1558.9412	779.9745	520.3189	11	N	6	**694.3762**	347.6920	232.1306
1655.9940	828.5009	552.6699	12	P	5	580.3333	290.6706	194.1163
1770.0369	**885.5224**	590.6842	13	N	4	483.2805	242.1442	161.7654
1883.1209	942.0644	628.3789	14	L	3	**369.2376**	185.1227	123.7511
1980.1737	**990.5908**	660.7298	15	P	2	256.1535	128.5807	86.0564
			16	R	1	159.1008	80.0543	53.7055

C(3):+160.16 K(8):+268.29

X-range:
0 - 0
MassTol: Y-zoom:
0.950 1.00
ImageSize:
(•) Sm ( ) Lg
MassType:
( ) AVG (•) MONO
Axis:
(•) 1 ( ) 2
Label:
(•) I ( ) M ( ) -
Ions:

a	☐ +	☐ 2+	☐ 3+
b	☑ +	☑ 2+	☐ 3+
c	☐ +	☐ 2+	☐ 3+
x	☐ +	☐ 2+	☐ 3+
y	☑ +	☑ 2+	☑ 3+
z	☐ +	☐ 2+	☐ 3+

hide H_2O/NH_3 ☐
zoom 112-122 ☐
zoom 124-133 ☐
GO

LVRPEVDVMCTAFHDNEETFLK, MH+ 2808.6071, m/z 936.8739
10HNE-1HSA-37Trypsin2-LTQ3.5939.5939.3.dta

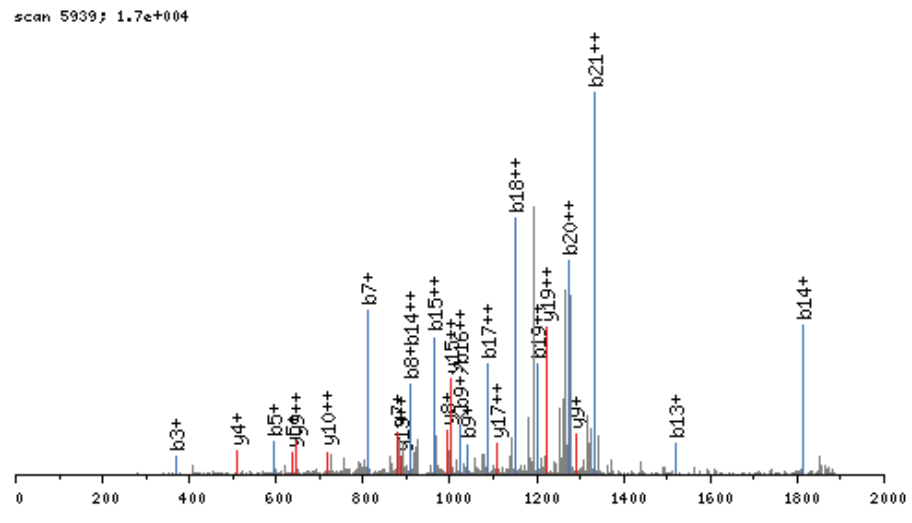

click image to zoom in; click top corners to zoom out [precursor±]

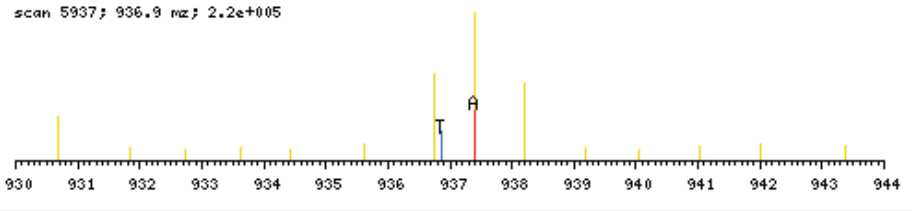

zoomed in precursor plot; T=theoretical m/z, A=acquired m/z

b^+	b^{2+}	#	AA	#	y^+	y^{2+}	y^{3+}
114.0919	57.5499	1	L	22			
213.1603	107.0841	2	V	21	2695.5230	1348.2654	899.1795
369.2614	185.1346	3	R	20	2596.4546	1298.7312	866.1567
466.3142	233.6610	4	P	19	2440.3535	**1220.6806**	814.1230
595.3568	298.1823	5	E	18	2343.3007	1172.1543	781.7721
694.4252	347.7165	6	V	17	2214.2581	**1107.6330**	738.7579
809.4521	405.2300	7	D	16	2115.1897	1058.0988	705.7351
908.5205	454.7642	8	V	15	2000.1628	**1000.5853**	667.3928
1039.5610	520.2844	9	M	14	1901.0943	951.0511	634.3700
1199.7213	600.3646	10	C	13	1770.0539	**885.5308**	590.6898
1300.7690	650.8884	11	T	12	1609.8936	805.4507	537.3031
1371.8061	686.4070	12	A	11	1508.8459	754.9268	503.6205
1518.8745	759.9412	13	F	10	1437.8088	**719.4083**	479.9415
1814.1463	**907.5771**	14	H	9	**1290.7403**	**645.8741**	430.9187
1929.1733	**965.0905**	15	D	8	**995.4686**	498.2382	332.4947
2043.2162	**1022.1120**	16	N	7	**880.4416**	440.7247	294.1524
2172.2588	**1086.6333**	17	E	6	766.3987	383.7033	256.1381
2301.3014	**1151.1546**	18	E	5	**637.3561**	319.1820	213.1239
2402.3490	**1201.6784**	19	T	4	**508.3135**	254.6607	170.1097
2549.4175	**1275.2126**	20	F	3	407.2658	204.1368	136.4272
2662.5015	**1331.7547**	21	L	2	260.1974	130.6026	87.4044
		22	K	1	147.1134	74.0606	49.7097

C(10):+160.16 H(14):+295.27

COMET Spectrum View by J.Eng (c) ISB 2001
(TPP v4.4 VUVUZELA rev 1, Build 201010121551 (MinGW))

X-range: 200 - 1800
MassTol: 0.950 Y-zoom: 2.00
ImageSize: Sm Lg
MassType: AVG MONO
Axis: 1 2
Label: I M -
Ions:

a	+	2+	3+
b	+	2+	3+
c	+	2+	3+
x	+	2+	3+
y	+	2+	3+
z	+	2+	3+

hide H_2O/NH_3
zoom 112-122
zoom 124-133
GO

LVRPEVDVMCTAFHDNEETFLK, MH+ 2808.6071, m/z 702.9072
10HNE-1HSA-37Trypsin3-LTQ3.5949.5949.4.dta

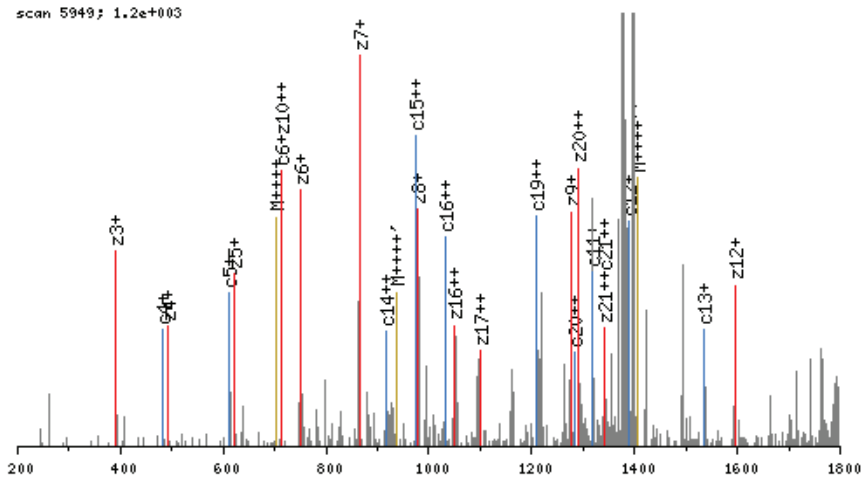

click image to zoom in; click top corners to zoom out [precursor±]

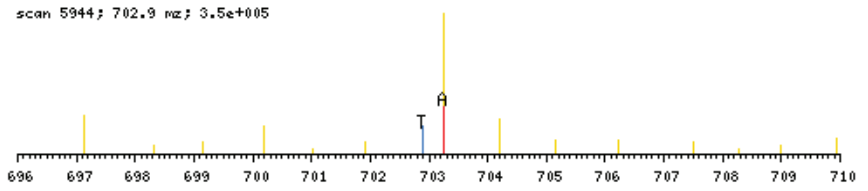

zoomed in precursor plot; T=theoretical m/z, A=acquired m/z

c^+	c^{2+}	c^{3+}	#	AA	#	z^+	z^{2+}	z^{3+}
131.1184	66.0631	44.3780	1	L	22			
230.1869	115.5973	77.4008	2	V	21	2679.5043	**1340.2560**	893.8400
386.2880	193.6479	129.4345	3	R	20	2580.4359	**1290.7218**	860.8172
483.3407	242.1743	161.7855	4	P	19	2424.3347	1212.6713	808.7835
612.3833	306.6956	204.7997	5	E	18	2327.2820	1164.1449	776.4325
711.4517	356.2298	237.8225	6	V	17	2198.2394	**1099.6236**	733.4183
826.4787	413.7433	276.1648	7	D	16	2099.1710	**1050.0894**	700.3955
925.5471	463.2775	309.1876	8	V	15	1984.1440	992.5759	662.0532
1056.5876	528.7977	352.8677	9	M	14	1885.0756	943.0417	629.0304
1216.7479	608.8779	406.2545	10	C	13	1754.0351	877.5215	585.3503
1317.7956	659.4017	439.9371	11	T	12	**1593.8748**	797.4413	531.9635
1388.8327	694.9202	463.6161	12	A	11	1492.8271	746.9175	498.2809
1535.9011	768.4545	512.6389	13	F	10	1421.7900	**711.3989**	474.6019
1831.1729	**916.0903**	611.0628	14	H	9	**1274.7216**	637.8647	425.5791
1946.1998	**973.6038**	649.4052	15	D	8	**979.4498**	490.2288	327.1552
2060.2427	**1030.6253**	687.4195	16	N	7	**864.4229**	432.7154	288.8128
2189.2853	1095.1466	730.4337	17	E	6	**750.3800**	375.6939	250.7985
2318.3279	1159.6679	773.4479	18	E	5	**621.3374**	311.1726	207.7843
2419.3756	**1210.1917**	807.1304	19	T	4	**492.2948**	246.6513	164.7701
2566.4440	**1283.7259**	856.1532	20	F	3	**391.2471**	196.1275	131.0876
2679.5281	**1340.2680**	893.8479	21	L	2	244.1787	122.5933	82.0648
			22	K	1	131.0946	66.0512	44.3701

C(10):+160.16 H(14):+295.27

X-range: 0 - 1200
MassTol: 0.950 Y-zoom: 4.00
ImageSize: (•) Sm ( ) Lg
MassType: ( ) AVG (•) MONO
Axis: (•) 1 ( ) 2
Label: (•) I ( ) M ( ) -
Ions:

a	[ ] +	[ ] 2+	[ ] 3+
b	[x] +	[ ] 2+	[ ] 3+
c	[ ] +	[ ] 2+	[ ] 3+
x	[ ] +	[ ] 2+	[ ] 3+
y	[x] +	[x] 2+	[ ] 3+
z	[ ] +	[ ] 2+	[ ] 3+

hide H_2O/NH_3 [ ]
zoom 112-122 [ ]
zoom 124-133 [ ]
GO

KYLYEIAR, MH+ 1213.7988, m/z 607.4030
10HNE-1HSA-37Trypsin4-LTQ2.4655.4655.2.dta

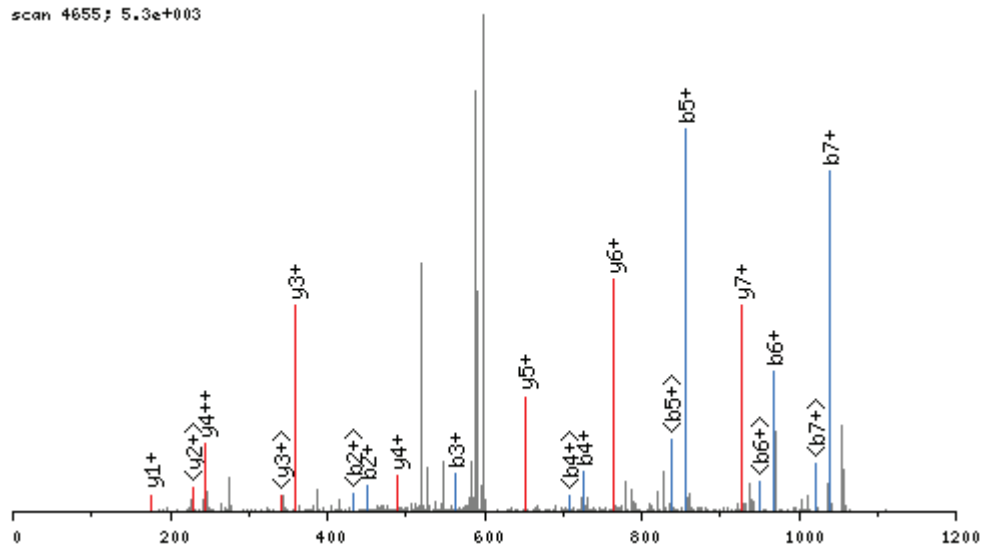

click image to zoom in; click top corners to zoom out [precursor±]

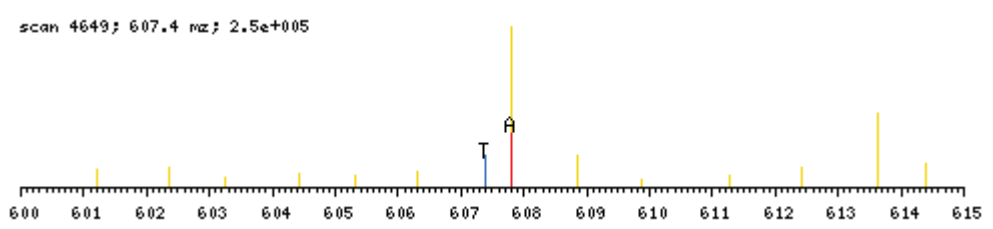

zoomed in precursor plot; T=theoretical m/z, A=acquired m/z

b^+	#	AA	#	y^+	y^{2+}
287.3126	1	K	8		
450.3759	2	Y	7	927.4940	464.2509
563.4600	3	L	6	764.4307	382.7192
726.5233	4	Y	5	651.3466	326.1772
855.5659	5	E	4	488.2833	244.6455
968.6500	6	I	3	359.2407	180.1243
1039.6871	7	A	2	246.1566	123.5822
	8	R	1	175.1195	88.0637

K(1):+286.30

X-range: 0 - 0
MassTol: 0.950 Y-zoom: 1.00
ImageSize: Sm Lg
MassType: AVG MONO
Axis: 1 2
Label: I M -
Ions:
a + 2+ 3+
b + 2+ 3+
c + 2+ 3+
x + 2+ 3+
y + 2+ 3+
z + 2+ 3+
hide H_2O/NH_3
zoom 112-122
zoom 124-133
GO

RHPYFYAPELLFFAK, MH+ 2057.2086, m/z 686.4077
10HNE-1HSA-37Trypsin5-LTQ3.6219.6219.3.dta

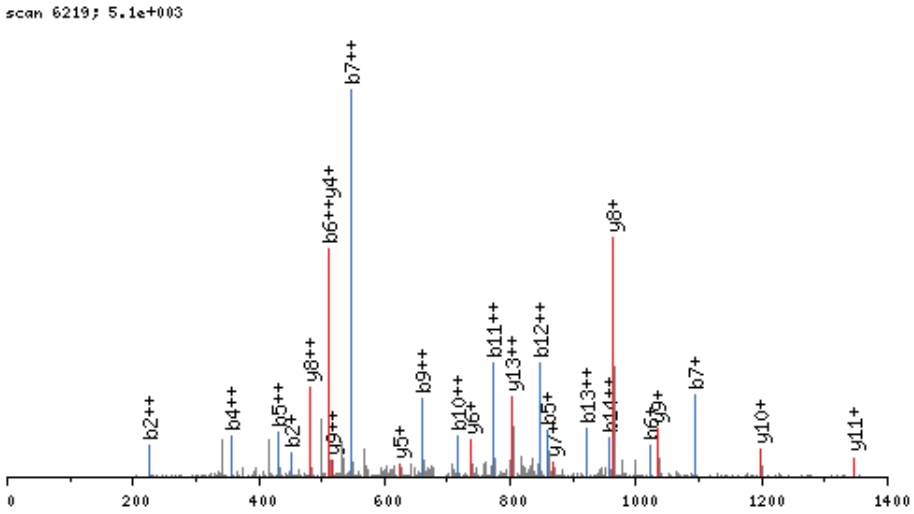

click image to zoom in; click top corners to zoom out [precursor±]

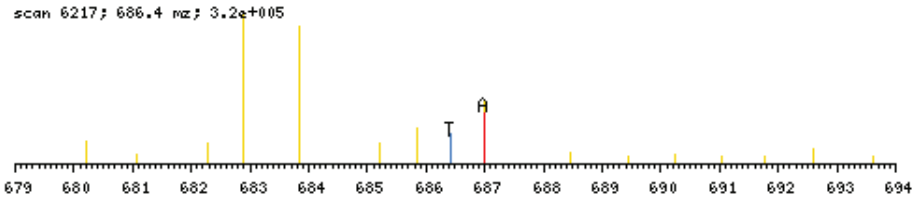

zoomed in precursor plot; T=theoretical m/z, A=acquired m/z

b^+	b^{2+}	#	AA	#	y^+	y^{2+}	y^{3+}
157.1089	79.0584	1	R	15			
452.3807	226.6943	2	H	14	1901.1075	951.0577	634.3744
549.4335	275.2207	3	P	13	1605.8357	803.4218	535.9505
712.4968	356.7523	4	Y	12	1508.7830	754.8954	503.5995
859.5652	430.2865	5	F	11	1345.7196	673.3637	449.2451
1022.6286	511.8182	6	Y	10	1198.6512	599.8295	400.2223
1093.6657	547.3367	7	A	9	1035.5879	518.2979	345.8678
1190.7184	595.8631	8	P	8	964.5508	482.7793	322.1888
1319.7610	660.3844	9	E	7	867.4980	434.2529	289.8379
1432.8451	716.9265	10	L	6	738.4554	369.7316	246.8237
1545.9291	773.4685	11	L	5	625.3714	313.1896	209.1290
1692.9976	847.0027	12	F	4	512.2873	256.6476	171.4343
1840.0660	920.5369	13	F	3	365.2189	183.1134	122.4115
1911.1031	956.0555	14	A	2	218.1505	109.5791	73.3887
		15	K	1	147.1134	74.0606	49.7097

H(2):+295.27

COMET Spectrum View by J.Eng (c) ISB 2001
(TPP v4.4 VUVUZELA rev 1, Build 201010121551 (MinGW))

X-range: 200 - 2000
MassTol: 0.950 Y-zoom: 1.00
ImageSize: (•) Sm ( ) Lg
MassType: ( ) AVG (•) MONO
Axis: (•) 1 ( ) 2
Label: (•) I ( ) M ( ) -
Ions:

a	☐ +	☐ 2+	☐ 3+
b	☐ +	☐ 2+	☐ 3+
c	☑ +	☑ 2+	☐ 3+
x	☐ +	☐ 2+	☐ 3+
y	☐ +	☐ 2+	☐ 3+
z	☑ +	☑ 2+	☑ 3+

hide H_2O/NH_3 ☐
zoom 112-122 ☐
zoom 124-133 ☐
GO

RHPYFYAPELLFFAK, MH+ 2057.2086, m/z 686.4077
10HNE-1HSA-37Trypsin5-LTQ4.8861.8861.3.dta

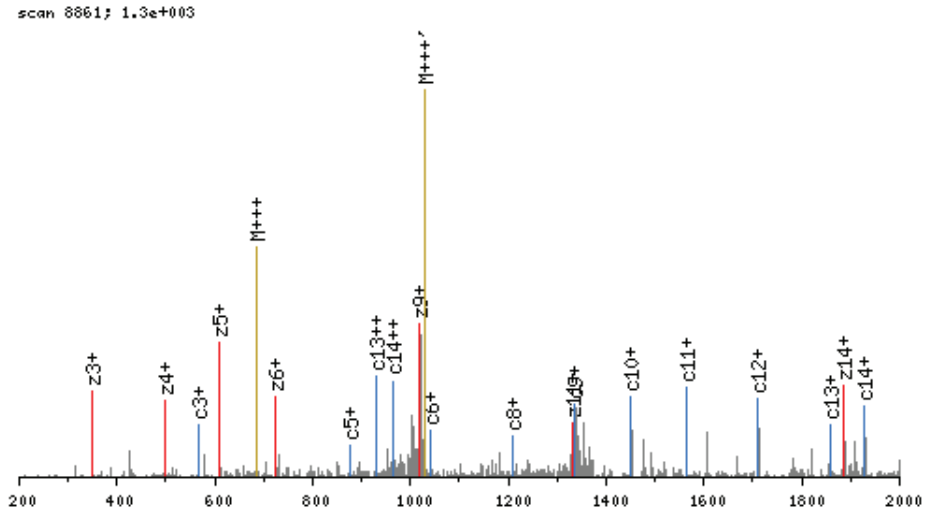

click image to zoom in; click top corners to zoom out [precursor±]

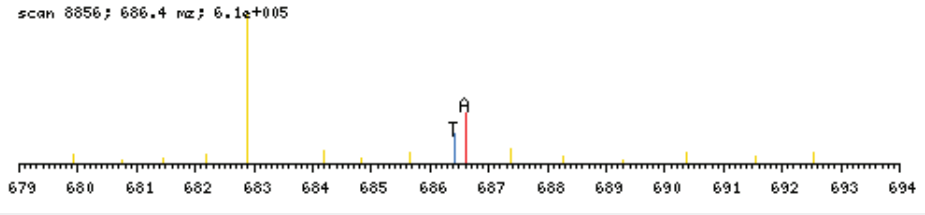

zoomed in precursor plot; T=theoretical m/z, A=acquired m/z

c^+	c^{2+}	#	AA	#	z^+	z^{2+}	z^{3+}
174.1355	87.5717	1	R	15			
469.4073	235.2075	2	H	14	1885.0888	943.0483	629.0348
566.4600	283.7339	3	P	13	1589.8170	795.4124	530.6109
729.5234	365.2656	4	Y	12	1492.7642	746.8860	498.2600
876.5918	438.7998	5	F	11	1329.7009	665.3544	443.9055
1039.6551	520.3315	6	Y	10	1182.6325	591.8202	394.8827
1110.6922	555.8500	7	A	9	1019.5692	510.2885	340.5283
1207.7450	604.3764	8	P	8	948.5321	474.7699	316.8492
1336.7876	668.8977	9	E	7	851.4793	426.2436	284.4983
1449.8716	725.4397	10	L	6	722.4367	361.7223	241.4841
1562.9557	781.9818	11	L	5	609.3526	305.1802	203.7894
1710.0241	855.5160	12	F	4	496.2686	248.6382	166.0947
1857.0925	929.0502	13	F	3	349.2002	175.1040	117.0719
1928.1296	964.5687	14	A	2	202.1317	101.5698	68.0491
		15	K	1	131.0946	66.0512	44.3701

H(2):+295.27

COMET Spectrum View by J.Eng (c) ISB 2001
(TPP v4.4 VUVUZELA rev 1, Build 201010121551 (MinGW))

X-range: 200 - 1400
MassTol: 0.950 Y-zoom: 1.00
ImageSize: (•) Sm ( ) Lg
MassType: ( ) AVG (•) MONO
Axis: (•) 1 ( ) 2
Label: (•) I ( ) M ( ) -
Ions:

a	[ ] +	[ ] 2+	[ ] 3+
b	[x] +	[x] 2+	[ ] 3+
c	[ ] +	[ ] 2+	[ ] 3+
x	[ ] +	[ ] 2+	[ ] 3+
y	[x] +	[x] 2+	[x] 3+
z	[ ] +	[ ] 2+	[ ] 3+

hide H_2O/NH_3 [ ]
zoom 112-122 [ ]
zoom 124-133 [ ]
GO

RHPYFYAPELLFFAKR, MH+ 2213.3097, m/z 738.4414
10HNE-1HSA-37Trypsin5-LTQ1.5395.5395.3.dta

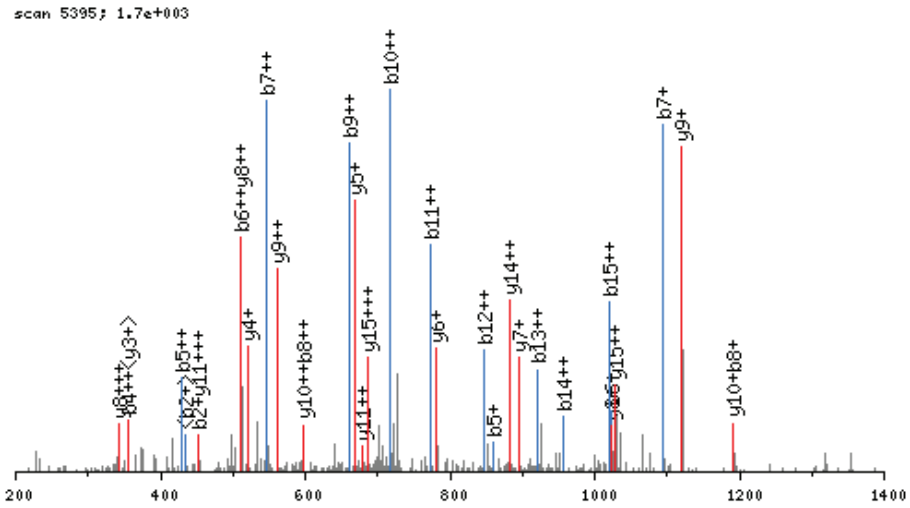

click image to zoom in; click top corners to zoom out [precursor±]

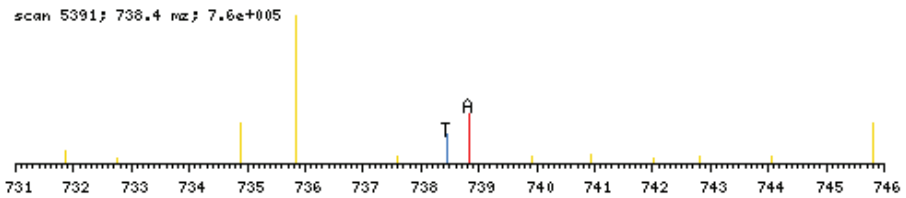

zoomed in precursor plot; T=theoretical m/z, A=acquired m/z

b^+	b^{2+}	#	AA	#	y^+	y^{2+}	y^{3+}
157.1089	79.0584	1	R	16			
452.3807	226.6943	2	H	15	2057.2086	**1029.1082**	**686.4081**
549.4335	275.2207	3	P	14	1761.9368	**881.4723**	587.9842
712.4968	**356.7523**	4	Y	13	1664.8841	832.9460	555.6332
859.5652	**430.2865**	5	F	12	1501.8207	751.4143	501.2788
1022.6286	**511.8182**	6	Y	11	1354.7523	**677.8801**	**452.2560**
1093.6657	**547.3367**	7	A	10	**1191.6890**	**596.3484**	397.9016
1190.7184	**595.8631**	8	P	9	**1120.6519**	**560.8299**	374.2225
1319.7610	**660.3844**	9	E	8	**1023.5991**	**512.3035**	**341.8716**
1432.8451	**716.9265**	10	L	7	**894.5565**	447.7822	298.8574
1545.9291	**773.4685**	11	L	6	**781.4725**	391.2401	261.1627
1692.9976	**847.0027**	12	F	5	**668.3884**	334.6981	223.4680
1840.0660	**920.5369**	13	F	4	**521.3200**	261.1639	174.4452
1911.1031	**956.0555**	14	A	3	374.2516	187.6297	125.4224
2039.1981	**1020.1029**	15	K	2	303.2145	152.1111	101.7434
		16	R	1	175.1195	88.0637	59.0451

H(2):+295.27

X-range: 400 - 1800
MassTol: 0.950 Y-zoom: 1.70
ImageSize: Sm Lg
MassType: AVG MONO
Axis: 1 2
Label: I M -
Ions:

a	+	2+	3+
b	+	2+	3+
c	+	2+	3+
x	+	2+	3+
y	+	2+	3+
z	+	2+	3+

hide H_2O/NH_3
zoom 112-122
zoom 124-133
GO

RHPYFYAPELLFFAKR, MH+ 2371.5195, m/z 593.6353
10HNE-1HSA-37Trypsin3-LTQ2.6320.6320.4.dta

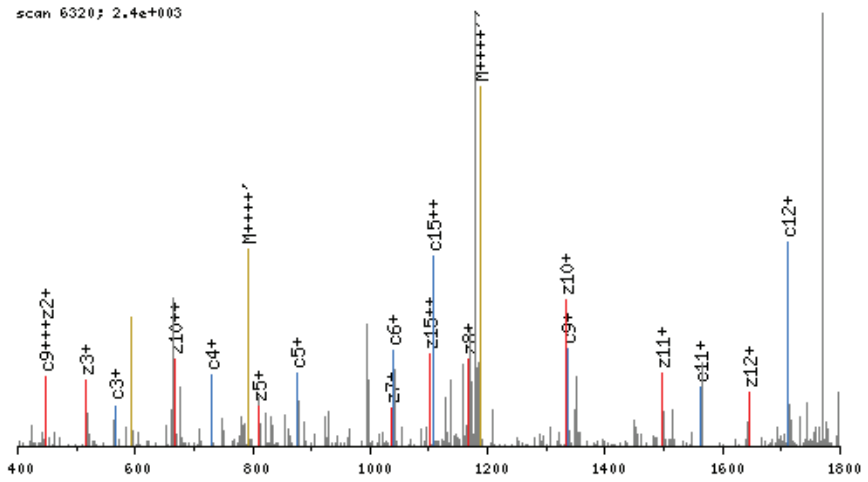

click image to zoom in; click top corners to zoom out [precursor±]

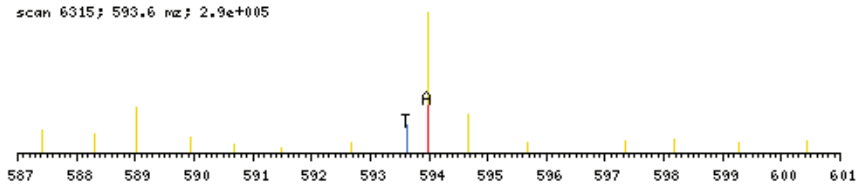

zoomed in precursor plot; T=theoretical m/z, A=acquired m/z

c^+	c^{2+}	c^{3+}	#	AA	#	z^+	z^{2+}	z^{3+}
174.1355	87.5717	58.7170	1	R	16			
469.4073	235.2075	157.1410	2	H	15	2199.3997	1100.2038	733.8051
566.4600	283.7339	189.4919	3	P	14	1904.1279	952.5679	635.3812
729.5234	365.2656	243.8463	4	Y	13	1807.0752	904.0415	603.0303
876.5918	438.7998	292.8691	5	F	12	1644.0118	822.5098	548.6758
1039.6551	520.3315	347.2236	6	Y	11	1496.9434	748.9756	499.6530
1110.6922	555.8500	370.9026	7	A	10	1333.8801	667.4440	445.2986
1207.7450	604.3764	403.2535	8	P	9	1262.8430	631.9254	421.6195
1336.7876	668.8977	446.2677	9	E	8	1165.7902	583.3990	389.2686
1449.8716	725.4397	483.9624	10	L	7	1036.7476	518.8777	346.2544
1562.9557	781.9818	521.6571	11	L	6	923.6636	462.3357	308.5597
1710.0241	855.5160	570.6799	12	F	5	810.5795	405.7937	270.8650
1857.0925	929.0502	619.7027	13	F	4	663.5111	332.2595	221.8422
1928.1296	964.5687	643.3818	14	A	3	516.4427	258.7252	172.8194
2214.4344	1107.7211	738.8167	15	K	2	445.4056	223.2067	149.1404
			16	R	1	159.1008	80.0543	53.7055

H(2):+295.27 K(15):+286.30

X-range: 200 - 1800
MassTol: 0.950 Y-zoom: 1.00
ImageSize: Sm Lg
MassType: AVG MONO
Axis: 1 2
Label: I M -
Ions:

a	+	2+	3+
b	+	2+	3+
c	+	2+	3+
x	+	2+	3+
y	+	2+	3+
z	+	2+	3+

hide H_2O/NH_3
zoom 112-122
zoom 124-133
GO

YKAAFTECCQAADK, MH+ 1821.1947, m/z 911.1010
10HNE-1HSA-37Trypsin4-LTQ3.4018.4018.2.dta

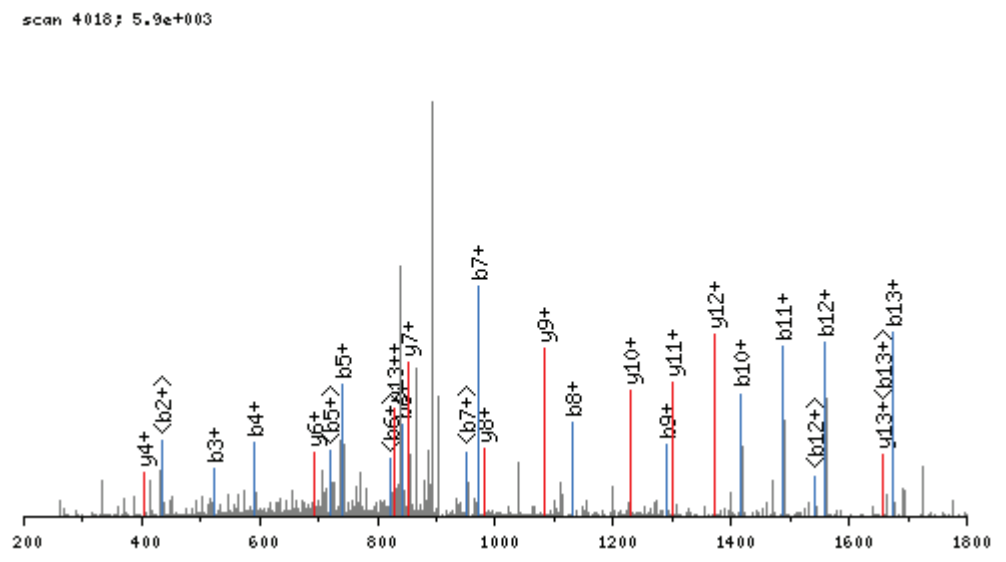

click image to zoom in; click top corners to zoom out [precursor±]

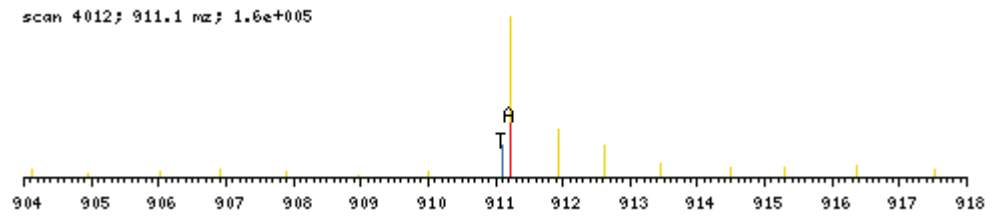

zoomed in precursor plot; T=theoretical m/z, A=acquired m/z

b^+	#	AA	#	y^+	y^{2+}
164.0712	1	Y	14		
450.3759	2	K	13	1658.1314	829.5696
521.4130	3	A	12	1371.8266	686.4172
592.4502	4	A	11	1300.7895	650.8987
739.5186	5	F	10	1229.7524	615.3801
840.5663	6	T	9	1082.6840	541.8459
969.6088	7	E	8	981.6363	491.3221
1129.7691	8	C	7	852.5937	426.8008
1289.9294	9	C	6	692.4334	346.7206
1417.9880	10	Q	5	532.2731	266.6405
1489.0251	11	A	4	404.2145	202.6112
1560.0623	12	A	3	333.1774	167.0926
1675.0892	13	D	2	262.1403	131.5741
	14	K	1	147.1134	74.0606

K(2):+286.30 C(8):+160.16 C(9):+160.16

X-range: 200 - 1800
MassTol: 0.950 Y-zoom: 1.00
ImageSize: Sm Lg
MassType: AVG MONO
Axis: 1 2
Label: I M -
Ions:

a	+	2+	3+
b	+	2+	3+
c	+	2+	3+
x	+	2+	3+
y	+	2+	3+
z	+	2+	3+

hide H_2O/NH_3
zoom 112-122
zoom 124-133
GO

YKAAFTECCQAADK, MH+ 1821.1947, m/z 607.7364
10HNE-1HSA-37Trypsin2-LTQ1.3847.3847.3.dta

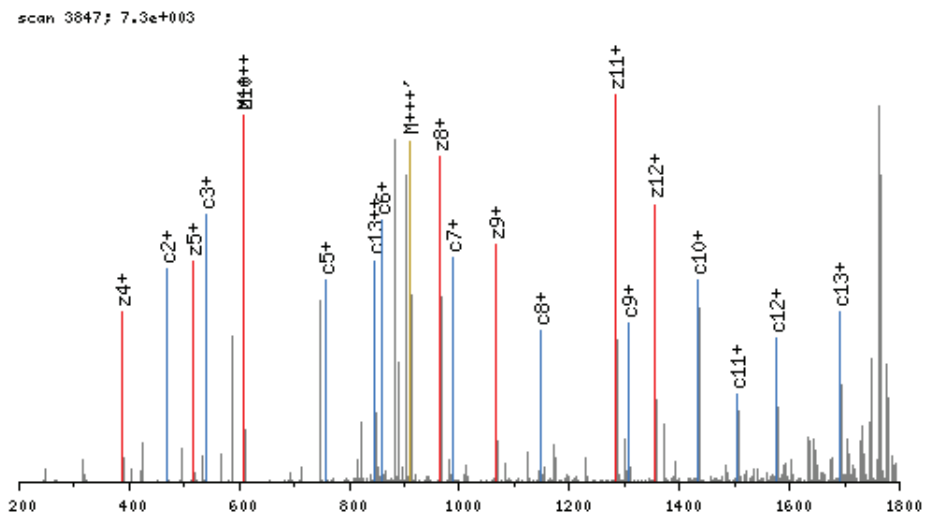

click image to zoom in; click top corners to zoom out [precursor±]

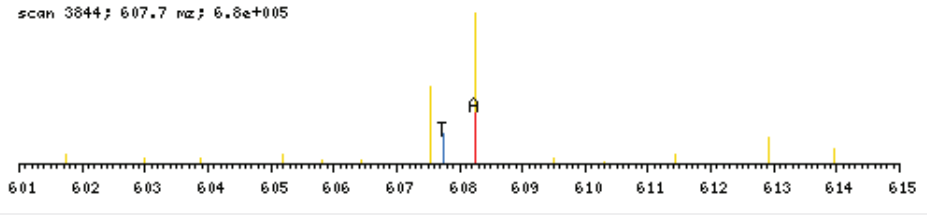

zoomed in precursor plot; T=theoretical m/z, A=acquired m/z

c^+	c^{2+}	#	AA	#	z^+	z^{2+}	z^{3+}
181.0977	91.0528	1	Y	14			
467.4025	234.2052	2	K	13	1642.1127	821.5602	548.0428
538.4396	269.7237	3	A	12	1355.8079	678.4079	452.6078
609.4767	305.2423	4	A	11	1284.7708	642.8893	428.9288
756.5451	378.7765	5	F	10	1213.7337	607.3707	405.2498
857.5928	429.3003	6	T	9	1066.6652	533.8365	356.2270
986.6354	493.8216	7	E	8	965.6176	483.3127	322.5444
1146.7957	573.9018	8	C	7	836.5750	418.7914	279.5302
1306.9560	653.9819	9	C	6	676.4147	338.7113	226.1434
1435.0146	718.0112	10	Q	5	516.2544	258.6311	172.7567
1506.0517	753.5298	11	A	4	388.1958	194.6018	130.0705
1577.0888	789.0483	12	A	3	317.1587	159.0833	106.3914
1692.1157	846.5618	13	D	2	246.1216	123.5647	82.7124
		14	K	1	131.0946	66.0512	44.3701

K(2):+286.30 C(8):+160.16 C(9):+160.16

X-range: 200 - 1100
MassTol: 0.950 Y-zoom: 4.00
ImageSize: Sm Lg
MassType: AVG MONO
Axis: 1 2
Label: I M -
Ions:
a + 2+ 3+
b + 2+ 3+
c + 2+ 3+
x + 2+ 3+
y + 2+ 3+
z + 2+ 3+
hide H_2O/NH_3
zoom 112-122
zoom 124-133
GO

YKAAFTECCQAADK, MH+ 1803.1842, m/z 601.7329
10HNE-1HSA-37Trypsin3-LTQ2.4214.4214.3.dta

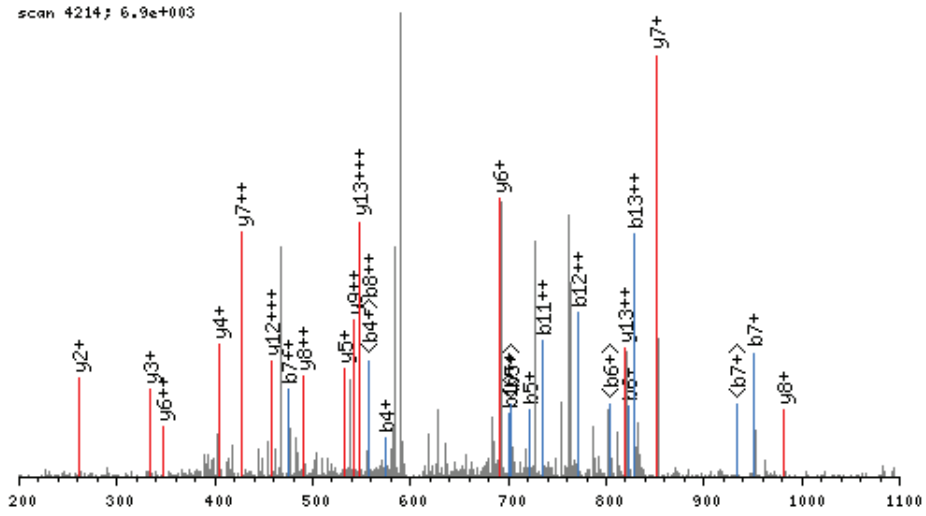

click image to zoom in; click top corners to zoom out [precursor±]

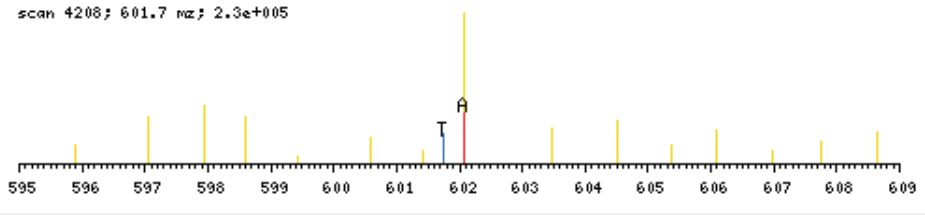

zoomed in precursor plot; T=theoretical m/z, A=acquired m/z

b^+	b^{2+}	#	AA	#	y^+	y^{2+}	y^{3+}
164.0712	82.5395	1	Y	14			
432.3654	216.6866	2	K	13	1640.1208	820.5643	547.3788
503.4025	252.2052	3	A	12	1371.8266	686.4172	457.9474
574.4396	287.7237	4	A	11	1300.7895	650.8987	434.2684
721.5080	361.2579	5	F	10	1229.7524	615.3801	410.5893
822.5557	411.7818	6	T	9	1082.6840	541.8459	361.5665
951.5983	476.3031	7	E	8	981.6363	491.3221	327.8840
1111.7586	556.3832	8	C	7	852.5937	426.8008	284.8698
1271.9189	636.4634	9	C	6	692.4334	346.7206	231.4830
1399.9775	700.4926	10	Q	5	532.2731	266.6405	178.0963
1471.0146	736.0112	11	A	4	404.2145	202.6112	135.4101
1542.0517	771.5298	12	A	3	333.1774	167.0926	111.7310
1657.0786	829.0432	13	D	2	262.1403	131.5741	88.0520
		14	K	1	147.1134	74.0606	49.7097

K(2):+268.29 C(8):+160.16 C(9):+160.16

X-range: 200 - 1800
MassTol: 0.950 Y-zoom: 1.00
ImageSize: (•) Sm ( ) Lg
MassType: ( ) AVG (•) MONO
Axis: (•) 1 ( ) 2
Label: (•) I ( ) M ( ) -
Ions:
a [ ] + [ ] 2+ [ ] 3+
b [ ] + [ ] 2+ [ ] 3+
c [x] + [x] 2+ [ ] 3+
x [ ] + [ ] 2+ [ ] 3+
y [ ] + [ ] 2+ [ ] 3+
z [x] + [x] 2+ [x] 3+
hide H_2O/NH_3 [ ]
zoom 112-122 [ ]
zoom 124-133 [ ]
GO

YKAAFTECCQAADK, MH+ 1803.1842, m/z 601.7329
10HNE-1HSA-37Trypsin5-LTQ4.4295.4295.3.dta

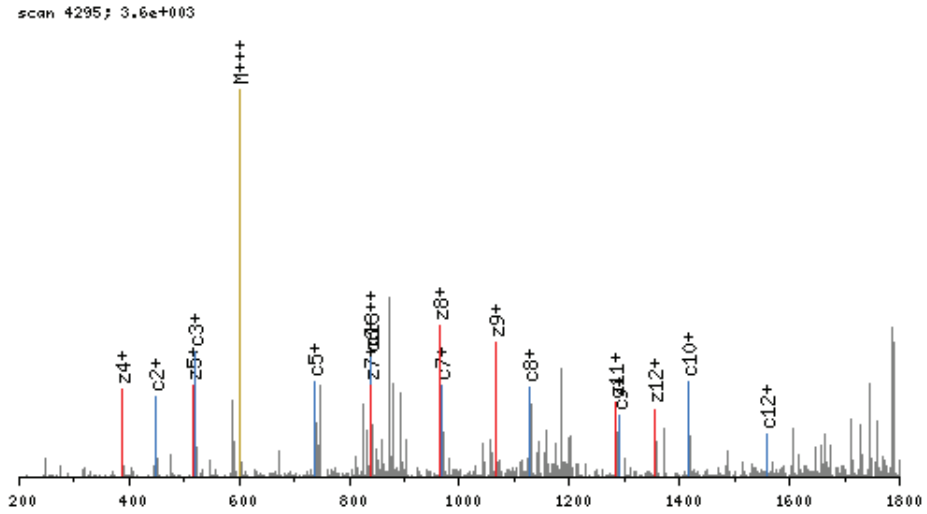

click image to zoom in; click top corners to zoom out [precursor±]

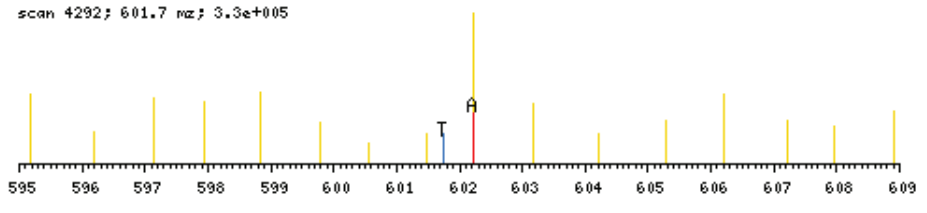

zoomed in precursor plot; T=theoretical m/z, A=acquired m/z

c^+	c^{2+}	#	AA	#	z^+	z^{2+}	z^{3+}
181.0977	91.0528	1	Y	14			
449.3919	225.1999	2	K	13	1624.1021	812.5550	542.0393
520.4290	260.7184	3	A	12	**1355.8079**	678.4079	452.6078
591.4661	296.2370	4	A	11	**1284.7708**	642.8893	428.9288
738.5346	369.7712	5	F	10	1213.7337	607.3707	405.2498
839.5822	420.2950	6	T	9	**1066.6652**	533.8365	356.2270
968.6248	484.8163	7	E	8	**965.6176**	483.3127	322.5444
1128.7851	564.8965	8	C	7	**836.5750**	418.7914	279.5302
1288.9454	644.9766	9	C	6	676.4147	338.7113	226.1434
1417.0040	709.0059	10	Q	5	**516.2544**	258.6311	172.7567
1488.0411	744.5245	11	A	4	**388.1958**	194.6018	130.0705
1559.0782	780.0430	12	A	3	317.1587	159.0833	106.3914
1674.1052	**837.5565**	13	D	2	246.1216	123.5647	82.7124
		14	K	1	131.0946	66.0512	44.3701

K(2):+268.29 C(8):+160.16 C(9):+160.16

X-range: 0 - 0
MassTol: 0.950 Y-zoom: 1.00
ImageSize: Sm Lg
MassType: AVG MONO
Axis: 1 2
Label: I M -
Ions:
a + 2+ 3+
b + 2+ 3+
c + 2+ 3+
x + 2+ 3+
y + 2+ 3+
z + 2+ 3+
hide H_2O/NH_3
zoom 112-122
zoom 124-133
GO

LKCASLQK, MH+ 1105.8743, m/z 369.2963
10HNE-1HSA-37Trypsin5-LTQ4.3307.3307.3.dta

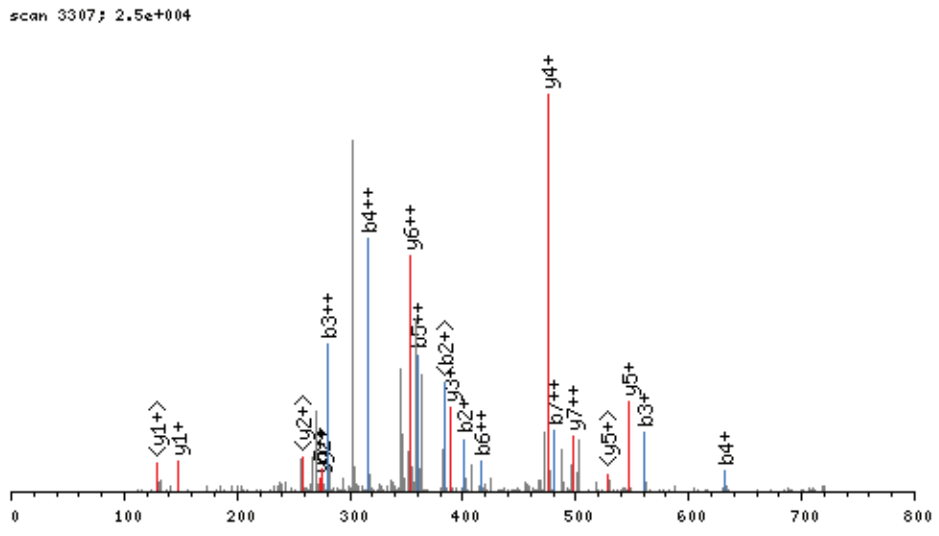

click image to zoom in; click top corners to zoom out [precursor±]

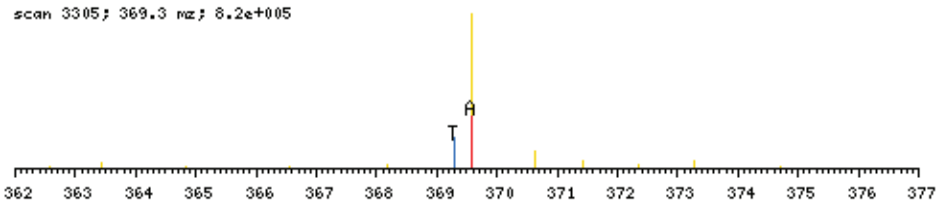

zoomed in precursor plot; T=theoretical m/z, A=acquired m/z

b^+	b^{2+}	#	AA	#	y^+	y^{2+}	y^{3+}
114.0919	57.5499	1	L	8			
400.3967	200.7022	2	K	7	992.7902	**496.8990**	331.6020
560.5570	**280.7824**	3	C	6	706.4854	**353.7466**	236.1670
631.5941	**316.3010**	4	A	5	**546.3251**	**273.6665**	182.7803
718.6261	**359.8170**	5	S	4	**475.2880**	238.1479	159.1012
831.7102	**416.3590**	6	L	3	**388.2560**	194.6319	130.0905
959.7688	**480.3883**	7	Q	2	**275.1719**	138.0899	92.3959
		8	K	1	**147.1134**	74.0606	49.7097

K(2):+286.30 C(3):+160.16

X-range:
0 - 0
MassTol: Y-zoom:
0.950 1.00
ImageSize:
(•) Sm ( ) Lg
MassType:
( ) AVG (•) MONO
Axis:
(•) 1 ( ) 2
Label:
(•) I ( ) M ( ) -
Ions:

a	☐ +	☐ 2+	☐ 3+
b	☑ +	☑ 2+	☐ 3+
c	☐ +	☐ 2+	☐ 3+
x	☐ +	☐ 2+	☐ 3+
y	☑ +	☑ 2+	☑ 3+
z	☐ +	☐ 2+	☐ 3+

hide H_2O/NH_3 ☐
zoom 112-122 ☐
zoom 124-133 ☐
GO

AFKAWAVAR, MH+ 1177.7889, m/z 393.2678
10HNE-1HSA-37Trypsin5-LTQ4.4933.4933.3.dta

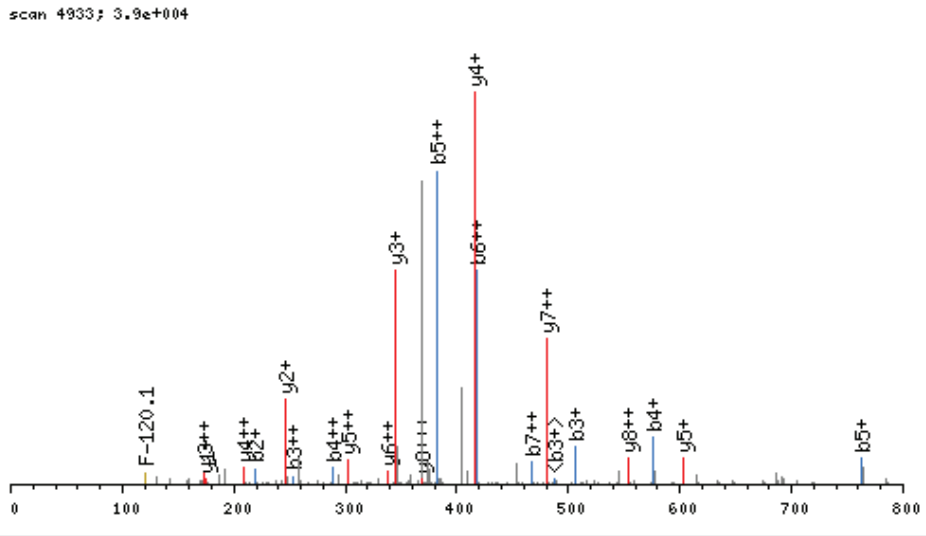

click image to zoom in; click top corners to zoom out [precursor±]

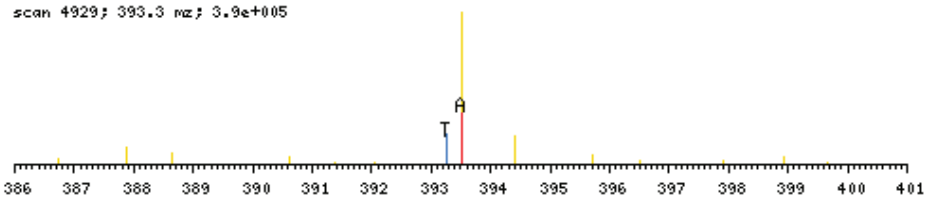

zoomed in precursor plot; T=theoretical m/z, A=acquired m/z

b^+	b^{2+}	#	AA	#	y^+	y^{2+}	y^{3+}
72.0449	36.5264	1	A	9			
219.1134	110.0606	2	F	8	1106.7518	**553.8798**	**369.5891**
505.4181	**253.2130**	3	K	7	959.6833	**480.3456**	320.5663
576.4552	**288.7315**	4	A	6	673.3786	**337.1932**	225.1314
762.5346	**381.7712**	5	W	5	**602.3415**	**301.6746**	201.4524
833.5717	**417.2897**	6	A	4	**416.2621**	**208.6350**	139.4259
932.6401	**466.8240**	7	V	3	**345.2250**	**173.1164**	115.7469
1003.6772	502.3425	8	A	2	**246.1566**	123.5822	82.7241
		9	R	1	**175.1195**	88.0637	59.0451

K(3):+286.30

X-range: 100 - 1300
MassTol: 0.950 Y-zoom: 1.00
ImageSize: Sm Lg
MassType: AVG MONO
Axis: 1 2
Label: I M -
Ions:
a + 2+ 3+
b + 2+ 3+
c + 2+ 3+
x + 2+ 3+
y + 2+ 3+
z + 2+ 3+
hide H_2O/NH_3
zoom 112-122
zoom 124-133
GO

AEFAEVSKLVTDLTK, MH+ 1809.1052, m/z 603.7066
10HNE-1HSA-37Trypsin5-LTQ1.5822.5822.3.dta

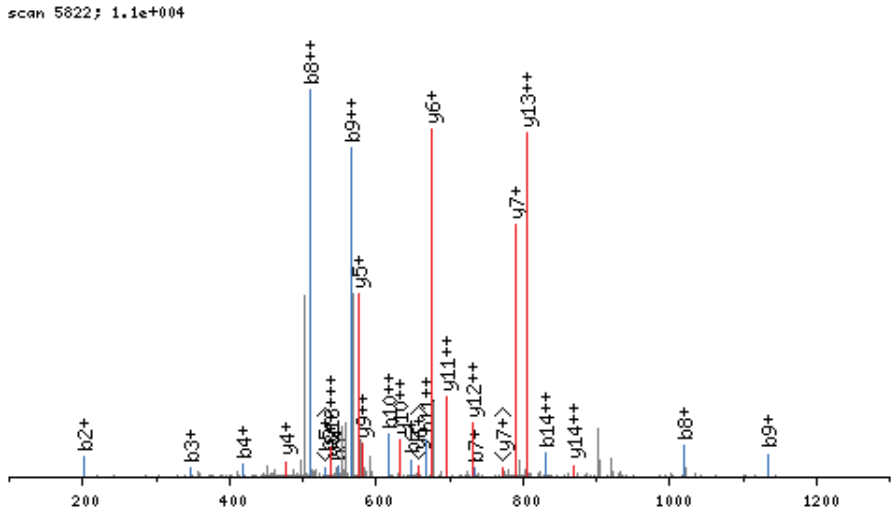

click image to zoom in; click top corners to zoom out [precursor±]

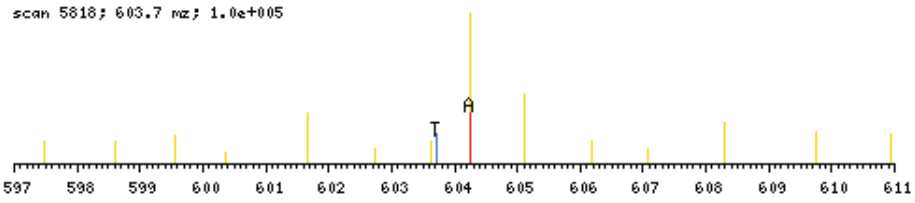

zoomed in precursor plot; T=theoretical m/z, A=acquired m/z

b^+	b^{2+}	#	AA	#	y^+	y^{2+}	y^{3+}
72.0449	36.5264	1	A	15			
201.0875	101.0477	2	E	14	1738.0681	869.5380	580.0279
348.1559	174.5819	3	F	13	1609.0255	805.0167	537.0137
419.1931	210.1004	4	A	12	1461.9571	731.4825	487.9909
548.2357	274.6217	5	E	11	1390.9200	695.9639	464.3119
647.3041	324.1559	6	V	10	1261.8774	631.4426	421.2977
734.3361	367.6720	7	S	9	1162.8090	581.9084	388.2749
1020.6409	510.8244	8	K	8	1075.7770	538.3924	359.2642
1133.7249	567.3664	9	L	7	789.4722	395.2400	263.8293
1232.7934	616.9006	10	V	6	676.3881	338.6980	226.1346
1333.8410	667.4244	11	T	5	577.3197	289.1638	193.1118
1448.8680	724.9379	12	D	4	476.2720	238.6399	159.4292
1561.9520	781.4799	13	L	3	361.2451	181.1265	121.0869
1662.9997	832.0038	14	T	2	248.1610	124.5844	83.3922
		15	K	1	147.1134	74.0606	49.7097

K(8):+286.30

X-range: 800 - 1900
MassTol: 0.950 Y-zoom: 1.00
ImageSize: (•) Sm ( ) Lg
MassType: ( ) AVG (•) MONO
Axis: (•) 1 ( ) 2
Label: (•) I ( ) M ( ) -
Ions:

a	[ ] +	[ ] 2+	[ ] 3+
b	[ ] +	[ ] 2+	[ ] 3+
c	[x] +	[ ] 2+	[ ] 3+
x	[ ] +	[ ] 2+	[ ] 3+
y	[ ] +	[ ] 2+	[ ] 3+
z	[x] +	[x] 2+	[ ] 3+

hide H_2O/NH_3 [ ]
zoom 112-122 [ ]
zoom 124-133 [ ]
GO

AEFAEVSKLVTDLTK, MH+ 1809.1052, m/z 905.0563
10HNE-1HSA-37Trypsin4-LTQ1.5795.5795.2.dta

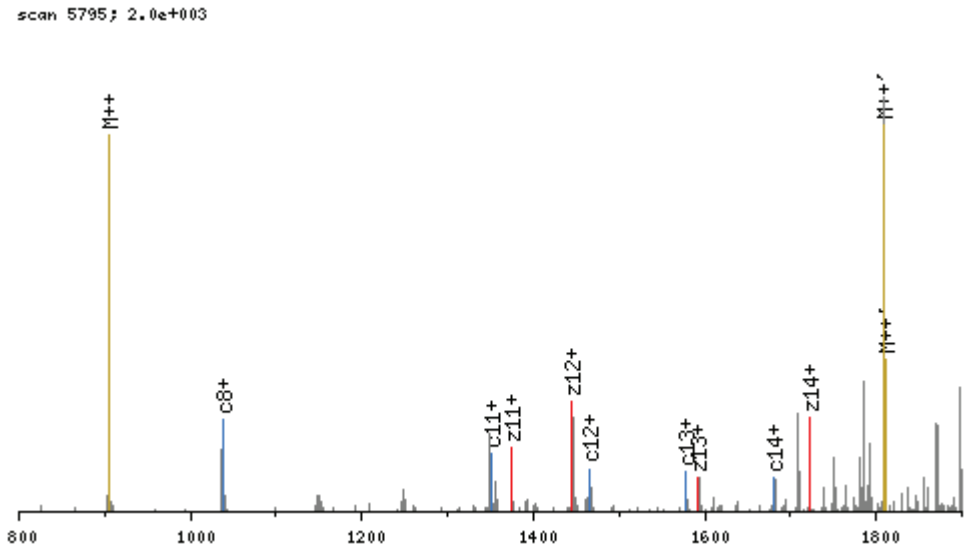

click image to zoom in; click top corners to zoom out [precursor±]

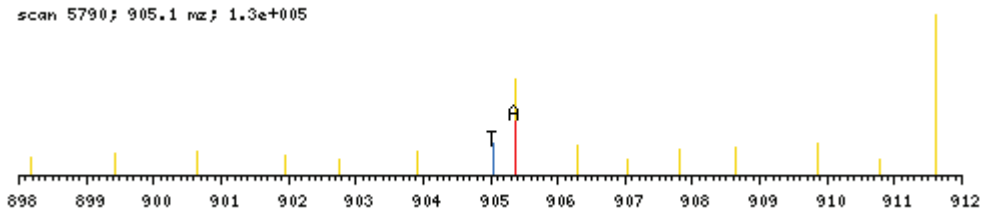

zoomed in precursor plot; T=theoretical m/z, A=acquired m/z

c^+	#	AA	#	z^+	z^{2+}
89.0715	1	A	15		
218.1141	2	E	14	1722.0494	861.5286
365.1825	3	F	13	1593.0068	797.0073
436.2196	4	A	12	1445.9384	723.4731
565.2622	5	E	11	1374.9013	687.9546
664.3306	6	V	10	1245.8587	623.4333
751.3626	7	S	9	1146.7903	573.8991
1037.6674	8	K	8	1059.7583	530.3830
1150.7515	9	L	7	773.4535	387.2306
1249.8199	10	V	6	660.3694	330.6886
1350.8676	11	T	5	561.3010	281.1544
1465.8945	12	D	4	460.2533	230.6306
1578.9786	13	L	3	345.2264	173.1171
1680.0263	14	T	2	232.1423	116.5751
	15	K	1	131.0946	66.0512

K(8):+286.30

COMET Spectrum View by J.Eng (c) ISB 2001
(TPP v4.4 VUVUZELA rev 1, Build 201010121551 (MinGW))

X-range: 400 - 1800
MassTol: 0.950 Y-zoom: 1.00
ImageSize: Sm Lg
MassType: AVG MONO
Axis: 1 2
Label: I M -
Ions:

a	+	2+	3+
b	+	2+	3+
c	+	2+	3+
x	+	2+	3+
y	+	2+	3+
z	+	2+	3+

hide H_2O/NH_3
zoom 112-122
zoom 124-133
GO

LVTDLTKVHTECCHGDLLECADDR, MH+ 3174.1035, m/z 1058.7060
10HNE-1HSA-37Trypsin4-LTQ2.4030.4030.3.dta

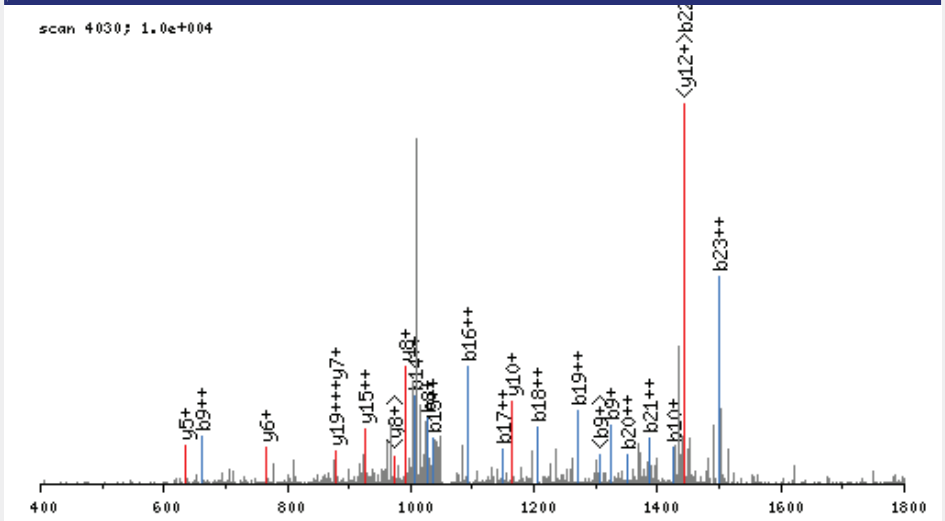

click image to zoom in; click top corners to zoom out [precursor±]

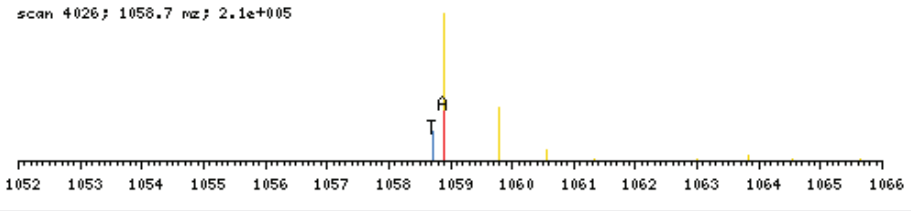

zoomed in precursor plot; T=theoretical m/z, A=acquired m/z

b^+	b^{2+}	#	AA	#	y^+	y^{2+}	y^{3+}
114.0919	57.5499	1	L	24			
213.1603	107.0841	2	V	23	3061.0195	1531.0136	1021.0117
314.2080	157.6079	3	T	22	2961.9511	1481.4794	987.9889
429.2349	215.1214	4	D	21	2860.9034	1430.9556	954.3063
542.3190	271.6634	5	L	20	2745.8764	1373.4421	915.9640
643.3667	322.1872	6	T	19	2632.7924	1316.9001	878.2693
929.6714	465.3396	7	K	18	2531.7447	1266.3763	844.5868
1028.7399	514.8738	8	V	17	2245.4399	1123.2239	749.1519
1324.0116	662.5097	9	H	16	2146.3715	1073.6897	716.1290
1425.0593	713.0336	10	T	15	1851.0997	926.0538	617.7051
1554.1019	777.5549	11	E	14	1750.0520	875.5299	584.0226
1714.2622	857.6350	12	C	13	1621.0094	811.0086	541.0084
1874.4225	937.7152	13	C	12	1460.8491	730.9285	487.6216
2011.4814	1006.2446	14	H	11	1300.6888	650.8483	434.2348
2068.5029	1034.7554	15	G	10	1163.6299	582.3189	388.5485
2183.5298	1092.2688	16	D	9	1106.6085	553.8081	369.5414
2296.6139	1148.8109	17	L	8	991.5815	496.2947	331.1991
2409.6980	1205.3529	18	L	7	878.4975	439.7526	293.5044
2538.7406	1269.8742	19	E	6	765.4134	383.2106	255.8097
2698.9009	1349.9543	20	C	5	636.3708	318.6893	212.7955
2769.9380	1385.4729	21	A	4	476.2105	238.6092	159.4087
2884.9649	1442.9864	22	D	3	405.1734	203.0906	135.7297
2999.9919	1500.4998	23	D	2	290.1464	145.5771	97.3874
		24	R	1	175.1195	88.0637	59.0451

K(7):+286.30 H(9):+295.27 C(12):+160.16 C(13):+160.16 C(20):+160.16

X-range: 400 - 1900
MassTol: 0.950 Y-zoom: 1.00
ImageSize: (•) Sm ( ) Lg
MassType: ( ) AVG (•) MONO
Axis: (•) 1 ( ) 2
Label: (•) I ( ) M ( ) -
Ions:

a	☐ +	☐ 2+	☐ 3+
b	☐ +	☐ 2+	☐ 3+
c	☑ +	☑ 2+	☐ 3+
x	☐ +	☐ 2+	☐ 3+
y	☐ +	☐ 2+	☐ 3+
z	☑ +	☑ 2+	☑ 3+

hide H_2O/NH_3 ☐
zoom 112-122 ☐
zoom 124-133 ☐
GO

VHTECCHGDLLECADDR, MH+ 2245.4399, m/z 749.1515
10HNE-1HSA-37Trypsin2-LTQ2.4160.4160.3.dta

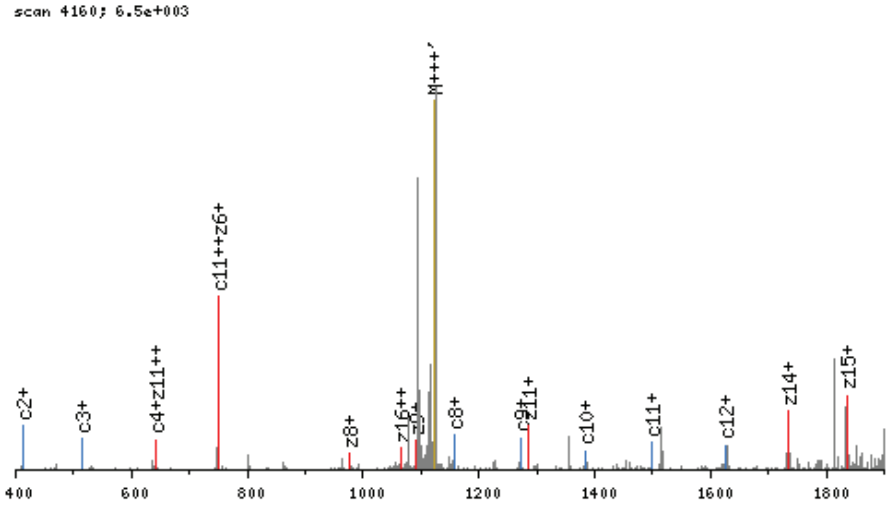

click image to zoom in; click top corners to zoom out [precursor±]

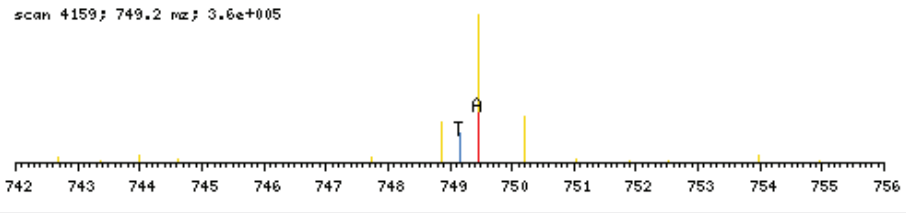

zoomed in precursor plot; T=theoretical m/z, A=acquired m/z

c^+	c^{2+}	#	AA	#	z^+	z^{2+}	z^{3+}
117.1028	59.0553	1	V	17			
412.3746	206.6912	2	H	16	2130.3528	**1065.6803**	710.7895
513.4222	257.2150	3	T	15	**1835.0810**	918.0444	612.3655
642.4648	321.7363	4	E	14	**1734.0333**	867.5206	578.6830
802.6251	401.8165	5	C	13	1604.9907	802.9993	535.6688
962.7854	481.8966	6	C	12	1444.8304	722.9191	482.2820
1099.8444	550.4261	7	H	11	**1284.6701**	**642.8390**	428.8953
1156.8658	578.9368	8	G	10	1147.6112	574.3095	383.2090
1271.8928	636.4503	9	D	9	**1090.5897**	545.7988	364.2018
1384.9768	692.9923	10	L	8	**975.5628**	488.2853	325.8595
1498.0609	**749.5344**	11	L	7	862.4787	431.7433	288.1648
1627.1035	814.0557	12	E	6	**749.3947**	375.2012	250.4701
1787.2638	894.1358	13	C	5	620.3521	310.6800	207.4559
1858.3009	929.6544	14	A	4	460.1918	230.5998	154.0691
1973.3278	987.1678	15	D	3	389.1547	195.0812	130.3901
2088.3548	1044.6813	16	D	2	274.1277	137.5678	92.0478
		17	R	1	159.1008	80.0543	53.7055

H(2):+295.27 C(5):+160.16 C(6):+160.16 C(13):+160.16

X-range: 200 - 1400
MassTol: 0.950 Y-zoom: 1.00
ImageSize: (•) Sm ( ) Lg
MassType: ( ) AVG (•) MONO
Axis: (•) 1 ( ) 2
Label: (•) I ( ) M ( ) -
Ions:

a	☐ +	☐ 2+	☐ 3+
b	☑ +	☑ 2+	☐ 3+
c	☐ +	☐ 2+	☐ 3+
x	☐ +	☐ 2+	☐ 3+
y	☑ +	☑ 2+	☑ 3+
z	☐ +	☐ 2+	☐ 3+

hide H_2O/NH_3 ☐
zoom 112-122 ☐
zoom 124-133 ☐
GO

VHTECCHGDLLECADDR, MH+ 2403.6528, m/z 801.8891
10HNE-1HSA-37Trypsin5-LTQ4.5591.5591.3.dta

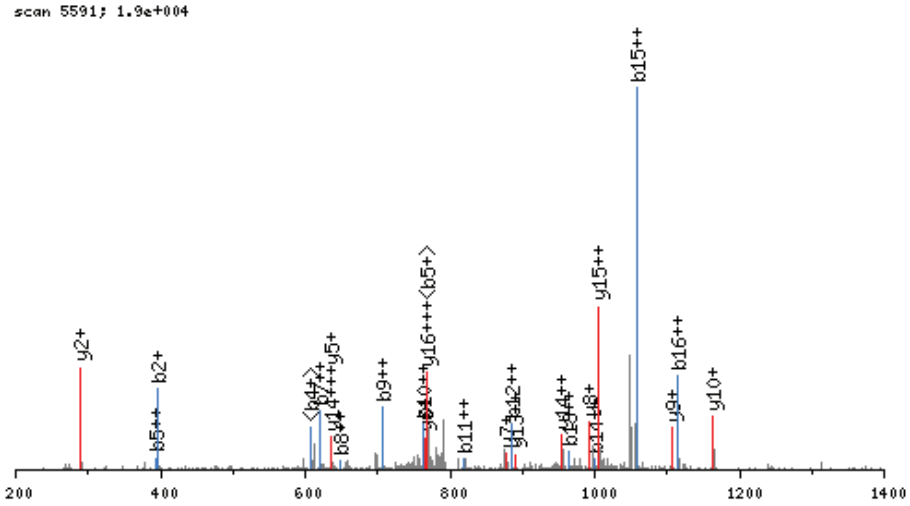

click image to zoom in; click top corners to zoom out [precursor±]

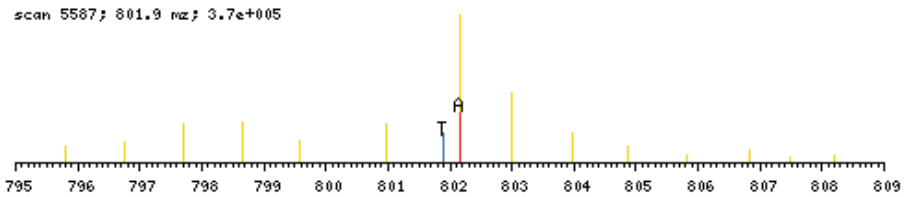

zoomed in precursor plot; T=theoretical m/z, A=acquired m/z

b^+	b^{2+}	#	AA	#	y^+	y^{2+}	y^{3+}
100.0762	50.5420	1	V	17			
395.3480	198.1779	2	H	16	2304.5844	1152.7961	**768.8667**
496.3957	248.7018	3	T	15	2009.3126	**1005.1602**	670.4427
625.4383	313.2231	4	E	14	1908.2649	**954.6364**	**636.7602**
785.5986	**393.3032**	5	C	13	1779.2223	**890.1151**	593.7460
945.7589	473.3834	6	C	12	1619.0620	810.0349	540.3592
1241.0307	**621.0192**	7	H	11	1458.9017	729.9548	486.9725
1298.0521	**649.5300**	8	G	10	**1163.6299**	582.3189	388.5485
1413.0791	**707.0435**	9	D	9	**1106.6085**	553.8081	369.5414
1526.1631	**763.5855**	10	L	8	**991.5815**	496.2947	331.1991
1639.2472	**820.1275**	11	L	7	**878.4975**	439.7526	293.5044
1768.2898	**884.6488**	12	E	6	**765.4134**	383.2106	255.8097
1928.4501	**964.7290**	13	C	5	**636.3708**	318.6893	212.7955
1999.4872	**1000.2475**	14	A	4	476.2105	238.6092	159.4087
2114.5142	**1057.7610**	15	D	3	405.1734	203.0906	135.7297
2229.5411	**1115.2745**	16	D	2	**290.1464**	145.5771	97.3874
		17	R	1	175.1195	88.0637	59.0451

H(2):+295.27 C(5):+160.16 C(6):+160.16 H(7):+295.27
C(13):+160.16

X-range: 200 - 2000
MassTol: 0.950 Y-zoom: 1.00
ImageSize: (•) Sm ( ) Lg
MassType: ( ) AVG (•) MONO
Axis: (•) 1 ( ) 2
Label: (•) I ( ) M ( ) -
Ions:

a	☐ +	☐ 2+	☐ 3+
b	☐ +	☐ 2+	☐ 3+
c	☑ +	☑ 2+	☐ 3+
x	☐ +	☐ 2+	☐ 3+
y	☐ +	☐ 2+	☐ 3+
z	☑ +	☑ 2+	☑ 3+

hide H_2O/NH_3 ☐
zoom 112-122 ☐
zoom 124-133 ☐
GO

VHTECCHGDLLECADDR, MH+ 2403.6528, m/z 801.8891
10HNE-1HSA-37Trypsin5-LTQ4.5590.5590.3.dta

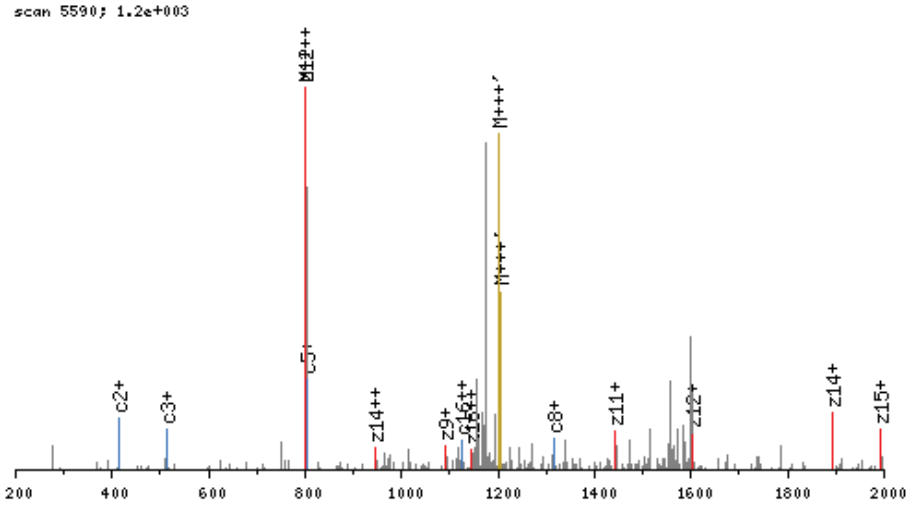

click image to zoom in; click top corners to zoom out [precursor±]

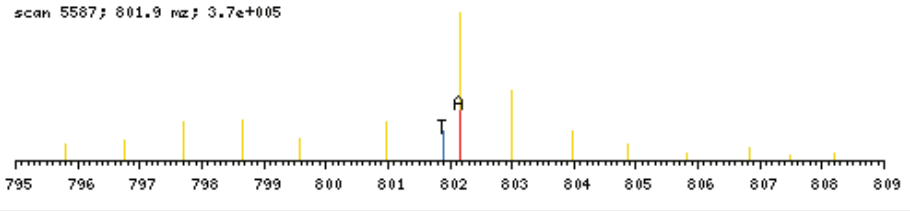

zoomed in precursor plot; T=theoretical m/z, A=acquired m/z

c^+	c^{2+}	#	AA	#	z^+	z^{2+}	z^{3+}
117.1028	59.0553	1	V	17			
412.3746	206.6912	2	H	16	2288.5656	1144.7867	763.5271
513.4222	257.2150	3	T	15	1993.2939	997.1508	665.1032
642.4648	321.7363	4	E	14	1892.2462	946.6270	631.4206
802.6251	401.8165	5	C	13	1763.2036	882.1057	588.4064
962.7854	481.8966	6	C	12	1603.0433	802.0256	535.0196
1258.0572	629.5325	7	H	11	1442.8830	721.9454	481.6329
1315.0787	658.0433	8	G	10	1147.6112	574.3095	383.2090
1430.1056	715.5567	9	D	9	1090.5897	545.7988	364.2018
1543.1897	772.0988	10	L	8	975.5628	488.2853	325.8595
1656.2738	828.6408	11	L	7	862.4787	431.7433	288.1648
1785.3163	893.1621	12	E	6	749.3947	375.2012	250.4701
1945.4766	973.2422	13	C	5	620.3521	310.6800	207.4559
2016.5138	1008.7608	14	A	4	460.1918	230.5998	154.0691
2131.5407	1066.2743	15	D	3	389.1547	195.0812	130.3901
2246.5676	1123.7877	16	D	2	274.1277	137.5678	92.0478
		17	R	1	159.1008	80.0543	53.7055

H(2):+295.27 C(5):+160.16 C(6):+160.16 H(7):+295.27
C(13):+160.16

COMET Spectrum View by J.Eng (c) ISB 2001
(TPP v4.4 VUVUZELA rev 1, Build 201010121551 (MinGW))

X-range: 300 - 1600
MassTol: 0.950 Y-zoom: 1.00
ImageSize: Sm Lg
MassType: AVG MONO
Axis: 1 2
Label: I M -
Ions:
a + 2+ 3+
b + 2+ 3+
c + 2+ 3+
x + 2+ 3+
y + 2+ 3+
z + 2+ 3+
hide H_2O/NH_3
zoom 112-122
zoom 124-133
GO

VHTECCHGDLLECADDRADLAK, MH+ 2901.9330, m/z 967.9825
10HNE-1HSA-37Trypsin4-LTQ3.5096.5096.3.dta

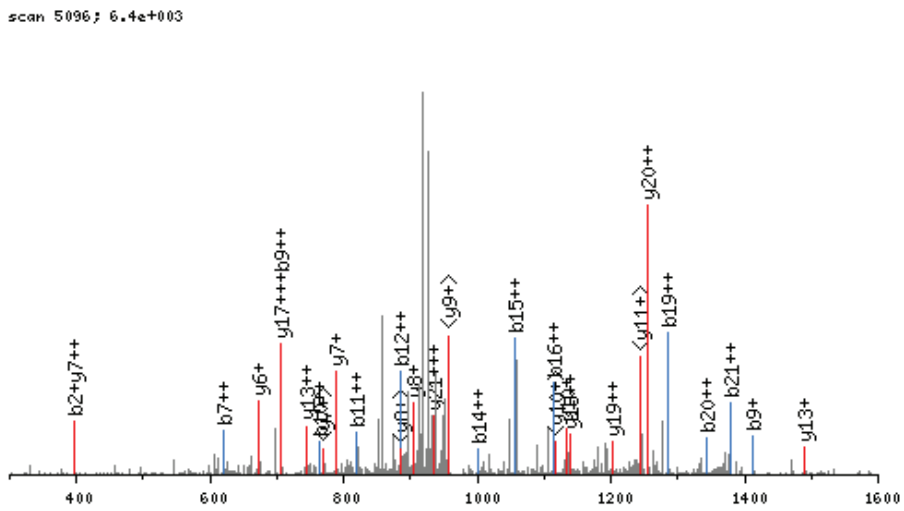

click image to zoom in; click top corners to zoom out [precursor±]

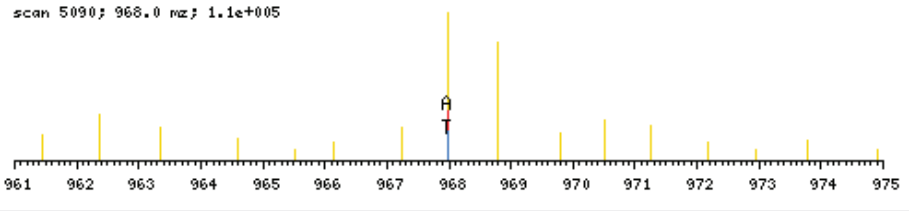

zoomed in precursor plot; T=theoretical m/z, A=acquired m/z

b^+	b^{2+}	#	AA	#	y^+	y^{2+}	y^{3+}
100.0762	50.5420	1	V	22			
395.3480	198.1779	2	H	21	2802.8646	1401.9362	**934.9601**
496.3957	248.7018	3	T	20	2507.5928	**1254.3003**	836.5361
625.4383	313.2231	4	E	19	2406.5451	**1203.7765**	802.8536
785.5986	393.3032	5	C	18	2277.5025	**1139.2552**	759.8394
945.7589	473.3834	6	C	17	2117.3422	1059.1750	**706.4526**
1241.0307	**621.0192**	7	H	16	1957.1819	979.0949	653.0659
1298.0521	649.5300	8	G	15	1661.9101	831.4590	554.6419
1413.0791	**707.0435**	9	D	14	1604.8887	802.9482	535.6348
1526.1631	**763.5855**	10	L	13	**1489.8617**	**745.4348**	497.2925
1639.2472	**820.1275**	11	L	12	1376.7777	688.8927	459.5978
1768.2898	**884.6488**	12	E	11	1263.6936	632.3507	421.9031
1928.4501	964.7290	13	C	10	**1134.6510**	567.8294	378.8889
1999.4872	**1000.2475**	14	A	9	974.4907	487.7493	325.5021
2114.5142	**1057.7610**	15	D	8	**903.4536**	452.2307	301.8231
2229.5411	**1115.2745**	16	D	7	**788.4266**	**394.7172**	263.4808
2385.6422	1193.3250	17	R	6	**673.3997**	337.2038	225.1384
2456.6793	1228.8436	18	A	5	517.2986	259.1532	173.1047
2571.7063	**1286.3570**	19	D	4	446.2615	223.6346	149.4257
2684.7903	**1342.8991**	20	L	3	331.2345	166.1212	111.0834
2755.8274	**1378.4176**	21	A	2	218.1505	109.5791	73.3887
		22	K	1	147.1134	74.0606	49.7097

H(2):+295.27 C(5):+160.16 C(6):+160.16 H(7):+295.27
C(13):+160.16

X-range: 200 - 1800
MassTol: 0.950 Y-zoom: 2.00
ImageSize: Sm Lg
MassType: AVG MONO
Axis: 1 2
Label: I M -
Ions:

a	+	2+	3+
b	+	2+	3+
c	✓ +	✓ 2+	✓ 3+
x	+	2+	3+
y	+	2+	3+
z	✓ +	✓ 2+	✓ 3+

hide H_2O/NH_3
zoom 112-122
zoom 124-133
GO

VHTECCHGDLLECADDRADLAK, MH+ 2901.9330, m/z 726.2387
10HNE-1HSA-37Trypsin3-LTQ1.4960.4960.4.dta

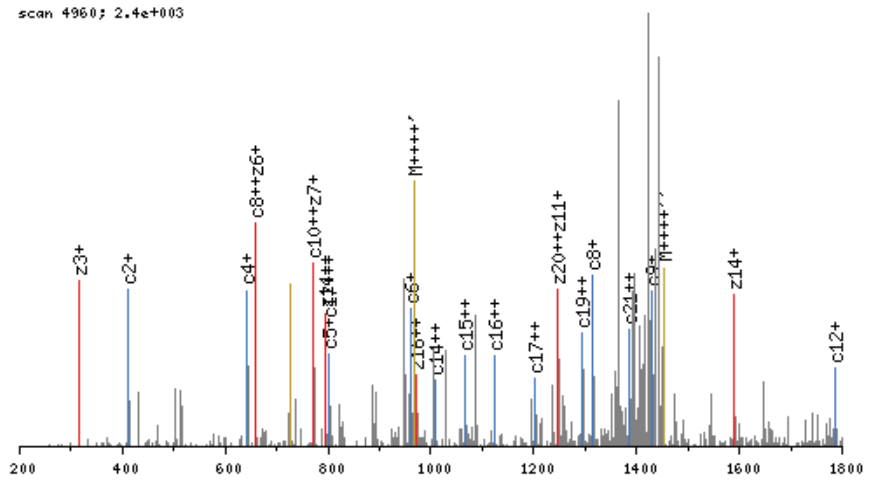

click image to zoom in; click top corners to zoom out [precursor±]

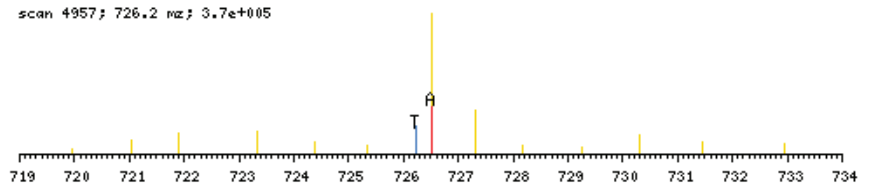

zoomed in precursor plot; T=theoretical m/z, A=acquired m/z

c^+	c^{2+}	c^{3+}	#	AA	#	z^+	z^{2+}	z^{3+}
117.1028	59.0553	39.7061	1	V	22			
412.3746	206.6912	138.1301	2	H	21	2786.8458	1393.9268	929.6205
513.4222	257.2150	171.8126	3	T	20	2491.5741	1246.2909	831.1966
642.4648	321.7363	214.8268	4	E	19	2390.5264	1195.7671	797.5140
802.6251	401.8165	268.2136	5	C	18	2261.4838	1131.2458	754.4998
962.7854	481.8966	321.6004	6	C	17	2101.3235	1051.1657	701.1130
1258.0572	629.5325	420.0243	7	H	16	1941.1632	971.0855	647.7263
1315.0787	658.0433	439.0314	8	G	15	1645.8914	823.4496	549.3024
1430.1056	715.5567	477.3738	9	D	14	1588.8699	794.9389	530.2952
1543.1897	772.0988	515.0684	10	L	13	1473.8430	737.4254	491.9529
1656.2738	828.6408	552.7631	11	L	12	1360.7589	680.8834	454.2582
1785.3163	893.1621	595.7773	12	E	11	1247.6749	624.3413	416.5635
1945.4766	973.2422	649.1641	13	C	10	1118.6323	559.8200	373.5493
2016.5138	1008.7608	672.8431	14	A	9	958.4720	479.7399	320.1625
2131.5407	1066.2743	711.1855	15	D	8	887.4349	444.2213	296.4835
2246.5676	1123.7877	749.5278	16	D	7	772.4079	386.7079	258.1412
2402.6688	1201.8383	801.5615	17	R	6	657.3810	329.1944	219.7989
2473.7059	1237.3568	825.2405	18	A	5	501.2799	251.1438	167.7652
2588.7328	1294.8703	863.5828	19	D	4	430.2427	215.6253	144.0861
2701.8169	1351.4124	901.2775	20	L	3	315.2158	158.1118	105.7438
2772.8540	1386.9309	924.9565	21	A	2	202.1317	101.5698	68.0491
			22	K	1	131.0946	66.0512	44.3701

H(2):+295.27 C(5):+160.16 C(6):+160.16 H(7):+295.27 C(13):+160.16

X-range: 200 - 1400
MassTol: 0.950 Y-zoom: 1.00
ImageSize: (•) Sm ( ) Lg
MassType: ( ) AVG (•) MONO
Axis: (•) 1 ( ) 2
Label: (•) I ( ) M ( ) -
Ions:

a	☐ +	☐ 2+	☐ 3+
b	☑ +	☑ 2+	☐ 3+
c	☐ +	☐ 2+	☐ 3+
x	☐ +	☐ 2+	☐ 3+
y	☑ +	☑ 2+	☑ 3+
z	☐ +	☐ 2+	☐ 3+

hide H_2O/NH_3 ☐
zoom 112-122 ☐
zoom 124-133 ☐
GO

ADLAKYICENQDSISSK, MH+ 2100.2623, m/z 700.7589
10HNE-1HSA-37Trypsin5-LTQ3.4681.4681.3.dta

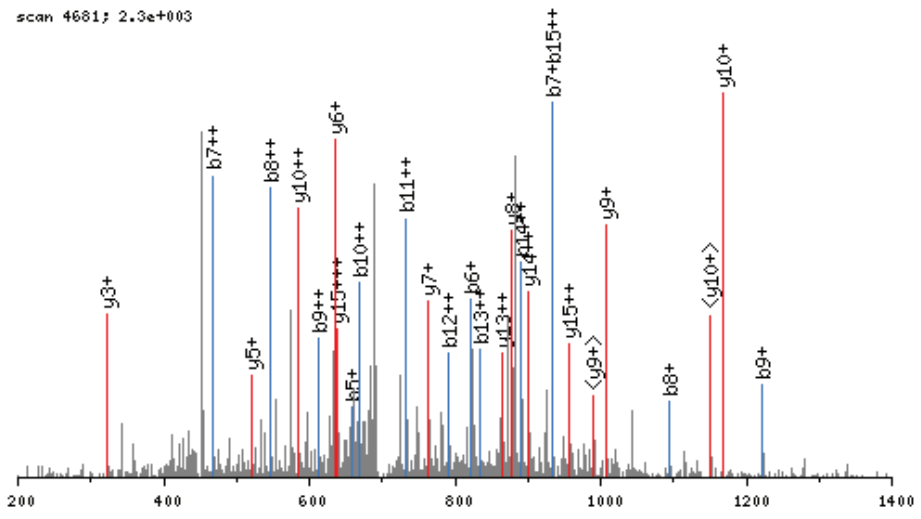

click image to zoom in; click top corners to zoom out [precursor±]

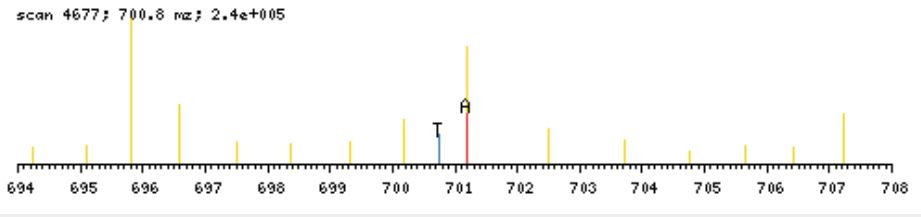

zoomed in precursor plot; T=theoretical m/z, A=acquired m/z

b^+	b^{2+}	#	AA	#	y^+	y^{2+}	y^{3+}
72.0449	36.5264	1	A	17			
187.0719	94.0399	2	D	16	2029.2251	1015.1165	677.0803
300.1559	150.5819	3	L	15	1914.1982	**957.6030**	**638.7379**
371.1931	186.1004	4	A	14	1801.1141	**901.0610**	601.0433
657.4978	329.2528	5	K	13	1730.0770	**865.5424**	577.3642
820.5612	410.7845	6	Y	12	1443.7722	722.3900	481.9293
933.6452	**467.3265**	7	I	11	1280.7089	640.8584	427.5749
1093.8055	**547.4067**	8	C	10	**1167.6248**	**584.3163**	389.8802
1222.8481	**611.9280**	9	E	9	**1007.4645**	504.2362	336.4934
1336.8911	**668.9494**	10	N	8	**878.4220**	439.7149	293.4792
1464.9496	**732.9787**	11	Q	7	**764.3790**	382.6934	255.4649
1579.9766	**790.4922**	12	D	6	**636.3204**	318.6641	212.7787
1667.0086	**834.0082**	13	S	5	**521.2935**	261.1507	174.4364
1780.0927	**890.5502**	14	I	4	434.2615	217.6346	145.4257
1867.1247	**934.0663**	15	S	3	**321.1774**	161.0926	107.7310
1954.1567	977.5823	16	S	2	234.1454	117.5766	78.7203
		17	K	1	147.1134	74.0606	49.7097

K(5):+286.30 C(8):+160.16

X-range: 400 - 1800
MassTol: 0.950 Y-zoom: 1.00
ImageSize: Sm Lg
MassType: AVG MONO
Axis: 1 2
Label: I M -
Ions:

a	+	2+	3+
b	+	2+	3+
c	+	2+	3+
x	+	2+	3+
y	+	2+	3+
z	+	2+	3+

hide H_2O/NH_3
zoom 112-122
zoom 124-133
GO

ADLAKYICENQDSISSK, MH+ 2100.2623, m/z 700.7589
10HNE-1HSA-37Trypsin3-LTQ2.4855.4855.3.dta

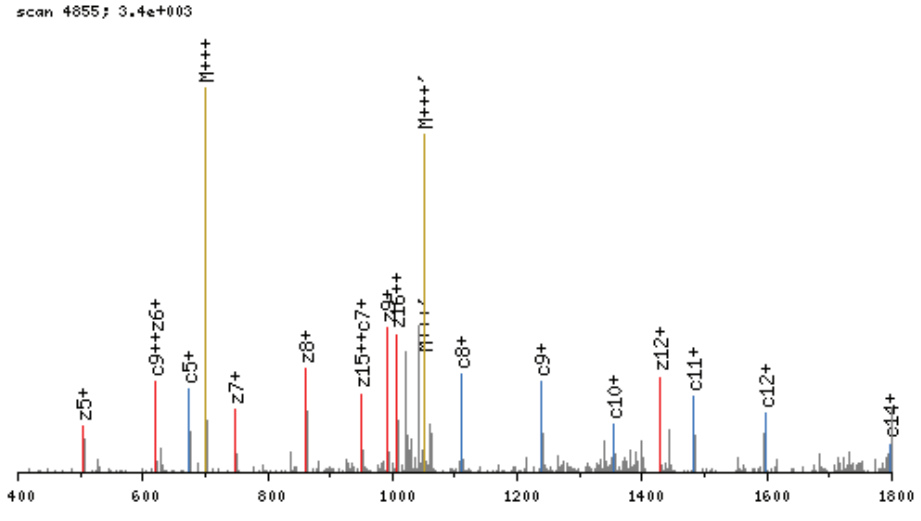

click image to zoom in; click top corners to zoom out [precursor±]

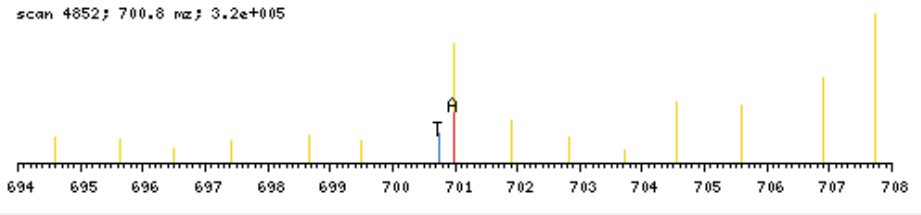

zoomed in precursor plot; T=theoretical m/z, A=acquired m/z

c^+	c^{2+}	#	AA	#	z^+	z^{2+}	z^{3+}
89.0715	45.0397	1	A	17			
204.0984	102.5531	2	D	16	2013.2064	**1007.1071**	671.7407
317.1825	159.0952	3	L	15	1898.1795	**949.5936**	633.3984
388.2196	194.6137	4	A	14	1785.0954	893.0516	595.7037
674.5244	337.7661	5	K	13	1714.0583	857.5331	572.0246
837.5877	419.2978	6	Y	12	**1427.7535**	714.3807	476.5897
950.6718	475.8398	7	I	11	1264.6902	632.8490	422.2353
1110.8321	555.9200	8	C	10	1151.6061	576.3070	384.5406
1239.8747	**620.4412**	9	E	9	**991.4458**	496.2268	331.1538
1353.9176	677.4627	10	N	8	**862.4032**	431.7055	288.1396
1481.9762	741.4920	11	Q	7	**748.3603**	374.6841	250.1253
1597.0031	799.0055	12	D	6	**620.3017**	310.6548	207.4391
1684.0352	842.5215	13	S	5	**505.2748**	253.1413	169.0968
1797.1192	899.0635	14	I	4	418.2427	209.6253	140.0861
1884.1512	942.5795	15	S	3	305.1587	153.0833	102.3914
1971.1833	986.0955	16	S	2	218.1267	109.5672	73.3808
		17	K	1	131.0946	66.0512	44.3701

K(5):+286.30 C(8):+160.16

X-range: 400 - 1800
MassTol: 0.950 Y-zoom: 1.00
ImageSize: (•) Sm ( ) Lg
MassType: ( ) AVG (•) MONO
Axis: (•) 1 ( ) 2
Label: (•) I ( ) M ( ) -
Ions:
a [ ] + [ ] 2+ [ ] 3+
b [x] + [x] 2+ [ ] 3+
c [ ] + [ ] 2+ [ ] 3+
x [ ] + [ ] 2+ [ ] 3+
y [x] + [x] 2+ [x] 3+
z [ ] + [ ] 2+ [ ] 3+
hide H_2O/NH_3 [ ]
zoom 112-122 [ ]
zoom 124-133 [ ]
GO

SHCIAEVENDEMPADLPSLAADFVESK, MH+ 3132.6875, m/z 1044.9007
10HNE-1HSA-37Trypsin5-LTQ4.8480.8480.3.dta

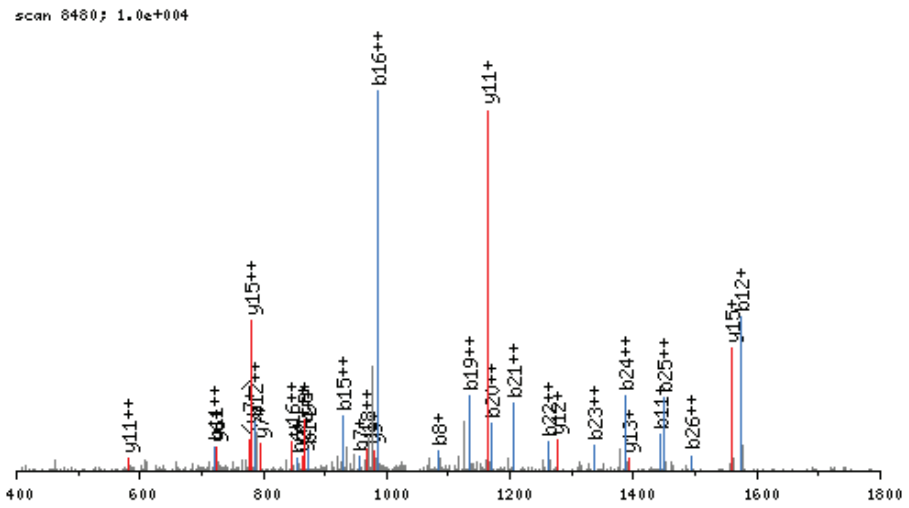

click image to zoom in; click top corners to zoom out [precursor]

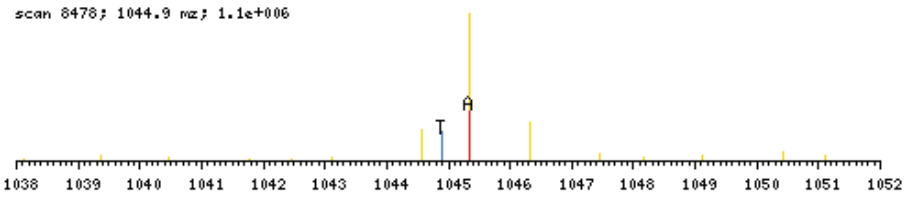

zoomed in precursor plot; T=theoretical m/z, A=acquired m/z

b^+	b^{2+}	#	AA	#	y^+	y^{2+}	y^{3+}
88.0399	44.5238	1	S	27			
383.3116	192.1597	2	H	26	3045.6555	1523.3317	1015.8904
543.4719	272.2399	3	C	25	2750.3837	1375.6958	917.4665
656.5560	328.7819	4	I	24	2590.2234	1295.6156	**864.0797**
727.5931	364.3005	5	A	23	2477.1394	1239.0736	826.3850
856.6357	428.8218	6	E	22	2406.1023	1203.5550	802.7060
955.7041	478.3560	7	V	21	2277.0597	1139.0337	759.6918
1084.7467	542.8773	8	E	20	2177.9913	1089.4995	726.6690
1198.7896	599.8987	9	N	19	2048.9487	1024.9782	683.6548
1313.8166	657.4122	10	D	18	1934.9057	**967.9568**	645.6405
1442.8592	**721.9335**	11	E	17	1819.8788	910.4433	607.2981
1573.8997	**787.4537**	12	M	16	1690.8362	**845.9220**	564.2839
1670.9524	835.9801	13	P	15	**1559.7957**	**780.4018**	520.6038
1741.9895	**871.4987**	14	A	14	1462.7430	731.8754	488.2529
1857.0165	**929.0122**	15	D	13	**1391.7058**	696.3568	464.5738
1970.1005	**985.5542**	16	L	12	**1276.6789**	638.8434	426.2315
2067.1533	1034.0806	17	P	11	**1163.5948**	**582.3013**	388.5368
2154.1853	1077.5966	18	S	10	1066.5421	533.7749	356.1859
2267.2694	**1134.1386**	19	L	9	**979.5100**	490.2589	327.1752
2338.3065	**1169.6572**	20	A	8	**866.4260**	433.7169	289.4805
2409.3436	**1205.1757**	21	A	7	**795.3889**	398.1983	265.8015
2524.3706	**1262.6892**	22	D	6	**724.3517**	362.6798	242.1225
2671.4390	**1336.2234**	23	F	5	609.3248	305.1663	203.7802
2770.5074	**1385.7576**	24	V	4	462.2564	231.6321	154.7573
2899.5500	**1450.2789**	25	E	3	363.1880	182.0979	121.7345
2986.5820	**1493.7949**	26	S	2	234.1454	117.5766	78.7203
		27	K	1	147.1134	74.0606	49.7097

H(2):+295.27 C(3):+160.16

COMET Spectrum View by J.Eng (c) ISB 2001
(TPP v4.4 VUVUZELA rev 1, Build 201010121551 (MinGW))

X-range: 500 - 2000
MassTol: 0.950 Y-zoom: 1.00
ImageSize: (•) Sm ( ) Lg
MassType: ( ) AVG (•) MONO
Axis: (•) 1 ( ) 2
Label: (•) I ( ) M ( ) -
Ions:

a	☐ +	☐ 2+	☐ 3+
b	☐ +	☐ 2+	☐ 3+
c	☑ +	☑ 2+	☐ 3+
x	☐ +	☐ 2+	☐ 3+
y	☐ +	☐ 2+	☐ 3+
z	☑ +	☑ 2+	☑ 3+

hide H_2O/NH_3 ☐
zoom 112-122 ☐
zoom 124-133 ☐
GO

SHCIAEVENDEMPADLPSLAADFVESK, MH+ 3132.6875, m/z 1044.9007
10HNE-1HSA-37Trypsin5-LTQ4.8598.8598.3.dta

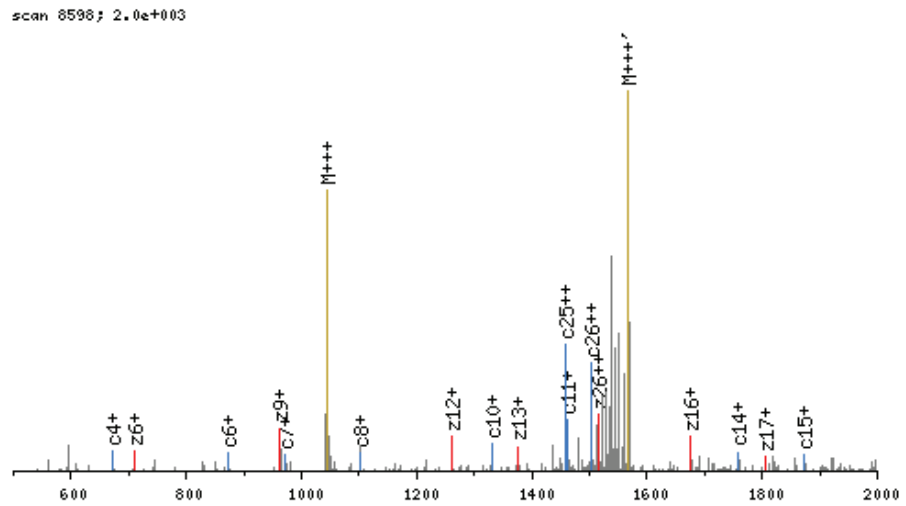

click image to zoom in; click top corners to zoom out [precursor±]

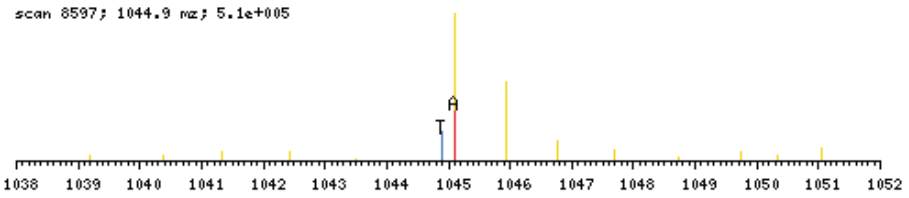

zoomed in precursor plot; T=theoretical m/z, A=acquired m/z

c^+	c^{2+}	#	AA	#	z^+	z^{2+}	z^{3+}
105.0664	53.0371	1	S	27			
400.3382	200.6730	2	H	26	3029.6368	1515.3223	1010.5508
560.4985	280.7532	3	C	25	2734.3650	1367.6864	912.1269
673.5825	337.2952	4	I	24	2574.2047	1287.6063	858.7401
744.6197	372.8137	5	A	23	2461.1207	1231.0642	821.0454
873.6623	437.3350	6	E	22	2390.0835	1195.5457	797.3664
972.7307	486.8692	7	V	21	2261.0409	1131.0244	754.3522
1101.7733	551.3905	8	E	20	2161.9725	1081.4902	721.3294
1215.8162	608.4120	9	N	19	2032.9299	1016.9689	678.3152
1330.8431	665.9255	10	D	18	1918.8870	959.9474	640.3009
1459.8857	730.4468	11	E	17	1803.8601	902.4339	601.9586
1590.9262	795.9670	12	M	16	1674.8175	837.9126	558.9444
1687.9790	844.4934	13	P	15	1543.7770	772.3924	515.2642
1759.0161	880.0120	14	A	14	1446.7242	723.8660	482.9133
1874.0430	937.5254	15	D	13	1375.6871	688.3475	459.2343
1987.1271	994.0675	16	L	12	1260.6602	630.8340	420.8919
2084.1799	1042.5938	17	P	11	1147.5761	574.2920	383.1973
2171.2119	1086.1099	18	S	10	1050.5233	525.7656	350.8463
2284.2960	1142.6519	19	L	9	963.4913	482.2496	321.8357
2355.3331	1178.1704	20	A	8	850.4072	425.7075	284.1410
2426.3702	1213.6890	21	A	7	779.3701	390.1890	260.4619
2541.3971	1271.2025	22	D	6	708.3330	354.6704	236.7829
2688.4655	1344.7367	23	F	5	593.3061	297.1570	198.4406
2787.5339	1394.2709	24	V	4	446.2377	223.6227	149.4178
2916.5765	1458.7922	25	E	3	347.1693	174.0885	116.3950
3003.6086	1502.3082	26	S	2	218.1267	109.5672	73.3808
		27	K	1	131.0946	66.0512	44.3701

H(2):+295.27 C(3):+160.16

X-range: 400 - 1800
MassTol: 0.950 Y-zoom: 1.00
ImageSize: Sm Lg
MassType: AVG MONO
Axis: 1 2
Label: I M -
Ions:
a + 2+ 3+
b + 2+ 3+
c + 2+ 3+
x + 2+ 3+
y + 2+ 3+
z + 2+ 3+
hide H_2O/NH_3
zoom 112-122
zoom 124-133
GO

SHCIAEVENDEMPADLPSLAADFVESK, MH+ 3148.8346, m/z 1050.2830
10HNE-1HSA-37Trypsin5-LTQ4.7927.7927.3.dta

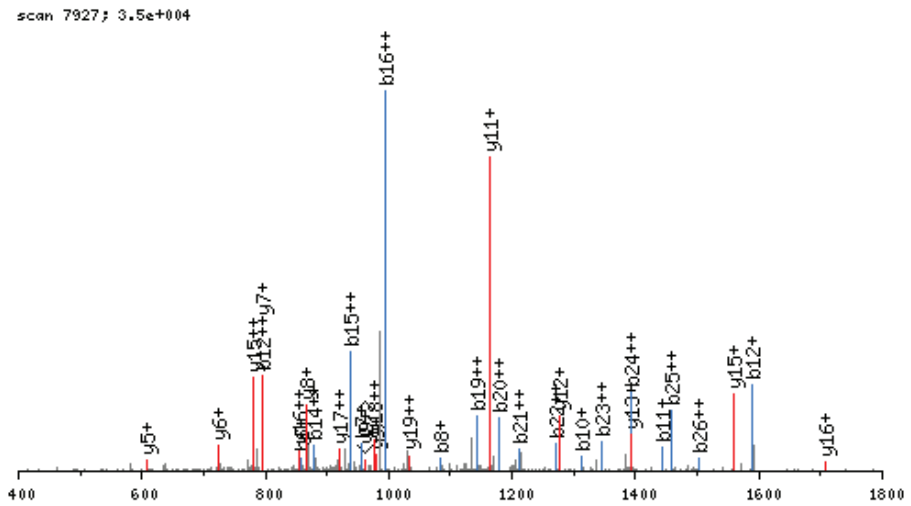

click image to zoom in; click top corners to zoom out [precursor]

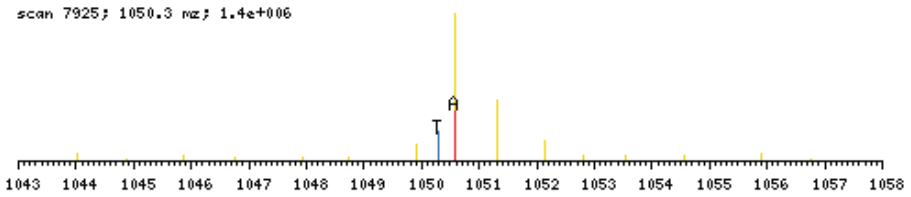

zoomed in precursor plot; T=theoretical m/z, A=acquired m/z

b^+	b^{2+}	#	AA	#	y^+	y^{2+}	y^{3+}
88.0399	44.5238	1	S	27			
383.3116	192.1597	2	H	26	3061.8026	1531.4052	1021.2727
543.4719	272.2399	3	C	25	2766.5308	1383.7693	922.8488
656.5560	328.7819	4	I	24	2606.3705	1303.6891	869.4620
727.5931	364.3005	5	A	23	2493.2864	1247.1471	831.7674
856.6357	428.8218	6	E	22	2422.2493	1211.6286	808.0883
955.7041	478.3560	7	V	21	2293.2067	1147.1073	765.0741
1084.7467	542.8773	8	E	20	2194.1383	1097.5731	732.0513
1198.7896	599.8987	9	N	19	2065.0957	1033.0518	689.0371
1313.8166	657.4122	10	D	18	1951.0528	976.0303	651.0228
1442.8592	721.9335	11	E	17	1836.0258	918.5168	612.6805
1590.0467	795.5273	12	M	16	1706.9832	853.9955	569.6663
1687.0995	844.0536	13	P	15	1559.7957	780.4018	520.6038
1758.1366	879.5722	14	A	14	1462.7430	731.8754	488.2529
1873.1635	937.0857	15	D	13	1391.7058	696.3568	464.5738
1986.2476	993.6277	16	L	12	1276.6789	638.8434	426.2315
2083.3003	1042.1541	17	P	11	1163.5948	582.3013	388.5368
2170.3324	1085.6701	18	S	10	1066.5421	533.7749	356.1859
2283.4164	1142.2121	19	L	9	979.5100	490.2589	327.1752
2354.4535	1177.7307	20	A	8	866.4260	433.7169	289.4805
2425.4907	1213.2492	21	A	7	795.3889	398.1983	265.8015
2540.5176	1270.7627	22	D	6	724.3517	362.6798	242.1225
2687.5860	1344.2969	23	F	5	609.3248	305.1663	203.7802
2786.6544	1393.8311	24	V	4	462.2564	231.6321	154.7573
2915.6970	1458.3524	25	E	3	363.1880	182.0979	121.7345
3002.7291	1501.8684	26	S	2	234.1454	117.5766	78.7203
		27	K	1	147.1134	74.0606	49.7097

H(2):+295.27 C(3):+160.16 M(12):+147.19

X-range: 400 - 2000
MassTol: 0.950 Y-zoom: 1.00
ImageSize: (•) Sm ( ) Lg
MassType: ( ) AVG (•) MONO
Axis: (•) 1 ( ) 2
Label: (•) I ( ) M ( ) -
Ions:
a [ ] + [ ] 2+ [ ] 3+
b [ ] + [ ] 2+ [ ] 3+
c [x] + [x] 2+ [ ] 3+
x [ ] + [ ] 2+ [ ] 3+
y [ ] + [ ] 2+ [ ] 3+
z [x] + [x] 2+ [x] 3+
hide H_2O/NH_3 [ ]
zoom 112-122 [ ]
zoom 124-133 [ ]
GO

SHCIAEVENDEMPADLPSLAADFVESK, MH+ 3148.8346, m/z 1050.2830
10HNE-1HSA-37Trypsin5-LTQ4.7926.7926.3.dta

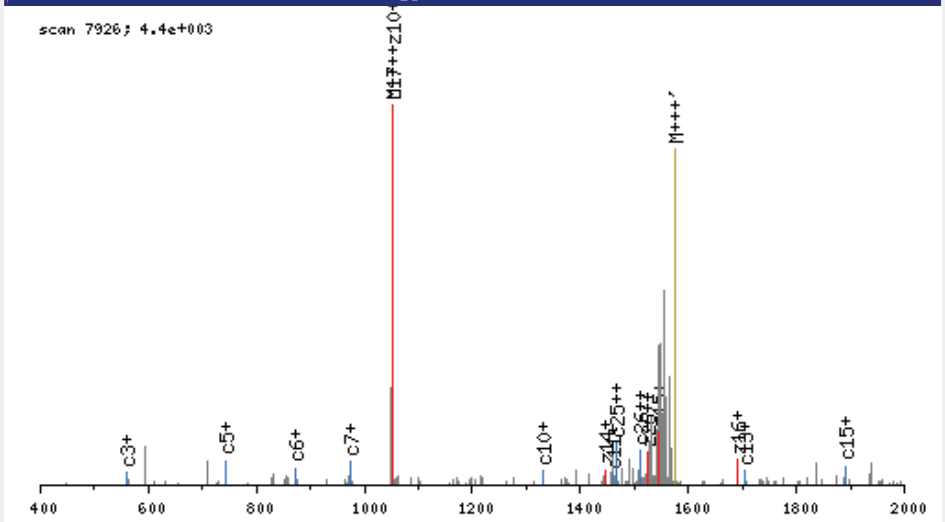

click image to zoom in; click top corners to zoom out [precursor±]

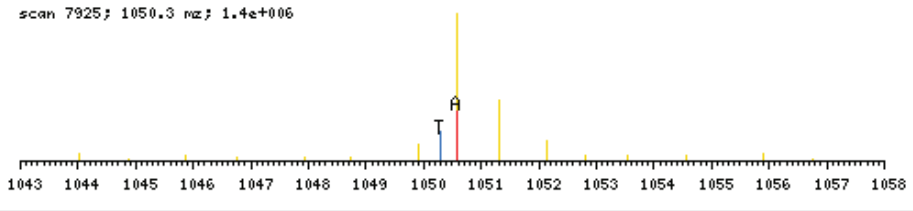

zoomed in precursor plot; T=theoretical m/z, A=acquired m/z

c^+	c^{2+}	#	AA	#	z^+	z^{2+}	z^{3+}
105.0664	53.0371	1	S	27			
400.3382	200.6730	2	H	26	3045.7838	**1523.3958**	1015.9332
560.4985	280.7532	3	C	25	2750.5120	1375.7599	917.5092
673.5825	337.2952	4	I	24	2590.3517	1295.6798	864.1225
744.6197	372.8137	5	A	23	2477.2677	1239.1378	826.4278
873.6623	437.3350	6	E	22	2406.2306	1203.6192	802.7487
972.7307	486.8692	7	V	21	2277.1880	1139.0979	759.7345
1101.7733	551.3905	8	E	20	2178.1196	1089.5637	726.7117
1215.8162	608.4120	9	N	19	2049.0770	1025.0424	683.6975
1330.8431	665.9255	10	D	18	1935.0340	968.0209	645.6832
1459.8857	730.4468	11	E	17	1820.0071	910.5075	607.3409
1607.0732	804.0405	12	M	16	**1690.9645**	845.9862	564.3267
1704.1260	852.5669	13	P	15	**1543.7770**	772.3924	515.2642
1775.1631	888.0855	14	A	14	**1446.7242**	723.8660	482.9133
1890.1901	945.5989	15	D	13	1375.6871	688.3475	459.2343
2003.2741	1002.1410	16	L	12	1260.6602	630.8340	420.8919
2100.3269	**1050.6674**	17	P	11	1147.5761	574.2920	383.1973
2187.3589	1094.1834	18	S	10	**1050.5233**	525.7656	350.8463
2300.4430	1150.7254	19	L	9	963.4913	482.2496	321.8357
2371.4801	1186.2440	20	A	8	850.4072	425.7075	284.1410
2442.5172	1221.7625	21	A	7	779.3701	390.1890	260.4619
2557.5442	1279.2760	22	D	6	708.3330	354.6704	236.7829
2704.6126	1352.8102	23	F	5	593.3061	297.1570	198.4406
2803.6810	1402.3444	24	V	4	446.2377	223.6227	149.4178
2932.7236	**1466.8657**	25	E	3	347.1693	174.0885	116.3950
3019.7556	**1510.3817**	26	S	2	218.1267	109.5672	73.3808
		27	K	1	131.0946	66.0512	44.3701

H(2):+295.27 C(3):+160.16 M(12):+147.19

COMET Spectrum View by J.Eng (c) ISB 2001
(TPP v4.4 VUVUZELA rev 1, Build 201010121551 (MinGW))

X-range: 0 - 0
MassTol: 0.950 Y-zoom: 1.00
ImageSize: Sm Lg
MassType: AVG MONO
Axis: 1 2
Label: I M -
Ions:
a + 2+ 3+
b + 2+ 3+
c + 2+ 3+
x + 2+ 3+
y + 2+ 3+
z + 2+ 3+
hide H_2O/NH_3
zoom 112-122
zoom 124-133
GO

RHPDYSVVLLLR, MH+ 1626.0565, m/z 542.6903
10HNE-1HSA-37Trypsin5-LTQ3.4975.4975.3.dta

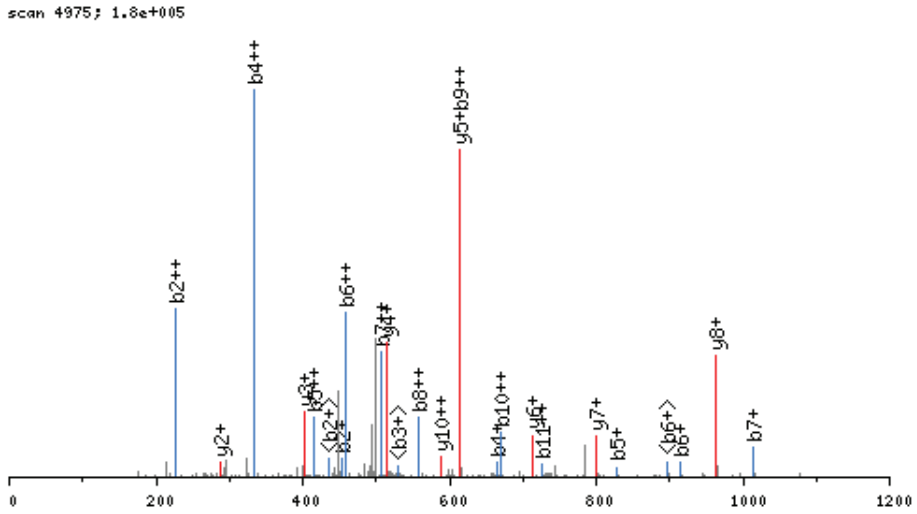

click image to zoom in; click top corners to zoom out [precursor±]

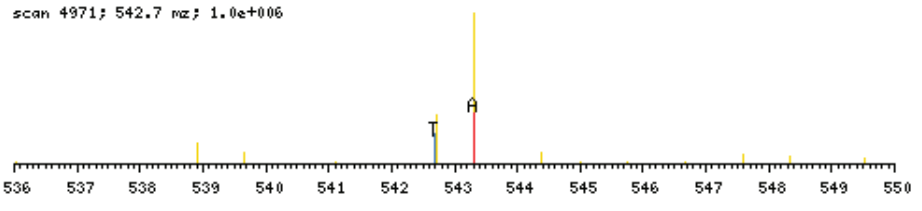

zoomed in precursor plot; T=theoretical m/z, A=acquired m/z

b^+	b^{2+}	#	AA	#	y^+	y^{2+}	y^{3+}
157.1089	79.0584	1	R	12			
452.3807	226.6943	2	H	11	1469.9554	735.4816	490.6570
549.4335	275.2207	3	P	10	1174.6836	587.8457	392.2331
664.4604	332.7341	4	D	9	1077.6308	539.3193	359.8822
827.5238	414.2658	5	Y	8	962.6039	481.8059	321.5398
914.5558	457.7818	6	S	7	799.5405	400.2742	267.1854
1013.6242	507.3160	7	V	6	712.5085	356.7582	238.1747
1112.6926	556.8502	8	V	5	613.4401	307.2240	205.1519
1225.7767	613.3922	9	L	4	514.3717	257.6898	172.1291
1338.8607	669.9343	10	L	3	401.2876	201.1477	134.4344
1451.9448	726.4763	11	L	2	288.2036	144.6057	96.7397
		12	R	1	175.1195	88.0637	59.0451

H(2):+295.27

X-range: 300 - 1700
MassTol: 0.950 Y-zoom: 1.00
ImageSize: (•) Sm ( ) Lg
MassType: ( ) AVG (•) MONO
Axis: (•) 1 ( ) 2
Label: (•) I ( ) M ( ) -
Ions:

a	☐ +	☐ 2+	☐ 3+
b	☐ +	☐ 2+	☐ 3+
c	☑ +	☑ 2+	☐ 3+
x	☐ +	☐ 2+	☐ 3+
y	☐ +	☐ 2+	☐ 3+
z	☑ +	☑ 2+	☑ 3+

hide H_2O/NH_3 ☐
zoom 112-122 ☐
zoom 124-133 ☐
GO

RHPDYSVVLLLR, MH+ 1626.0565, m/z 542.6903
10HNE-1HSA-37Trypsin3-LTQ3.5329.5329.3.dta

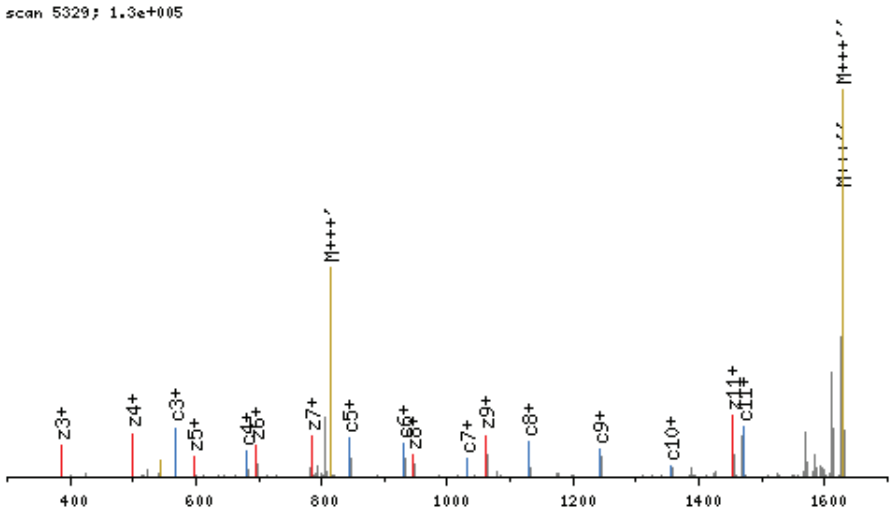

click image to zoom in; click top corners to zoom out [precursor±]

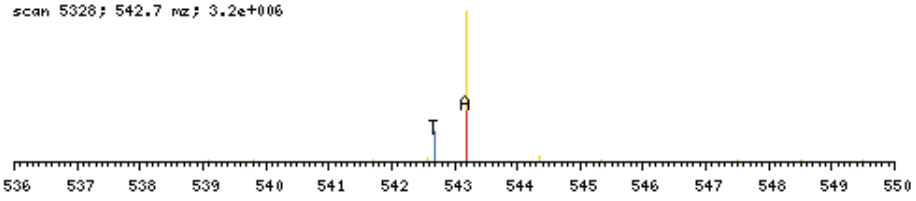

zoomed in precursor plot; T=theoretical m/z, A=acquired m/z

c^+	c^{2+}	#	AA	#	z^+	z^{2+}	z^{3+}
174.1355	87.5717	1	R	12			
469.4073	235.2075	2	H	11	1453.9366	727.4722	485.3174
566.4600	283.7339	3	P	10	1158.6649	579.8363	386.8935
681.4870	341.2474	4	D	9	1061.6121	531.3100	354.5426
844.5503	422.7791	5	Y	8	946.5852	473.7965	316.2003
931.5823	466.2951	6	S	7	783.5218	392.2648	261.8458
1030.6507	515.8293	7	V	6	696.4898	348.7488	232.8351
1129.7192	565.3635	8	V	5	597.4214	299.2146	199.8123
1242.8032	621.9055	9	L	4	498.3530	249.6804	166.7895
1355.8873	678.4476	10	L	3	385.2689	193.1384	129.0949
1468.9713	734.9896	11	L	2	272.1848	136.5963	91.4002
		12	R	1	159.1008	80.0543	53.7055

H(2):+295.27

X-range: 200 - 1000
MassTol: 0.950 Y-zoom: 1.00
ImageSize: (•) Sm ( ) Lg
MassType: ( ) AVG (•) MONO
Axis: (•) 1 ( ) 2
Label: (•) I ( ) M ( ) -
Ions:

a	☐ +	☐ 2+	☐ 3+
b	☑ +	☑ 2+	☐ 3+
c	☐ +	☐ 2+	☐ 3+
x	☐ +	☐ 2+	☐ 3+
y	☑ +	☑ 2+	☑ 3+
z	☐ +	☐ 2+	☐ 3+

hide H_2O/NH_3 ☐
zoom 112-122 ☐
zoom 124-133 ☐
GO

HPDYSVVLLLR, MH+ 1469.9554, m/z 490.6566
10HNE-1HSA-37Trypsin4-LTQ1.5285.5285.3.dta

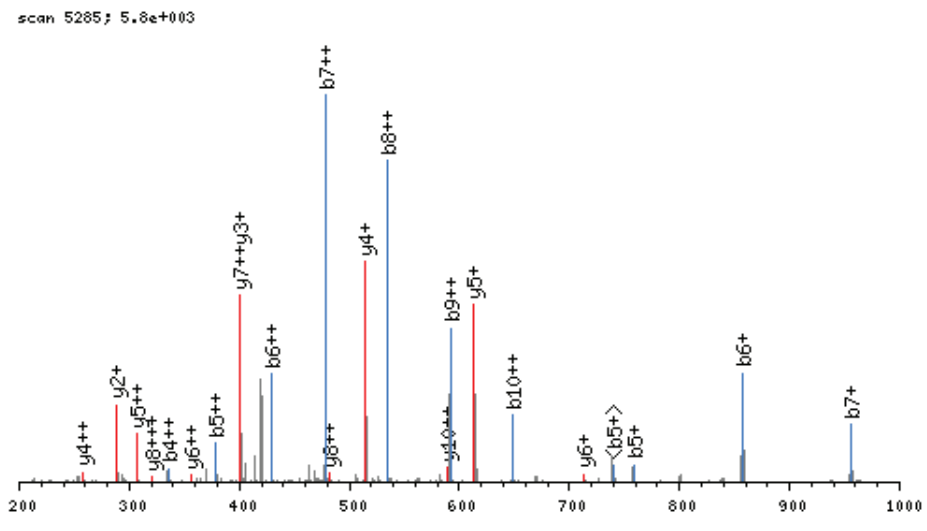

click image to zoom in; click top corners to zoom out [precursor±]

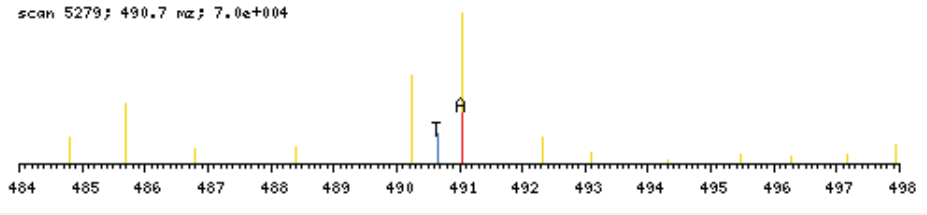

zoomed in precursor plot; T=theoretical m/z, A=acquired m/z

b^+	b^{2+}	#	AA	#	y^+	y^{2+}	y^{3+}
296.2796	148.6437	1	H	11			
393.3324	197.1701	2	P	10	1174.6836	587.8457	392.2331
508.3593	254.6836	3	D	9	1077.6308	539.3193	359.8822
671.4226	336.2152	4	Y	8	962.6039	481.8059	321.5398
758.4547	379.7312	5	S	7	799.5405	400.2742	267.1854
857.5231	429.2655	6	V	6	712.5085	356.7582	238.1747
956.5915	478.7997	7	V	5	613.4401	307.2240	205.1519
1069.6756	535.3417	8	L	4	514.3717	257.6898	172.1291
1182.7596	591.8837	9	L	3	401.2876	201.1477	134.4344
1295.8437	648.4258	10	L	2	288.2036	144.6057	96.7397
		11	R	1	175.1195	88.0637	59.0451

H(1):+295.27

X-range: 400 - 1400
MassTol: 0.950 Y-zoom: 1.00
ImageSize: (•) Sm ( ) Lg
MassType: ( ) AVG (•) MONO
Axis: (•) 1 ( ) 2
Label: (•) I ( ) M ( ) -
Ions:

a	☐ +	☐ 2+	☐ 3+
b	☑ +	☑ 2+	☐ 3+
c	☐ +	☐ 2+	☐ 3+
x	☐ +	☐ 2+	☐ 3+
y	☑ +	☑ 2+	☑ 3+
z	☐ +	☐ 2+	☐ 3+

hide H_2O/NH_3 ☐
zoom 112-122 ☐
zoom 124-133 ☐
GO

HPDYSVVLLLRLAKTYETTLEK, MH+ 2747.6421, m/z 916.5522
10HNE-1HSA-37Trypsin5-LTQ1.5575.5575.3.dta

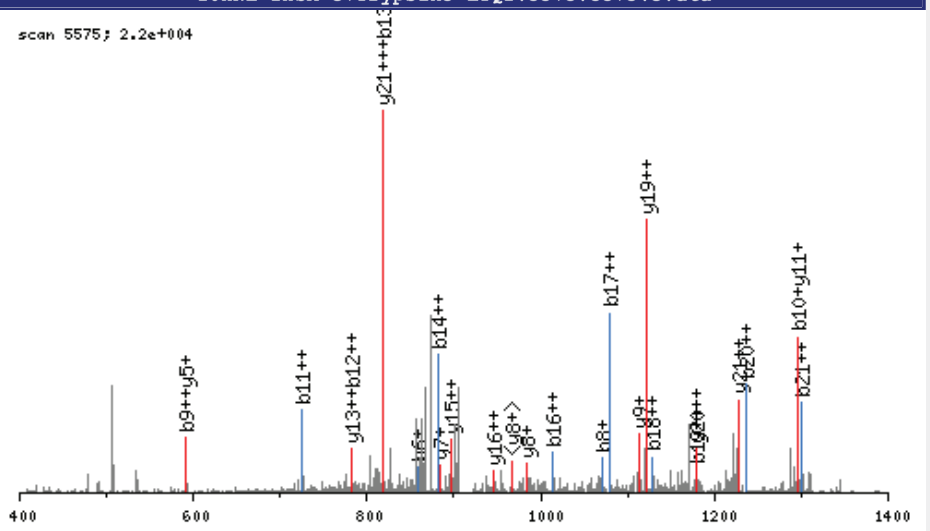

click image to zoom in; click top corners to zoom out [precursor±]

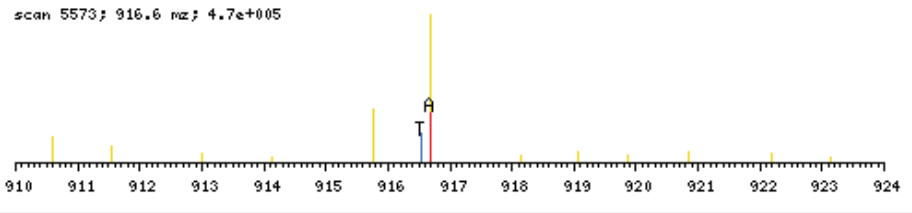

zoomed in precursor plot; T=theoretical m/z, A=acquired m/z

b^+	b^{2+}	#	AA	#	y^+	y^{2+}	y^{3+}
296.2796	148.6437	1	H	22			
393.3324	197.1701	2	P	21	2452.3703	**1226.6891**	**818.1287**
508.3593	254.6836	3	D	20	2355.3175	**1178.1627**	785.7777
671.4226	336.2152	4	Y	19	2240.2906	**1120.6492**	747.4354
758.4547	379.7312	5	S	18	2077.2273	1039.1175	693.0810
857.5231	429.2655	6	V	17	1990.1952	995.6015	664.0703
956.5915	478.7997	7	V	16	1891.1268	**946.0673**	631.0475
1069.6756	535.3417	8	L	15	1792.0584	**896.5331**	598.0247
1182.7596	**591.8837**	9	L	14	1678.9743	839.9911	560.3300
1295.8437	648.4258	10	L	13	1565.8903	**783.4491**	522.6353
1451.9448	**726.4763**	11	R	12	1452.8062	726.9070	484.9406
1565.0289	**783.0183**	12	L	11	**1296.7051**	648.8565	432.9069
1636.0660	**818.5369**	13	A	10	1183.6210	592.3144	395.2122
1764.1609	**882.5844**	14	K	9	**1112.5839**	556.7959	371.5332
1865.2086	933.1082	15	T	8	**984.4890**	492.7484	328.8349
2028.2719	**1014.6399**	16	Y	7	**883.4413**	442.2246	295.1523
2157.3145	**1079.1612**	17	E	6	720.3780	360.6929	240.7979
2258.3622	**1129.6850**	18	T	5	**591.3354**	296.1716	197.7837
2359.4099	**1180.2089**	19	T	4	490.2877	245.6478	164.1011
2472.4940	**1236.7509**	20	L	3	389.2400	195.1239	130.4186
2601.5366	**1301.2722**	21	E	2	276.1559	138.5819	92.7239
		22	K	1	147.1134	74.0606	49.7097

H(1):+295.27

X-range: 200 - 1800
MassTol: 0.950 Y-zoom: 1.00
ImageSize: Sm Lg
MassType: AVG MONO
Axis: 1 2
Label: I M -
Ions:

a	+	2+	3+
b	+	2+	3+
c	+	2+	3+
x	+	2+	3+
y	+	2+	3+
z	+	2+	3+

hide H_2O/NH_3
zoom 112-122
zoom 124-133
GO

HPDYSVVLLLRLAKTYETTLEK, MH+ 2747.6421, m/z 550.3342
1HNE-1HSA-37Trypsin4-LTQ2.5688.5688.5.dta

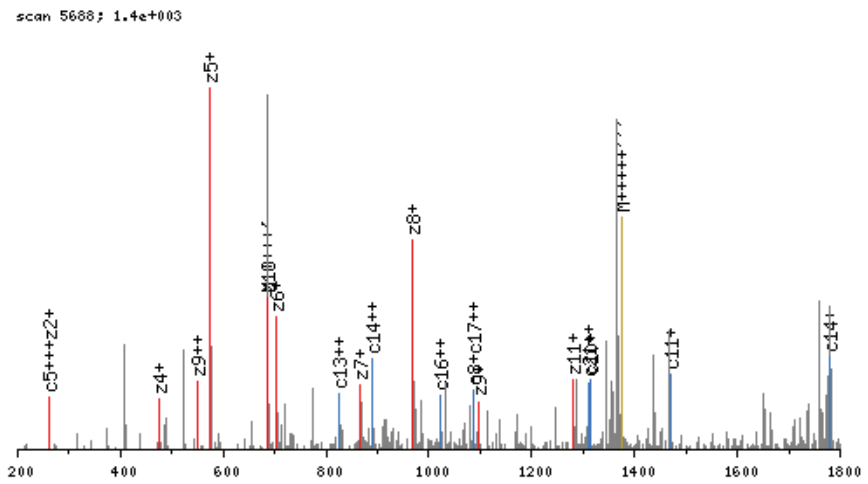

click image to zoom in; click top corners to zoom out [precursor±]

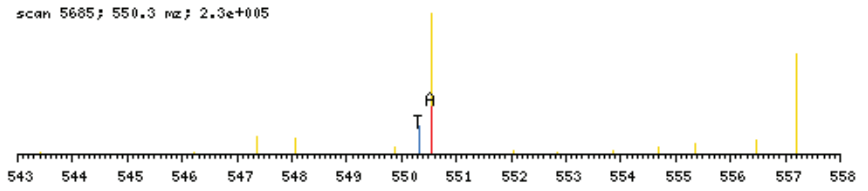

zoomed in precursor plot; T=theoretical m/z, A=acquired m/z

c^+	c^{2+}	c^{3+}	#	AA	#	z^+	z^{2+}	z^{3+}
313.3062	157.1570	105.1073	1	H	22			
410.3589	205.6834	137.4582	2	P	21	2436.3516	1218.6797	812.7891
525.3859	263.1968	175.8005	3	D	20	2339.2988	1170.1533	780.4382
688.4492	344.7285	230.1549	4	Y	19	2224.2719	1112.6398	742.0958
775.4812	388.2445	259.1656	5	S	18	2061.2085	1031.1082	687.7414
874.5496	437.7787	292.1884	6	V	17	1974.1765	987.5922	658.7307
973.6180	487.3129	325.2112	7	V	16	1875.1081	938.0580	625.7079
1086.7021	543.8550	362.9059	8	L	15	1776.0397	888.5238	592.6851
1199.7862	600.3970	400.6006	9	L	14	1662.9556	831.9817	554.9904
1312.8702	656.9390	438.2953	10	L	13	1549.8716	775.4397	517.2957
1468.9713	734.9896	490.3290	11	R	12	1436.7875	718.8977	479.6010
1582.0554	791.5316	528.0237	12	L	11	1280.6864	640.8471	427.5673
1653.0925	827.0502	551.7027	13	A	10	1167.6023	584.3051	389.8727
1781.1875	891.0977	594.4010	14	K	9	1096.5652	548.7865	366.1936
1882.2352	941.6215	628.0836	15	T	8	968.4702	484.7390	323.4953
2045.2985	1023.1532	682.4380	16	Y	7	867.4226	434.2152	289.8127
2174.3411	1087.6745	725.4522	17	E	6	704.3592	352.6835	235.4583
2275.3888	1138.1983	759.1348	18	T	5	575.3166	288.1622	192.4441
2376.4364	1188.7221	792.8174	19	T	4	474.2690	237.6384	158.7615
2489.5205	1245.2642	830.5121	20	L	3	373.2213	187.1146	125.0790
2618.5631	1309.7855	873.5263	21	E	2	260.1372	130.5725	87.3843
			22	K	1	131.0946	66.0512	44.3701

H(1):+295.27

X-range: 200 - 900
MassTol: 0.950 Y-zoom: 1.00
ImageSize: Sm Lg
MassType: AVG MONO
Axis: 1 2
Label: I M -
Ions:
a + 2+ 3+
b + 2+ 3+
c + 2+ 3+
x + 2+ 3+
y + 2+ 3+
z + 2+ 3+
hide H_2O/NH_3
zoom 112-122
zoom 124-133
GO

LAKTYETTLEK, MH+ 1454.9149, m/z 485.6432
1HNE-1HSA-37Trypsin5-LTQ1.4046.4046.3.dta

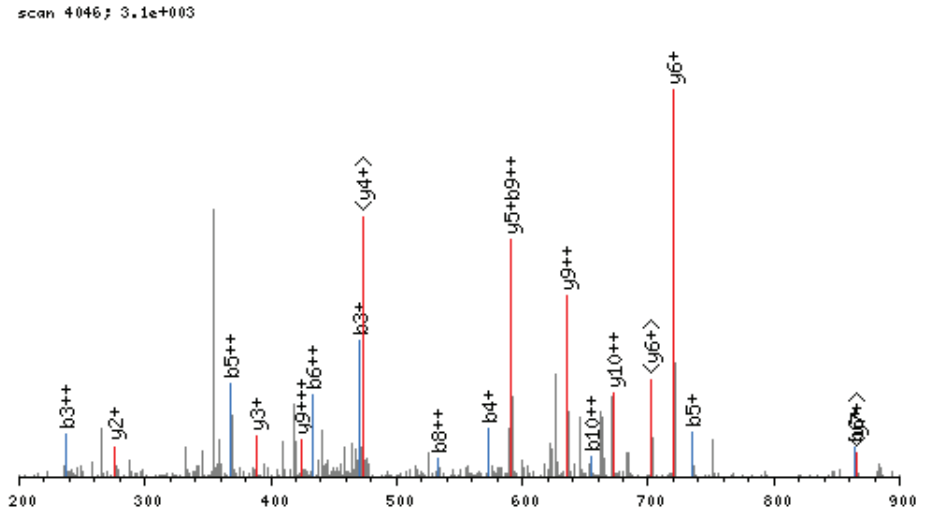

click image to zoom in; click top corners to zoom out [precursor±]

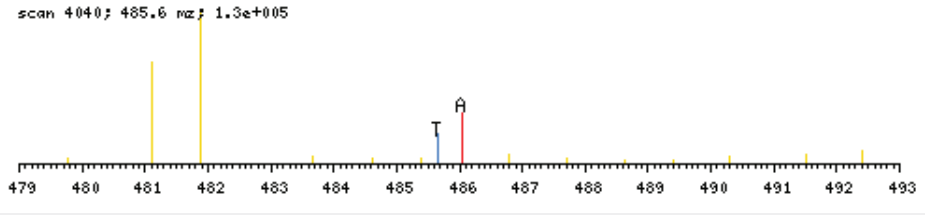

zoomed in precursor plot; T=theoretical m/z, A=acquired m/z

b^+	b^{2+}	#	AA	#	y^+	y^{2+}	y^{3+}
114.0919	57.5499	1	L	11			
185.1290	93.0684	2	A	10	1341.8309	**671.4193**	447.9488
471.4338	**236.2208**	3	K	9	1270.7937	**635.9008**	**424.2698**
572.4815	286.7446	4	T	8	984.4890	492.7484	328.8349
735.5448	**368.2763**	5	Y	7	883.4413	442.2246	295.1523
864.5874	**432.7976**	6	E	6	**720.3780**	360.6929	240.7979
965.6351	483.3214	7	T	5	**591.3354**	296.1716	197.7837
1066.6827	**533.8453**	8	T	4	490.2877	245.6478	164.1011
1179.7668	**590.3873**	9	L	3	**389.2400**	195.1239	130.4186
1308.8094	**654.9086**	10	E	2	**276.1559**	138.5819	92.7239
		11	K	1	147.1134	74.0606	49.7097

K(3):+286.30

X-range: 200 - 900
MassTol: 0.950 Y-zoom: 6.00
ImageSize: (•) Sm ( ) Lg
MassType: ( ) AVG (•) MONO
Axis: (•) 1 ( ) 2
Label: (•) I ( ) M ( ) -
Ions:
a [ ] + [ ] 2+ [ ] 3+
b [x] + [x] 2+ [ ] 3+
c [ ] + [ ] 2+ [ ] 3+
x [ ] + [ ] 2+ [ ] 3+
y [x] + [x] 2+ [x] 3+
z [ ] + [ ] 2+ [ ] 3+
hide H_2O/NH_3 [ ]
zoom 112-122 [ ]
zoom 124-133 [ ]
GO

LAKTYETTLEK, MH+ 1436.9044, m/z 479.6396
10HNE-1HSA-37Trypsin3-LTQ2.4333.4333.3.dta

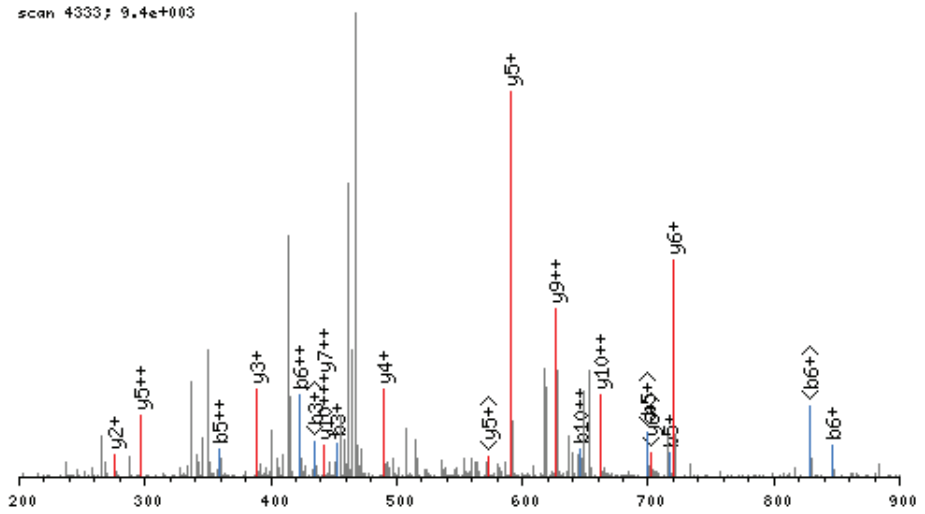

click image to zoom in; click top corners to zoom out [precursor±]

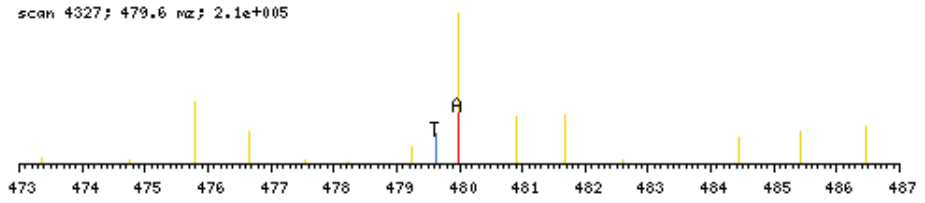

zoomed in precursor plot; T=theoretical m/z, A=acquired m/z

b^+	b^{2+}	#	AA	#	y^+	y^{2+}	y^{3+}
114.0919	57.5499	1	L	11			
185.1290	93.0684	2	A	10	1323.8203	**662.4141**	**441.9453**
453.4232	227.2155	3	K	9	1252.7832	**626.8955**	418.2663
554.4709	277.7394	4	T	8	984.4890	492.7484	328.8349
717.5342	**359.2710**	5	Y	7	883.4413	**442.2246**	295.1523
846.5768	**423.7923**	6	E	6	**720.3780**	360.6929	240.7979
947.6245	474.3162	7	T	5	**591.3354**	**296.1716**	197.7837
1048.6722	524.8400	8	T	4	**490.2877**	245.6478	164.1011
1161.7562	581.3820	9	L	3	**389.2400**	195.1239	130.4186
1290.7988	**645.9033**	10	E	2	**276.1559**	138.5819	92.7239
		11	K	1	147.1134	74.0606	49.7097

K(3):+268.29

X-range: 200 - 1500
MassTol: 0.950 Y-zoom: 1.00
ImageSize: Sm Lg
MassType: AVG MONO
Axis: 1 2
Label: I M -
Ions:

a	+	2+	3+
b	+	2+	3+
c	+	2+	3+
x	+	2+	3+
y	+	2+	3+
z	+	2+	3+

hide H_2O/NH_3
zoom 112-122
zoom 124-133
GO

LAKTYETTLEK, MH+ 1436.9044, m/z 479.6396
10HNE-1HSA-37Trypsin5-LTQ4.4608.4608.3.dta

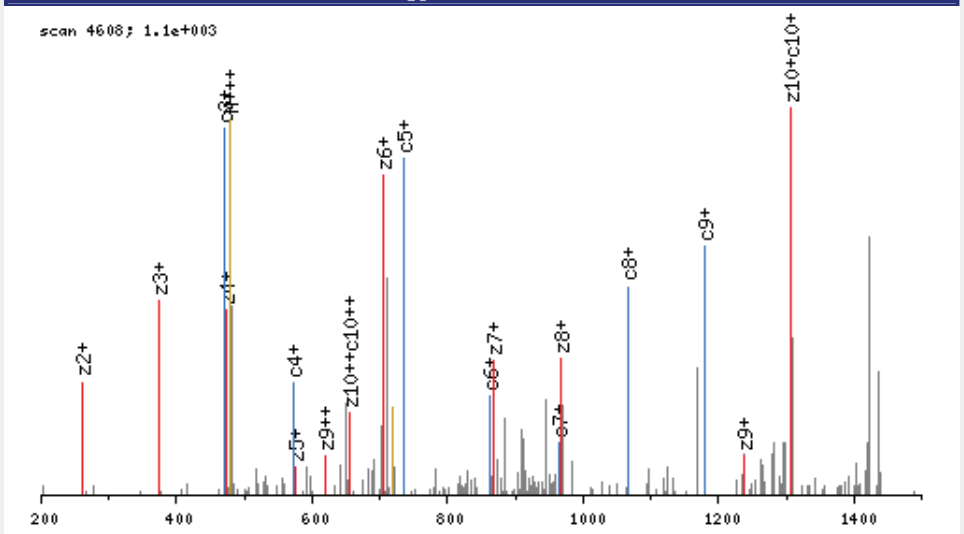

click image to zoom in; click top corners to zoom out [precursor±]

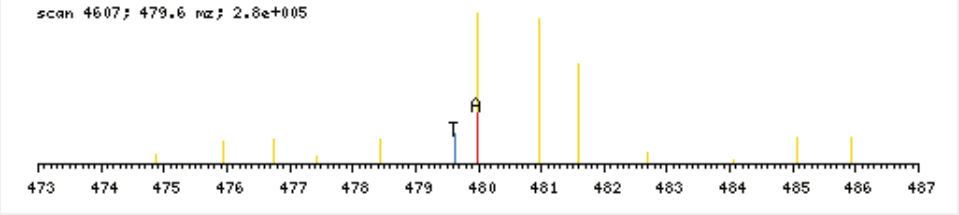

zoomed in precursor plot; T=theoretical m/z, A=acquired m/z

c^+	c^{2+}	#	AA	#	z^+	z^{2+}	z^{3+}
131.1184	66.0631	1	L	11			
202.1556	101.5817	2	A	10	1307.8016	654.4047	436.6057
470.4498	235.7288	3	K	9	1236.7645	618.8861	412.9267
571.4974	286.2526	4	T	8	968.4702	484.7390	323.4953
734.5608	367.7843	5	Y	7	867.4226	434.2152	289.8127
863.6034	432.3056	6	E	6	704.3592	352.6835	235.4583
964.6510	482.8294	7	T	5	575.3166	288.1622	192.4441
1065.6987	533.3533	8	T	4	474.2690	237.6384	158.7615
1178.7828	589.8953	9	L	3	373.2213	187.1146	125.0790
1307.8254	654.4166	10	E	2	260.1372	130.5725	87.3843
		11	K	1	131.0946	66.0512	44.3701

K(3):+268.29

X-range: 200 - 1800
MassTol: 0.950 Y-zoom: 1.00
ImageSize: (•) Sm ( ) Lg
MassType: ( ) AVG (•) MONO
Axis: (•) 1 ( ) 2
Label: (•) I ( ) M ( ) -
Ions:
a [ ] + [ ] 2+ [ ] 3+
b [x] + [x] 2+ [ ] 3+
c [ ] + [ ] 2+ [ ] 3+
x [ ] + [ ] 2+ [ ] 3+
y [x] + [x] 2+ [x] 3+
z [ ] + [ ] 2+ [ ] 3+
hide H_2O/NH_3 [ ]
zoom 112-122 [ ]
zoom 124-133 [ ]
GO

TYETTLEKCCAAADPHECYAK, MH+ 2676.6676, m/z 892.8941
10HNE-1HSA-37Trypsin5-LTQ4.4613.4613.3.dta

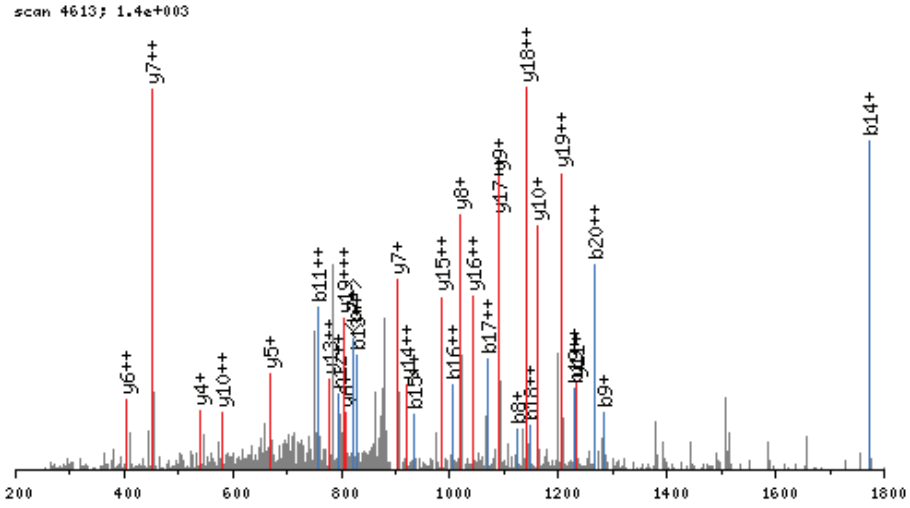

click image to zoom in; click top corners to zoom out [precursor±]

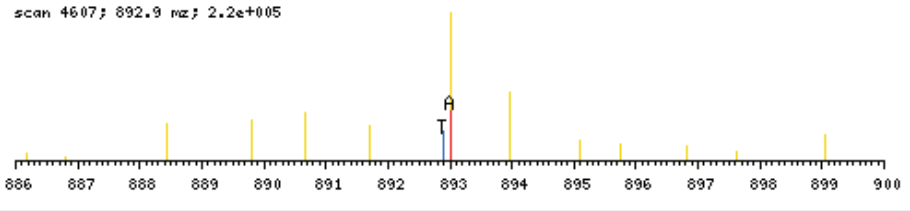

zoomed in precursor plot; T=theoretical m/z, A=acquired m/z

b^+	b^{2+}	#	AA	#	y^+	y^{2+}	y^{3+}
102.0555	51.5317	1	T	21			
265.1188	133.0633	2	Y	20	2575.6200	1288.3139	859.2119
394.1614	197.5846	3	E	19	2412.5566	**1206.7822**	**804.8574**
495.2091	248.1085	4	T	18	2283.5140	**1142.2609**	761.8432
596.2568	298.6323	5	T	17	2182.4664	**1091.7371**	728.1607
709.3408	355.1743	6	L	16	2081.4187	**1041.2133**	694.4781
838.3834	419.6956	7	E	15	1968.3346	**984.6712**	656.7834
1124.6882	562.8480	8	K	14	1839.2920	**920.1499**	613.7692
1284.8485	642.9282	9	C	13	1552.9872	**776.9975**	518.3343
1445.0088	723.0083	10	C	12	1392.8269	696.9174	464.9475
1516.0459	**758.5269**	11	A	11	**1232.6666**	616.8372	411.5608
1587.0830	**794.0454**	12	A	10	**1161.6295**	**581.3187**	387.8817
1658.1202	**829.5640**	13	A	9	**1090.5924**	545.8001	364.2027
1773.1471	887.0775	14	D	8	**1019.5553**	510.2816	340.5237
1870.1999	**935.6038**	15	P	7	**904.5284**	**452.7681**	302.1813
2007.2588	**1004.1333**	16	H	6	**807.4756**	**404.2417**	269.8304
2136.3014	**1068.6546**	17	E	5	**670.4167**	335.7123	224.1441
2296.4617	**1148.7347**	18	C	4	**541.3741**	271.1910	181.1299
2459.5250	**1230.2664**	19	Y	3	381.2138	191.1108	127.7431
2530.5621	**1265.7850**	20	A	2	218.1505	109.5791	73.3887
		21	K	1	147.1134	74.0606	49.7097

K(8):+286.30 C(9):+160.16 C(10):+160.16 C(18):+160.16

X-range: 400 - 1800
MassTol: 0.950 Y-zoom: 1.00
ImageSize: Sm Lg
MassType: AVG MONO
Axis: 1 2
Label: I M -
Ions:
a + 2+ 3+
b + 2+ 3+
c + 2+ 3+
x + 2+ 3+
y + 2+ 3+
z + 2+ 3+
hide H_2O/NH_3
zoom 112-122
zoom 124-133
GO

TYETTLEKCCAAADPHECYAK, MH+ 2676.6676, m/z 669.9224
10HNE-1HSA-37Trypsin3-LTQ3.4087.4087.4.dta

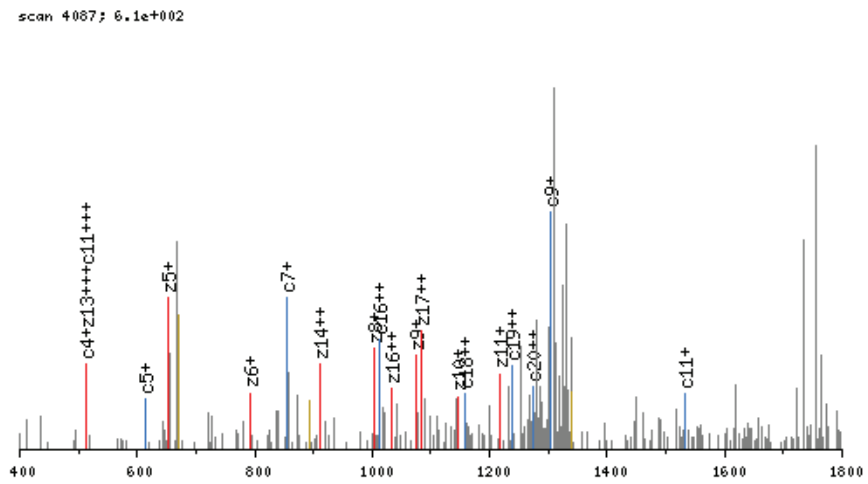

click image to zoom in; click top corners to zoom out [precursor±]

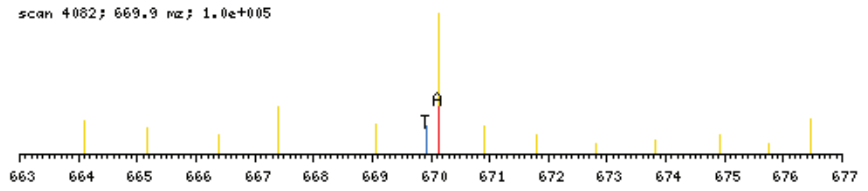

zoomed in precursor plot; T=theoretical m/z, A=acquired m/z

c^+	c^{2+}	c^{3+}	#	AA	#	z^+	z^{2+}	z^{3+}
119.0821	60.0449	40.3659	1	T	21			
282.1454	141.5766	94.7203	2	Y	20	2559.6012	1280.3045	853.8723
411.1880	206.0979	137.7345	3	E	19	2396.5379	1198.7729	799.5179
512.2357	256.6217	171.4171	4	T	18	2267.4953	1134.2516	756.5037
613.2833	307.1456	205.0997	5	T	17	2166.4476	1083.7277	722.8211
726.3674	363.6876	242.7943	6	L	16	2065.4000	1033.2039	689.1385
855.4100	428.2089	285.8085	7	E	15	1952.3159	976.6619	651.4438
1141.7148	571.3613	381.2435	8	K	14	1823.2733	912.1406	608.4297
1301.8751	651.4414	434.6302	9	C	13	1536.9685	768.9882	512.9947
1462.0354	731.5216	488.0170	10	C	12	1376.8082	688.9080	459.6080
1533.0725	767.0402	511.6960	11	A	11	1216.6479	608.8279	406.2212
1604.1096	802.5587	535.3751	12	A	10	1145.6108	573.3093	382.5422
1675.1467	838.0773	559.0541	13	A	9	1074.5737	537.7908	358.8631
1790.1737	895.5907	597.3964	14	D	8	1003.5366	502.2722	335.1841
1887.2264	944.1171	629.7474	15	P	7	888.5096	444.7587	296.8418
2024.2853	1012.6466	675.4337	16	H	6	791.4569	396.2324	264.4908
2153.3279	1077.1679	718.4479	17	E	5	654.3980	327.7029	218.8045
2313.4882	1157.2480	771.8346	18	C	4	525.3554	263.1816	175.7903
2476.5516	1238.7797	826.1891	19	Y	3	365.1951	183.1014	122.4036
2547.5887	1274.2982	849.8681	20	A	2	202.1317	101.5698	68.0491
			21	K	1	131.0946	66.0512	44.3701

K(8):+286.30 C(9):+160.16 C(10):+160.16 C(18):+160.16

X-range: 200 - 1600
MassTol: 0.950 Y-zoom: 1.00
ImageSize: (•) Sm ( ) Lg
MassType: ( ) AVG (•) MONO
Axis: (•) 1 ( ) 2
Label: (•) I ( ) M ( ) -
Ions:
a [ ] + [ ] 2+ [ ] 3+
b [x] + [ ] 2+ [ ] 3+
c [ ] + [ ] 2+ [ ] 3+
x [ ] + [ ] 2+ [ ] 3+
y [x] + [x] 2+ [ ] 3+
z [ ] + [ ] 2+ [ ] 3+
hide H_2O/NH_3 [ ]
zoom 112-122 [ ]
zoom 124-133 [ ]
GO

CCAAADPHECYAK, MH+ 1711.2001, m/z 856.1037
10HNE-1HSA-37Trypsin2-LTQ1.3482.3482.2.dta

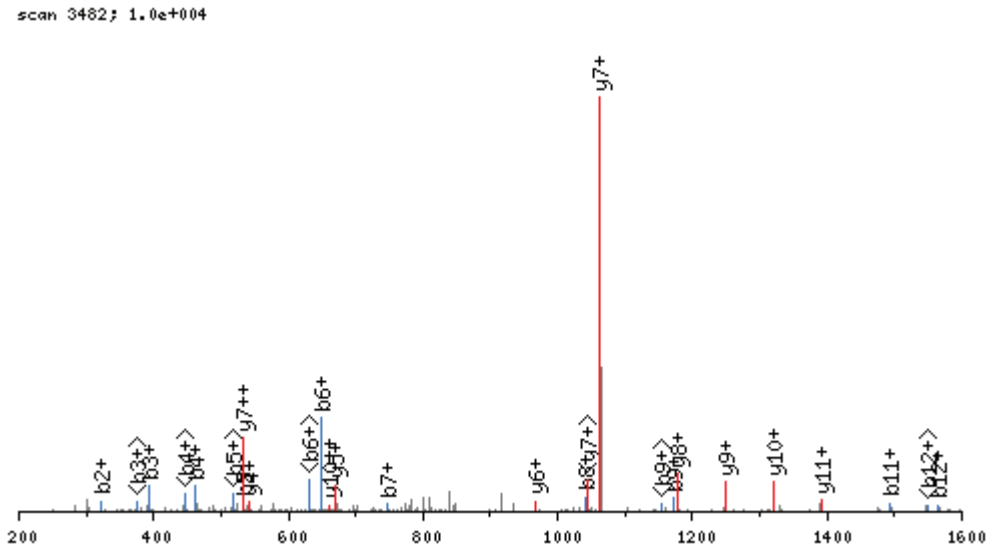

click image to zoom in; click top corners to zoom out [precursor±]

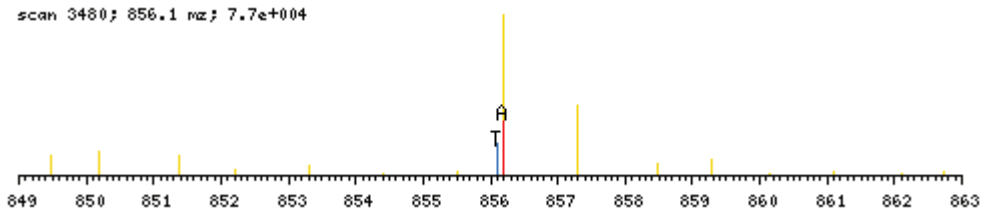

zoomed in precursor plot; T=theoretical m/z, A=acquired m/z

b^+	#	AA	#	y^+	y^{2+}
161.1681	1	C	13		
321.3284	2	C	12	1551.0398	776.0238
392.3655	3	A	11	1390.8795	695.9437
463.4027	4	A	10	1319.8424	660.4251
534.4398	5	A	9	1248.8053	624.9066
649.4667	6	D	8	1177.7682	589.3880
746.5195	7	P	7	1062.7412	531.8745
1041.7913	8	H	6	965.6885	483.3481
1170.8338	9	E	5	670.4167	335.7123
1330.9941	10	C	4	541.3741	271.1910
1494.0575	11	Y	3	381.2138	191.1108
1565.0946	12	A	2	218.1505	109.5791
	13	K	1	147.1134	74.0606

C(1):+160.16 C(2):+160.16 H(8):+295.27
C(10):+160.16

X-range: 300 - 1400
MassTol: 0.950 Y-zoom: 1.00
ImageSize: (•) Sm ( ) Lg
MassType: ( ) AVG (•) MONO
Axis: (•) 1 ( ) 2
Label: (•) I ( ) M ( ) -
Ions:

a	[ ] +	[ ] 2+	[ ] 3+
b	[x] +	[x] 2+	[ ] 3+
c	[ ] +	[ ] 2+	[ ] 3+
x	[ ] +	[ ] 2+	[ ] 3+
y	[x] +	[x] 2+	[x] 3+
z	[ ] +	[ ] 2+	[ ] 3+

hide H_2O/NH_3 [ ]
zoom 112-122 [ ]
zoom 124-133 [ ]
GO

VFDEFKPLVEEPQNLIK, MH+ 2203.3057, m/z 735.1068
10HNE-1HSA-37Trypsin4-LTQ1.5563.5563.3.dta

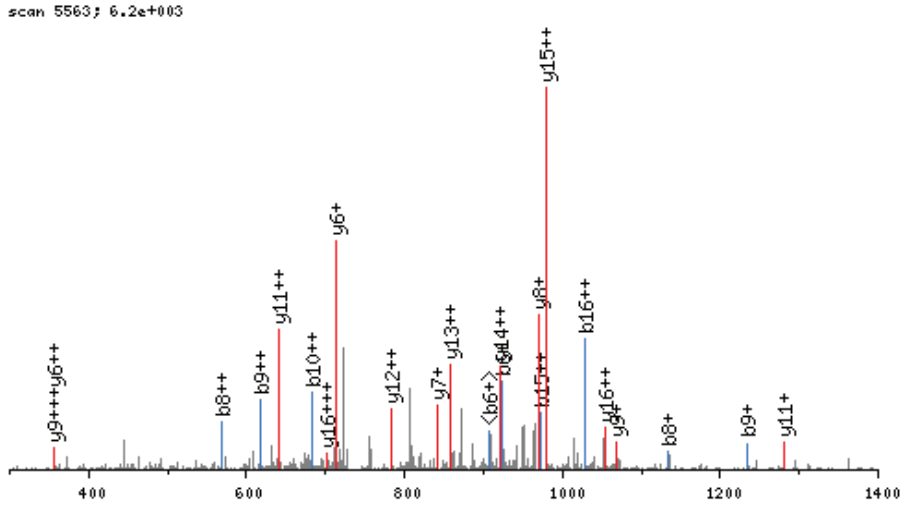

click image to zoom in; click top corners to zoom out [precursor±]

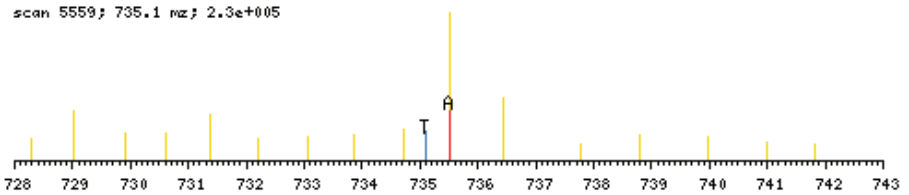

zoomed in precursor plot; T=theoretical m/z, A=acquired m/z

b^+	b^{2+}	#	AA	#	y^+	y^{2+}	y^{3+}
100.0762	50.5420	1	V	17			
247.1447	124.0762	2	F	16	2104.2373	**1052.6226**	**702.0843**
362.1716	181.5897	3	D	15	1957.1689	**979.0884**	653.0615
491.2142	246.1110	4	E	14	1842.1420	**921.5749**	614.7192
638.2826	319.6452	5	F	13	1713.0994	**857.0536**	571.7050
924.5874	462.7976	6	K	12	1566.0310	**783.5194**	522.6822
1021.6401	511.3240	7	P	11	**1279.7262**	**640.3670**	427.2473
1134.7242	**567.8660**	8	L	10	1182.6734	591.8406	394.8964
1233.7926	**617.4002**	9	V	9	**1069.5893**	535.2986	**357.2017**
1362.8352	**681.9215**	10	E	8	**970.5209**	485.7644	324.1789
1491.8778	746.4428	11	E	7	**841.4783**	421.2431	281.1647
1588.9306	794.9692	12	P	6	**712.4357**	**356.7218**	238.1505
1716.9892	858.9985	13	Q	5	615.3830	308.1954	205.7995
1831.0321	916.0200	14	N	4	487.3244	244.1661	163.1134
1944.1161	**972.5620**	15	L	3	373.2815	187.1447	125.0990
2057.2002	**1029.1040**	16	I	2	260.1974	130.6026	87.4044
		17	K	1	147.1134	74.0606	49.7097

K(6):+286.30

X-range: 300 - 1900
MassTol: 0.950 Y-zoom: 1.00
ImageSize: (•) Sm ( ) Lg
MassType: ( ) AVG (•) MONO
Axis: (•) 1 ( ) 2
Label: (•) I ( ) M ( ) -
Ions:

a	☐ +	☐ 2+	☐ 3+
b	☐ +	☐ 2+	☐ 3+
c	☑ +	☑ 2+	☐ 3+
x	☐ +	☐ 2+	☐ 3+
y	☐ +	☐ 2+	☐ 3+
z	☑ +	☑ 2+	☑ 3+

hide H_2O/NH_3 ☐
zoom 112-122 ☐
zoom 124-133 ☐
GO

VFDEFKPLVEEPQNLIK, MH+ 2203.3057, m/z 735.1068
10HNE-1HSA-37Trypsin3-LTQ3.6050.6050.3.dta

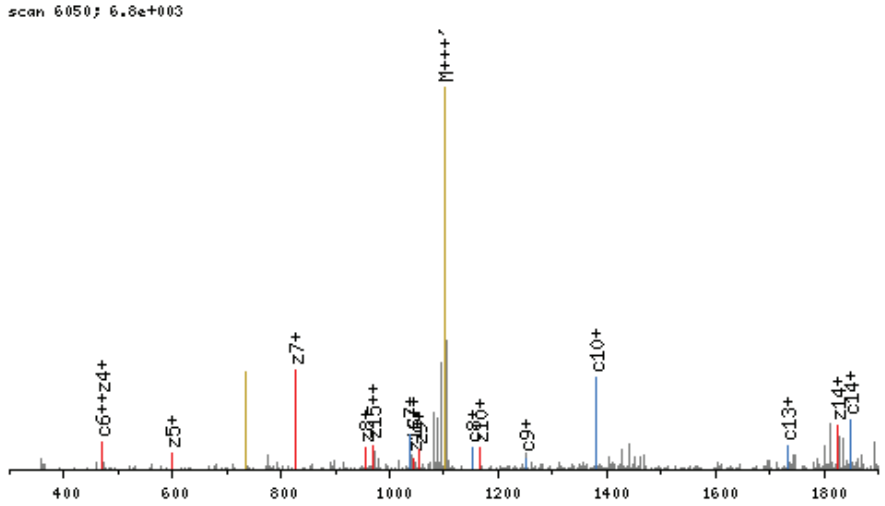

click image to zoom in; click top corners to zoom out [precursor±]

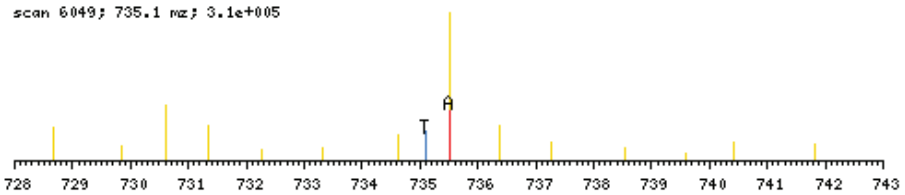

zoomed in precursor plot; T=theoretical m/z, A=acquired m/z

c^+	c^{2+}	#	AA	#	z^+	z^{2+}	z^{3+}
117.1028	59.0553	1	V	17			
264.1712	132.5895	2	F	16	2088.2186	**1044.6132**	696.7447
379.1981	190.1030	3	D	15	1941.1502	**971.0790**	647.7219
508.2407	254.6243	4	E	14	**1826.1232**	913.5655	609.3796
655.3092	328.1585	5	F	13	1697.0806	849.0442	566.3654
941.6139	**471.3109**	6	K	12	1550.0122	775.5100	517.3426
1038.6667	519.8373	7	P	11	1263.7075	632.3576	421.9077
1151.7508	576.3793	8	L	10	**1166.6547**	583.8313	389.5568
1250.8192	625.9135	9	V	9	**1053.5706**	527.2892	351.8621
1379.8618	690.4348	10	E	8	**954.5022**	477.7550	318.8393
1508.9044	754.9561	11	E	7	**825.4596**	413.2337	275.8251
1605.9571	803.4825	12	P	6	696.4170	348.7124	232.8109
1734.0157	867.5118	13	Q	5	**599.3643**	300.1860	200.4600
1848.0586	924.5332	14	N	4	**471.3057**	236.1568	157.7738
1961.1427	981.0753	15	L	3	357.2628	179.1353	119.7595
2074.2268	1037.6173	16	I	2	244.1787	122.5933	82.0648
		17	K	1	131.0946	66.0512	44.3701

K(6):+286.30

X-range: 300 - 1400
MassTol: 0.950 Y-zoom: 1.00
ImageSize: Sm Lg
MassType: AVG MONO
Axis: 1 2
Label: I M -
Ions:

a	+	2+	3+
b	+	2+	3+
c	+	2+	3+
x	+	2+	3+
y	+	2+	3+
z	+	2+	3+

hide H_2O/NH_3
zoom 112-122
zoom 124-133
GO

QNCELFEQLGEYKFQNALLVR, MH+ 2757.6374, m/z 919.8840
10HNE-1HSA-37Trypsin4-LTQ1.5673.5673.3.dta

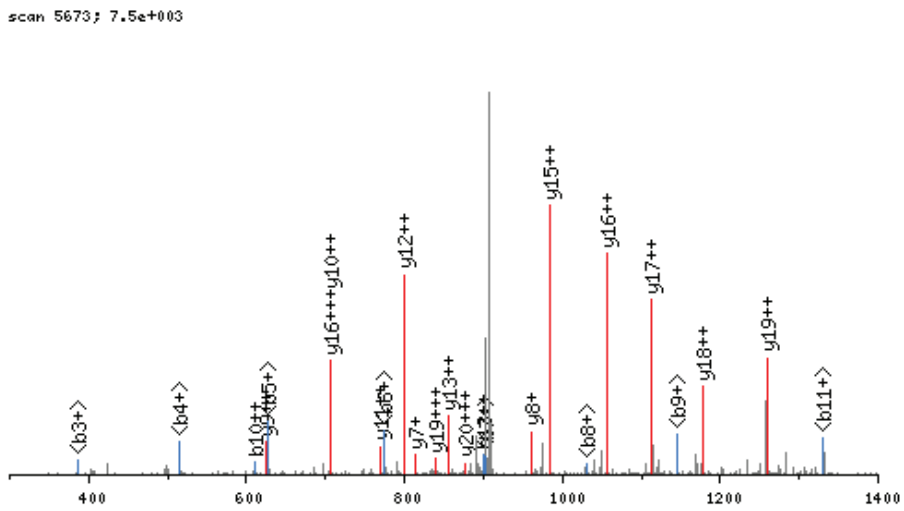

click image to zoom in; click top corners to zoom out [precursor±]

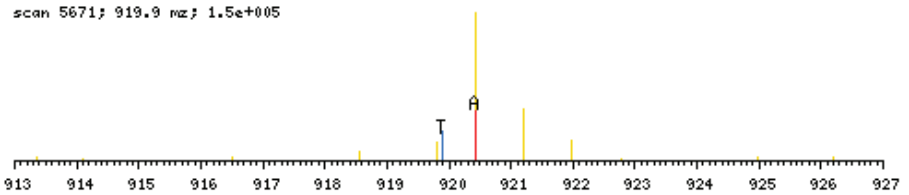

zoomed in precursor plot; T=theoretical m/z, A=acquired m/z

b^+	b^{2+}	#	AA	#	y^+	y^{2+}	y^{3+}
129.0664	65.0371	1	Q	21			
243.1093	122.0586	2	N	20	2629.5788	1315.2933	**877.1981**
403.2696	202.1387	3	C	19	2515.5358	**1258.2718**	**839.1838**
532.3122	266.6600	4	E	18	2355.3755	**1178.1917**	785.7971
645.3963	323.2021	5	L	17	2226.3330	**1113.6704**	742.7829
792.4647	396.7363	6	F	16	2113.2489	**1057.1284**	**705.0882**
921.5073	461.2576	7	E	15	1966.1805	**983.5942**	656.0654
1049.5659	525.2868	8	Q	14	1837.1379	919.0729	613.0512
1162.6499	581.8289	9	L	13	1709.0793	**855.0436**	570.3650
1219.6714	**610.3396**	10	G	12	1595.9952	**798.5015**	532.6703
1348.7140	674.8609	11	E	11	1538.9738	**769.9908**	513.6631
1511.7773	756.3926	12	Y	10	1409.9312	**705.4695**	470.6489
1798.0821	**899.5450**	13	K	9	1246.8679	**623.9378**	416.2945
1945.1505	973.0792	14	F	8	**960.5631**	480.7855	320.8596
2073.2091	1037.1085	15	Q	7	**813.4947**	407.2512	271.8368
2187.2520	1094.1299	16	N	6	685.4361	343.2220	229.1506
2258.2891	1129.6485	17	A	5	571.3932	286.2005	191.1363
2371.3732	1186.1905	18	L	4	500.3560	250.6819	167.4572
2484.4573	1242.7325	19	L	3	387.2720	194.1399	129.7625
2583.5257	1292.2668	20	V	2	274.1879	137.5979	92.0679
		21	R	1	175.1195	88.0637	59.0451

C(3):+160.16 K(13):+286.30

X-range: 200 - 1200
MassTol: 0.950 Y-zoom: 7.00
ImageSize: Sm Lg
MassType: AVG MONO
Axis: 1 2
Label: I M -
Ions:
a + 2+ 3+
b + 2+ 3+
c + 2+ 3+
x + 2+ 3+
y + 2+ 3+
z + 2+ 3+
hide H_2O/NH_3
zoom 112-122
zoom 124-133
GO

KVPQVSTPTLVEVSR, MH+ 1798.1481, m/z 600.0542
10HNE-1HSA-37Trypsin4-LTQ2.5227.5227.3.dta

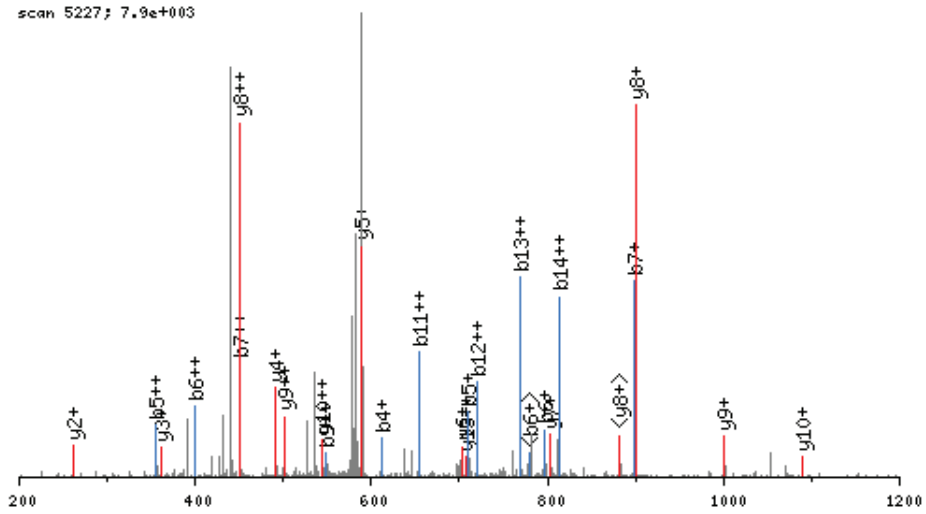

click image to zoom in; click top corners to zoom out [precursor±]

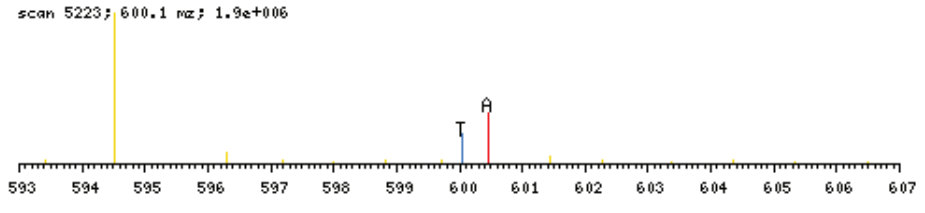

zoomed in precursor plot; T=theoretical m/z, A=acquired m/z

b^+	b^{2+}	#	AA	#	y^+	y^{2+}	y^{3+}
287.3126	144.1602	1	K	15			
386.3810	193.6944	2	V	14	1511.8433	756.4256	504.6197
483.4338	242.2208	3	P	13	1412.7749	706.8914	471.5969
611.4924	306.2501	4	Q	12	1315.7222	658.3650	439.2459
710.5608	355.7843	5	V	11	1187.6636	594.3357	396.5597
797.5928	399.3003	6	S	10	1088.5952	544.8015	363.5369
898.6405	449.8242	7	T	9	1001.5631	501.2855	334.5263
995.6932	498.3505	8	P	8	900.5155	450.7616	300.8437
1096.7409	548.8744	9	T	7	803.4627	402.2353	268.4928
1209.8250	605.4164	10	L	6	702.4150	351.7114	234.8102
1308.8934	654.9506	11	V	5	589.3310	295.1694	197.1155
1437.9360	719.4719	12	E	4	490.2625	245.6352	164.0927
1537.0044	769.0061	13	V	3	361.2199	181.1139	121.0785
1624.0364	812.5221	14	S	2	262.1515	131.5797	88.0557
		15	R	1	175.1195	88.0637	59.0451

K(1):+286.30

X-range: 200 - 1900
MassTol: 0.950 Y-zoom: 1.00
ImageSize: (•) Sm ( ) Lg
MassType: ( ) AVG (•) MONO
Axis: (•) 1 ( ) 2
Label: (•) I ( ) M ( ) -
Ions:

	+	2+	3+
a	☐	☐	☐
b	☐	☐	☐
c	☑	☑	☐
x	☐	☐	☐
y	☐	☐	☐
z	☑	☑	☑

hide H_2O/NH_3 ☐
zoom 112-122 ☐
zoom 124-133 ☐
GO

KVPQVSTPTLVEVSR, MH+ 1798.1481, m/z 600.0542
10HNE-1HSA-37Trypsin5-LTQ4.5805.5805.3.dta

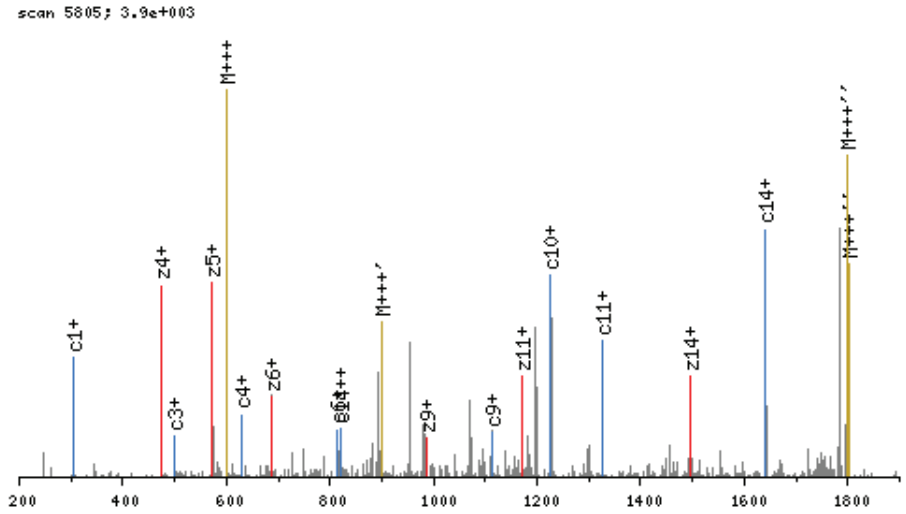

click image to zoom in; click top corners to zoom out [precursor±]

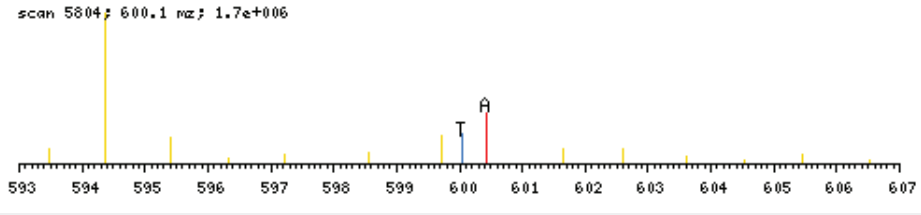

zoomed in precursor plot; T=theoretical m/z, A=acquired m/z

c^+	c^{2+}	#	AA	#	z^+	z^{2+}	z^{3+}
304.3392	152.6735	1	K	15			
403.4076	202.2077	2	V	14	1495.8246	748.4162	499.2801
500.4603	250.7341	3	P	13	1396.7562	698.8820	466.2573
628.5189	314.7634	4	Q	12	1299.7034	650.3556	433.9064
727.5873	364.2976	5	V	11	1171.6449	586.3263	391.2202
814.6194	407.8136	6	S	10	1072.5764	536.7921	358.1974
915.6670	458.3374	7	T	9	985.5444	493.2761	329.1867
1012.7198	506.8638	8	P	8	884.4967	442.7523	295.5041
1113.7675	557.3876	9	T	7	787.4440	394.2259	263.1532
1226.8515	613.9297	10	L	6	686.3963	343.7021	229.4706
1325.9200	663.4639	11	V	5	573.3122	287.1600	191.7760
1454.9625	727.9852	12	E	4	474.2438	237.6258	158.7532
1554.0310	777.5194	13	V	3	345.2012	173.1045	115.7390
1641.0630	821.0354	14	S	2	246.1328	123.5703	82.7162
		15	R	1	159.1008	80.0543	53.7055

K(1):+286.30

X-range: 200 - 1100
MassTol: 0.950 Y-zoom: 7.00
ImageSize: Sm Lg
MassType: AVG MONO
Axis: 1 2
Label: I M -
Ions:
a + 2+ 3+
b + 2+ 3+
c + 2+ 3+
x + 2+ 3+
y + 2+ 3+
z + 2+ 3+
hide H_2O/NH_3
zoom 112-122
zoom 124-133
GO

KVPQVSTPTLVEVSR, MH+ 1780.1375, m/z 594.0507
10HNE-1HSA-37Trypsin5-LTQ1.4522.4522.3.dta

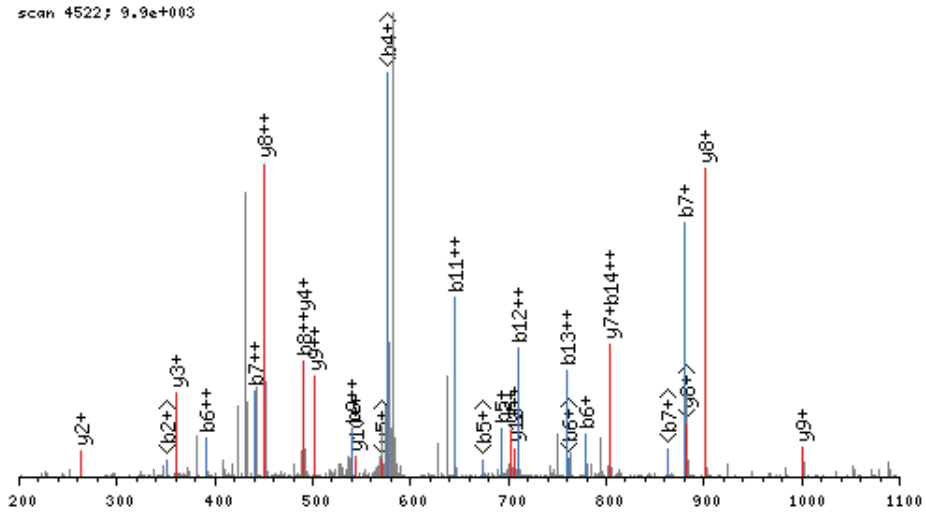

click image to zoom in; click top corners to zoom out [precursor±]

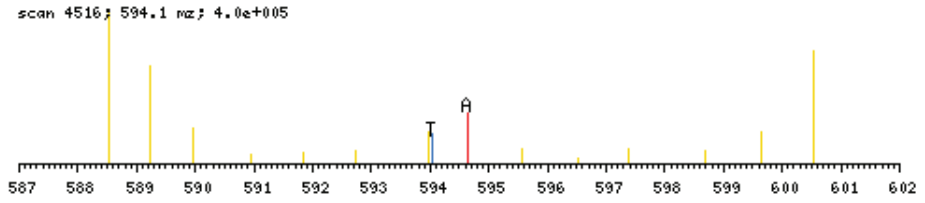

zoomed in precursor plot; T=theoretical m/z, A=acquired m/z

b^+	b^{2+}	#	AA	#	y^+	y^{2+}	y^{3+}
269.3020	135.1549	1	K	15			
368.3705	184.6891	2	V	14	1511.8433	756.4256	504.6197
465.4232	233.2155	3	P	13	1412.7749	706.8914	471.5969
593.4818	297.2448	4	Q	12	1315.7222	658.3650	439.2459
692.5502	346.7790	5	V	11	1187.6636	594.3357	396.5597
779.5822	390.2950	6	S	10	1088.5952	544.8015	363.5369
880.6299	440.8189	7	T	9	1001.5631	501.2855	334.5263
977.6827	489.3453	8	P	8	900.5155	450.7616	300.8437
1078.7304	539.8691	9	T	7	803.4627	402.2353	268.4928
1191.8144	596.4111	10	L	6	702.4150	351.7114	234.8102
1290.8828	645.9453	11	V	5	589.3310	295.1694	197.1155
1419.9254	710.4666	12	E	4	490.2625	245.6352	164.0927
1518.9938	760.0008	13	V	3	361.2199	181.1139	121.0785
1606.0259	803.5168	14	S	2	262.1515	131.5797	88.0557
		15	R	1	175.1195	88.0637	59.0451

K(1):+268.29

X-range: 200 - 1800
MassTol: 0.950 Y-zoom: 5.00
ImageSize: (•) Sm ( ) Lg
MassType: ( ) AVG (•) MONO
Axis: (•) 1 ( ) 2
Label: (•) I ( ) M ( ) -
Ions:

	+	2+	3+
a	☐	☐	☐
b	☐	☐	☐
c	☑	☑	☐
x	☐	☐	☐
y	☐	☐	☐
z	☑	☑	☑

hide H_2O/NH_3 ☐
zoom 112-122 ☐
zoom 124-133 ☐
GO

KVPQVSTPTLVEVSR, MH+ 1780.1375, m/z 594.0507
10HNE-1HSA-37Trypsin5-LTQ4.5994.5994.3.dta

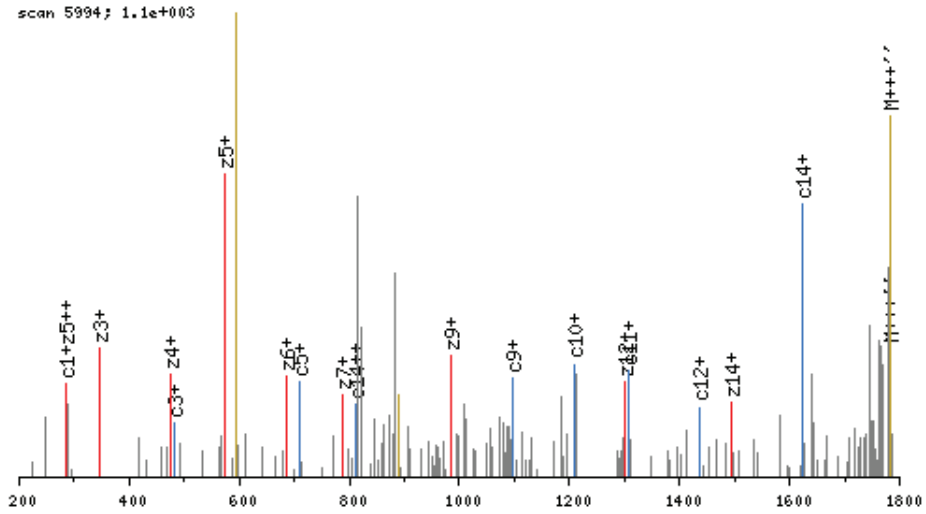

click image to zoom in; click top corners to zoom out [precursor±]

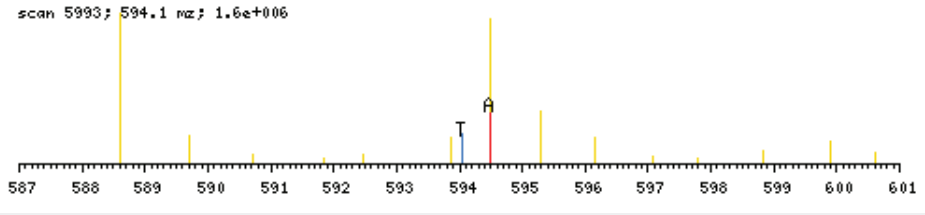

zoomed in precursor plot; T=theoretical m/z, A=acquired m/z

c^+	c^{2+}	#	AA	#	z^+	z^{2+}	z^{3+}
286.3286	143.6682	1	K	15			
385.3970	193.2024	2	V	14	1495.8246	748.4162	499.2801
482.4498	241.7288	3	P	13	1396.7562	698.8820	466.2573
610.5083	305.7581	4	Q	12	1299.7034	650.3556	433.9064
709.5768	355.2923	5	V	11	1171.6449	586.3263	391.2202
796.6088	398.8083	6	S	10	1072.5764	536.7921	358.1974
897.6565	449.3321	7	T	9	985.5444	493.2761	329.1867
994.7092	497.8585	8	P	8	884.4967	442.7523	295.5041
1095.7569	548.3824	9	T	7	787.4440	394.2259	263.1532
1208.8410	604.9244	10	L	6	686.3963	343.7021	229.4706
1307.9094	654.4586	11	V	5	573.3122	287.1600	191.7760
1436.9520	718.9799	12	E	4	474.2438	237.6258	158.7532
1536.0204	768.5141	13	V	3	345.2012	173.1045	115.7390
1623.0524	812.0301	14	S	2	246.1328	123.5703	82.7162
		15	R	1	159.1008	80.0543	53.7055

K(1):+268.29

X-range: 200 - 1000
MassTol: 0.950 Y-zoom: 1.00
ImageSize: (•) Sm ( ) Lg
MassType: ( ) AVG (•) MONO
Axis: (•) 1 ( ) 2
Label: (•) I ( ) M ( ) -
Ions:

a	☐ +	☐ 2+	☐ 3+
b	☑ +	☑ 2+	☐ 3+
c	☐ +	☐ 2+	☐ 3+
x	☐ +	☐ 2+	☐ 3+
y	☑ +	☑ 2+	☑ 3+
z	☐ +	☐ 2+	☐ 3+

hide H_2O/NH_3 ☐
zoom 112-122 ☐
zoom 124-133 ☐
GO

VTKCCTESLVNR, MH+ 1625.1787, m/z 542.3977
10HNE-1HSA-37Trypsin2-LTQ3.3654.3654.3.dta

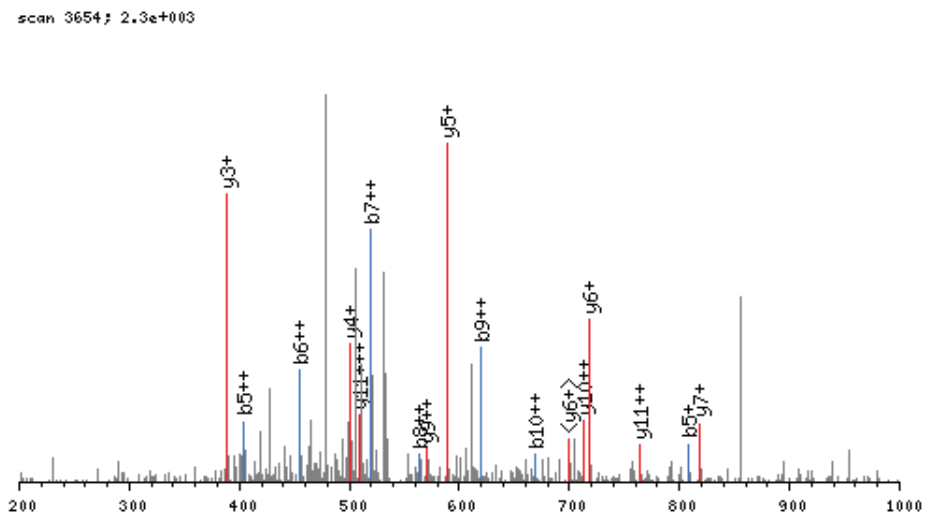

click image to zoom in; click top corners to zoom out [precursor±]

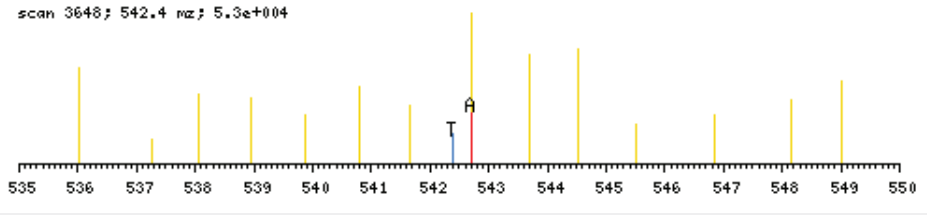

zoomed in precursor plot; T=theoretical m/z, A=acquired m/z

b^+	b^{2+}	#	AA	#	y^+	y^{2+}	y^{3+}
100.0762	50.5420	1	V	12			
201.1239	101.0659	2	T	11	1526.1103	763.5590	509.3753
487.4287	244.2183	3	K	10	1425.0626	713.0352	475.6927
647.5890	324.2984	4	C	9	1138.7578	569.8828	380.2578
807.7493	404.3786	5	C	8	978.5975	489.8027	326.8711
908.7970	454.9024	6	T	7	818.4372	409.7225	273.4843
1037.8396	519.4237	7	E	6	717.3895	359.1987	239.8017
1124.8716	562.9397	8	S	5	588.3469	294.6774	196.7875
1237.9557	619.4817	9	L	4	501.3149	251.1614	167.7769
1337.0241	669.0160	10	V	3	388.2308	194.6193	130.0822
1451.0670	726.0374	11	N	2	289.1624	145.0851	97.0594
		12	R	1	175.1195	88.0637	59.0451

K(3):+286.30 C(4):+160.16 C(5):+160.16

X-range: 200 - 2000
MassTol: 0.950 Y-zoom: 1.00
ImageSize: (•) Sm ( ) Lg
MassType: ( ) AVG (•) MONO
Axis: (•) 1 ( ) 2
Label: (•) I ( ) M ( ) -
Ions:
a [ ] + [ ] 2+ [ ] 3+
b [x] + [ ] 2+ [ ] 3+
c [ ] + [ ] 2+ [ ] 3+
x [ ] + [ ] 2+ [ ] 3+
y [x] + [x] 2+ [ ] 3+
z [ ] + [ ] 2+ [ ] 3+
hide H_2O/NH_3 [ ]
zoom 112-122 [ ]
zoom 124-133 [ ]
GO

EFNAETFTFHADICTLSEK, MH+ 2418.3657, m/z 1209.6865
10HNE-1HSA-37Trypsin5-LTQ4.7385.7385.2.dta

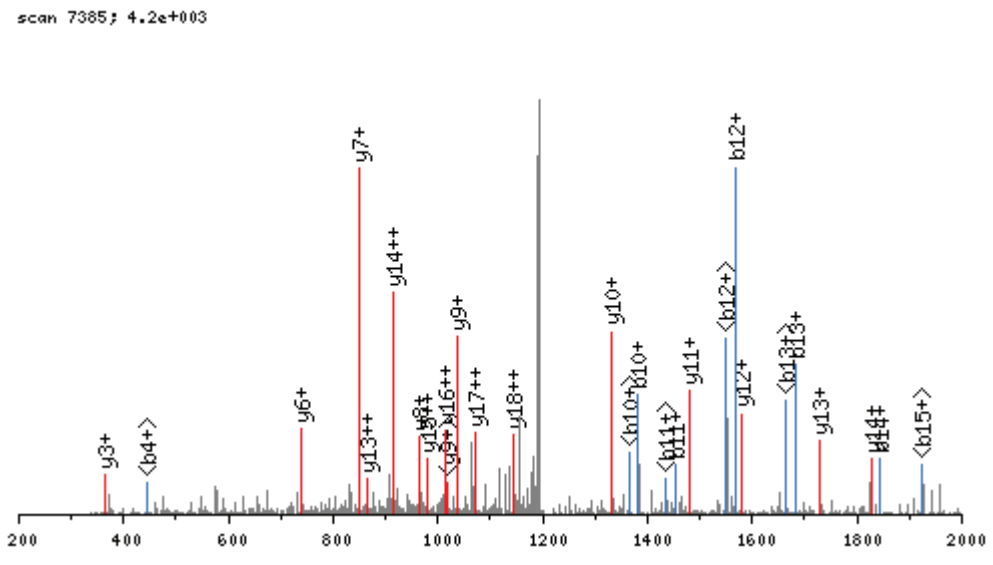

click image to zoom in; click top corners to zoom out [precursor±]

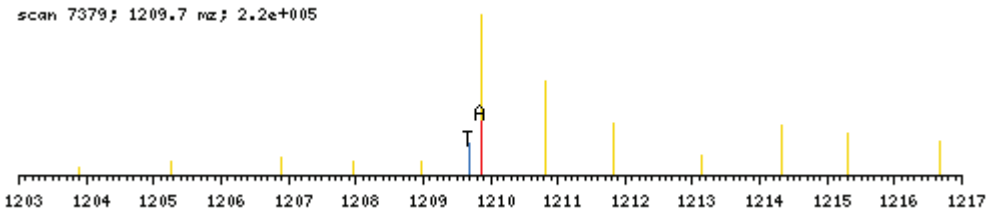

zoomed in precursor plot; T=theoretical m/z, A=acquired m/z

b^+	#	AA	#	y^+	y^{2+}
130.0504	1	E	19		
277.1188	2	F	18	2289.3232	1145.1655
391.1618	3	N	17	2142.2547	1071.6313
462.1989	4	A	16	2028.2118	1014.6098
591.2415	5	E	15	1957.1747	979.0913
692.2891	6	T	14	1828.1321	914.5700
839.3576	7	F	13	1727.0844	864.0461
940.4052	8	T	12	1580.0160	790.5119
1087.4737	9	F	11	1478.9683	739.9881
1382.7454	10	H	10	1331.8999	666.4539
1453.7825	11	A	9	1036.6281	518.8180
1568.8095	12	D	8	965.5910	483.2994
1681.8936	13	I	7	850.5641	425.7860
1842.0539	14	C	6	737.4800	369.2439
1943.1015	15	T	5	577.3197	289.1638
2056.1856	16	L	4	476.2720	238.6399
2143.2176	17	S	3	363.1880	182.0979
2272.2602	18	E	2	276.1559	138.5819
	19	K	1	147.1134	74.0606

H(10):+295.27 C(14):+160.16

X-range: 400 - 1800
MassTol: 0.950 Y-zoom: 1.00
ImageSize: (•) Sm ( ) Lg
MassType: ( ) AVG (•) MONO
Axis: (•) 1 ( ) 2
Label: (•) I ( ) M ( ) -
Ions:

a	☐ +	☐ 2+	☐ 3+
b	☐ +	☐ 2+	☐ 3+
c	☑ +	☑ 2+	☐ 3+
x	☐ +	☐ 2+	☐ 3+
y	☐ +	☐ 2+	☐ 3+
z	☑ +	☑ 2+	☑ 3+

hide H_2O/NH_3 ☐
zoom 112-122 ☐
zoom 124-133 ☐
GO

EFNAETFTFHADICTLSEK, MH+ 2418.3657, m/z 806.7934
10HNE-1HSA-37Trypsin3-LTQ1.5945.5945.3.dta

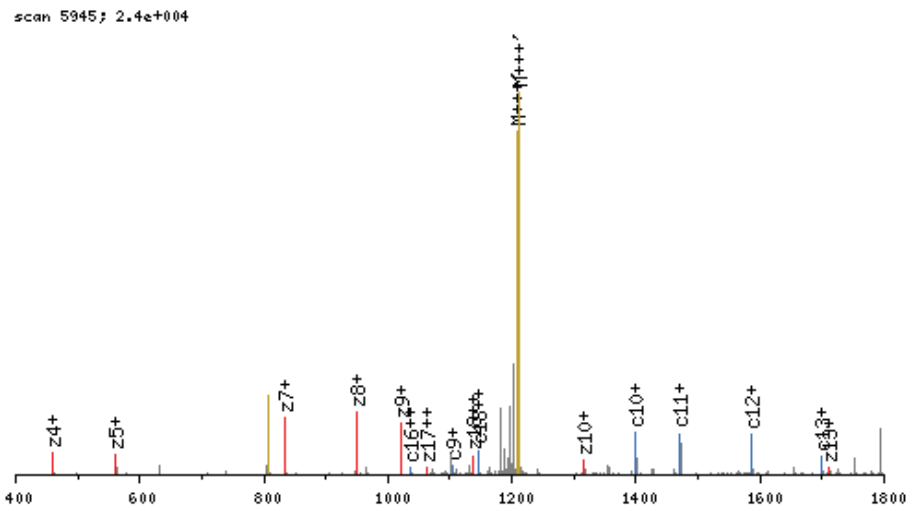

click image to zoom in; click top corners to zoom out [precursor±]

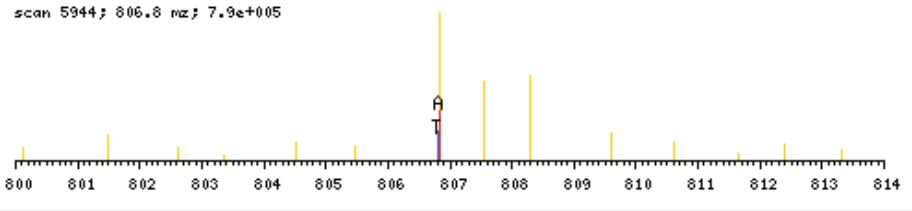

zoomed in precursor plot; T=theoretical m/z, A=acquired m/z

c^+	c^{2+}	#	AA	#	z^+	z^{2+}	z^{3+}
147.0770	74.0424	1	E	19			
294.1454	147.5766	2	F	18	2273.3044	**1137.1561**	758.4400
408.1883	204.5981	3	N	17	2126.2360	**1063.6219**	709.4172
479.2254	240.1166	4	A	16	2012.1931	1006.6005	671.4029
608.2680	304.6379	5	E	15	1941.1560	971.0819	647.7239
709.3157	355.1618	6	T	14	1812.1134	906.5606	604.7097
856.3841	428.6960	7	F	13	**1711.0657**	856.0368	571.0271
957.4318	479.2198	8	T	12	1563.9973	782.5026	522.0043
1104.5002	552.7540	9	F	11	1462.9496	731.9787	488.3218
1399.7720	700.3899	10	H	10	**1315.8812**	658.4445	439.2989
1470.8091	735.9085	11	A	9	**1020.6094**	510.8086	340.8750
1585.8360	793.4219	12	D	8	**949.5723**	475.2901	317.1960
1698.9201	849.9640	13	I	7	**834.5454**	417.7766	278.8537
1859.0804	930.0441	14	C	6	721.4613	361.2346	241.1590
1960.1281	980.5680	15	T	5	**561.3010**	281.1544	187.7722
2073.2121	**1037.1100**	16	L	4	**460.2533**	230.6306	154.0897
2160.2442	1080.6260	17	S	3	347.1693	174.0885	116.3950
2289.2868	**1145.1473**	18	E	2	260.1372	130.5725	87.3843
		19	K	1	131.0946	66.0512	44.3701

H(10):+295.27 C(14):+160.16

X-range: 300 - 1500
MassTol: 0.950 Y-zoom: 1.00
ImageSize: Sm Lg
MassType: AVG MONO
Axis: 1 2
Label: I M -
Ions:
a + 2+ 3+
b + 2+ 3+
c + 2+ 3+
x + 2+ 3+
y + 2+ 3+
z + 2+ 3+
hide H_2O/NH_3
zoom 112-122
zoom 124-133
GO

EFNAETFTFHADICTLSEKER, MH+ 2703.5064, m/z 901.8403
10HNE-1HSA-37Trypsin5-LTQ1.5376.5376.3.dta

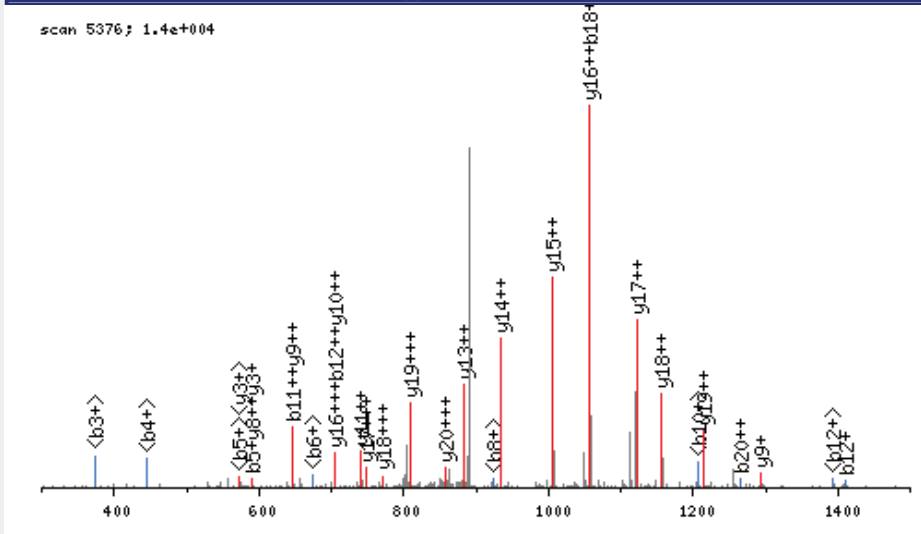

click image to zoom in; click top corners to zoom out [precursor±]

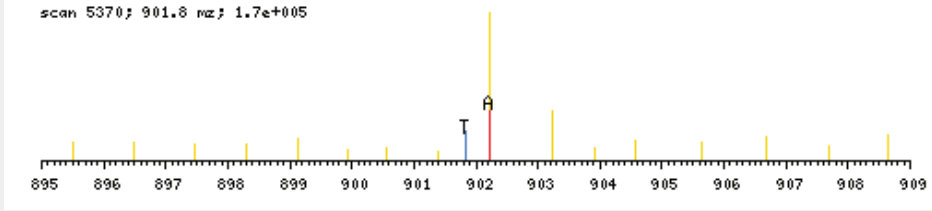

zoomed in precursor plot; T=theoretical m/z, A=acquired m/z

b^+	b^{2+}	#	AA	#	y^+	y^{2+}	y^{3+}
130.0504	65.5291	1	E	21			
277.1188	139.0633	2	F	20	2574.4638	1287.7358	**858.8265**
391.1618	196.0848	3	N	19	2427.3954	**1214.2016**	**809.8037**
462.1989	231.6033	4	A	18	2313.3525	**1157.1801**	**771.7894**
591.2415	296.1246	5	E	17	2242.3153	**1121.6616**	**748.1103**
692.2891	346.6485	6	T	16	2113.2728	**1057.1403**	**705.0961**
839.3576	420.1827	7	F	15	2012.2251	**1006.6165**	671.4136
940.4052	470.7065	8	T	14	1865.1567	**933.0822**	622.3908
1087.4737	544.2407	9	F	13	1764.1090	**882.5584**	588.7082
1224.5326	612.7702	10	H	12	1617.0406	809.0242	539.6854
1295.5697	**648.2888**	11	A	11	1479.9817	**740.4947**	493.9991
1410.5966	**705.8022**	12	D	10	1408.9445	**704.9762**	470.3201
1523.6807	762.3443	13	I	9	**1293.9176**	**647.4627**	431.9778
1683.8410	842.4244	14	C	8	1180.8335	**590.9207**	394.2831
1784.8887	892.9482	15	T	7	1020.6732	510.8405	340.8963
1897.9727	949.4903	16	L	6	919.6256	460.3167	307.2137
1985.0048	993.0063	17	S	5	806.5415	403.7747	269.5190
2114.0473	**1057.5276**	18	E	4	719.5095	360.2586	240.5084
2400.3521	1200.6800	19	K	3	**590.4669**	295.7373	197.4942
2529.3947	**1265.2013**	20	E	2	304.1621	152.5850	102.0592
		21	R	1	175.1195	88.0637	59.0451

C(14):+160.16 K(19):+286.30

X-range:
500 - 1300
MassTol: Y-zoom:
0.950 1.00
ImageSize:
(•) Sm ( ) Lg
MassType:
( ) AVG (•) MONO
Axis:
(•) 1 ( ) 2
Label:
(•) I ( ) M ( ) -
Ions:

a	[ ] +	[ ] 2+	[ ] 3+
b	[ ] +	[ ] 2+	[ ] 3+
c	[x] +	[ ] 2+	[ ] 3+
x	[ ] +	[ ] 2+	[ ] 3+
y	[ ] +	[ ] 2+	[ ] 3+
z	[x] +	[x] 2+	[ ] 3+

hide H_2O/NH_3 [ ]
zoom 112-122 [ ]
zoom 124-133 [ ]
GO

KQTALVELVK, MH+ 1286.9091, m/z 643.9582
10HNE-1HSA-37Trypsin5-LTQ4.5504.5504.2.dta

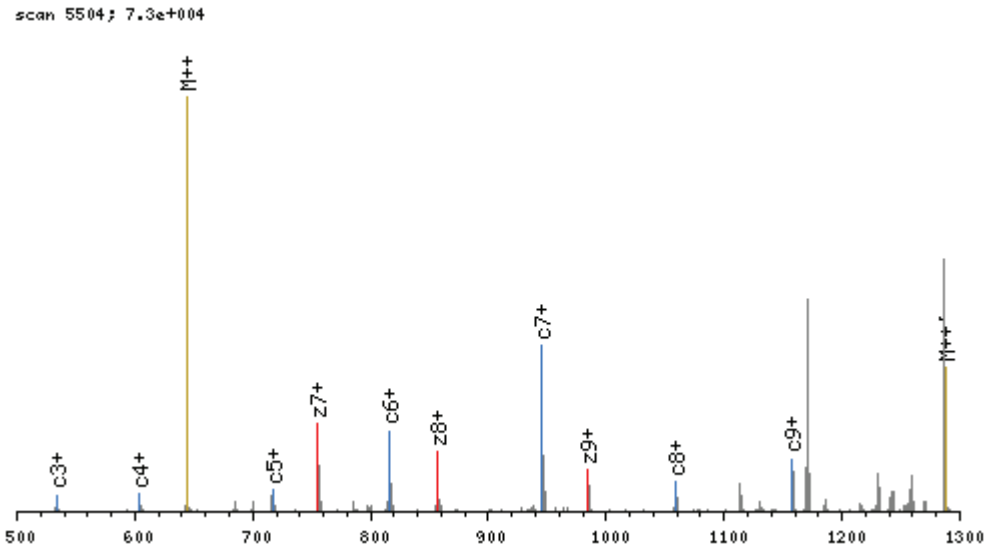

click image to zoom in; click top corners to zoom out [precursor±]

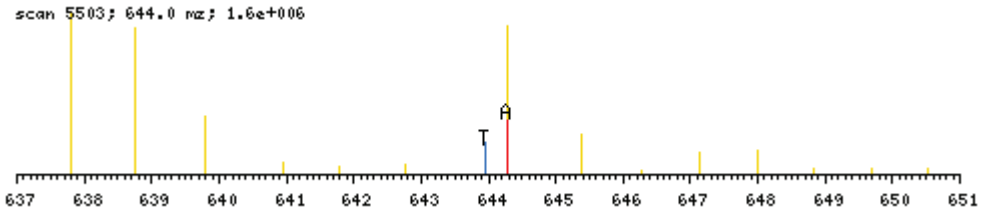

zoomed in precursor plot; T=theoretical m/z, A=acquired m/z

c^+	#	AA	#	z^+	z^{2+}
304.3392	1	K	10		
432.3977	2	Q	9	984.5855	492.7967
533.4454	3	T	8	856.5270	428.7674
604.4825	4	A	7	755.4793	378.2436
717.5666	5	L	6	684.4422	342.7250
816.6350	6	V	5	571.3581	286.1830
945.6776	7	E	4	472.2897	236.6488
1058.7617	8	L	3	343.2471	172.1275
1157.8301	9	V	2	230.1630	115.5854
	10	K	1	131.0946	66.0512

K(1):+286.30

X-range: 100 - 800
MassTol: 0.950 Y-zoom: 1.00
ImageSize: Sm Lg
MassType: AVG MONO
Axis: 1 2
Label: I M -
Ions:
a + 2+ 3+
b + 2+ 3+
c + 2+ 3+
x + 2+ 3+
y + 2+ 3+
z + 2+ 3+
hide H_2O/NH_3
zoom 112-122
zoom 124-133
GO

KQTALVELVK, MH+ 1268.8985, m/z 423.6377
10HNE-1HSA-37Trypsin4-LTQ3.5169.5169.3.dta

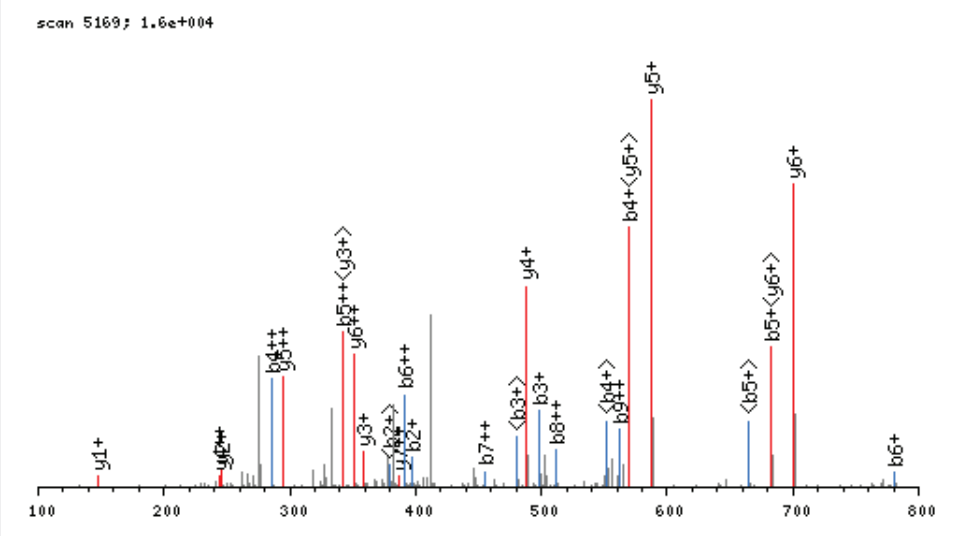

click image to zoom in; click top corners to zoom out [precursor±]

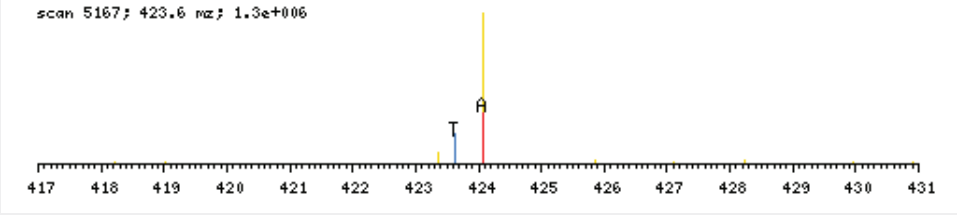

zoomed in precursor plot; T=theoretical m/z, A=acquired m/z

b^+	b^{2+}	#	AA	#	y^+	y^{2+}	y^{3+}
269.3020	135.1549	1	K	10			
397.3606	199.1842	2	Q	9	1000.6043	500.8060	334.2066
498.4083	249.7081	3	T	8	872.5457	436.7768	291.5204
569.4454	285.2266	4	A	7	771.4980	386.2529	257.8379
682.5295	341.7686	5	L	6	700.4609	350.7344	234.1589
781.5979	391.3029	6	V	5	587.3768	294.1923	196.4642
910.6405	455.8242	7	E	4	488.3084	244.6581	163.4414
1023.7245	512.3662	8	L	3	359.2658	180.1368	120.4272
1122.7930	561.9004	9	V	2	246.1818	123.5948	82.7325
		10	K	1	147.1134	74.0606	49.7097

K(1):+268.29

X-range: 200 - 1300
MassTol: 0.950 Y-zoom: 1.00
ImageSize: (•) Sm ( ) Lg
MassType: ( ) AVG (•) MONO
Axis: (•) 1 ( ) 2
Label: (•) I ( ) M ( ) -
Ions:

a	☐ +	☐ 2+	☐ 3+
b	☐ +	☐ 2+	☐ 3+
c	☑ +	☑ 2+	☐ 3+
x	☐ +	☐ 2+	☐ 3+
y	☐ +	☐ 2+	☐ 3+
z	☑ +	☑ 2+	☑ 3+

hide H_2O/NH_3 ☐
zoom 112-122 ☐
zoom 124-133 ☐
GO

KQTALVELVK, MH+ 1268.8985, m/z 423.6377
10HNE-1HSA-37Trypsin3-LTQ3.4934.4934.3.dta

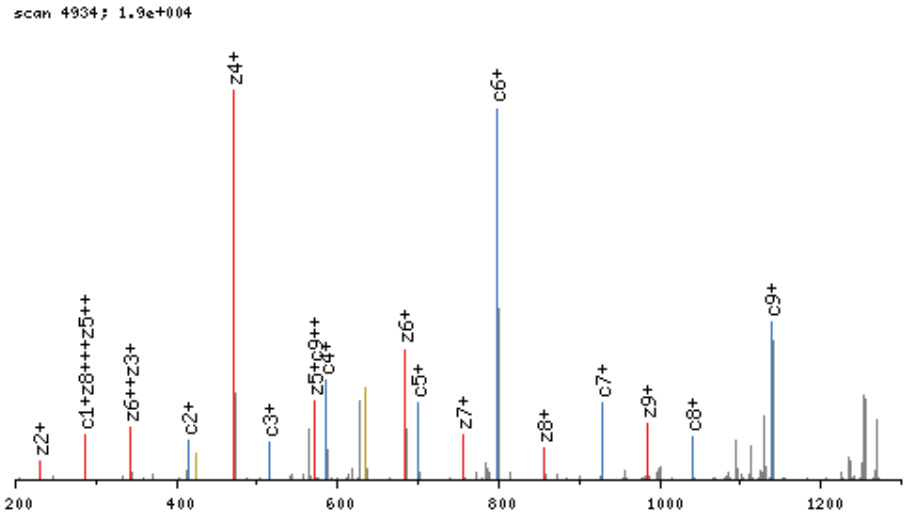

click image to zoom in; click top corners to zoom out [precursor±]

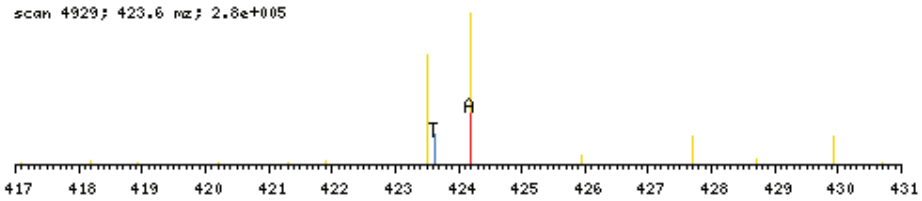

zoomed in precursor plot; T=theoretical m/z, A=acquired m/z

c^+	c^{2+}	#	AA	#	z^+	z^{2+}	z^{3+}
286.3286	143.6682	1	K	10			
414.3872	207.6975	2	Q	9	984.5855	492.7967	328.8671
515.4348	258.2213	3	T	8	856.5270	428.7674	286.1809
586.4720	293.7399	4	A	7	755.4793	378.2436	252.4983
699.5560	350.2819	5	L	6	684.4422	342.7250	228.8193
798.6244	399.8161	6	V	5	571.3581	286.1830	191.1246
927.6670	464.3374	7	E	4	472.2897	236.6488	158.1018
1040.7511	520.8795	8	L	3	343.2471	172.1275	115.0876
1139.8195	570.4137	9	V	2	230.1630	115.5854	77.3929
		10	K	1	131.0946	66.0512	44.3701

K(1):+268.29

X-range:
300 - 1800
MassTol: Y-zoom:
0.950 1.00
ImageSize:
(•) Sm ( ) Lg
MassType:
( ) AVG (•) MONO
Axis:
(•) 1 ( ) 2
Label:
(•) I ( ) M ( ) -
Ions:

a	☐ +	☐ 2+	☐ 3+
b	☑ +	☐ 2+	☐ 3+
c	☐ +	☐ 2+	☐ 3+
x	☐ +	☐ 2+	☐ 3+
y	☑ +	☑ 2+	☐ 3+
z	☐ +	☐ 2+	☐ 3+

hide H_2O/NH_3 ☐
zoom 112-122 ☐
zoom 124-133 ☐
GO

EQLKAVMDDFAAFVEK, MH+ 1999.1253, m/z 1000.0663
10HNE-1HSA-37Trypsin3-LTQ1.7119.7119.2.dta

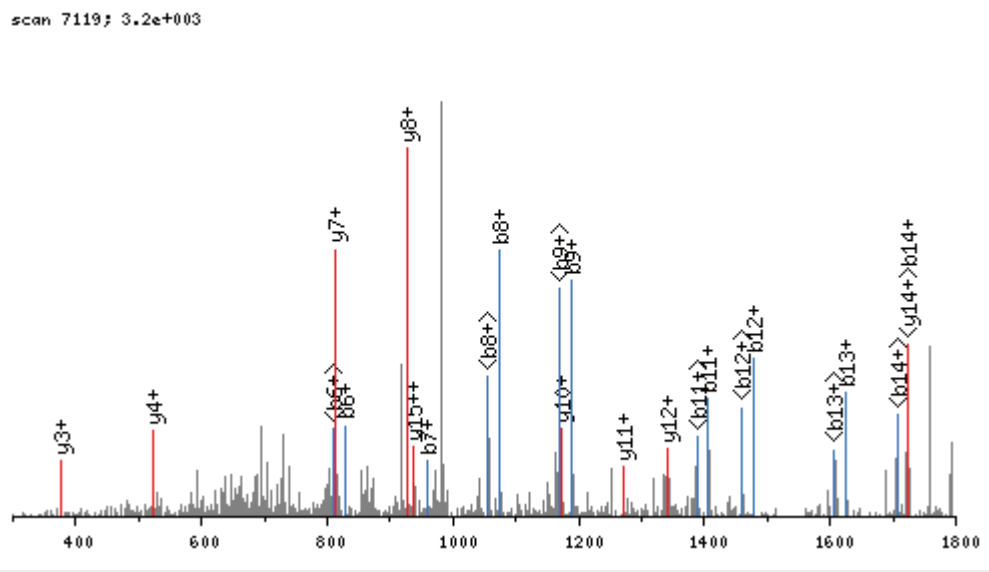

click image to zoom in; click top corners to zoom out [precursor±]

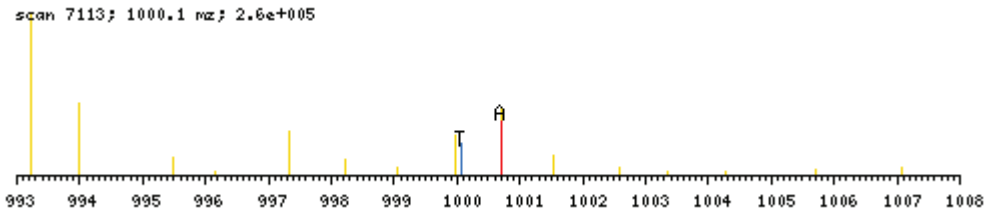

zoomed in precursor plot; T=theoretical m/z, A=acquired m/z

b^+	#	AA	#	y^+	y^{2+}
130.0504	1	E	16		
258.1090	2	Q	15	1870.0827	**935.5453**
371.1931	3	L	14	1742.0242	871.5160
657.4978	4	K	13	1628.9401	814.9740
728.5350	5	A	12	**1342.6353**	671.8216
827.6034	6	V	11	**1271.5982**	636.3030
958.6439	7	M	10	**1172.5298**	586.7688
1073.6708	8	D	9	1041.4893	521.2486
1188.6977	9	D	8	**926.4624**	463.7351
1335.7662	10	F	7	**811.4354**	406.2216
1406.8033	11	A	6	664.3670	332.6874
1477.8404	12	A	5	593.3299	297.1689
1624.9088	13	F	4	**522.2928**	261.6503
1723.9772	14	V	3	**375.2244**	188.1161
1853.0198	15	E	2	276.1559	138.5819
	16	K	1	147.1134	74.0606

K(4):+286.30

X-range: 400 - 1900
MassTol: 0.950 Y-zoom: 1.00
ImageSize: Sm Lg
MassType: AVG MONO
Axis: 1 2
Label: I M -
Ions:

a	+	2+	3+
b	+	2+	3+
c	+	2+	3+
x	+	2+	3+
y	+	2+	3+
z	+	2+	3+

hide H_2O/NH_3
zoom 112-122
zoom 124-133
GO

EQLKAVMDDFAAFVEK, MH+ 1999.1253, m/z 667.0466
10HNE-1HSA-37Trypsin5-LTQ4.8836.8836.3.dta

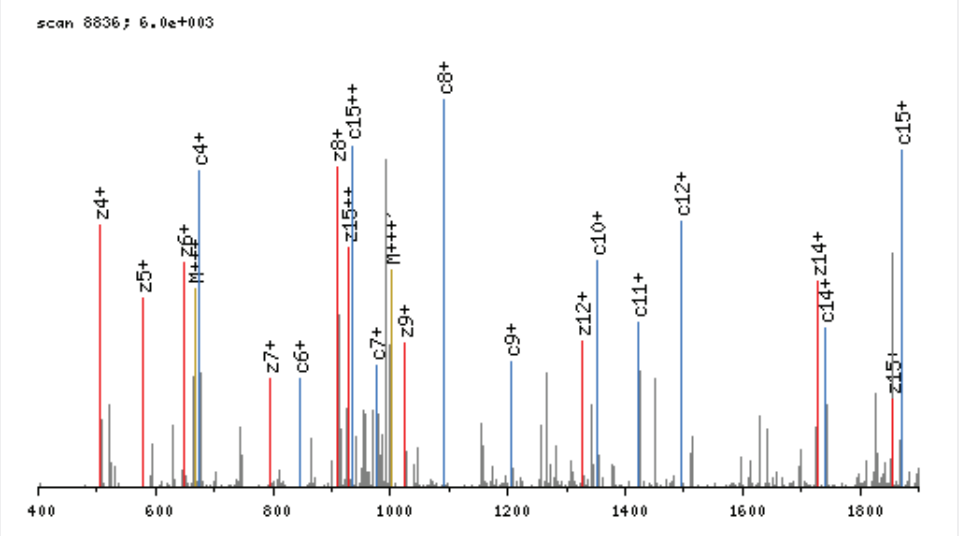

click image to zoom in; click top corners to zoom out [precursor±]

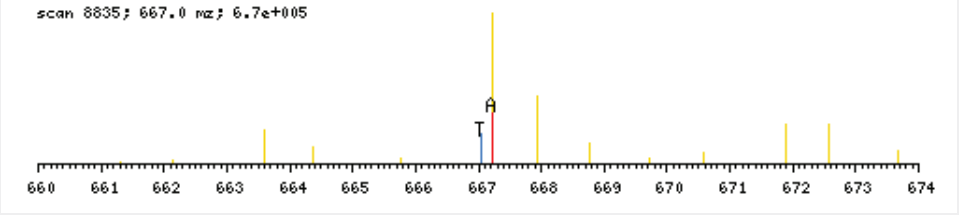

zoomed in precursor plot; T=theoretical m/z, A=acquired m/z

c^+	c^{2+}	#	AA	#	z^+	z^{2+}	z^{3+}
147.0770	74.0424	1	E	16			
275.1355	138.0717	2	Q	15	1854.0640	927.5359	618.6932
388.2196	194.6137	3	L	14	1726.0054	863.5066	576.0070
674.5244	337.7661	4	K	13	1612.9214	806.9646	538.3123
745.5615	373.2847	5	A	12	1326.6166	663.8122	442.8774
844.6299	422.8189	6	V	11	1255.5795	628.2937	419.1984
975.6704	488.3391	7	M	10	1156.5111	578.7594	386.1756
1090.6973	545.8526	8	D	9	1025.4706	513.2392	342.4954
1205.7243	603.3661	9	D	8	910.4436	455.7257	304.1531
1352.7927	676.9003	10	F	7	795.4167	398.2123	265.8108
1423.8298	712.4188	11	A	6	648.3483	324.6781	216.7880
1494.8669	747.9374	12	A	5	577.3112	289.1595	193.1089
1641.9353	821.4716	13	F	4	506.2740	253.6409	169.4299
1741.0038	871.0058	14	V	3	359.2056	180.1067	120.4071
1870.0463	935.5271	15	E	2	260.1372	130.5725	87.3843
		16	K	1	131.0946	66.0512	44.3701

K(4):+286.30

X-range: 200 - 1300
MassTol: 0.950 Y-zoom: 1.00
ImageSize: (•) Sm ( ) Lg
MassType: ( ) AVG (•) MONO
Axis: (•) 1 ( ) 2
Label: (•) I ( ) M ( ) -
Ions:

a	[ ] +	[ ] 2+	[ ] 3+
b	[x] +	[x] 2+	[ ] 3+
c	[ ] +	[ ] 2+	[ ] 3+
x	[ ] +	[ ] 2+	[ ] 3+
y	[x] +	[x] 2+	[x] 3+
z	[ ] +	[ ] 2+	[ ] 3+

hide H_2O/NH_3 [ ]
zoom 112-122 [ ]
zoom 124-133 [ ]
GO

EQLKAVMDDFAAFVEK, MH+ 1981.1148, m/z 661.0431
10HNE-1HSA-37Trypsin3-LTQ2.7320.7320.3.dta

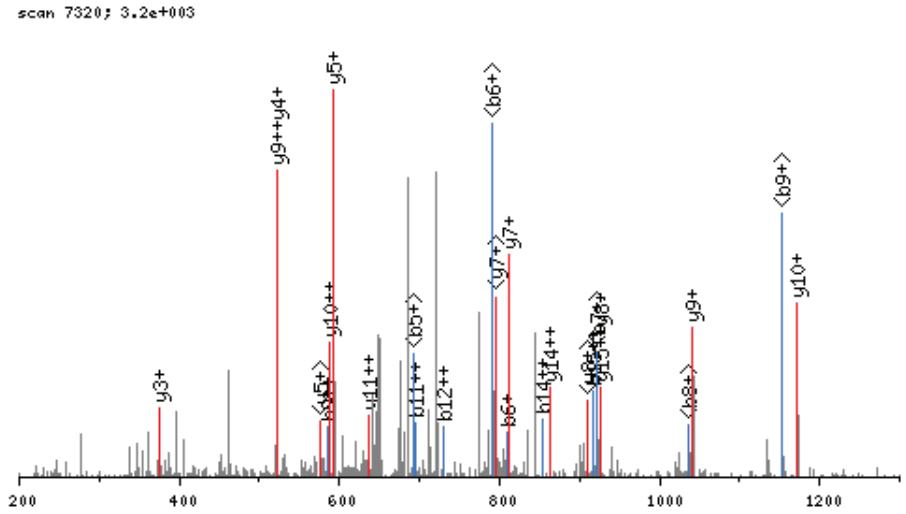

click image to zoom in; click top corners to zoom out [precursor±]

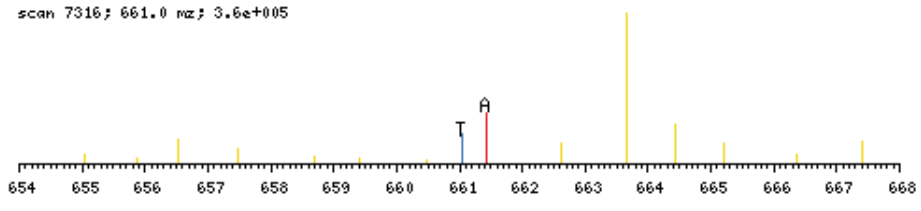

zoomed in precursor plot; T=theoretical m/z, A=acquired m/z

b^+	b^{2+}	#	AA	#	y^+	y^{2+}	y^{3+}
130.0504	65.5291	1	E	16			
258.1090	129.5584	2	Q	15	1852.0722	**926.5400**	618.0293
371.1931	186.1004	3	L	14	1724.0136	**862.5107**	575.3431
639.4873	320.2475	4	K	13	1610.9295	805.9687	537.6484
710.5244	355.7661	5	A	12	1342.6353	671.8216	448.2170
809.5928	405.3003	6	V	11	1271.5982	**636.3030**	424.5380
940.6333	470.8206	7	M	10	**1172.5298**	**586.7688**	391.5151
1055.6602	528.3340	8	D	9	**1041.4893**	**521.2486**	347.8350
1170.6872	**585.8475**	9	D	8	**926.4624**	463.7351	309.4927
1317.7556	659.3817	10	F	7	**811.4354**	406.2216	271.1504
1388.7927	**694.9003**	11	A	6	664.3670	332.6874	222.1276
1459.8298	**730.4188**	12	A	5	**593.3299**	297.1689	198.4485
1606.8982	803.9530	13	F	4	**522.2928**	261.6503	174.7695
1705.9666	**853.4872**	14	V	3	**375.2244**	188.1161	125.7467
1835.0092	**918.0085**	15	E	2	276.1559	138.5819	92.7239
		16	K	1	147.1134	74.0606	49.7097

K(4):+268.29

X-range: 400 - 1800
MassTol: 0.950 Y-zoom: 1.00
ImageSize: Sm Lg
MassType: AVG MONO
Axis: 1 2
Label: I M -
Ions:

a	+	2+	3+
b	+	2+	3+
c	+	2+	3+
x	+	2+	3+
y	+	2+	3+
z	+	2+	3+

hide H_2O/NH_3
zoom 112-122
zoom 124-133
GO

EQLKAVMDDFAAFVEK, MH+ 1981.1148, m/z 661.0431
10HNE-1HSA-37Trypsin2-LTQ1.7146.7146.3.dta

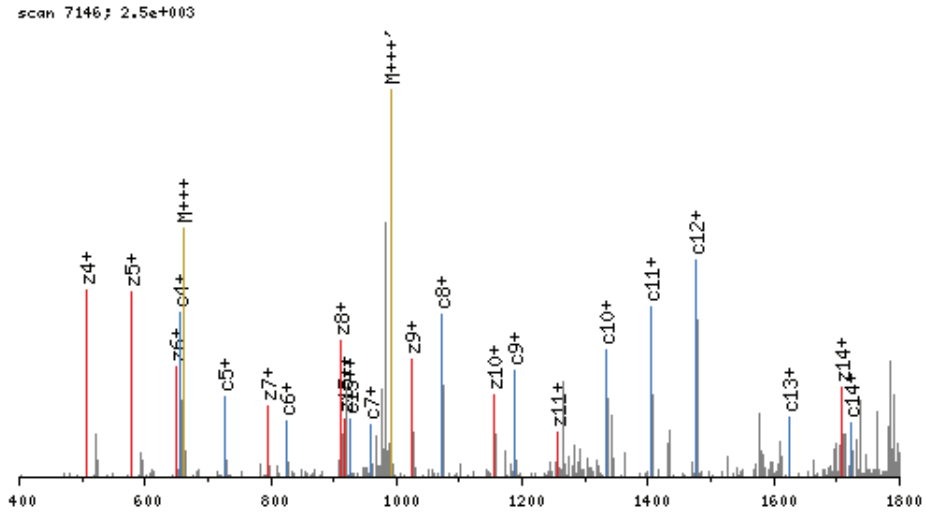

click image to zoom in; click top corners to zoom out [precursor±]

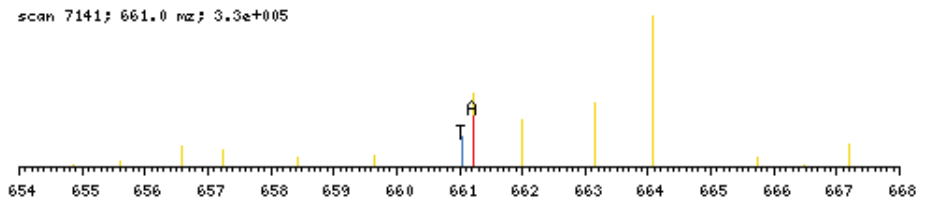

zoomed in precursor plot; T=theoretical m/z, A=acquired m/z

c^+	c^{2+}	#	AA	#	z^+	z^{2+}	z^{3+}
147.0770	74.0424	1	E	16			
275.1355	138.0717	2	Q	15	1836.0534	918.5306	612.6897
388.2196	194.6137	3	L	14	1707.9949	854.5013	570.0035
656.5138	328.7608	4	K	13	1594.9108	797.9593	532.3088
727.5509	364.2794	5	A	12	1326.6166	663.8122	442.8774
826.6194	413.8136	6	V	11	1255.5795	628.2937	419.1984
957.6598	479.3338	7	M	10	1156.5111	578.7594	386.1756
1072.6868	536.8473	8	D	9	1025.4706	513.2392	342.4954
1187.7137	594.3608	9	D	8	910.4436	455.7257	304.1531
1334.7821	667.8950	10	F	7	795.4167	398.2123	265.8108
1405.8193	703.4135	11	A	6	648.3483	324.6781	216.7880
1476.8564	738.9321	12	A	5	577.3112	289.1595	193.1089
1623.9248	812.4663	13	F	4	506.2740	253.6409	169.4299
1722.9932	862.0005	14	V	3	359.2056	180.1067	120.4071
1852.0358	926.5218	15	E	2	260.1372	130.5725	87.3843
		16	K	1	131.0946	66.0512	44.3701

K(4):+268.29

X-range: 500 - 1400
MassTol: 0.950 Y-zoom: 1.00
ImageSize: Sm Lg
MassType: AVG MONO
Axis: 1 2
Label: I M -
Ions:
a + 2+ 3+
b + 2+ 3+
c + 2+ 3+
x + 2+ 3+
y + 2+ 3+
z + 2+ 3+
hide H_2O/NH_3
zoom 112-122
zoom 124-133
GO

DLGEENFKALVLIAFAQYLQQCPFEDHVK, MH+ 3523.8187, m/z 881.7101
10HNE-1HSA-Trypsin6-Orbit2.04363.04363.4.dta

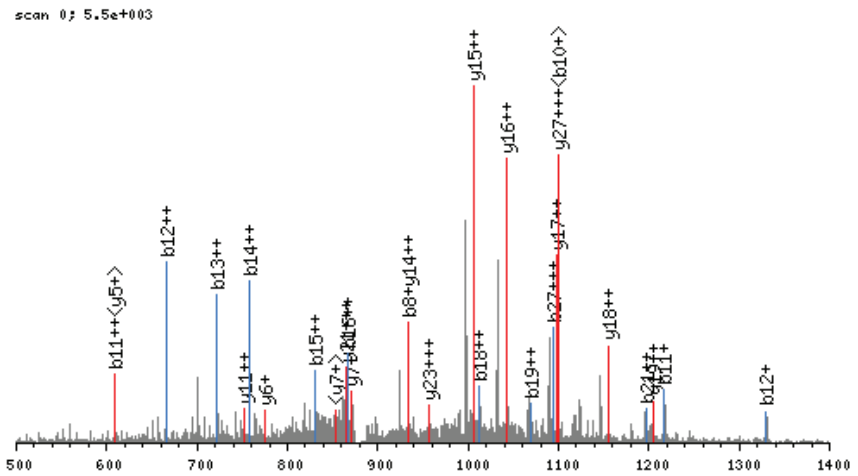

click image to zoom in; click top corners to zoom out

b^+	b^{2+}	b^{3+}	#	AA	#	y^+	y^{2+}	y^{3+}
116.0348	58.5213	39.3501	1	D	29			
229.1188	115.0633	77.0448	2	L	28	3408.7918	1704.8998	1136.9358
286.1403	143.5741	96.0520	3	G	27	3295.7077	1648.3578	**1099.2411**
415.1829	208.0954	139.0662	4	E	26	3238.6863	1619.8470	1080.2340
544.2255	272.6167	182.0804	5	E	25	3109.6437	1555.3258	1037.2198
658.2684	329.6381	220.0947	6	N	24	2980.6011	1490.8045	994.2056
805.3368	403.1723	269.1175	7	F	23	2866.5582	1433.7830	**956.1913**
933.4318	467.2198	311.8158	8	K	22	2719.4897	1360.2488	907.1685
1004.4689	502.7384	335.4949	9	A	21	2591.3948	1296.2013	**864.4701**
1117.5530	559.2804	373.1895	10	L	20	2520.3577	1260.6827	840.7911
1216.6214	**608.8146**	406.2123	11	V	19	2407.2736	**1204.1407**	803.0964
1329.7054	**665.3566**	443.9070	12	L	18	2308.2052	**1154.6065**	770.0736
1442.7895	**721.8987**	481.6017	13	I	17	2195.1211	**1098.0645**	732.3789
1513.8266	**757.4172**	505.2808	14	A	16	2082.0371	**1041.5224**	694.6842
1660.8950	**830.9514**	554.3036	15	F	15	2010.9999	**1006.0039**	671.0052
1731.9321	**866.4700**	577.9826	16	A	14	1863.9315	**932.4697**	621.9824
1859.9907	930.4993	620.6688	17	Q	13	1792.8944	896.9511	598.3034
2023.0541	**1012.0309**	675.0232	18	Y	12	1664.8358	832.9218	555.6172
2136.1381	**1068.5730**	712.7179	19	L	11	1501.7725	**751.3902**	501.2627
2264.1967	1132.6023	755.4041	20	Q	10	1388.6884	694.8481	463.5680
2392.2553	**1196.6315**	798.0903	21	Q	9	1260.6299	630.8188	420.8818
2653.3952	1327.2015	885.1369	22	C	8	1132.5713	566.7896	378.1956
2750.4479	1375.7279	917.4879	23	P	7	**871.4314**	436.2196	291.1490
2897.5164	1449.2621	966.5107	24	F	6	**774.3786**	387.6932	258.7981
3026.5589	1513.7834	1009.5249	25	E	5	627.3102	314.1590	209.7753
3141.5859	1571.2969	1047.8672	26	D	4	498.2676	249.6377	166.7611
3278.6448	1639.8263	**1093.5535**	27	H	3	383.2407	192.1243	128.4188
3377.7132	1689.3605	1126.5763	28	V	2	246.1818	123.5948	82.7325
			29	K	1	147.1134	74.0606	49.7097

C(22):+261.14

X-range: 200 - 1200
MassTol: 0.950 Y-zoom: 1.00
ImageSize: Sm Lg
MassType: AVG MONO
Axis: 1 2
Label: I M -
Ions:

a	+	2+	3+
b	+	2+	3+
c	+	2+	3+
x	+	2+	3+
y	+	2+	3+
z	+	2+	3+

hide H_2O/NH_3
zoom 112-122
zoom 124-133
GO

ALVLIAFAQYLQQCPFEDHVK, MH+ 2591.3948, m/z 648.6042
10HNE-1HSA-Trypsin6-Orbit2.04329.04329.4.dta

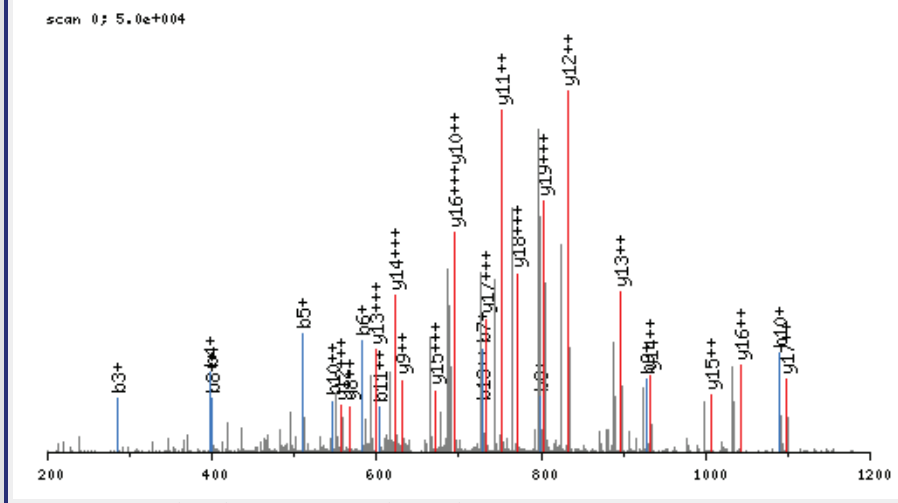

click image to zoom in; click top corners to zoom out

b^+	b^{2+}	b^{3+}	#	AA	#	y^+	y^{2+}	y^{3+}
72.0449	36.5264	24.6869	1	A	21			
185.1290	93.0684	62.3816	2	L	20	2520.3577	1260.6827	840.7911
284.1974	142.6026	95.4044	3	V	19	2407.2736	1204.1407	803.0964
397.2815	199.1447	133.0990	4	L	18	2308.2052	1154.6065	770.0736
510.3655	255.6867	170.7937	5	I	17	2195.1211	1098.0645	732.3789
581.4027	291.2052	194.4728	6	A	16	2082.0371	1041.5224	694.6842
728.4711	364.7394	243.4956	7	F	15	2010.9999	1006.0039	671.0052
799.5082	400.2580	267.1746	8	A	14	1863.9315	932.4697	621.9824
927.5668	464.2873	309.8608	9	Q	13	1792.8944	896.9511	598.3034
1090.6301	545.8190	364.2152	10	Y	12	1664.8358	832.9218	555.6172
1203.7142	602.3610	401.9099	11	L	11	1501.7725	751.3902	501.2627
1331.7727	666.3903	444.5961	12	Q	10	1388.6884	694.8481	463.5680
1459.8313	730.4196	487.2823	13	Q	9	1260.6299	630.8188	420.8818
1720.9712	860.9895	574.3290	14	C	8	1132.5713	566.7896	378.1956
1818.0240	909.5159	606.6799	15	P	7	871.4314	436.2196	291.1490
1965.0924	983.0501	655.7027	16	F	6	774.3786	387.6932	258.7981
2094.1350	1047.5714	698.7169	17	E	5	627.3102	314.1590	209.7753
2209.1619	1105.0849	737.0592	18	D	4	498.2676	249.6377	166.7611
2346.2208	1173.6143	782.7455	19	H	3	383.2407	192.1243	128.4188
2445.2893	1223.1485	815.7683	20	V	2	246.1818	123.5948	82.7325
			21	K	1	147.1134	74.0606	49.7097

C(14):+261.14

COMET Spectrum View by J.Eng (c) ISB 2001
(TPP v4.4 VUVUZELA rev 1, Build 201010121551 (MinGW))

X-range: 100 - 800
MassTol: 0.950 Y-zoom: 1.00
ImageSize: (•) Sm ( ) Lg
MassType: ( ) AVG (•) MONO
Axis: (•) 1 ( ) 2
Label: (•) I ( ) M ( ) -
Ions:
a [ ] + [ ] 2+ [ ] 3+
b [x] + [x] 2+ [ ] 3+
c [ ] + [ ] 2+ [ ] 3+
x [ ] + [ ] 2+ [ ] 3+
y [x] + [x] 2+ [x] 3+
z [ ] + [ ] 2+ [ ] 3+
hide H_2O/NH_3 [ ]
zoom 112-122 [ ]
zoom 124-133 [ ]
GO

SLHTLFGDK, MH+ 1175.6676, m/z 392.5607
10HNE-1HSA-Trypsin6-Orbit3.03026.03026.3.dta

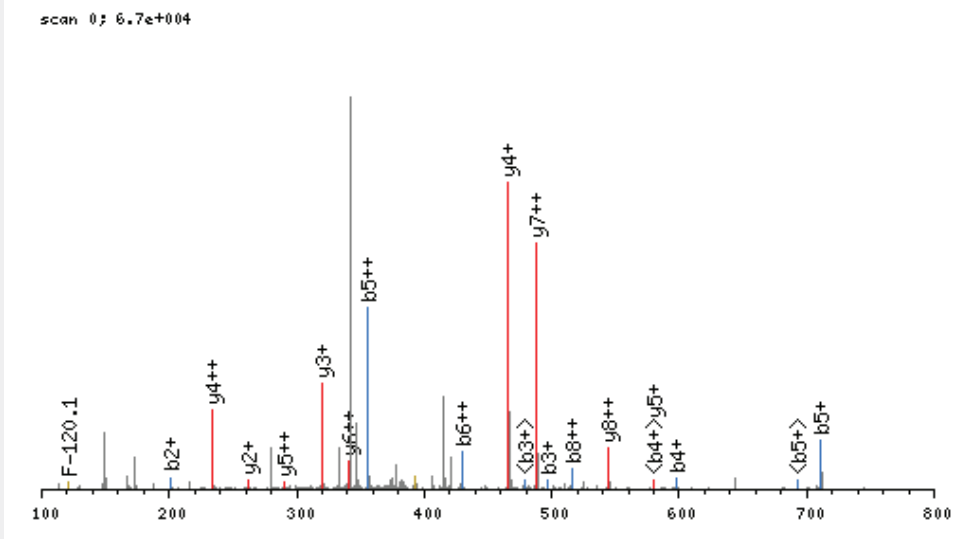

click image to zoom in; click top corners to zoom out

b^+	b^{2+}	#	AA	#	y^+	y^{2+}	y^{3+}
88.0399	44.5238	1	S	9			
201.1239	101.0659	2	L	8	1088.6356	**544.8217**	363.5504
496.3135	248.6607	3	H	7	975.5515	**488.2797**	325.8557
597.3612	299.1845	4	T	6	680.3619	**340.6849**	227.4592
710.4453	**355.7265**	5	L	5	**579.3142**	**290.1610**	193.7766
857.5137	**429.2607**	6	F	4	**466.2302**	**233.6190**	156.0819
914.5351	457.7715	7	G	3	**319.1618**	160.0848	107.0591
1029.5621	**515.2849**	8	D	2	**262.1403**	131.5741	88.0520
		9	K	1	147.1134	74.0606	49.7097

H(3):+295.19

COMET Spectrum View by J.Eng (c) ISB 2001
(TPP v4.4 VUVUZELA rev 1, Build 201010121551 (MinGW))

X-range: 200 - 1700
MassTol: 0.950 Y-zoom: 1.00
ImageSize: (•) Sm ( ) Lg
MassType: ( ) AVG (•) MONO
Axis: (•) 1 ( ) 2
Label: (•) I ( ) M ( ) -
Ions:

a	☐ +	☐ 2+	☐ 3+
b	☑ +	☑ 2+	☐ 3+
c	☐ +	☐ 2+	☐ 3+
x	☐ +	☐ 2+	☐ 3+
y	☑ +	☑ 2+	☑ 3+
z	☐ +	☐ 2+	☐ 3+

hide H_2O/NH_3 ☐
zoom 112-122 ☐
zoom 124-133 ☐
GO

RHPYFYAPELLFFAK, MH+ 2057.1264, m/z 686.3803
10HNE-1HSA-Trypsin6-Orbit2.03830.03830.3.dta

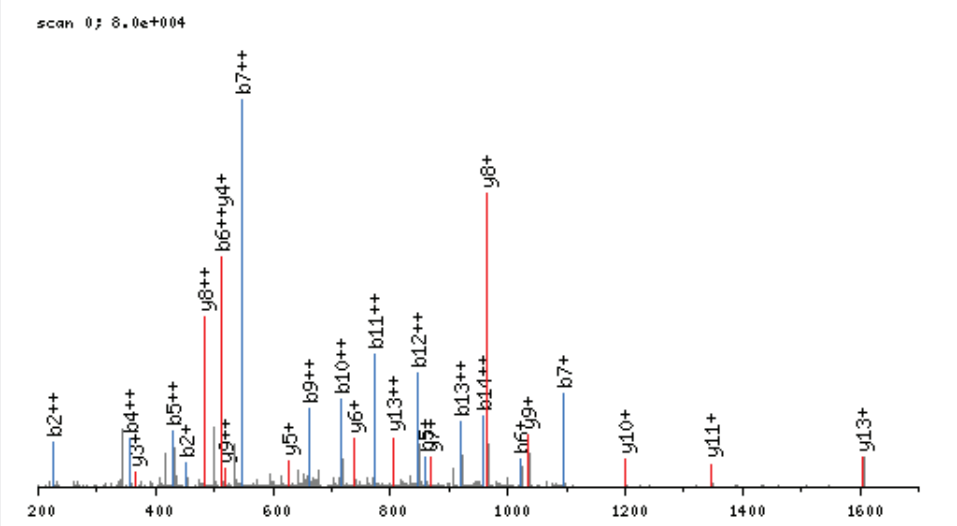

click image to zoom in; click top corners to zoom out

b^+	b^{2+}	#	AA	#	y^+	y^{2+}	y^{3+}
157.1089	79.0584	1	R	15			
452.2985	226.6532	2	H	14	1901.0253	951.0166	634.3470
549.3513	275.1796	3	P	13	1605.8357	803.4218	535.9505
712.4146	356.7112	4	Y	12	1508.7830	754.8954	503.5995
859.4830	430.2454	5	F	11	1345.7196	673.3637	449.2451
1022.5464	511.7771	6	Y	10	1198.6512	599.8295	400.2223
1093.5835	547.2957	7	A	9	1035.5879	518.2979	345.8678
1190.6362	595.8220	8	P	8	964.5508	482.7793	322.1888
1319.6788	660.3433	9	E	7	867.4980	434.2529	289.8379
1432.7629	716.8854	10	L	6	738.4554	369.7316	246.8237
1545.8470	773.4274	11	L	5	625.3714	313.1896	209.1290
1692.9154	846.9616	12	F	4	512.2873	256.6476	171.4343
1839.9838	920.4958	13	F	3	365.2189	183.1134	122.4115
1911.0209	956.0144	14	A	2	218.1505	109.5791	73.3887
		15	K	1	147.1134	74.0606	49.7097

H(2):+295.19

X-range: 200 - 1000
MassTol: 0.950 Y-zoom: 1.00
ImageSize: Sm Lg
MassType: AVG MONO
Axis: 1 2
Label: I M -
Ions:

a	+	2+	3+
b	+	2+	3+
c	+	2+	3+
x	+	2+	3+
y	+	2+	3+
z	+	2+	3+

hide H_2O/NH_3
zoom 112-122
zoom 124-133
GO

RHPYFYAPELLFFAKR, MH+ 2371.3582, m/z 593.5950
10HNE-1HSA-Trypsin6-Orbit2.04047.04047.4.dta

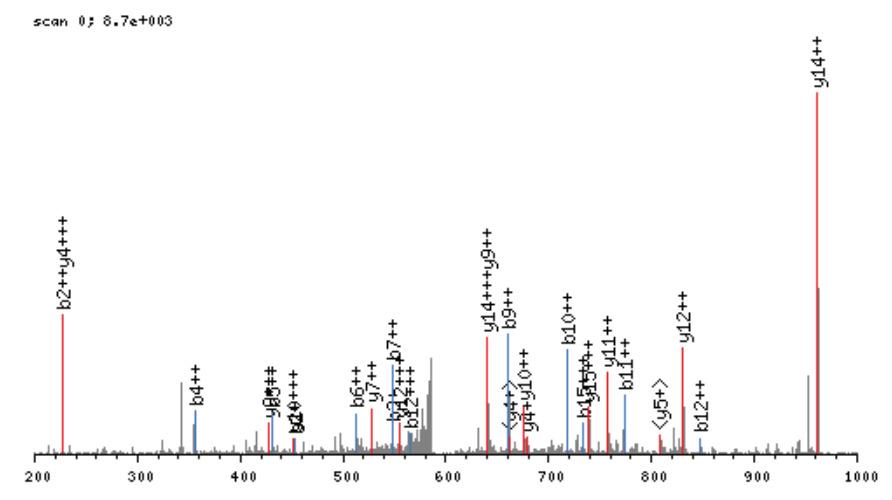

click image to zoom in; click top corners to zoom out

b^+	b^{2+}	b^{3+}	#	AA	#	y^+	y^{2+}	y^{3+}
157.1089	79.0584	53.0415	1	R	16			
452.2985	226.6532	151.4381	2	H	15	2215.2571	1108.1325	739.0909
549.3513	275.1796	183.7890	3	P	14	1920.0675	960.5377	640.6944
712.4146	356.7112	238.1434	4	Y	13	1823.0148	912.0113	608.3435
859.4830	430.2454	287.1662	5	F	12	1659.9514	830.4796	553.9890
1022.5464	511.7771	341.5207	6	Y	11	1512.8830	756.9454	504.9662
1093.5835	547.2957	365.1997	7	A	10	1349.8197	675.4138	450.6118
1190.6362	595.8220	397.5506	8	P	9	1278.7826	639.8952	426.9327
1319.6788	660.3433	440.5648	9	E	8	1181.7298	591.3688	394.5818
1432.7629	716.8854	478.2595	10	L	7	1052.6872	526.8475	351.5676
1545.8470	773.4274	515.9542	11	L	6	939.6031	470.3055	313.8729
1692.9154	846.9616	564.9770	12	F	5	826.5191	413.7635	276.1782
1839.9838	920.4958	613.9998	13	F	4	679.4507	340.2292	227.1554
1911.0209	956.0144	637.6789	14	A	3	532.3823	266.6950	178.1326
2197.2465	1099.1272	733.0874	15	K	2	461.3451	231.1765	154.4536
			16	R	1	175.1195	88.0637	59.0451

H(2):+295.19 K(15):+286.23

X-range: 200 - 1100
MassTol: 0.950 Y-zoom: 1.00
ImageSize: (•) Sm ( ) Lg
MassType: ( ) AVG (•) MONO
Axis: (•) 1 ( ) 2
Label: (•) I ( ) M ( ) -
Ions:
a [ ] + [ ] 2+ [ ] 3+
b [x] + [x] 2+ [ ] 3+
c [ ] + [ ] 2+ [ ] 3+
x [ ] + [ ] 2+ [ ] 3+
y [x] + [x] 2+ [x] 3+
z [ ] + [ ] 2+ [ ] 3+
hide H_2O/NH_3 [ ]
zoom 112-122 [ ]
zoom 124-133 [ ]
GO

YKAAFTECCQAADK, MH+ 1820.8564, m/z 607.6236
10HNE-1HSA-Trypsin6-Orbit1.02272.02272.3.dta

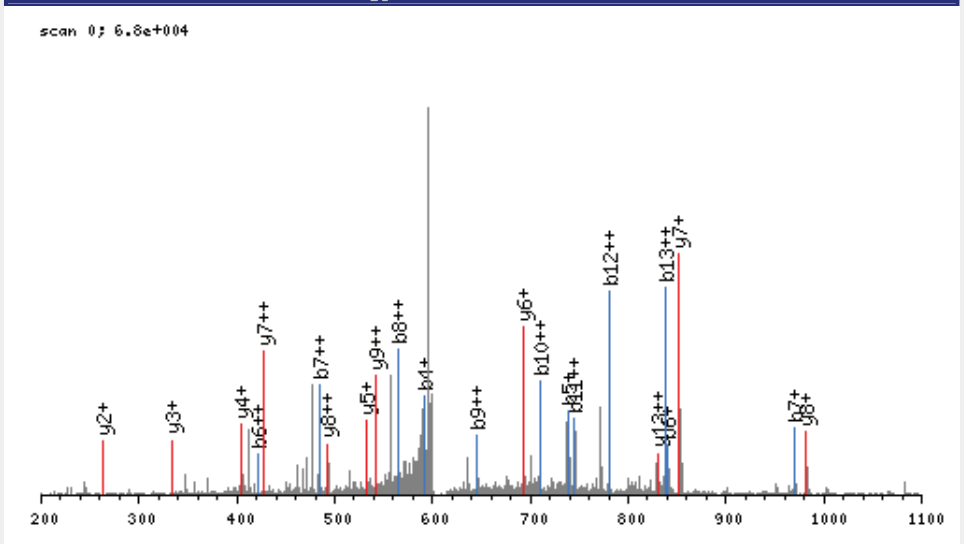

click image to zoom in; click top corners to zoom out

b^+	b^{2+}	#	AA	#	y^+	y^{2+}	y^{3+}
164.0712	82.5395	1	Y	14			
450.2968	225.6523	2	K	13	1657.7930	**829.4004**	553.2696
521.3339	261.1709	3	A	12	1371.5674	686.2876	457.8610
592.3710	296.6894	4	A	11	1300.5303	650.7690	434.1820
739.4394	370.2236	5	F	10	1229.4932	615.2505	410.5029
840.4871	**420.7475**	6	T	9	1082.4247	**541.7163**	361.4801
969.5297	**485.2688**	7	E	8	**981.3771**	**491.1924**	327.7976
1129.5604	**565.2841**	8	C	7	**852.3345**	**426.6711**	284.7834
1289.5911	**645.2995**	9	C	6	**692.3038**	346.6558	231.4398
1417.6497	**709.3287**	10	Q	5	**532.2731**	266.6405	178.0963
1488.6868	**744.8473**	11	A	4	**404.2145**	202.6112	135.4101
1559.7239	**780.3659**	12	A	3	**333.1774**	167.0926	111.7310
1674.7508	**837.8793**	13	D	2	**262.1403**	131.5741	88.0520
		14	K	1	147.1134	74.0606	49.7097

K(2):+286.23 C(8):+160.03 C(9):+160.03

X-range: 100 - 700
MassTol: 0.950 Y-zoom: 1.00
ImageSize: (•) Sm ( ) Lg
MassType: ( ) AVG (•) MONO
Axis: (•) 1 ( ) 2
Label: (•) I ( ) M ( ) -
Ions:

a	[ ] +	[ ] 2+	[ ] 3+
b	[x] +	[x] 2+	[ ] 3+
c	[ ] +	[ ] 2+	[ ] 3+
x	[ ] +	[ ] 2+	[ ] 3+
y	[x] +	[x] 2+	[x] 3+
z	[ ] +	[ ] 2+	[ ] 3+

hide H_2O/NH_3 [ ]
zoom 112-122 [ ]
zoom 124-133 [ ]
GO

LKCASLQK, MH+ 1105.6655, m/z 369.2267
10HNE-1HSA-Trypsin6-Orbit2.01837.01837.3.dta

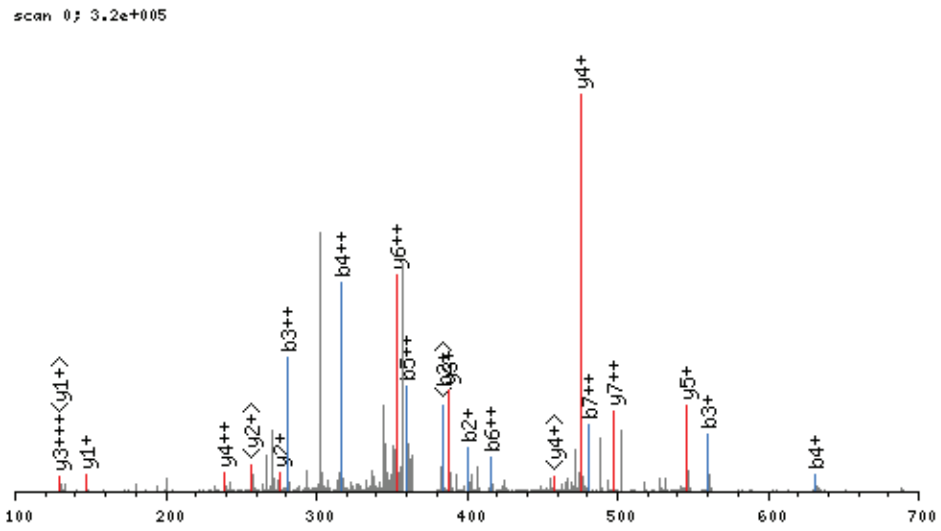

click image to zoom in; click top corners to zoom out

b^+	b^{2+}	#	AA	#	y^+	y^{2+}	y^{3+}
114.0919	57.5499	1	L	8			
400.3175	200.6627	2	K	7	992.5815	**496.7946**	331.5324
560.3482	**280.6780**	3	C	6	706.3558	**353.6818**	236.1238
631.3853	**316.1966**	4	A	5	**546.3251**	273.6665	182.7803
718.4174	**359.7126**	5	S	4	**475.2880**	**238.1479**	159.1012
831.5014	**416.2546**	6	L	3	**388.2560**	194.6319	**130.0905**
959.5600	**480.2839**	7	Q	2	**275.1719**	138.0899	92.3959
		8	K	1	**147.1134**	74.0606	49.7097

K(2):+286.23 C(3):+160.03

X-range: 100 - 900
MassTol: 0.950 Y-zoom: 1.00
ImageSize: (•) Sm ( ) Lg
MassType: ( ) AVG (•) MONO
Axis: (•) 1 ( ) 2
Label: (•) I ( ) M ( ) -
Ions:

a	☐ +	☐ 2+	☐ 3+
b	☑ +	☑ 2+	☐ 3+
c	☐ +	☐ 2+	☐ 3+
x	☐ +	☐ 2+	☐ 3+
y	☑ +	☑ 2+	☑ 3+
z	☐ +	☐ 2+	☐ 3+

hide H_2O/NH_3 ☐
zoom 112-122 ☐
zoom 124-133 ☐
GO

AFKAWAVAR, MH+ 1177.7097, m/z 393.2414
10HNE-1HSA-Trypsin6-Orbit2.02804.02804.3.dta

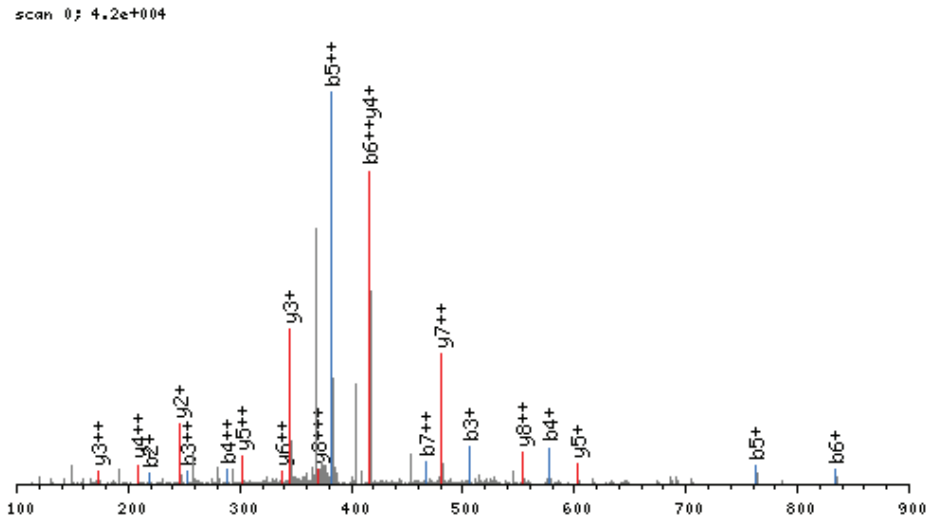

click image to zoom in; click top corners to zoom out

b^+	b^{2+}	#	AA	#	y^+	y^{2+}	y^{3+}
72.0449	36.5264	1	A	9			
219.1134	110.0606	2	F	8	1106.6726	**553.8402**	**369.5628**
505.3390	**253.1734**	3	K	7	959.6042	**480.3060**	320.5400
576.3761	**288.6920**	4	A	6	673.3786	**337.1932**	225.1314
762.4554	**381.7316**	5	W	5	**602.3415**	**301.6746**	201.4524
833.4925	**417.2502**	6	A	4	**416.2621**	**208.6350**	139.4259
932.5610	**466.7844**	7	V	3	**345.2250**	**173.1164**	115.7469
1003.5981	502.3029	8	A	2	**246.1566**	123.5822	82.7241
		9	R	1	175.1195	88.0637	59.0451

K(3):+286.23

X-range: 500 - 1700
MassTol: 0.950 Y-zoom: 1.00
ImageSize: Sm Lg
MassType: AVG MONO
Axis: 1 2
Label: I M -
Ions:

a	+	2+	3+
b	+	2+	3+
c	+	2+	3+
x	+	2+	3+
y	+	2+	3+
z	+	2+	3+

hide H_2O/NH_3
zoom 112-122
zoom 124-133
GO

SHCIAEVENDEMPADLPSLAADFVESK, MH+ 3132.4757, m/z 1044.8301
10HNE-1HSA-Trypsin6-Orbit2.03858.03858.3.dta

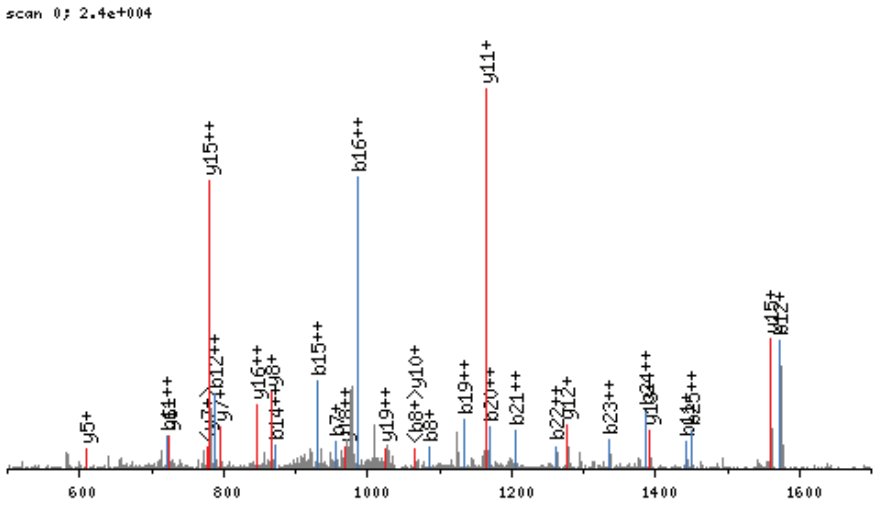

click image to zoom in; click top corners to zoom out

b^+	b^{2+}	#	AA	#	y^+	y^{2+}	y^{3+}
88.0399	44.5238	1	S	27			
383.2294	192.1186	2	H	26	3045.4437	1523.2258	1015.8198
543.2601	272.1340	3	C	25	2750.2541	1375.6310	917.4233
656.3442	328.6760	4	I	24	2590.2234	1295.6156	864.0797
727.3813	364.1946	5	A	23	2477.1394	1239.0736	826.3850
856.4239	428.7159	6	E	22	2406.1023	1203.5550	802.7060
955.4923	478.2501	7	V	21	2277.0597	1139.0337	759.6918
1084.5349	542.7714	8	E	20	2177.9913	1089.4995	726.6690
1198.5778	599.7928	9	N	19	2048.9487	**1024.9782**	683.6548
1313.6048	657.3063	10	D	18	1934.9057	**967.9568**	645.6405
1442.6474	**721.8276**	11	E	17	1819.8788	910.4433	607.2981
1573.6879	**787.3478**	12	M	16	1690.8362	**845.9220**	564.2839
1670.7406	835.8742	13	P	15	**1559.7957**	**780.4018**	520.6038
1741.7777	**871.3928**	14	A	14	1462.7430	731.8754	488.2529
1856.8047	**928.9063**	15	D	13	**1391.7058**	696.3568	464.5738
1969.8887	**985.4483**	16	L	12	**1276.6789**	638.8434	426.2315
2066.9415	1033.9747	17	P	11	**1163.5948**	582.3013	388.5368
2153.9735	1077.4907	18	S	10	**1066.5421**	533.7749	356.1859
2267.0576	**1134.0327**	19	L	9	979.5100	490.2589	327.1752
2338.0947	**1169.5513**	20	A	8	**866.4260**	433.7169	289.4805
2409.1318	**1205.0698**	21	A	7	**795.3889**	398.1983	265.8015
2524.1588	**1262.5833**	22	D	6	**724.3517**	362.6798	242.1225
2671.2272	**1336.1175**	23	F	5	**609.3248**	305.1663	203.7802
2770.2956	**1385.6517**	24	V	4	462.2564	231.6321	154.7573
2899.3382	**1450.1730**	25	E	3	363.1880	182.0979	121.7345
2986.3702	1493.6890	26	S	2	234.1454	117.5766	78.7203
		27	K	1	147.1134	74.0606	49.7097

H(2):+295.19 C(3):+160.03

COMET Spectrum View by J.Eng (c) ISB 2001
(TPP v4.4 VUVUZELA rev 1, Build 201010121551 (MinGW))

X-range: 500 - 1700
MassTol: 0.950 Y-zoom: 1.00
ImageSize: Sm Lg
MassType: AVG MONO
Axis: 1 2
Label: I M -
Ions:

	+	2+	3+
a	☐	☐	☐
b	☑	☑	☐
c	☐	☐	☐
x	☐	☐	☐
y	☑	☑	☑
z	☐	☐	☐

hide H_2O/NH_3 ☐
zoom 112-122 ☐
zoom 124-133 ☐
GO

SHCIAEVENDEMPADLPSLAADFVESK, MH+ 3148.4707, m/z 1050.1617
10HNE-1HSA-Trypsin6-Orbit1.03632.03632.3.dta

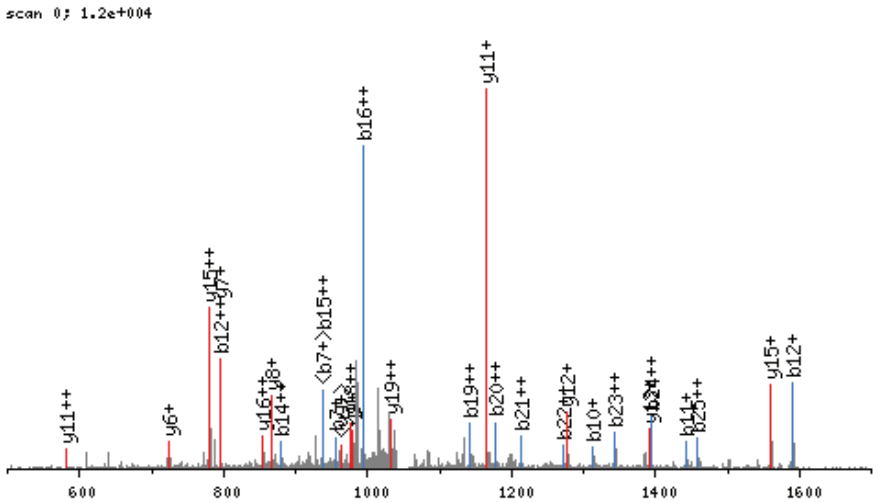

click image to zoom in; click top corners to zoom out

b^+	b^{2+}	#	AA	#	y^+	y^{2+}	y^{3+}
88.0399	44.5238	1	S	27			
383.2294	192.1186	2	H	26	3061.4386	1531.2232	1021.1514
543.2601	272.1340	3	C	25	2766.2490	1383.6284	922.7549
656.3442	328.6760	4	I	24	2606.2184	1303.6131	869.4113
727.3813	364.1946	5	A	23	2493.1343	1247.0711	831.7166
856.4239	428.7159	6	E	22	2422.0972	1211.5525	808.0376
955.4923	478.2501	7	V	21	2293.0546	1147.0312	765.0234
1084.5349	542.7714	8	E	20	2193.9862	1097.4970	732.0006
1198.5778	599.7928	9	N	19	2064.9436	**1032.9757**	688.9864
1313.6048	657.3063	10	D	18	1950.9007	**975.9542**	650.9721
1442.6474	721.8276	11	E	17	1835.8737	918.4408	612.6298
1589.6828	**795.3453**	12	M	16	1706.8311	**853.9195**	569.6156
1686.7355	843.8717	13	P	15	**1559.7957**	**780.4018**	520.6038
1757.7726	**879.3902**	14	A	14	1462.7430	731.8754	488.2529
1872.7996	**936.9037**	15	D	13	**1391.7058**	696.3568	464.5738
1985.8837	**993.4457**	16	L	12	**1276.6789**	638.8434	426.2315
2082.9364	1041.9721	17	P	11	**1163.5948**	**582.3013**	388.5368
2169.9684	1085.4881	18	S	10	1066.5421	533.7749	356.1859
2283.0525	**1142.0302**	19	L	9	**979.5100**	490.2589	327.1752
2354.0896	**1177.5487**	20	A	8	**866.4260**	433.7169	289.4805
2425.1267	**1213.0673**	21	A	7	**795.3889**	398.1983	265.8015
2540.1537	**1270.5808**	22	D	6	**724.3517**	362.6798	242.1225
2687.2221	**1344.1150**	23	F	5	609.3248	305.1663	203.7802
2786.2905	**1393.6492**	24	V	4	462.2564	231.6321	154.7573
2915.3331	**1458.1705**	25	E	3	363.1880	182.0979	121.7345
3002.3651	1501.6865	26	S	2	234.1454	117.5766	78.7203
		27	K	1	147.1134	74.0606	49.7097

H(2):+295.19 C(3):+160.03 M(12):+147.04

COMET Spectrum View by J.Eng (c) ISB 2001
(TPP v4.4 VUVUZELA rev 1, Build 201010121551 (MinGW))

X-range: 200 - 1200
MassTol: 0.950 Y-zoom: 1.00
ImageSize: (•) Sm ( ) Lg
MassType: ( ) AVG (•) MONO
Axis: (•) 1 ( ) 2
Label: (•) I ( ) M ( ) -
Ions:

a	☐ +	☐ 2+	☐ 3+
b	☑ +	☑ 2+	☐ 3+
c	☐ +	☐ 2+	☐ 3+
x	☐ +	☐ 2+	☐ 3+
y	☑ +	☑ 2+	☑ 3+
z	☐ +	☐ 2+	☐ 3+

hide H_2O/NH_3 ☐
zoom 112-122 ☐
zoom 124-133 ☐
GO

RHPDYSVVLLLR, MH+ 1625.9743, m/z 542.6629
10HNE-1HSA-Trypsin6-Orbit3.03322.03322.3.dta

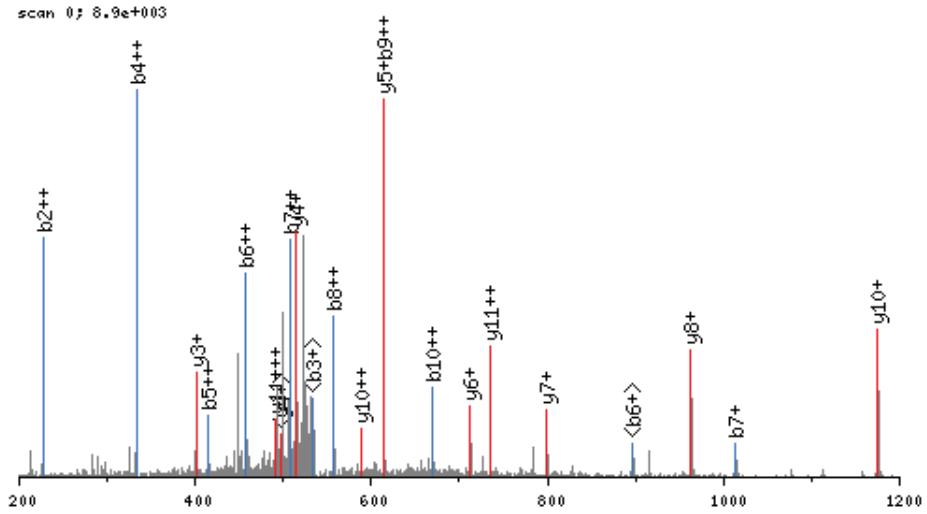

click image to zoom in; click top corners to zoom out

b^+	b^{2+}	#	AA	#	y^+	y^{2+}	y^{3+}
157.1089	79.0584	1	R	12			
452.2985	**226.6532**	2	H	11	1469.8732	**735.4405**	**490.6296**
549.3513	275.1796	3	P	10	**1174.6836**	**587.8457**	392.2331
664.3782	**332.6930**	4	D	9	1077.6308	539.3193	359.8822
827.4416	**414.2247**	5	Y	8	**962.6039**	481.8059	321.5398
914.4736	**457.7407**	6	S	7	**799.5405**	400.2742	267.1854
1013.5420	**507.2749**	7	V	6	**712.5085**	356.7582	238.1747
1112.6104	**556.8091**	8	V	5	**613.4401**	307.2240	205.1519
1225.6945	**613.3512**	9	L	4	**514.3717**	257.6898	172.1291
1338.7785	**669.8932**	10	L	3	**401.2876**	201.1477	134.4344
1451.8626	726.4352	11	L	2	288.2036	144.6057	96.7397
		12	R	1	175.1195	88.0637	59.0451

H(2):+295.19

X-range: 300 - 1400
MassTol: 0.950 Y-zoom: 1.00
ImageSize: (•) Sm ( ) Lg
MassType: ( ) AVG (•) MONO
Axis: (•) 1 ( ) 2
Label: (•) I ( ) M ( ) -
Ions:

a	☐ +	☐ 2+	☐ 3+
b	☑ +	☑ 2+	☐ 3+
c	☐ +	☐ 2+	☐ 3+
x	☐ +	☐ 2+	☐ 3+
y	☑ +	☑ 2+	☑ 3+
z	☐ +	☐ 2+	☐ 3+

hide H_2O/NH_3 ☐
zoom 112-122 ☐
zoom 124-133 ☐
GO

QNCELFEQLGEYKFQNALLVR, MH+ 2757.4286, m/z 919.8144
10HNE-1HSA-Trypsin6-Orbit2.03895.03895.3.dta

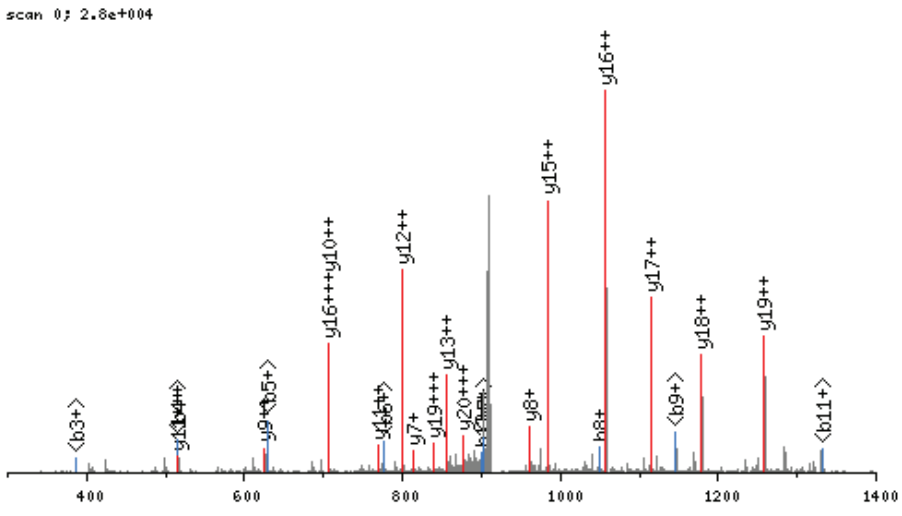

click image to zoom in; click top corners to zoom out

b^+	b^{2+}	#	AA	#	y^+	y^{2+}	y^{3+}
129.0664	65.0371	1	Q	21			
243.1093	122.0586	2	N	20	2629.3700	1315.1889	**877.1286**
403.1400	202.0739	3	C	19	2515.3271	**1258.1675**	**839.1142**
532.1826	266.5952	4	E	18	2355.2964	**1178.1521**	785.7707
645.2667	323.1372	5	L	17	2226.2538	**1113.6308**	742.7565
792.3351	396.6715	6	F	16	2113.1698	**1057.0888**	**705.0618**
921.3777	461.1928	7	E	15	1966.1013	**983.5546**	656.0390
1049.4363	525.2220	8	Q	14	1837.0587	919.0333	613.0248
1162.5203	581.7641	9	L	13	1709.0002	**855.0040**	570.3386
1219.5418	610.2748	10	G	12	1595.9161	**798.4620**	532.6439
1348.5844	674.7961	11	E	11	1538.8946	**769.9512**	**513.6368**
1511.6477	756.3278	12	Y	10	1409.8520	**705.4299**	470.6226
1797.8733	**899.4406**	13	K	9	1246.7887	**623.8983**	416.2681
1944.9418	972.9748	14	F	8	**960.5631**	480.7855	320.8596
2073.0003	1037.0041	15	Q	7	**813.4947**	407.2512	271.8368
2187.0433	1094.0255	16	N	6	685.4361	343.2220	229.1506
2258.0804	1129.5441	17	A	5	571.3932	286.2005	191.1363
2371.1644	1186.0861	18	L	4	500.3560	250.6819	167.4572
2484.2485	1242.6282	19	L	3	387.2720	194.1399	129.7625
2583.3169	1292.1624	20	V	2	274.1879	137.5979	92.0679
		21	R	1	175.1195	88.0637	59.0451

C(3):+160.03 K(13):+286.23

COMET Spectrum View by J.Eng (c) ISB 2001
(TPP v4.4 VUVUZELA rev 1, Build 201010121551 (MinGW))

X-range: 300 - 1000
MassTol: 0.950 Y-zoom: 7.00
ImageSize: (•) Sm ( ) Lg
MassType: ( ) AVG (•) MONO
Axis: (•) 1 ( ) 2
Label: (•) I ( ) M ( ) -
Ions:

a	☐ +	☐ 2+	☐ 3+
b	☑ +	☑ 2+	☐ 3+
c	☐ +	☐ 2+	☐ 3+
x	☐ +	☐ 2+	☐ 3+
y	☑ +	☑ 2+	☑ 3+
z	☐ +	☐ 2+	☐ 3+

hide H_2O/NH_3 ☐
zoom 112-122 ☐
zoom 124-133 ☐
GO

KVPQVSTPTLVEVSR, MH+ 1798.0690, m/z 600.0278
10HNE-1HSA-Trypsin6-Orbit2.02814.02814.3.dta

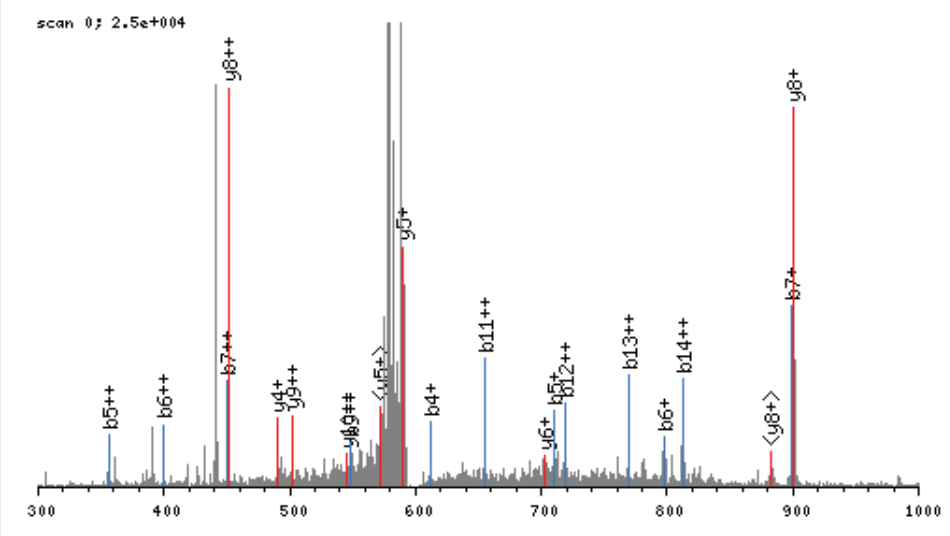

click image to zoom in; click top corners to zoom out

b^+	b^{2+}	#	AA	#	y^+	y^{2+}	y^{3+}
287.2335	144.1206	1	K	15			
386.3019	193.6549	2	V	14	1511.8433	756.4256	504.6197
483.3546	242.1812	3	P	13	1412.7749	706.8914	471.5969
611.4132	306.2105	4	Q	12	1315.7222	658.3650	439.2459
710.4816	355.7447	5	V	11	1187.6636	594.3357	396.5597
797.5137	399.2607	6	S	10	1088.5952	544.8015	363.5369
898.5613	449.7846	7	T	9	1001.5631	501.2855	334.5263
995.6141	498.3110	8	P	8	900.5155	450.7616	300.8437
1096.6618	548.8348	9	T	7	803.4627	402.2353	268.4928
1209.7459	605.3768	10	L	6	702.4150	351.7114	234.8102
1308.8143	654.9110	11	V	5	589.3310	295.1694	197.1155
1437.8569	719.4323	12	E	4	490.2625	245.6352	164.0927
1536.9253	768.9665	13	V	3	361.2199	181.1139	121.0785
1623.9573	812.4826	14	S	2	262.1515	131.5797	88.0557
		15	R	1	175.1195	88.0637	59.0451

K(1):+286.23

X-range: 300 - 1100
MassTol: 0.950 Y-zoom: 3.00
ImageSize: Sm Lg
MassType: AVG MONO
Axis: 1 2
Label: I M -
Ions:

a	+	2+	3+
b	+	2+	3+
c	+	2+	3+
x	+	2+	3+
y	+	2+	3+
z	+	2+	3+

hide H_2O/NH_3
zoom 112-122
zoom 124-133
GO

KVPQVSTPTLVEVSR, MH+ 1780.0584, m/z 594.0243
10HNE-1HSA-Trypsin6-Orbit1.02940.02940.3.dta

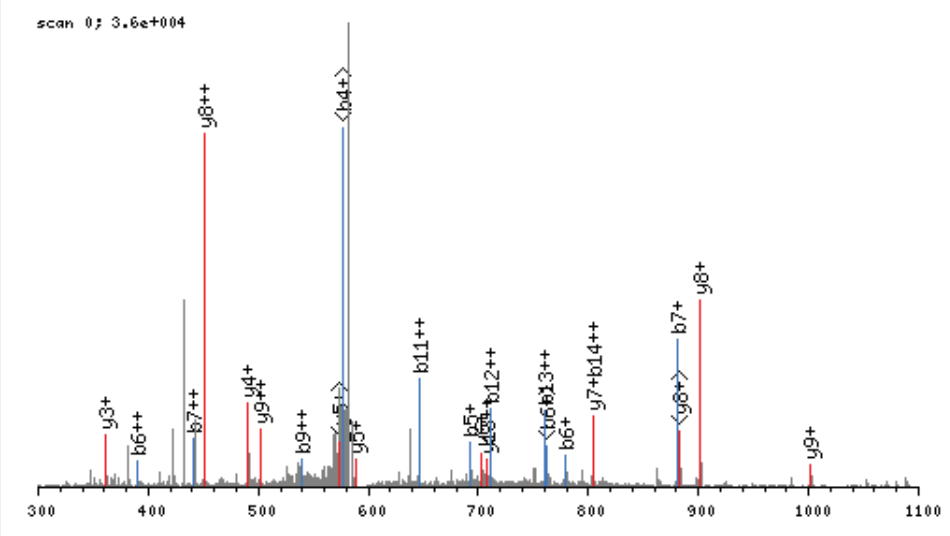

click image to zoom in; click top corners to zoom out

b^+	b^{2+}	#	AA	#	y^+	y^{2+}	y^{3+}
269.2229	135.1154	1	K	15			
368.2913	184.6496	2	V	14	1511.8433	756.4256	504.6197
465.3441	233.1760	3	P	13	1412.7749	706.8914	471.5969
593.4027	297.2052	4	Q	12	1315.7222	658.3650	439.2459
692.4711	346.7394	5	V	11	1187.6636	594.3357	396.5597
779.5031	390.2555	6	S	10	1088.5952	544.8015	363.5369
880.5508	440.7793	7	T	9	1001.5631	501.2855	334.5263
977.6035	489.3057	8	P	8	900.5155	450.7616	300.8437
1078.6512	539.8295	9	T	7	803.4627	402.2353	268.4928
1191.7353	596.3716	10	L	6	702.4150	351.7114	234.8102
1290.8037	645.9058	11	V	5	589.3310	295.1694	197.1155
1419.8463	710.4271	12	E	4	490.2625	245.6352	164.0927
1518.9147	759.9613	13	V	3	361.2199	181.1139	121.0785
1605.9467	803.4773	14	S	2	262.1515	131.5797	88.0557
		15	R	1	175.1195	88.0637	59.0451

K(1):+268.22

X-range: 200 - 800
MassTol: 0.950 Y-zoom: 1.00
ImageSize: Sm Lg
MassType: AVG MONO
Axis: 1 2
Label: I M -
Ions:

a	+	2+	3+
b	+	2+	3+
c	+	2+	3+
x	+	2+	3+
y	+	2+	3+
z	+	2+	3+

hide H_2O/NH_3
zoom 112-122
zoom 124-133
GO

KQTALVELVK, MH+ 1286.8299, m/z 429.6148
10HNE-1HSA-Trypsin6-Orbit1.02905.02905.3.dta

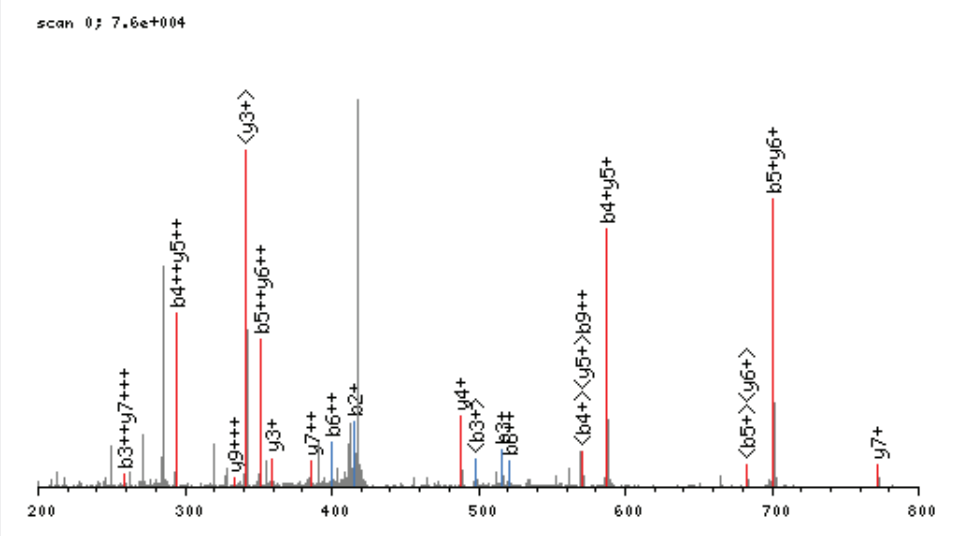

click image to zoom in; click top corners to zoom out

b^+	b^{2+}	#	AA	#	y^+	y^{2+}	y^{3+}
287.2335	144.1206	1	K	10			
415.2920	208.1499	2	Q	9	1000.6043	500.8060	**334.2066**
516.3397	**258.6738**	3	T	8	872.5457	436.7768	291.5204
587.3768	**294.1923**	4	A	7	**771.4980**	**386.2529**	**257.8379**
700.4609	**350.7344**	5	L	6	**700.4609**	**350.7344**	234.1589
799.5293	**400.2686**	6	V	5	**587.3768**	**294.1923**	196.4642
928.5719	464.7899	7	E	4	**488.3084**	244.6581	163.4414
1041.6560	**521.3319**	8	L	3	**359.2658**	180.1368	120.4272
1140.7244	**570.8661**	9	V	2	246.1818	123.5948	82.7325
		10	K	1	147.1134	74.0606	49.7097

K(1):+286.23

COMET Spectrum View by J.Eng (c) ISB 2001
(TPP v4.4 VUVUZELA rev 1, Build 201010121551 (MinGW))

X-range: 100 - 800
MassTol: 0.950 Y-zoom: 1.00
ImageSize: Sm Lg
MassType: AVG MONO
Axis: 1 2
Label: I M -
Ions:

a	+	2+	3+
b	+	2+	3+
c	+	2+	3+
x	+	2+	3+
y	+	2+	3+
z	+	2+	3+

hide H_2O/NH_3
zoom 112-122
zoom 124-133
GO

KQTALVELVK, MH+ 1268.8193, m/z 423.6113
10HNE-1HSA-Trypsin6-Orbit3.02993.02993.3.dta

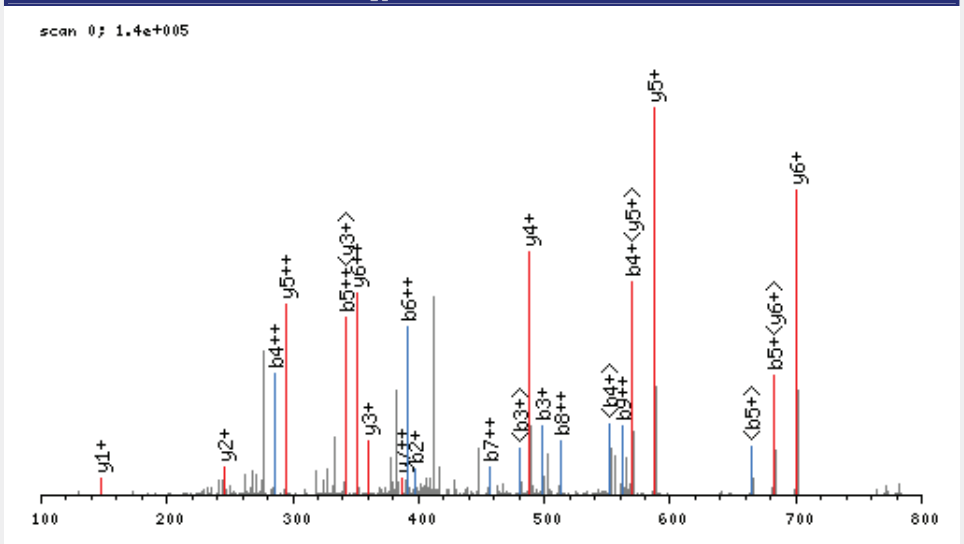

click image to zoom in; click top corners to zoom out

b^+	b^{2+}	#	AA	#	y^+	y^{2+}	y^{3+}
269.2229	135.1154	1	K	10			
397.2815	199.1447	2	Q	9	1000.6043	500.8060	334.2066
498.3292	249.6685	3	T	8	872.5457	436.7768	291.5204
569.3663	285.1870	4	A	7	771.4980	386.2529	257.8379
682.4503	341.7291	5	L	6	700.4609	350.7344	234.1589
781.5188	391.2633	6	V	5	587.3768	294.1923	196.4642
910.5613	455.7846	7	E	4	488.3084	244.6581	163.4414
1023.6454	512.3266	8	L	3	359.2658	180.1368	120.4272
1122.7138	561.8608	9	V	2	246.1818	123.5948	82.7325
		10	K	1	147.1134	74.0606	49.7097

K(1):+268.22

X-range: 200 - 1300
MassTol: 0.950 Y-zoom: 1.00
ImageSize: (•) Sm ( ) Lg
MassType: ( ) AVG (•) MONO
Axis: (•) 1 ( ) 2
Label: (•) I ( ) M ( ) -
Ions:

a	☐ +	☐ 2+	☐ 3+
b	☑ +	☑ 2+	☐ 3+
c	☐ +	☐ 2+	☐ 3+
x	☐ +	☐ 2+	☐ 3+
y	☑ +	☑ 2+	☑ 3+
z	☐ +	☐ 2+	☐ 3+

hide H_2O/NH_3 ☐
zoom 112-122 ☐
zoom 124-133 ☐
GO

EQLKAVMDDFAAFVEK, MH+ 1999.0462, m/z 667.0202
10HNE-1HSA-Trypsin6-Orbit1.03946.03946.3.dta

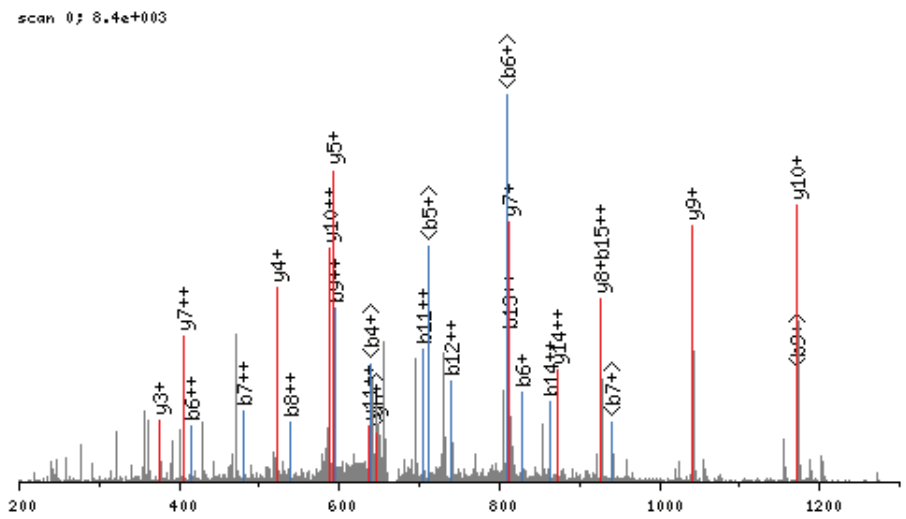

click image to zoom in; click top corners to zoom out

b^+	b^{2+}	#	AA	#	y^+	y^{2+}	y^{3+}
130.0504	65.5291	1	E	16			
258.1090	129.5584	2	Q	15	1870.0036	935.5057	624.0064
371.1931	186.1004	3	L	14	1741.9450	**871.4764**	581.3202
657.4187	329.2133	4	K	13	1628.8610	814.9344	543.6255
728.4558	364.7318	5	A	12	1342.6353	671.8216	448.2170
827.5242	**414.2660**	6	V	11	1271.5982	**636.3030**	424.5380
958.5647	**479.7863**	7	M	10	**1172.5298**	**586.7688**	391.5151
1073.5917	**537.2997**	8	D	9	**1041.4893**	521.2486	347.8350
1188.6186	**594.8132**	9	D	8	**926.4624**	463.7351	309.4927
1335.6870	668.3474	10	F	7	**811.4354**	**406.2216**	271.1504
1406.7241	**703.8660**	11	A	6	664.3670	332.6874	222.1276
1477.7612	**739.3845**	12	A	5	**593.3299**	297.1689	198.4485
1624.8297	**812.9187**	13	F	4	**522.2928**	261.6503	174.7695
1723.8981	**862.4529**	14	V	3	**375.2244**	188.1161	125.7467
1852.9407	**926.9742**	15	E	2	276.1559	138.5819	92.7239
		16	K	1	147.1134	74.0606	49.7097

K(4):+286.23